PLACE IN RETURN BOX to remove this checkout from your record.
TO AVOID FINES return on or before date due.

DATE DUE	DATE DUE	DATE DUE

MSU Is An Affirmative Action/Equal Opportunity Institution

c:\circ\datedue.pm3-p.1

CYCLIC LOAD EFFECTS ON MODEL PILE BEHAVIOR IN FROZEN SAND

By

David L. Stelzer

A DISSERTATION

Submitted to
Michigan State University
in partial fulfillment of the requiresments
for the degree of

DOCTOR OF PHILOSOPHY

Department of Civil and Environmental Engineering

1989

604356

ABSTRACT

CYCLIC LOAD EFFECTS ON MODEL PILE BEHAVIOR IN FROZEN SAND

By

David L. Stelzer

Small cyclic loads, 3 to 5 percent of the long-term sustained load, superimposed on a static load will increase settlement (displacement) rates of friction piles embedded in frozen ground. Determination of the basic mechanisms responsible for this increase in pile settlement rates and a suitable theory for their prediction were the objectives of this research.

A series of model steel piles with controlled surface geometries (lug size, shape, and spacing) were frozen in sand and loaded while carefully controlling test variables. The data collected provided information on the displacement mechanisms operating at the pile/frozen soil interface. Pile settlement rates due to static and incremental static loading were analyzed and compared to rate increases resulting from superimposed dynamic loads. Variables controlled during these tests included cyclic load amplitude, frequency of load application, static load magnitude, and temperature. Sand density and ice volume fractions were controlled during sample preparation.

Experimental results showed that cyclic loads significantly increased model pile displacement rates over

those observed for the sustained load, but were smaller than rates inferred from published results. Typically, superimposing a small cyclic load (with amplitude X) produced a displacement rate increase approximately equivalent to the rate increase produced by adding a small static load (magnitude close to 0.6 times X) to a similar pile. The measured displacement (creep) rates appeared to be independent of frequency in the range of 0.1 Hz to 10 Hz for small cyclic loads superimposed on a sustained load. Data corresponding to frequencies which induced resonant response in parts of the loading system were excluded from this study.

Larger lugs (more than 2 times maximum particle size) compressed frozen sand at their leading edge and densified the adjacent frozen soil. Particle crushing along with formation of a zone of material flow and/or slippage occurred in front of and around the lugs. Ice melting at particle contact points and water movement to adjacent locations with lower stress accompanied this slip process. The onset of increasing pile displacement rates (tertiary creep) was shown to be a function of lug height and spacing.

To my family

ACKNOWLEDGEMENT

The author wishes to express appreciation to the National Science Foundation for supporting this work under grant No. CEE-8412275. Financial support from the Department of Civil and Environmental Engineering at Michigan State University, arranged by Dr. Mark B. Snyder and Dr. William B. Taylor, was appreciated.

The author is grateful to Prof. O.B. Andersland for his excellent guidance throughout the course of these studies. Prof. Andersland's advice was thoughtful and helpful. Drs. Robert K. Wen, Gary L. Cloud, and Grahame J. Larson deserve special thanks for serving on the author's guidance committee and reviewing this dissertation.

My wife Karen and daughter Gabriel deserve special recognition for providing their emotional support and love.

TABLE OF CONTENTS

LIST OF TABLES..... x

LIST OF FIGURES..... xi

LIST OF SYMBOLS..... xxi

CHAPTER I. INTRODUCTION..... 1

1.1. Frozen Soil Pile Foundations..... 1

1.2 Cyclic Pile Loading: Research Problem and Objectives..... 5

CHAPTER II. LITERATURE REVIEW..... 7

2.1. Mechanical Properties of Frozen Soils..... 7

2.1.1. Effect of Frozen Soil Composition on Behavior..... 7

2.1.2. Frozen Soil Creep Strength..... 10

2.1.3. Temperature Dependence of Frozen Soil Strength..... 20

2.1.4. Constitutive Equations for Frozen Soils..... 23

2.1.5. Frozen Soil Strength Testing..... 31

2.2. Response of Frozen Ground to Dynamic Loading... 32

2.2.1 Dynamically Loaded Foundations in Unfrozen Soils..... 32

2.2.2. Stress-Strain and Energy Absorbing Properties..... 33

2.2.3. Deformation Influenced by Cyclic Loading..... 35

2.3. Adhesion and Friction Between Pile and Soil.... 39

2.3.1. Mechanical Interaction Between Frozen Soil and Pile..... 42

2.3.2. Pile/Soil Adfreeze Bond Estimation... 42

2.4. Review of Pile Design Methods..... 43

2.5. Pile Settlement Estimation Equations..... 52

2.5.1. Shear Deformation of Soil Along Pile Shaft..... 52

2.5.2. Penetration Deformation of Soil at Pile Base..... 56

2.5.3. Expansion of a Cylindrical Cavity by Pile Settlement..... 63

2.6. Cyclic Loading of Piles and Pile Driving..... 65

CHAPTER III MATERIALS, SAMPLE PREPARATION, EQUIPMENT, AND TESTING PROCEDURES..... 71

3.1. Materials..... 71

3.2. Sample Preparation 72

3.3. Temperature Control Equipment..... 78

3.4. Displacement Measurement Equipment..... 79

3.5. Pile Loading and Load Measurement Equipment... 80

3.6. Testing Procedures..... 81

3.7. Model Pile Loading Procedures..... 82

3.8. Displacement-Time Data Plotting Techniques.... 85

3.9. Determination of Pile Settlement Equation Parameters..... 87

CHAPTER IV EXPERIMENTAL RESULTS..... 90

4.1. Sample Inspection After Testing..... 90

4.2. Full Duration Loads on Lugged Model Piles..... 92

4.3. Step Loads on Lugged Model Piles..... 104

4.3.1. Step Load Increase Magnitudes..... 114

4.3.2. Repeated Step Load Increases..... 121

4.3.3. Rapid Adjustment to a Nearly Steady State..... 126

4.4. Short Duration Loads on Model Lugged Piles.... 133

4.5. Multiple Short Duration Loads on Lugged Model Piles..... 148

4.6. Threaded Rods as Model Piles..... 151

CHAPTER V DISCUSSION AND APPLICATIONS..... 169

5.1. Creep Equation Parameters from Static Loads... 169

5.2. Pile Capacity From Straight Shaft..... 173

5.3. Load Capacity From Pile Lugs..... 182

5.4. Temperature Dependance of Pile Capacity..... 185

5.5. Dynamic Effects on Model Pile Load Capacities. 187

5.6. Limits of Model Pile Displacement..... 194

5.7. Comparison to Uniaxial Compression Tests..... 201

5.8 Comparison to Ladanyi's (1976) Cone Penetration Tests..... 205

5.9. Large n Values from Cyclic Loads on Model Piles..... 206

5.10. Applications to Field Piles..... 212

5.10.1. Analysis of a Pile Failure..... 212

5.10.2. Another Perspective on a Proposed ASTM Standard..... 216

5.10.3. Additional Pile Capacity from Driven Piles..... 217

5.10.4. Additional Research on Static and Cyclic Pile Loads..... 219

CHAPTER VI SUMMARY AND CONCLUSIONS..... 221

6.1 Summary..... 221

6.2 Conclusions..... 222

6.2.1. Creep Settlement Parameters..... 223

6.2.2. Dynamic Load Effect on Settlement Rates..... 224

6.2.3. Pile Surface Roughness and Load Capacity..... 225

APPENDIX A FIGURES FOR DETERMINATION OF TABLE 4.1 CREEP PARAMETERS..... 227

APPENDIX B PILE TEST DATA..... 267

REFERENCE LIST 315

LIST OF TABLES

Table 2.1. Relative Importance of Material and Field- and/or Test-Condition Parameters on Dynamic Properties of Frozen Soils. (after Vinson, 1978).

Table 4.1. Creep Equation Parameters from Full Duration Tests of Lugged Piles.

Table 4.2 Creep Equation Parameters for Lugged Piles from Step Loads.

Table 4.3 Displacement Rate Increases from Short Duration Load Increases on Lugged Piles.

Table 4.4. Threaded Pile Test Results

Table 4.5. Displacement Rate Increases from Multiple Short Duration Loads on Lugged Piles.

Table 5.1. Creep Equation Parameters from Full Duration Tests of Lugged Piles With and (Estimated) Without Resistance on Shaft Behind Lug.

Table 5.2. Determination of Temperature Dependent Creep Equation Exponents. (Data From Table 4.2)

Table 5.3. Lugged Pile Test Data at for Model Steel Piles Frozen in Sand at -3 deg C with Particle Sizes 0.42 to 0.59 mm.

Table 5.4. Temperature Adjustments for Parameswaren's (1985) Cyclic Uniaxial Compression Tests.

LIST OF FIGURES

Figure 1.1. Temperature profile in the ground, permafrost area (from Andersland, 1987).

Figure 2.1. Frozen sand strength mechanisms (after Ting et al., 1983).

Figure 2.2. Compression tests with frozen Ottawa Sand (after Sayles, 1973). (a) Stress-Strain Curves; (b) Mohr Envelopes.

Figure 2.3. Schematic representation of the failure envelope for frozen Ottawa Sand (after Ladanyi, 1981).

Figure 2.4. Mohr envelopes for creep strength of Ottawa Sand (T = -3.85 deg C) (after Ladanyi, 1981).

Figure 2.5. Failure strain versus strain-rate for a frozen sand (after Ladanyi, 1981).

Figure 2.6. Compressive strength vs. strain rate (after Bragg and Andersland, 1980).

Figure 2.7. Temperature dependence of uniaxial compression strength for various frozen materials (after Ladanyi, 1972).

Figure 2.8. Constant-stress creep tests (after Andersland,et al. 1978).
(a) Creep curve variations.
(b) Basic creep curve.
(c) True strain rate versus time.

Figure 2.9. Creep curve for step loading (after Ladanyi, 1972).

Figure 2.10. Damping ratio of frozen soil (after Vinson, 1978). (a) Versus frequency. (b) Versus temperature.

Figure 2.11. Effect of cyclic stress on temperature of frozen sand (after Parameswaran, 1985).

Figure 2.12. Typical strain relations for frozen sand (after Trimble and Mitchell, 1982).

Figure 2.13. Idealized plate in contact with ice and frozen soil (after Weaver and Morgenstern, 1981a).
(a) Air trapped during sample preparation allows slip at ice/plate interface.
(b) Interaction between plate protrusions and soil grains.
(c) Shear plane developes in ice.

Figure 2.14. Vyalov relationship between failure stress and time (after Neukirchner, 1988).

Figure 2.15. Load test of steel pipe pile (after Linell and Lobacz, 1980).

Figure 2.16. Long-term cohesion of frozen soils (after Weaver and Morgenstern, 1981b).

Figure 2.17. Design chart for friction piles in frozen Ottawa Sand (after Weaver and Morgenstern, 1981b).

Figure 2.18. Design chart for friction end-bearing piles in frozen Ottawa Sand (after Weaver and Morgenstern, 1981b).

Figure 2.19. Uncoupling of effects due to pile shaft and base (after Weaver and Morgenstern, 1981b).

Figure 2.20. Notation for the theory of tapered piles (after Ladanyi and Guichaoua 1985).

Figure 2.21. Vibratory frequency versus force amplitudes for model piles embedded in unfrozen sand (after Schmid 1969).

Figure 2.22. Wave form of model piles at various resonance frequencies (after Schmid 1969).

Figure 2.23. Typical creep curve showing the displacement of wood pile in frozen clay with time (after Parameswaren 1984).

Figure 3.1. Model pile embedded in frozen sand. Lug provides controlled surface roughness.

Figure 3.2. Model pile testing equipment.

Figure 3.3. Typical model pile displacement curves.

Figure 3.4. Typical log(time)-log(displacement) curves for model pile movement in frozen sand.

Figure 3.5. Primary-creep parameters from time-creep-strain data. (after Andersland, et al. 1978).

Figure 4.1. Time-displacement curves for model steel piles with 3.18 mm lug heights in frozen sand.

Figure 4.2. Log(time)-log(displacement) curves for a pile test using various C-type starting points. (a) Test #105.

Figure 4.2b. Log(time)-log(displacement) curves for Test #114 with various starting points.

Figure 4.2b. Log(time)-log(displacement) curves for Test #111 with various starting points.

Figure 4.3. Time-displacement curves for model piles with 3.18 mm lug heights in frozen sand @ -3 ° C and 25.4 mm displacement limits. (a) With 0 mm C-type starting points.

Figure 4.3b. With 1 mm C-type starting points.

Figure 4.3c. With 3 mm C-type starting points.

Figure 4.3d. With 4.4 mm C-type starting points.

Figure 4.3e. With 6 mm C-type starting points.

Figure 4.4. Time-displacement behavior of similar piles subjected to similar loads in frozen sand using a 1 mm C-type starting point.

Figure 4.5. Time-displacement behavior of two similar model piles in frozen sand subjected to similar load increases. Plots used 5.75 mm C-type starting points.

Figure 4.6. Time-displacement behavior of a model pile before and after a load increase. (a) Load increased after a relatively small pile displacement.

Figure 4.6b. Load increased after a relatively large displacement.

Figure 4.7. Time-displacement curves of a single pile test in frozen sand after a load increase. (a) Using C-type starting points.

Figure 4.7b. Using B-type starting points.

Figure 4.8. Time-displacement behavior of a tapered-lug model pile (Test #60) loaded by several steps including a superimposed dynamic load.

Figure 4.9. Time-displacement of a tapered-lug model pile before and after loading. (a) Static load increase at 9.73 mm displacement of Test #60.

Figure 4.9b. Static load increase at 12.96 mm displacement of Test #60.

Figure 4.9c. Static load increase at 19.76 mm displacement of Test #60.

Figure 4.10. Comparison of load increases on a model pile (Test #60) using C-type starting points.

Figure 4.11. Time-displacement behavior of a model steel pile (Test #29) loaded by several steps.

Figure 4.12. Time-displacement behavior of a model steel pile before and after loading. (a) First step load during Test #29.

Figure 4.12b. Second step load during Test #29.

Figure 4.13. Time-displacement behavior of a model pile (Test #33) frozen in a dense sand and loaded by steps including a superimposed dynamic load.

Figure 4.14. Time-displacement behavior of a model pile (Test #33) in dense sand before and after a load increase. (a) Step load 2.38 mm after beginning of Test #33.

Figure 4.14b. Step load added at 7.46 mm after beginning of Test #33.

Figure 4.14c. Temperature increased from - 3 deg C to -2 deg C at 9.51 mm after the beginning of Test #33.

Figure 4.15. Time-displacement behavior of a lugged pile (Test #35) shown with several superimposed dynamic loads and one static load increase.

Figure 4.16. Time-displacement behavior of a lugged pile (Test #51) in polycrystalline ice with a constant load.

Figure 4.17. Time-displacement curves for a model pile in frozen sand at -3 deg C with periods of unloading.

Figure 4.18. Time-displacement behavior of a single pile (Test #92) shown 1 mm after restoration of the static pile load.

Figure 4.19. Time-displacement curve for a model pile in frozen sand showing the relationship for short duration load increases VIII through XI of Test #92.

Figure 4.20. Short duration time-displacement curves for a model pile in frozen sand, load increases VIII Through XI of Sample #92.

Figure 4.21. Time-displacement behavior of model piles subjected to superimposed dynamic loads. (a) Curve of tapered lug pile (Test #60) in loose sand at -3 deg C.

Figure 4.21b. Curve of 0.79 mm lug in dense sand (Test #33) at -3 deg C.

Figure 4.21c. Curve of 0.79 mm lug in polycrystalline ice (Test #35) at -3 deg C.

Figure 4.21d. Curve of 0.79 mm lug in loose sand (Test #88) at -3 deg C.

Figure 4.22. Time-displacement behavior of a single pile (Test #123) loaded by successively larger loads during a short total duration.

Figure 4.23. Time-displacement of threaded rods in frozen sand.

Figure 4.24. Time-displacement behavior of threaded rods in frozen sand. (a) Threaded rod time-displacement curves started 0.14 mm after initial loading.

Figure 4.24b. Threaded rod time-displacement curves started 0.3 mm after initial loading.

Figure 4.24c. Threaded rod time-displacement curves started 0.7 mm after initial loading.

Figure 4.25. Time-displacement behavior for 16 thread per inch piles embedded in frozen sand.

Figure 4.26. Time-displacement behavior for 72 thread per inch piles embedded in frozen sand.

Figure 4.27. Time-displacement behavior of a 72 thread per inch pile embedded in polycrystalline ice and sand.

Figure 4.28. Time-displacement behavior for a 24 thread per inch pile embedded in polycrystalline ice.

Figure 4.29. Time-displacement behavior for a 24 thread per inch pile embedded in polycrystalline ice. (a) Static load increase of 52%.

Figure 4.29b. Static load increase of 27%.

Figure 4.30. Enlarged time-displacement behavior for a 24 threaded per inch pile (Test #64) in polycrystalline ice showing a displacement rate increase from a cyclic load.

Figure 4.31. Time-displacement behavior for a 24 thread per inch pile (Test #86) in loose frozen sand with periods of superimposed cyclic loads.

Figure 4.32. Enlarged due to a superimposed cyclic load. (a) Time-displacement behavior after 0.65 mm displacement.

Figure 4.32b. Time-displacement behavior after 0.95 mm Displacement.

Figure 5.1. Piles with different lug sizes approach steady state (b=1) at various rates.

Figure 5.2 Idealized comparison of compaction ahead of pile lugs having different lug heights.

Figure 5.3. Comparison between penetration tip and pile lug. (a) Cavity expansion model (after Ladanyi, 1976). (b) Region of increased pressure around pile lug.

Figure 5.4. Difference in creep equation proof load results from difference in pile lug size.

Figure 5.5. Difference in creep equation proof load shown for lugged pile with different embedments along their straight shaft portions.

Figure 5.6. Comparison of straight-shaft pile behaviors at various constant displacement rates.

Figure 5.7. Best fit lines are shown to generalize peak capacity and residual capacity of straight-shaft piles (data from Figure 5.6).

Figure 5.8. Creep parameter n increases with decreasing lug size.

Figure 5.9. Load capacity of lugged model piles based on step-load test.

Figure 5.10. Dynamic loading effect on displacement rates (normalized) versus frequency.

Figure 5.11. Displacement rate ratio versus displacement rate before dynamic ($\pm$) and static (+) loadings.

Figure 5.12. Displacement rate increases due to short duration load increases, static and dynamic.

Figure 5.13. Relationship between displacement limit and displacement at failure.

Figure 5.14. Comparison of thread spacing to pile displacement at failure.

Figure 5.15. Displacement-time curve for concrete pile in frozen soil (Parameswaren 1982).

Figure 5.16. Pile test results-Shaw Creek site (Luscher et al. 1983).

Figure A.1. Time-displacement curves for model steel piles in frozen sand at -3 deg C with 3.18 mm lug heights and 19.0 mm (average) displacement limits.

Figure A.2. Time-displacement curves for model piles in frozen sand at -3 deg C with 3.18 mm lug heights, 19.0 mm displacement limits. (a) 0 mm C-type plot starting points.

Figure A.2b. 1 mm C-type plot starting points.

Figure A.2c. 3 mm C-Type plot starting points.

Figure A.3. Time-displacement curves for model steel piles in frozen sand at -3 deg C with 3.18 mm lug heights and 76 mm (average) displacement limits.

Figure A.4. Time-displacement curves for model piles in frozen sand at -3 deg C with 3.18 mm lug heights, 76 mm displacement limits. (a) 0 mm C-type plot starting points.

Figure A.4b. 1 mm C-type plot starting points.

Figure A.4c. 3 mm C-Type plot starting points.

Figure A.4d. 5 mm C-Type plot starting points.

Figure A.5. Time-displacement curves for model steel piles in frozen sand at -3 deg C with 1.59 mm lug heights and 25.4 mm (average) displacement limits.

Figure A.6. Time-displacement curves for model piles in frozen sand at -3 deg C with 1.59 mm lug heights. (a) 0 mm C-type starting points and 25.4 mm displacement limits.

Figure A.6b. 1 mm C-type starting points and 25.4 mm displacement limits.

Figure A.6c. 3 mm C-type starting points and 25.4 mm displacement limits.

Figure A.6d. 6 mm C-type starting points and 25.4 mm displacement limits.

Figure A.6e. 0 mm C-type starting points and 19.0 mm displacement limits.

Figure A.6f. 1 mm C-type starting points and 19.0 mm displacement limits.

Figure A.6g. 3 mm C-type starting points and 19.0 mm displacement limits.

Figure A.7. Time-displacement curves for model steel piles in frozen sand at -3 deg C with 1.59 mm lug heights and 76 mm (average) displacement limits.

Figure A.8. Time-displacement curves for model piles in frozen sand at -3 deg C with 1.59 mm lug heights, 76 mm displacement limits. (a) 0 mm C-type plot starting points.

Figure A.8b. 1 mm C-type plot starting points.

Figure A.8c. 3 mm C-Type plot starting points.

Figure A.8d. 5 mm C-Type plot starting points.

Figure A.9. Time-displacement curves for model steel piles in frozen sand at -3 deg C with 0.79 mm lug heights and 24.1 mm (average) displacement limits.

Figure A.10. Time-displacement curves for model piles in frozen sand at -3 deg C with 0.79 mm lug heights, 24.1 mm displacement limits. (a) 0 mm C-type plot starting points.

Figure A.10b. 1 mm C-type plot starting points.

Figure A.10c. 3 mm C-Type plot starting points.

Figure A.10d. 6 mm C-Type plot starting points.

Figure A.10e. 12 mm C-Type plot starting points.

Figure A.11. Time-displacement curves for model piles in frozen sand (0.74 to 0.84 mm grain size) at -3 deg C with 0.79 mm lug heights and 76 mm (avg.) displacement limits.

Figure A.12. Time-displacement curves for model piles in frozen sand at -3 deg C with 0.79 mm lug heights, 76 mm displacement limits. (a) 0 mm C-type plot starting points.

Figure A.12b. 1 mm C-type plot starting points.

Figure A.12c. 3 mm C-Type plot starting points.

Figure A.12d. 6 mm C-Type plot starting points.

Figure A.13. Time-displacement curves for model steel piles in frozen sand at -3 deg C with 0.79 mm lug heights and 76 mm (average) displacement limits.

Figure A.14. Time-displacement curves for model steel piles in frozen sand (0.74 to 0.84 mm) at -2 deg C with 0.79 mm lug heights and 76 mm (average) displacement limits.

Figure A.15. Time-displacement curves for model piles in frozen sand at -2 deg C with 0.79 mm lug heights, 76 mm displacement limits. (a) 0 mm C-type plot starting points.

Figure A.15b. 1 mm C-type plot starting points.

Figure A.15c. 3 mm C-Type plot starting points.

Figure A.15d. 6 mm C-Type plot starting points.

Figure B.1. Pile Test #20.

Figure B.2. Pile Test #22.

Figure B.3. Pile Test #23.

Figure B.4. Pile Test #24.

Figure B.5. Pile Test #25.

Figure B.6. Pile Test #26.

Figure B.7. Pile Test #27.

Figure B.8. Pile Test #28.

Figure B.9. Pile Test #30.

Figure B.10. Pile Test #31.

Figure B.11. Pile Test #32.

Figure B.12. Pile Test #34.

Figure B.13. Pile Test #38.

Figure B.14. Pile Test #39.

Figure B.15. Pile Test #40.

Figure B.16. Pile Test #41.

Figure B.17. Pile Test #42.

Figure B.18. Pile Test #43.

Figure B.19. Pile Test #44.

Figure B.20. Pile Test #45.

Figure B.21. Pile Test #46.

Figure B.22. Pile Test #48.

Figure B.23. Pile Test #49.

Figure B.24. Pile Test #52.

Figure B.25. Pile Test #54.

Figure B.26. Pile Test #61.

Figure B.27. Pile Test #62.

Figure B.28. Pile Test #65.

Figure B.29. Pile Test #67.

Figure B.30. Pile Test #69.

Figure B.31. Pile Test #70.

Figure B.32. Pile Test #71.

Figure B.33. Pile Test #73.

Figure B.34. Pile Test #74.

Figure B.35. Pile Test #75.

Figure B.36. Pile Test #76.

Figure B.37. Pile Test #78.

Figure B.38. Pile Test #79.

Figure B.39. Pile Test #80.

Figure B.40. Pile Test #81.

Figure B.41. Pile Test #82.

Figure B.42. Pile Test #85.

Figure B.43. Pile Test #88.

LIST OF SYMBOLS

A, actual area

a, pile radius

A_F, area of shear plane

b, a creep parameter

c, material dependent constants

c, system damping coefficient

c_{lt}, long term cohesion

D, damping ratio of a soil

$E_o(T)$, a fictitious Young's modulus at a constant temperature, T

F, a function

f, a function of the type of materials and the conditions at the pile/frozen soil interface

$f(\theta)$, a function of temperature

G, shear modulus

G^*, complex shear modulus

G, a function

k, system spring coefficient

k, material dependent constants

L, length of pile

L_o, initial length

M, dynamic magnification factor

m, a constant based on the pile's surface roughness

N, normal pressure between soil and pile

n, a creep parameter

P, constant pile load

P_c, pile proof load

P_c', adjusted pile proof load

P_E, pile end bearing

p_i, pressure induced by soil expansion

p_o, initial earth pressure

$\bar{p}_o$, hydrostatic pressure

P_s, pile capacity

Q, pile capacity due to cylinder expansion

R', universal gas constant

r, distance from pile's center

r_i, expanded cavity radius

r_{io}, initial cavity radius

$\dot{s}$, a constant displacement rate

s_i, a fictitious instantaneous displacement

s(t), total displacement in terms of time

T, temperature

t, time

t_f, time to failure

t_F, time at start of tertiary creep

t_o, material and temperature dependant constant which correspond to short term tests at a given temperature and stress level

TR, transmissibility of applied force

$\tan\zeta$, friction coefficient alonf pile surface

U, apparent activation energy

$\dot{u}$, velocity of a soil element at distance r

u_a, pile displacement

V_s the volume displaced by punch penetration
(if penetration, less than the punch radius)

V_i the volume of the expanded cavity

V_{io}, initial cavity volume

u_i, displacement of the cavity in the radial direction

α, slope of tapered pile surface from pile axis

β, ratio of applied load frequency to natural frequency of system

$\dot{\gamma}$, shear distortion rate

δ, pile displacement

$\dot{\delta}$, pile displacement rate

$\dot{\delta}_c$, arbitrary (reference) pile displacement rate

$\dot{\epsilon}$, axial strain rate

θ = absolute value of temperature

θ_c, (arbitrarily) 1 deg C

ξ, damping ratio

σ, true stress

σ, lateral stress on the pile

σ_C, uniaxial compressive strength for frozen soils

σ_c, temperature-dependant proof stress

σ_{co}, proof stress at 0 deg C

σ_{cuo}, creep proof stress at a temperature close to
the freezing point

$\sigma_{cu\theta}$, a temperature-dependant creep proof stress

$\sigma_{c\theta}$, proof stress at temperature T

σ_E, pressure at the pile base

σ_e, effective stress

σ_f, long term allowable stress

σ_i, initial instantaneous stress

$\sigma_k(T)$, temperature dependant proof stress

σ_m, mean stress

σ_o, material and temperature dependant constant which correspond to short term tests at a given temperature and stress level

σ_r, radial stress

σ_{re}, radial stress at radius r_e

σ_T, uniaxial tensile strength for frozen soils

σ_t, circumferential stress

σ_1, σ_3, correspond to axial and confining pressures in the triaxial cell

τ, shear force between unfrozen soil and the pile

τ, shear stress at a distance

τ_a, long term adfreeze strength between pile and frozen soils

τ_F, stress along shear plane at failure

τ_{lt}, long term shear strength

ϕ_{lt}, friction angle of the Mohr envelope for this frozen soil

ϕ, friction angle of the Mohr failure envelope for this soil

ω, temperature-dependant exponent

ω, natural frequency of system

$\dot{\varepsilon}^{(c)}$, creep strain rate

ε, true strain

ε^i, instantaneous strain

$\dot{\varepsilon}_c$, an arbitrary creep strain rate

$\varepsilon^{(c)}$, creep strain

$\dot{\varepsilon}_e$, equivalent strain rate

ε_e, effective strain

ε^{ie}, instantaneous elastic strain

ε^{ip}, instantaneous plastic strain

ε_k, an arbitrary small strain (for calculation purposes)

INTRODUCTION

1.1. Frozen Soil Pile Foundations

In permafrost regions, pile foundations can be used advantageously for several reasons (Linell and Lobacz, 1980). They allow the structure to be raised above ground level so that an air space remains below the floor. This isolates the building from the annual frost heave and thaw subsidence of the uppermost ground layer. The air space insulates permafrost from heated buildings and helps maintain the frozen ground temperature. Because strength of permafrost is temperature-dependent, a foundation pile's load capacity will be higher for colder permafrost. Piles transfer loads deep into the ground to higher strength permafrost layers which are less susceptible to ground surface temperature fluctuations. When local building materials are scarce, piles can be the most economical way to provide stable foundations.

Pile installation in permafrost generally depends on the type and temperature of frozen soil encountered (Heydinger, 1987). Piles may be driven, as in unfrozen soils, into fine-grained relatively-warm permafrost. In harder permafrost, oversize holes may be drilled or augered so that the pile can be set in and eventually frozen into a slurry of natural soil, sand, or silt. A combination of these two methods (Manikian, 1983) involves drilling an

undersize hole before driving a steel pile. Warm water is sometimes added to an undersize hole to lower driving resistance.

Reinforced concrete, steel, and timber are commonly used for foundation piles placed in permafrost (Linell and Lobacz, 1980). In some areas timber is more readily available, can be relatively inexpensive, has versatile lengths (up to 70 feet), and (if properly preserved) is long lasting. Steel H sections and pipe piles are often chosen because of their high load capacity, suitability to driving, and resistance to weathering if protected. Concrete piles have many of a steel pile's good points but are less acceptable because of their weakness to tension forces that may develop during annual freezing at the ground surface. Cast-in-place concrete piles are even less acceptable because cement hydration adds heat to the permafrost and because the concrete may freeze and weaken before complete curing has occured.

The time dependance of frozen soil stress-strain relationships leads to one of the major problems with piles in permafrost. Prediction of long-term load capacity and settlement must, by necessity, be based on short-term testing. Extrapolation of short-term pile data to a long-term load capacity prediction is complicated by many factors, including soil temperature, soil type, pile type, soil/pile adhesion, and pile installation method. Some

examples of these complicating factors include:

a) Seasonal soil temperature changes due to climatic changes (Lachenbruch, 1988) and/or physical ground surface changes (Brown et al, 1969) which adversely effect pile load capacity (Figure 1.1).

b) Ice formed in frozen soils, often randomly, during deposition and/or freezing can greatly effect pile settlement and load capacity (Nixon and McRoberts, 1976)

c) Salts or other contaminants in the frozen pore water may not be obvious without testing, yet may significantly reduce a pile's load capacity (Nixon, 1987).

d) Pile geometry has been shown (Ladanyi and Guichoua, 1985) to have a large effect on pile capacity and allowable settlement.

e) Pile/soil adhesion varies with the pile material and soil type (Linell and Lobacz, 1980).

f) Piles embedded in frozen slurries have the highest pile/soil adhesion values (Linell and Lobacz 1980).

g) Pile testing for load capacity must wait until the slurry has frozen and any excessive lateral pressures induced by freezing have returned to equilibrium values (Neukirchner, 1988).

Due to the high cost of full-scale pile testing, many of the problems associated with piles and other foundations

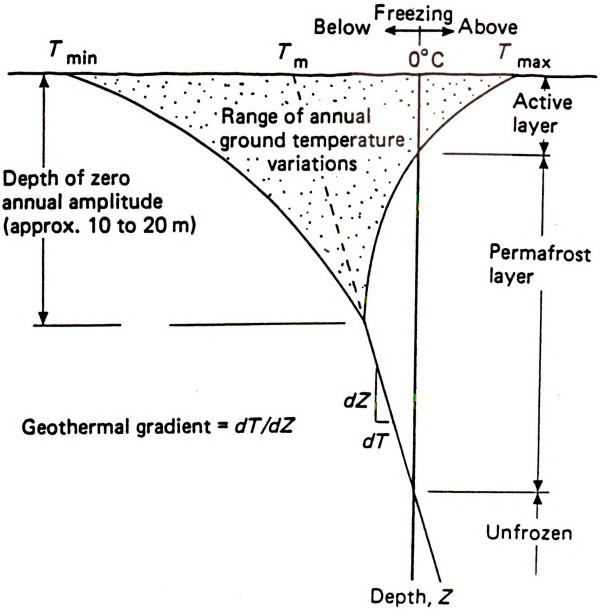

Figure 1.1. Temperature profile in the ground, permafrost area (from Andersland, 1987).

have been investigated in a controlled laboratory environment using frozen soil samples or models. Once the problem has been thoughly studied in the laboratory (and warrents further consideration) full-scale field tests may be conducted more economically.

1.2. Cyclic Pile Loading: Research Problem and Objectives

Piles supporting structures in permafrost areas will settle under imposed loads over a period of years. Load capacity is normally calculated on the basis of adfreeze bond at the pile/frozen soil interface. This adfreeze bond is determined from long- and short-term creep tests under static loads. In field situations, a cyclic load is often superimposed on the static load. These cyclic loads may include vibrating machinery (turbines, power generators, and compressors) or travelling loads (cranes, fork lift trucks, ect). Shock and transient vibrations are also caused by forges and pile drivers. Field observations have shown that the steady-state pile settlement rates (creep) in frozen soils are enhanced by the superimposed cyclic loads. Larger settlement rates can reduce the service life of existing piles or create a need, during design stages, for more piles. This laboratory research project was initiated to quantify these displacement rate increases and identify contributing factors.

Pile settlement in frozen ground is typically

predicted on the basis of a creep equation relating shear stresses at the soil/pile interface to pile displacement rates. Creep parameters are used to characterize soil type, soil/ice structure, temperature, and loading conditions. This study used model steel piles in a laboratory setting to carefully change and control test variables in order to increase our understanding of the processes responsible for pile settlement. Variables included cyclic load amplitude, frequency of load application, static load magnitude, and temperature. Sand density and ice volume fraction were controlled during sample preparation.

Load capacity of friction piles in frozen ground is known to increase significantly when the pile surface is roughened by the addition of protrusions or lugs. A series of model steel piles with controlled surface geometries (lug size, shape, and spacing) were frozen in sand and loaded to provide information on the displacement mechanisms operating at the pile/frozen soil interface. Criteria were sought which would help define the pile surface roughness geometry that most effectively controls pile settlement and increases pile capacity. Details are presented in subsquent chapters.

LITERATURE REVIEW

2.1. Mechanical Properties of Frozen Soils

Frozen soil is a complex mixture of mineral and/or organic particles, unfrozen water, polycrystalline ice, and air (Vyalov, 1965). The strength of a frozen granular soil results from ice strength, soil strength (interparticle friction, dilatency, and particle interlocking), and soil/ice interaction when subjected to a given strain rate at a specified temperature and stress state (Ting et al., 1983). Ice is responsible for creep, the time-dependant deformation of a frozen soil under sustained loading. For long-term loads creep deformation is important to engineering design and prediction of its magnitude and rate (with respect to stress, stress history, temperature, and soil composition) becomes necessary.

2.1.1. Effect of Frozen Soil Composition on Behavior

Weaver (1979) classified frozen soil into four significant catagories: dirty ice (0.9-1.0 Mg/m^3), very dirty ice (1.0-1.7 Mg/m^3), ice-poor frozen soil (1.7-2.0 Mg/m^3), and ice-rich frozen soil containing inclusions of ice. Ladanyi (1981) added the category of unsaturated frozen soil to these frozen soil types.

The behavior of a frozen sand is described in Figure 2.1. Starting with the peak uniaxial strength of ice, ice

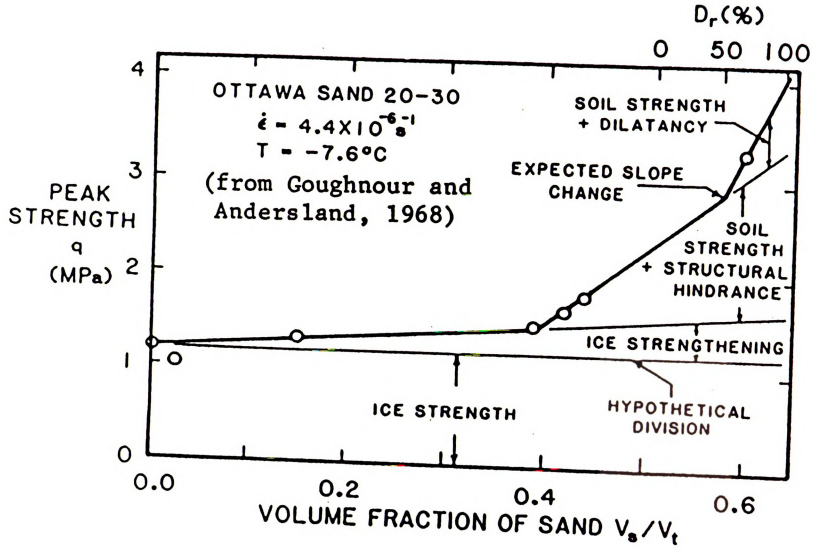

Figure 2.1. Frozen sand strength mechanisms (after Ting et al., 1983).

strength is shown to slowly increase due to an ice strengthing effect of the scattered sand grains. Kaplar (1971) and Goughnour and Andersland (1968) stated that particle contact was established at 40% and 42% sand volume, respectively. Peak strength can be seen to sharply increase above these sand volume fractions. The soil grains, when unfrozen, will develop strength from friction, dilatency, and particle interference, all of which are dependant on confining pressure and void ratio (Ting et al., 1983). The ice is thought to stabilize the soil skeleton (structural hinderence in Figure 2.1) due to strong ice to unfrozen-water film to sand-grain bonds between sand particles. At relative densities greater than 50%, ice/sand adhesion is thought to enhance dilatency effects and increase peak strength.

The behavior of ice-rich sand is dependant on the amount of ice and its orientation to soil stresses. For conservative design, some authors (Nixon and McRoberts, 1976) consider ice-rich soils to have only the strength of ice. Kaplar (1971), Alkire (1972), and Baker (1979) have shown that strength decreases rapidly when ice saturation, within frozen soils, is decreased.

The size of soil grains will also effect strength by altering how water is frozen within the soil. Water molecules bond to the surface of clay particles and remain unfrozen at normal freezing temperatures (Dillon and

Andersland, 1966; Anderson and Tice, 1972). The nature of some clays will prevent freezing of significant amounts of water down to -30 deg C. (Tsytovich, 1960). Scott (1969) reports little unfrozen water in sand at any temperature below freezing. Capillary flow in some silts can cause ice lenses to form (Anderson et al., 1978) parallel to the freezing front.

Salt dissolved in pore water of a clay will reduce frozen soil strength at a given temperature by increasing unfrozen water contents (Nixon and Lem, 1984). Ruedrich and Perkins (1974) showed that the maximum uniaxial strength of a sand was reduced by the addition of salt to pore water. Alwahab (1983) observed a significant reduction in model pile load capacities when pore water of frozen sand was changed from distilled water to relatively hard tap water.

2.1.2. Frozen Soil Creep Strength

Tsytovich (1975) described the process of creep in frozen soils. When stress is applied to a frozen soil, ice will melt at pressure points within the soil mass. The melt water will then move to locations of lower (confining) pressure and refreeze. Soil grains encountering less resistance will deform and/or break bonds within the remaining ice matrix and rearrange themselves in a generally denser configuration. Breaking the cohesive bond

tends to weaken a soil while particle rearrangement tends to strenghten the soil due to better particle interlock. If the strengthing process dominates, the deformation rate will continue to slow down and may never reach a constant deformation rate. If the weakening process dominates, the deformation rate will reach a minimum value then increase. Failure is often considered to start when the rate increases. The rate will increase until rupture or when the soil has little or no resistance to stress.

Creep within the ice matrix requires consideration of the applied stress, time to failure, minimum creep rate, temperature, and deformation at failure. In order to quantify the strength of a frozen soil, a series of triaxial tests are generally used to define the friction angle, ϕ and the time-and-temperature dependent cohesion, $c(t,\theta)$ (Andersland et al., 1978). Ladanyi (1972) notes that constant-temperature compression-creep tests (Vyalov, 1962; Sayles and Epanchin, 1966) determined that the onset of failure will occur at similar magnitudes of strain. For frozen fine-grained soils (Andersland et al., 1978), large strains can develop during secondary creep and failure is assumed to occur at a strain of 20% (design consideration may limit failure to a lower strain).

In general, longer load durations correspond to lower allowable stresses. Vyalov (1959) described long term frozen soil strength by

$$\sigma_f = \frac{\sigma_o}{\ln (t_f + t^*) - \ln (t_o)} \qquad (2.1)$$

where

$$t^* = t_o \exp(\sigma_o / \sigma_i) \qquad (2.2)$$

and σ_f is the long term strength, σ_i is the initial instantaneous strength, t_f is the time to failure, and the material and temperature dependant constants are represented by σ_o and t_o. Vyalov (1963) said that t^* could be neglected for long term strengths. Sayles (1973) found, for practical load durations, that the long term allowable stress for triaxial tests of frozen Ottawa sand approached a minimum level, thus

$$\sigma_f \approx (\sigma_1 - \sigma_3) \approx \frac{\sigma_o}{\ln (t_f / t_o)} \qquad (2.3)$$

where σ_1 and σ_3 correspond to axial and confining pressures in the triaxial cell and the parameters σ_o, t_o correspond to short term tests at a given temperature and stress level.

As mentioned before, at a sand concentration close to 40% and greater, frozen sand begins to develop strength from the ice matrix, interparticle friction, and dilatency. In Figure 2.2(a), Sayles (1973) explained that the ice matrix is relatively stiff and provides its peak strength at about 1 % strain while friction and dilatency develop more slowly and provide a second peak at about 10% strain.

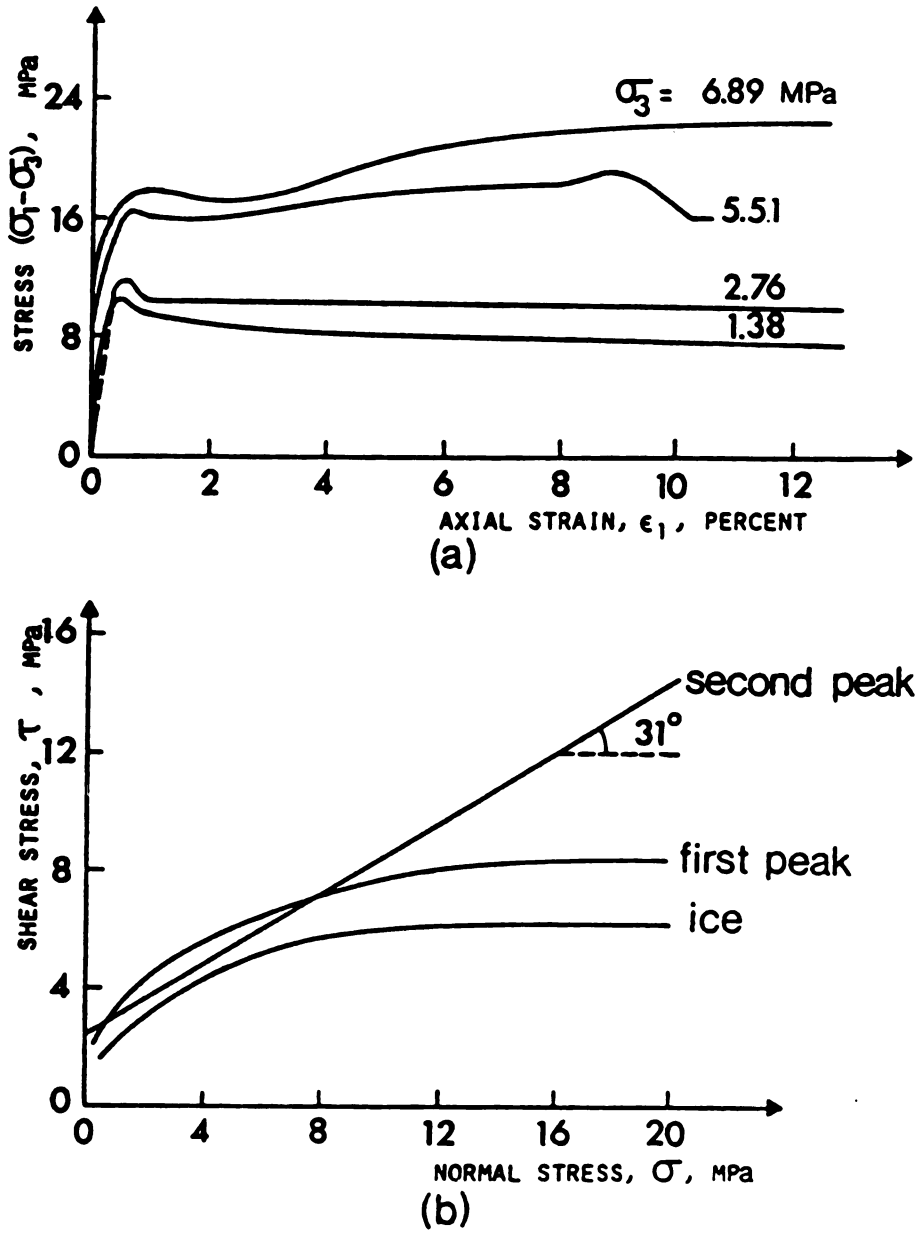

Figure 2.2. Compression tests with frozen Ottawa Sand (after Sayles, 1973). (a) Stress-Strain Curves; (b) Mohr Envelopes.

The stress conditions at the first peaks of these tests are plotted as a Mohr envelope in Figure 2.2(b) and labeled "first peak". This is similar to the Mohr envelope developed from tests of ice samples. After the first peak, friction and dilatency continue to slowly develop and produce a second peak in Figure 2.2(a) at the higher confining pressures of 6.89 MPa and 5.51 MPa. The stress conditions at 8.9% axial strain for the 5.51 MPa test and at 10% for the other triaxial confining tests are plotted as a Mohr envelope and labeled "second peak" in Figure 2.2(b). This is shown at an angle of 31 deg from the horizontal and is (approximately) the friction angle for this sand when tested unfrozen.

Ladanyi (1981) used information from Sayles (1973) and Chamberlain, et al. (1972) to produce Figure 2.3. The strength of ice dominates region A and peak strengths were determined at about 1% strain. Region B represents peak stress conditions found near 1% strain and at approximately 10% strain (where dilatency and friction added strength to the frozen sand). In region C, confining pressure partly melted the ice matrix and its contribution to strength was reduced. The high confining pressures of region D crushed sand grains and melted the pore ice so that the resulting behavior is similar to unfrozen sand under undrained conditions. Ladanyi (1981) notes that most permafrost stress conditions would fall into regions A and B at

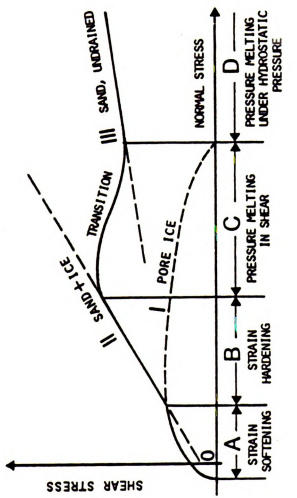

Figure 2.3. Schematic representation of the failure envelope for frozen Ottawa Sand (after Ladanyi, 1981).

confining pressures below 55 MPa.

Sayles (1973) also showed Mohr envelopes for creep strength from triaxial creep tests at various times to failure (Figure 2.4). The envelope for the longest time (to failure) can be seen at 29 deg from horizontal, which is close to the apparent angle of internal friction (30 deg) of the same sand when unfrozen. Andersland and AlNouri (1970) showed that the apparent angle of internal friction was similar for frozen and unfrozen sands and also showed this angle to be close to zero for frozen clays.

The ratio of σ_C/σ_T (uniaxial compressive strength/tensile strength) for frozen soils is usually lower than 5 (Ladanyi, 1981) which contrasts with the value of $\sigma_C/\sigma_T = 8$ for an ideal elastic-brittle material (Griffith, 1924). At higher temperatures (Ladanyi, 1981) or at slower strain rates (Haynes et al., 1975), σ_C/σ_T approaches unity and shows plastic behavior. Bragg and Andersland (1980) showed, in Figure 2.5, an abrupt change from a plastic behavior (with a failure strain greater than 4%) at strain rates less than 0.00025/sec. to a more brittle behavior (with a failure strain less than 1%) at strain rates greater than 0.00025/sec.

In Figure 2.6, a break in the -2 deg C curve at the strain rate of 0.00001/sec is thought to be associated with pressure melting at sand grain contacts. If refreezing did not occur immediately after melting, the unfrozen water

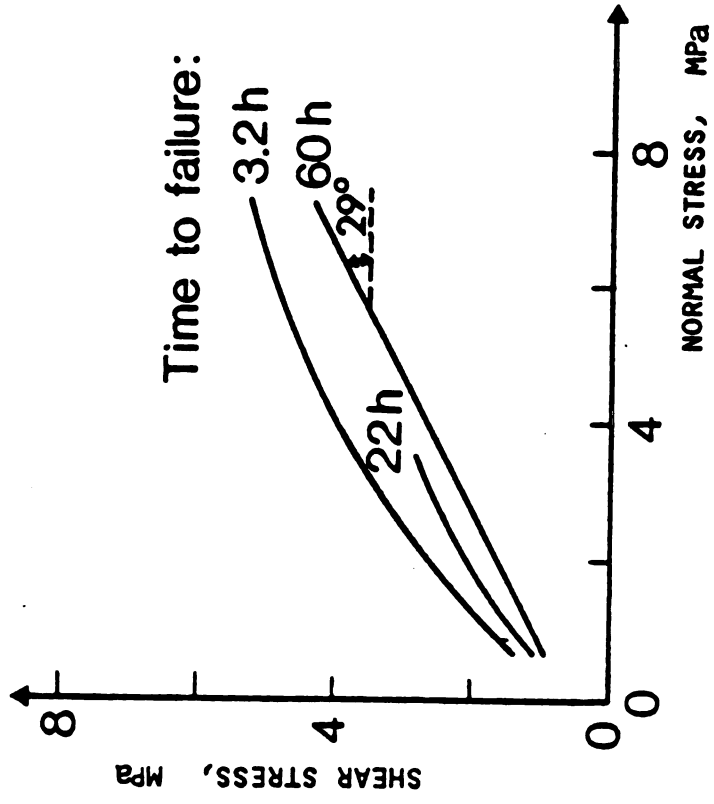

Figure 2.4. Mohr envelopes for creep strength of Ottawa Sand (T = -3.85 deg C) (after Ladanyi, 1981).

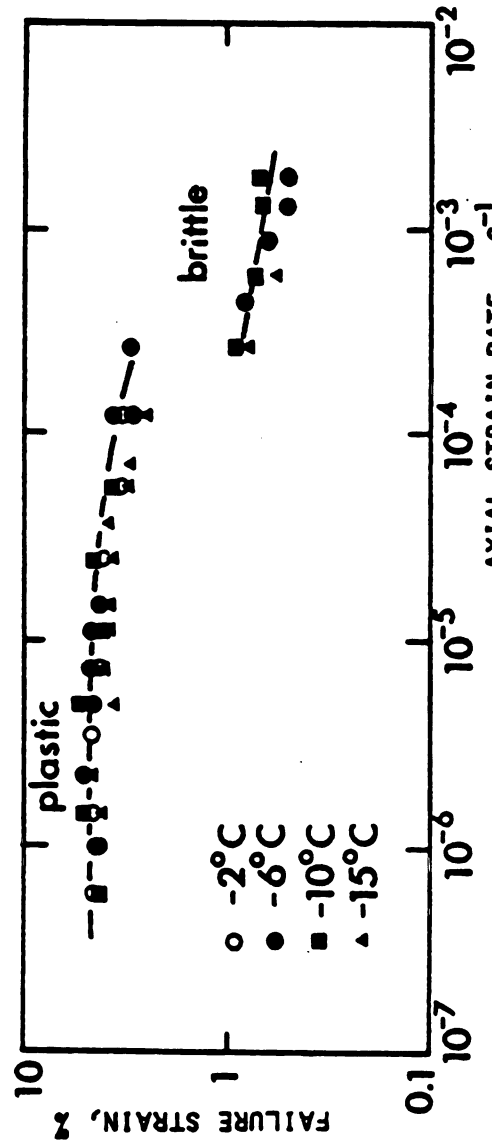

Figure 2.5. Failure strain versus strain-rate for a frozen sand (after Ladanyi, 1981).

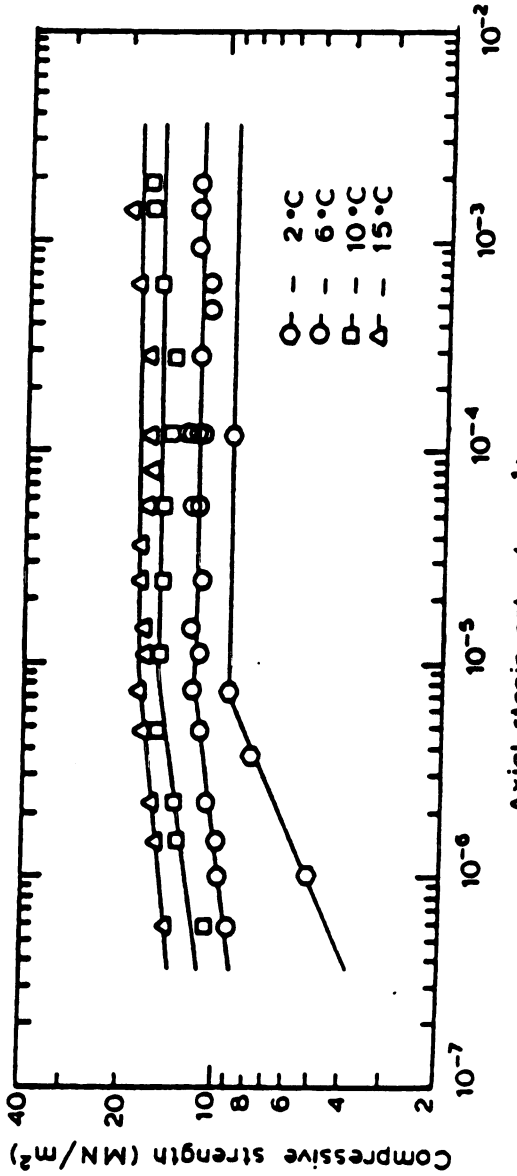

Figure 2.6. Compressive strength vs. strain rate (after Bragg and Andersland, 1980).

content could be increased and thereby decrease the strength of the sample. This strength decrease could alter the stress versus strain-rate curve. Samples tested at strain rates higher than 0.00001/sec may fracture some bonds in the ice matrix of frozen soils (Ladanyi, 1981).

2.1.3. Temperature Dependence of Frozen Soil Strength

The basic relationship of (increased) frozen soil strength with (decreased) temperature is shown in Figure 2.7 from Sayles (1966). The theory of rate process has been used to describe chemical processes (Glasstone et al, 1941) and deformation of unfrozen soils (Mitchell et al, 1968). It has also been used by other investigators (Andersland and Akili, 1967; Goughnour and Andersland, 1968; Andersland and ANouri, 1970; Andersland and Douglas, 1970) to describe the temperature-dependant behavior of frozen soils. According to this theory, deformation occurs when energy (thermal or mechanical) is added to "flow units" (of molecular size within the considered solid) so that the energy barriers preventing relative movement between these flow units are overcome. Andersland and Alnouri (1970) expressed creep rate $\dot{\varepsilon}^{(c)}$ as

$$\dot{\varepsilon}^{(c)} = A \exp[(-U / R') / (T)] \qquad (2.4)$$

where R′ is the universal gas constant, T is absolute temperature, and U is apparent activation energy. Ladanyi

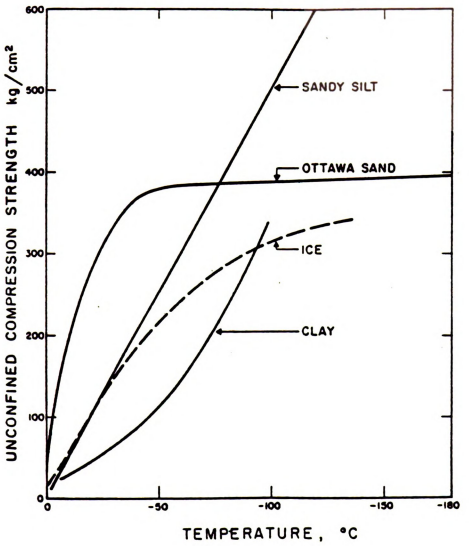

Figure 2.7. Temperature dependence of uniaxial compression strength for various frozen materials (after Ladanyi, 1972).

(1972) transformed this equation to

$$\sigma_{C\theta} = \sigma_{CO} \exp \left[\frac{(\theta)\ (-U / R')}{(273\ n)\ (273 - \theta)}\right] \qquad (2.5)$$

with

$$\theta = 273 - T \qquad (2.6)$$

where σ_{CO} is the proof stress at 0 deg C and $\sigma_{C\theta}$ is the proof stress at temperature T.

There has been disagreement over the usefulness of the rate process theory. Hoeskstra (1969) stated that this theory shouldn't be used with substances that change phase with temperature as frozen clays do. Ladanyi (1972) pointed out that the activation energies obtained by plotting the natural logarithms of creep rates versus reciprocals of absolute temperature are very high (389 kJ/mol in one case) compared to the value of 84 kJ/mol found by Gold (1970) for polycrystalline ice. To explain this discrepency, Andersland and Douglas (1970) stated that the activation energy determined during frozen soil deformation may be effected by mechanical changes occuring in the soil. Recent research by Orth (1985) supports the rate process theory for frozen sands and also notes that nonunique activation energies for ice (80 kJ/mol at below -8 deg C and 120 kJ/mole at above -8 deg C) found by Frost and Ashby (1982) support his and earlier findings.

Ladanyi (1972, 1981, 1985) has stated that the most

convenient means of describing the temperature-dependent frozen soil strength, $\sigma_{c\theta}$ is by empirical relationships such as Vyalov's (1962) power law which was normalized by Assur (1963) and shown by Ladanyi (1972) as

$$\sigma_{c\theta} = \sigma_{co} [1 + (\theta / \theta_c)]^{\omega} \qquad (2.7)$$

where θ_c is (arbitrarily) 1 deg C and θ is defined by equation 2.6. Ladanyi (1972) states that $\omega = 1$ can be used to approximate change over limited temperature intervals.

2.1.4. Constitutive Equations for Frozen Soils

Some typical creep curves for frozen soils under uniaxial compression are shown in Figure 2.8. (Andersland et al., 1978) Figure 2.8(b) shows the three general stages of constant temperature deformation behavior for frozen soils and other materials that exibit creep. The first stage is primary creep where the deformation rate initially increases rapidly, then slowly decreases. The behavior of some silts and sands do not leave this stage except when subjected to high stresses and/or high temperatures. The second stage is characterized by a constant deformation rate. Ice and ice-rich soils may have an extended period of secondary creep. The third stage of creep is indicated by an increasing deformation rate which leads to failure of the sample. Figure 2.8(c) shows that the second stage of creep contains the minimum deformation rate.

Because of the large strains obtained for creep tests

Figure 2.8. Constant-stress creep tests
(after Andersland, et al. 1978).
(a) Creep curve variations.
(b) Basic creep curve
(c) True strain rate versus time.

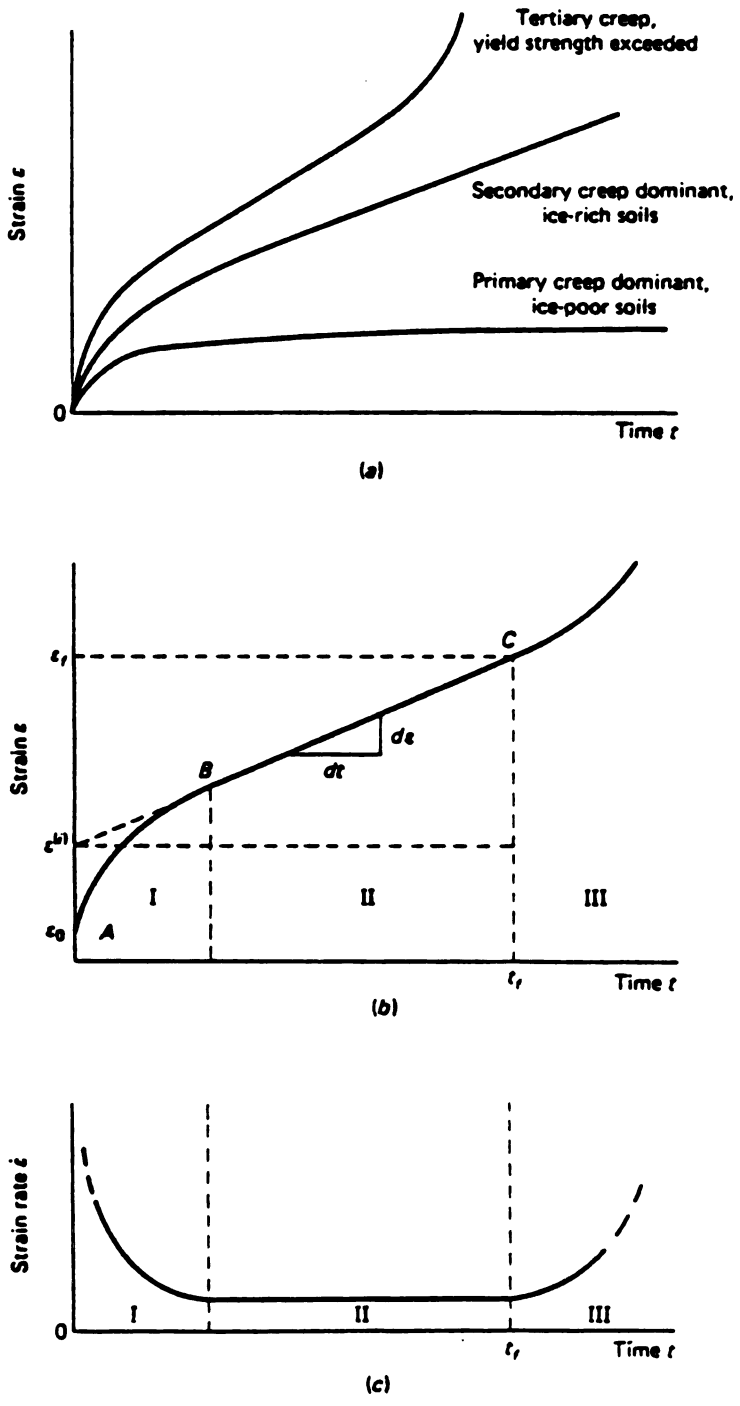
Tertiary creep,
yield strength exceeded
Secondary creep dominant,
ice-rich soils
Primary creep dominant,
ice-poor soils
Strain ε
0
Time t
(a)
C
ε_f
dε
dt
B
$\varepsilon_{(1)}$
I
II
III
ε_0
A
t_f
Time t
(b)
Strain rate $\dot{\varepsilon}$
0
I
II
III
t_f
Time t
(c)

Figure 2.8.

on frozen soils, true stress, σ is used as

$$\sigma = P / A \tag{2.8}$$

where A is the actual area and P is the constant load. True strain, ε can be shown as

$$\varepsilon = \ln (L / L_o) \tag{2.9}$$

Primary creep has been described by Hult (1966) as having an instantaneous strain, ε^i and a creep strain $\varepsilon^{(c)}$. The instantaneous strain contains an elastic portion, ε^{ie}, and a plastic portion, ε^{ip}. The instantaneous plastic strain has been written (Marin et al., 1951; Ladanyi, 1972) as

$$\varepsilon^{ip} = \varepsilon_k \left[\frac{\sigma}{\sigma_k(T)}\right]^k \tag{2.10}$$

where ε_k is an arbitrary small strain (for calculation purposes), $\sigma_k(T)$ is the temperature dependant proof stress, and k is a constant which is somewhat dependant on temperature. The elastic instantaneous strain, ε^{ie} can be shown as

$$\varepsilon^{ie} = \frac{\sigma}{\varepsilon_o(T)} \tag{2.11}$$

where $E_o(T)$ is a fictitious Young's modulus at a constant temperature, T. It has been suggested by Hult that ε^{ip} may be neglected because it is relatively small. Vyalov (1959)

showed that the entire instantaneous creep strain may be neglected when loading exceeds one day because ε^{i} becomes relatively small (less than 10%) as compared to the creep strain, $\varepsilon^{(c)}$.

The primary creep strain $\varepsilon^{(c)}$ can be described by

$$\varepsilon^{(c)} = f(\sigma, t, T) \tag{2.12}$$

where σ is true stress, t is time, and T is temperature. Vyalov (1962) proposed an equation of the type that has been used by later researchers (Ladanyi and Johnston, 1974; Eckardt, 1982) for constant-temperature constant-stress conditions as

$$\varepsilon^{(c)} = \left[\frac{\dot{\varepsilon}_c}{b}\right]^{b} \left[\frac{\sigma}{\sigma_c}\right]^{n} t^{b} \tag{2.13}$$

where b and n are creep parameters, $\dot{\varepsilon}_c$ is an arbitrary strain rate, and σ_c is the temperature-dependant proof stress (determined by the choice of $\dot{\varepsilon}_c$). This equation can also represent secondary creep when b equals 1. Differentiation of this equation yields the creep rate,

$$\dot{\varepsilon}^{(c)} = \left[\frac{\dot{\varepsilon}_c}{b}\right]^{b} \left[\frac{\sigma}{\sigma_c}\right]^{n} b \; t^{b-1} \tag{2.14}$$

which may be used to form a ratio of two creep rates (with similar test conditions except load) as

$$\frac{\dot{\varepsilon}_2}{\dot{\varepsilon}_1} = \left[\frac{\sigma_2}{\sigma_1}\right]^n \qquad (2.15)$$

when b = 1 and/or $t_2 \approx t_1$.

Secondary creep may be described (Hult, 1966) by a method that approximates the accumulated total strain, as a combination of a fictitious instantaneous strain, $\varepsilon^{(i)}$

$$\varepsilon^{(i)} = F(\sigma, T) \qquad (2.16)$$

plus a period of constant creep rate,

$$\dot{\varepsilon}^{(c)} = G(\sigma, T) \qquad (2.17)$$

in a total strain equation form as

$$\varepsilon = \varepsilon^{(i)} + \dot{\varepsilon}^{(c)}\, t \qquad (2.18)$$

where t is total time, σ is a constant stress, and T is a constant temperature. A series of creep tests, with each test at a constant temperature and a constant stress level, can then be used to calculate functions F and G so that Equation 2.18 can approximate total strain of this material while it is in secondary creep. Ladanyi (1972) showed a summation procedure to obtain total strain when a frozen soil is loaded in steps and each step reaches secondary creep (Figure 2.9).

Vyalov (1962) described creep of ice-poor soils by

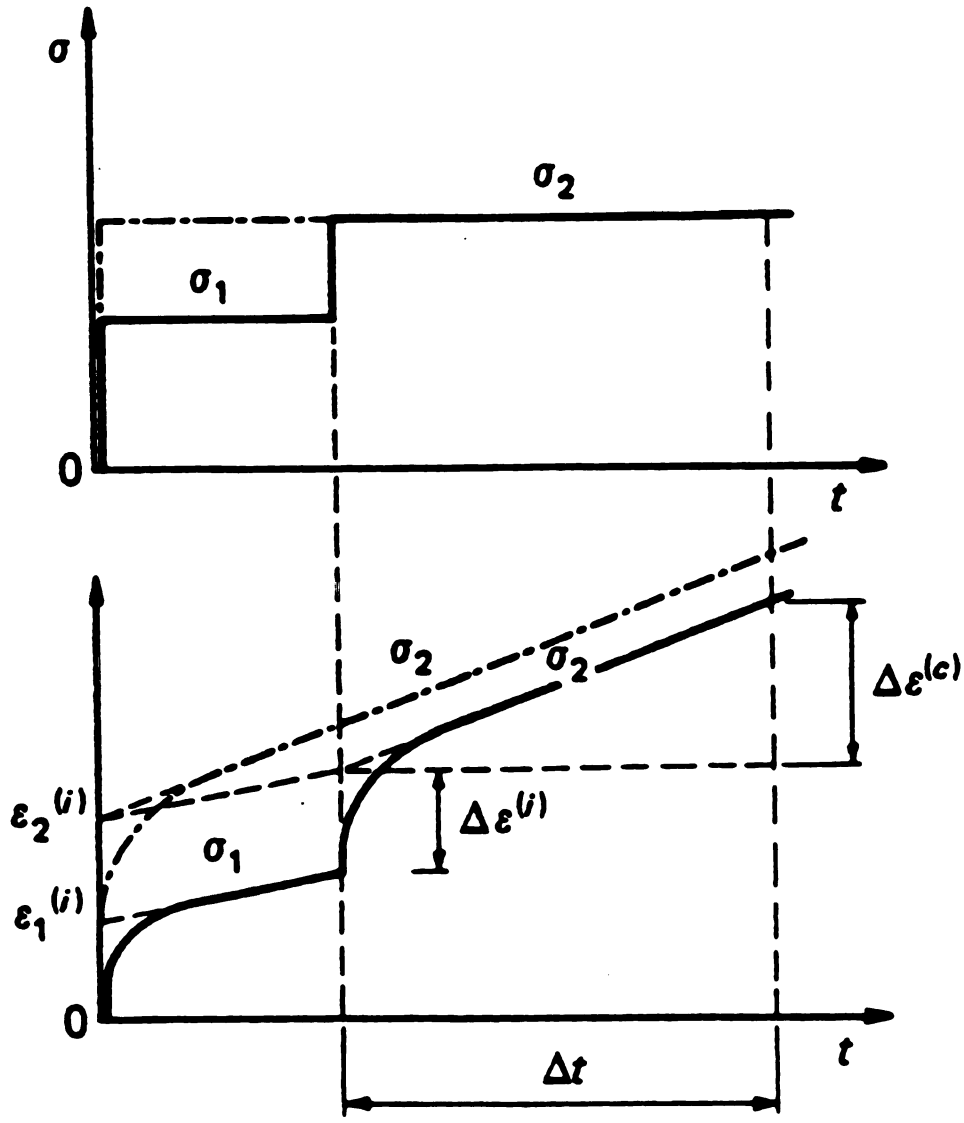

Figure 2.9. Creep curve for step loading (after Ladanyi, 1972).

$$\varepsilon = \left[\frac{1}{\omega\ (\sigma + 1)^{k}}\right]^{c} \quad \sigma^{c} \quad t^{b} \tag{2.19}$$

where ε is strain, σ is constant stress, t is time, θ is the number of degrees below freezing, and ω,k,c,b are material dependent constants. Ladanyi (1972) added the effect of confining stress to this equation so that

$$\varepsilon_1 = D\ [\ \sigma_1 - j(\sigma_3)\ ]^{c}\ t^{b} \tag{2.20}$$

with

$$j = \frac{(\ 1 + \sin\phi\ )}{(\ 1 - \sin\phi\ )} \tag{2.21}$$

and

$$D = \left[\frac{1}{\omega\ (\sigma + 1)^{k}}\right]^{c} \tag{2.22}$$

where ϕ is the friction angle of the Mohr failure envelope for this soil. Ladanyi and Johnston believed it reasonable to assume j = 1 when $\sigma_1 / j\sigma_3$ is less than 1.25 so that Equation 2.19 becomes

$$\varepsilon_1 = D\ (\sigma_1 - \sigma_3)^{c}\ t^{b} \tag{2.23}$$

for confined compression creep tests. Weaver and Morgenstern (1981b), interested in predicting pile settlement, reviewed existing uniaxial and triaxial compression tests to select the constitutive relationship that best fit data for ice-poor frozen soil creep behavior. An equation from Ladanyi (1972) for multiaxial stress

conditions was selected

$$\varepsilon_e = D \left\{ \left[\frac{j+2}{3}\right]\sigma_e + (1-j)\sigma_m \right\}^c t^b \qquad (2.24)$$

where ε_e is the effective strain, σ_e is the effective stress, and σ_m is the mean stress. When j = 1, this equation becomes

$$\varepsilon_e = D (\sigma_e)^c t^b \qquad (2.25)$$

2.1.5. Frozen Soil Strength Testing

Constant-strain-rate tests, relaxation tests, and creep tests are commonly performed on frozen soils to determine time dependent strength properties. During a constant-strain-rate test, the samples are strained at a constant rate and the resulting range of stresses are recorded. Scott (1969) states that this test avoids the problems of sudden loading found in the creep test and relaxation test. A relaxation test will load a sample quickly to a given strain then hold that strain while recording the resulting stress levels. Vyalov, et al. (1969) used this type of test to determine long term strengths of frozen soils. A creep test will load a sample quickly to a given stress then maintain this stress for the remainder of the test. Sometimes this test is altered by increasing the creep load incrementally after given periods of time.

Under similar conditions, similar values of $(\dot{\sigma}/\varepsilon)_{max}$

were found by constant-strain-rate tests and constant-stress creep tests (Mellor, 1979). Goughnour and Andersland (1968) have shown how data from constant-stress creep tests may be visualized as data from constant-strain-rate tests (and vice versa).

Some conditions of testing have been found to alter test results. Baker (1978a, 1978b) found that sample ends need to be carefully prepared. Andersland and AlNouri (1970) found temperature history to be important. Additional information on frozen soil test conditions can be found in Sayles, et al. (1987) which recommended standard testing methods.

2.2. Response of Frozen Ground to Dynamic Loading

The literature mentioned in this section includes topics on unfrozen soils due to the lack of frozen soil information in this subject area.

2.2.1. Dynamically Loaded Foundations in Unfrozen Soils

Richart et al. (1970) has shown methods which use measured or estimated dynamic stress-strain properties to estimate the response of shallow foundations on elastic half-spaces to dynamic loading. These methods include geometrical damping, the spreading of wave energy from a source on top of a half-space, but neglect the internal damping of the soil. Richart et al. (1970) noted that the

assumption of no internal or material damping, when the damping ratio, D, of a soil was less than 3% (as many unfrozen soils have), would alter the computed shear modulus, G by less than 6% from the complex shear modulus, G^*, computed with the influence of damping. Assuming soil to be elastic (no internal damping) made computation of a foundation's response to dynamic loading easier and nearly as accurate. Figure 2.10 shows damping ratios for frozen soils which are considerably higher than 3% for soil temperatures higher than -10 deg C. Use of elastic theory methods for dynamic response of frozen soils may produce unacceptable errors.

2.2.2. Stress-Strain and Energy Absorbing Properties

Frequency, amplitude, and load duration are important to solving dynamic loading problems (Vinson, 1978). Two common problems encountered in geotechnical engineering are: (1) high frequency, low amplitude, and sustained loading from vibrating machinery or (2) low frequency, higher amplitude, transient or irregular loading from explosions or earthquakes. The properties generally tested for are included in two groups: (1) dynamic stress-strain properties which include various wave types and velocities, Young's moduli, and shear moduli or (2) energy absorption properties which include various stress-strain, phase-lag, and damping measurements.

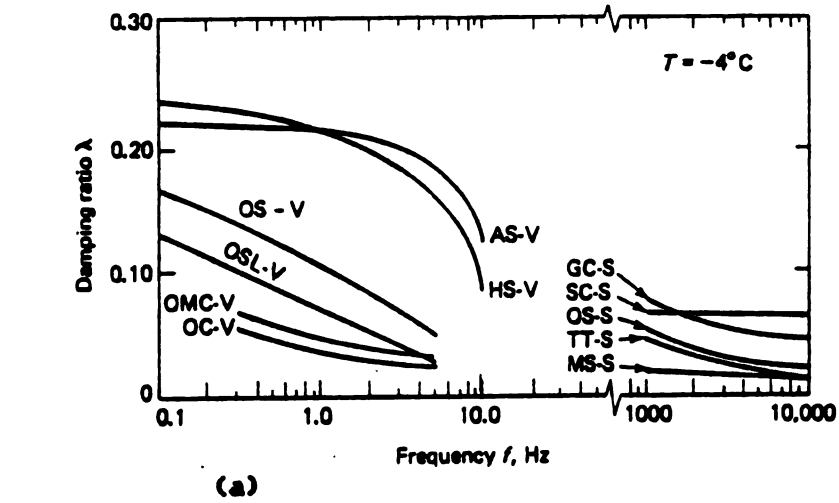

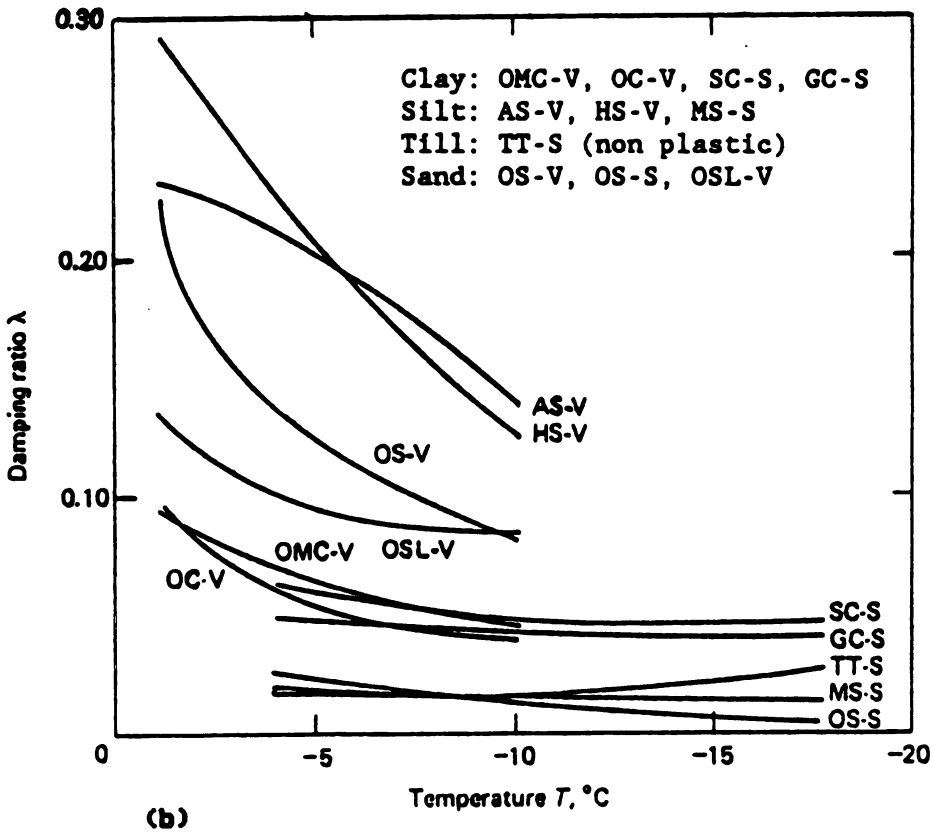

Figure 2.10. Damping ratio of frozen soil (after Vinson, 1978). (a) Versus frequency. (b) Versus temperature.

Cyclic loading superimposed on a statically loaded pile normally includes a low frequency, low amplitude, sustained cyclic load with a much larger static load. Although many dynamic triaxial, dynamic uniaxial compression, and resonant column tests (Kaplar, 1969; Stevens, 1975; Chaichanavong, 1976; Vinson et al., 1977) consider only a cyclic load or superimpose a cyclic load on a hydrostatic load, they provide some insight on how frequency and amplitude of loading effect various soils. Table 2.1 was compiled by Vinson (1978) to show the relative importance of the frozen physical conditions and testing conditions on the dynamic stress-strain and energy absorbing properties.

2.2.3. Deformation Influenced by Cyclic Loading

Some triaxial and uniaxial compression tests on frozen soils show how dynamic loading can effect total strain. Strain rates appear to be relevant to the problem of increased pile displacement rates due to cyclic loading. Parameswaren (1985), in Figure 2.11, showed large strain rate increases after a cyclic load (dashed lines) was superimposed on a static load (solid lines). A temperature increase was measured within the sample during the dynamic loading from which Parameswaren (1985) calculated a volume of unfrozen water and speculated how this might accelerate strain rates. In uniaxial compression tests of frozen sand

Table 2.1. Relative Importance of Various Parameters on Dynamic Properties of Frozen Soils (after Vinson, 1978).

Material parameters:		
Material type and composition	Very important; dynamic stress-strain properties for coarse-grained soils can be nearly an order of magnitude greater than for fine-grained soils	Very important; energy-absorbing properties can differ by an order of magnitude or greater for different soil types
Material density or void ratio (for fully saturated soils)	Important; over a range of void ratios from 0.3 to ice, dynamic stress-strain properties can decrease by a factor of 5; over the range of void ratios associated with a given soil type the influence of dynamic stress-strain properties will not be as great; dynamic stress-strain properties of ice decrease substantially with decreasing density	Probably unimportant; there may be a slight decrease in damping ratio with decreasing density over the range associated with the given soil type
Ice content or degree of ice saturation per unfrozen water content	Very important; however, occurrence of coarse-grained soils with 90% ice saturation is rare in nature; degree of ice saturation for fine-grained soils is related to unfrozen water content and the influence in this case is reflected by temperature	Important; see comments under Dynamic stress-strain properties
Field- and/or test-condition parameters:		
Temperature	Very important for frozen soils, particularly in the range 0 to $-5^{\circ}C$	Very important for frozen soils in the range 0 to $-5^{\circ}C$; relatively unimportant in the range -5 to $-20^{\circ}C$
Strain (or stress) amplitude of loading	Unimportant for axial strain amplitudes less than $10^{-3}\%$ for frozen soils and ice; important for axial strain amplitudes between 10^{-3} and $10^{-1}\%$ for frozen soils	Unimportant for axial strain amplitudes less than $10^{-3}\%$; important for axial strain amplitudes between 10^{-3} and $10^{-1}\%$ for most frozen soils
Frequency of loading	Relatively unimportant	Probably important
Confining pressure	Important for coarse-grained soils and ice; unimportant for fine-grained soils	Unimportant

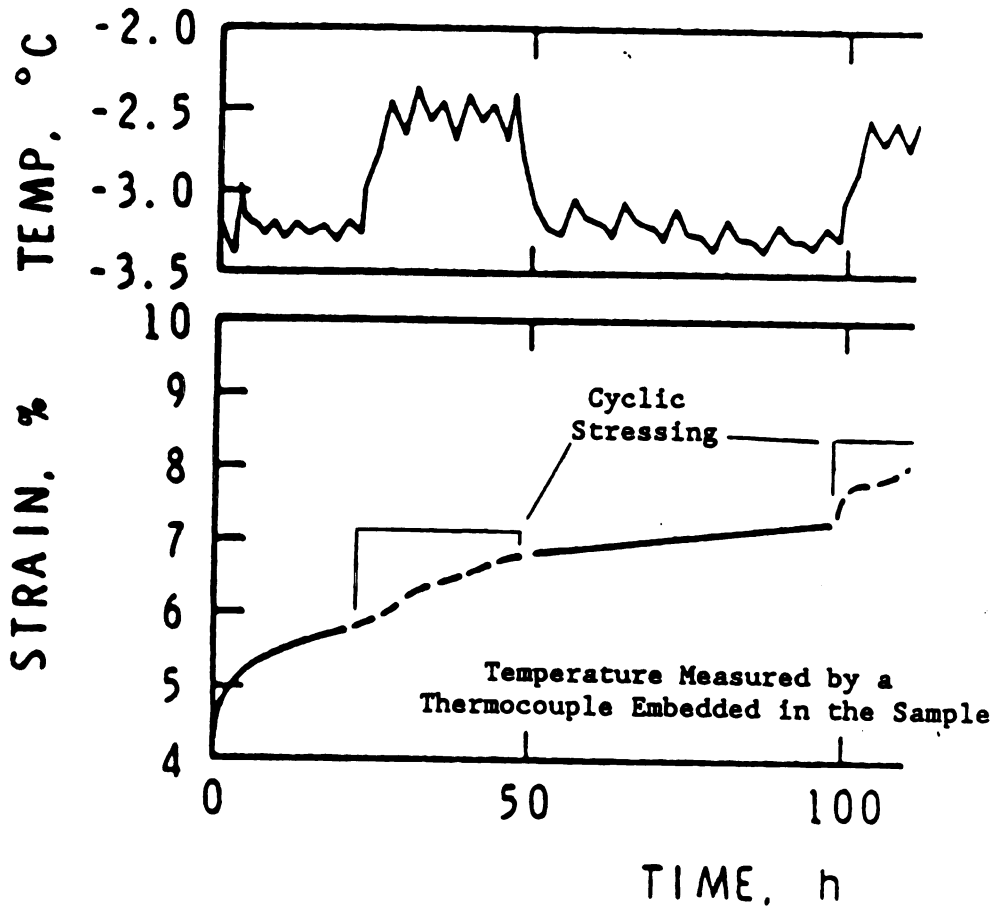

Figure 2.11. Effect of cyclic stress on temperature of frozen sand (after Parameswaran, 1985).

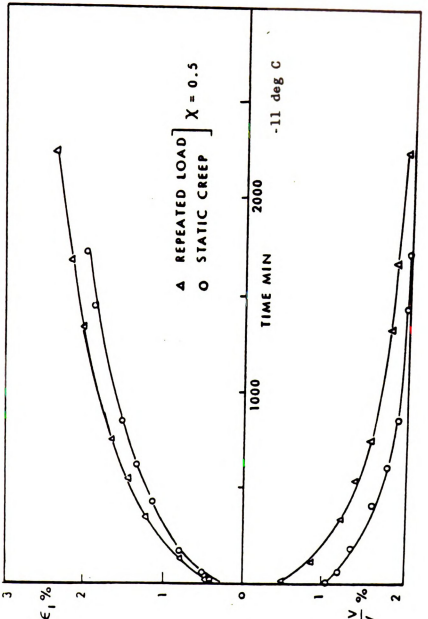

Figure 2.12. Typical strain relations for frozen sand (after Trimble and Mitchell, 1982).

at 11 deg C, Trimble and Mitchell (1982) compared a constant stress sample to a sample that was repeatedly: 1) loaded to the same constant load for 0.25 seconds and then 2) completely unloaded for 0.25 seconds. Figure 2.12 shows that volumetric strains, total strains, and strain rates of these tests are similar.

2.3. Adhesion and Friction Between Pile and Soil

Adhesion has been extensively studied by Jellinek (1957a, 1957b, 1960a, 1960b, 1960c, 1967) with results reported for tensile and shear tests on ice adhesion to stainless steel, lucite, fused quartz, and polystyrene. Jellinek (1957b) proposed that a transition layer of unfrozen water lies between the ice and the other materials. Strong tensile and lesser shear strengths were found between the ice and the other materials (Jellinek, 1967). Experimental control of adhesion is reported (Jellinek, 1957a; Alwahab, 1983) to be difficult so that a lot of scatter exists in experimental results. Weaver and Morgenstern (1981a, Figure 2.13) suggest that entrapped air could weaken bond at the ice/pile interface.

Friction between a pile and soil grains can be thought of as occuring in unfrozen soil. The shear force between unfrozen soil and the pile, can be described as

$$\tau = N f \qquad (2.26)$$

Figure 2.13. Idealized plate in contact with ice and frozen soil (after Weaver and Morgenstern, 1981a).
(a) Air trapped during sample preparation allows slip ice/plate interface.
(b) Interaction between plate protrusions and soil grains.
(c) Shear plane developes in ice.

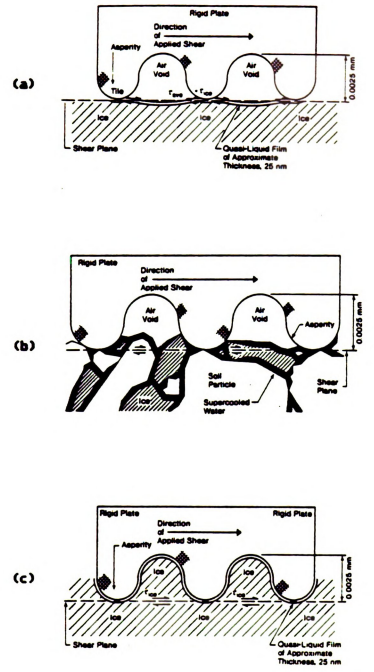
(a)
Rigid Plate
Direction of Applied Shear
Asperity
Air Void
Air Void
Tile
Ice
Ice
Ice
0.0025 mm
Shear Plane
Quasi-Liquid Film of Approximate Thickness, 25 nm
(b)
Rigid Plate
Direction of Applied Shear
Air Void
Air Void
Asperity
0.0025 mm
Soil Particle
Shear Plane
Ice
Supercooled Water
(c)
Rigid Plate
Rigid Plate
Direction of Applied Shear
Asperity
Ice
Ice
0.0025 mm
Ice
Ice
Ice
Shear Plane
Quasi-Liquid Film of Approximate Thickness, 25 nm

Figure 2.13.

where N is the normal pressure between soil and pile and f is a function of the type of materials and the conditions at the pile/frozen soil interface. Normal pressure can vary considerably due to pile installation methods (Ladanyi and Guichaoua, 1986). Friction can be virtually eliminated if a very cold pile forms an ice coating as it freezes its surrounding sand slurry (Linell and Lobacz, 1980).

2.3.1. Mechanical Interaction Between Frozen Soil and Pile

Mechanical interaction may evolve as a physical rearrangement of the soil particles with respect to the pile. Alwahab (1983) added oversize protrusions (lugs) to model piles which created, when loaded, regions of increased pressure ahead of these lugs. These pressures are similar to those pressures attributed to cavity expansion in frozen soils (Ladanyi, 1976). Increasing the diameters of these lugs clearly increased the model pile load capacities. Weaver and Morgenstern (1981a) showed indications that shear behavior at the interface between metal plates and frozen soils was dependent on plate roughness and soil type.

2.3.2. Pile/Soil Adfreeze Bond Estimation

Adfreeze bond at the pile/frozen soil interface, used for estimating pile load capacity, has often been considered (Linell and Lobacz, 1980; Weaver and

Morgenstern, 1981b) to be some fraction of the shear strength of the frozen soil surrounding the pile. Weaver and Morgenstern (1981b) considered the long term adfreeze strength between pile and frozen soils, τ_a to be

$$\tau_a = m \tau_{lt} \tag{2.27}$$

where m is a constant based on the pile's surface roughness. Long term shear strength was then defined as

$$\tau_{lt} = c_{lt} + \sigma \tan(\phi_{lt}) \tag{2.28}$$

where c_{lt} is long term cohesion, σ is the lateral stress on the pile, and ϕ_{lt} is the friction angle of the Mohr envelope for this frozen soil. Weaver and Morgenstern (1981b) considered $\sigma \tan(\phi_{lt})$ to be small compared to c_{lt}, hence they assumed the long-term adfreeze bond to be

$$\tau_a = m c_{lt} \tag{2.29}$$

Values of m were described as ranging from 0.6 for steel to 1.0 for corrugated steel.

2.4. Review of Pile Design Methods

The best information for pile design in permafrost can be obtained from full-scale piles (Linell and Lobacz, 1980)

built at the project site by the anticipated construction method and load tested during the surrounding permafrost's warmest condition. Factors such as soil type, soil temperature, pile installation, and pile type are thereby combined in the right proportions so that loading the test pile is similar to loading a design pile. However, pile test information is not generally available during the early planning of a project or may be considered unnecessary for small projects (which could be overdesigned and verified later). Preliminary designs may be estimated from knowledge of the project's soil types, soil temperatures, confined triaxial compression test parameters, pile size, and anticipated pile loads (Weaver and Morgenstern, 1981b).

A proposed standard method by the American Society for Testing and Materials (ASTM) entitled "Standard Method of Testing Individual Piles in Permafrost Under Static Axial Compressive Load" has recently been outlined by Neukirchner (1988). While this standard has not yet been approved, it uses many procedures accepted in "Piles Under Static Axial Compressive Load" (ASTM D-1143), the existing standard for unfrozen soils. The biggest difference between the "unfrozen" and "frozen" methods concerns loading procedures. The "unfrozen" test increases the pile load in several steps (25% of design load) and generally holds each incremental load for less than 2 hours. The "frozen" test

procedure uses two test piles, each one loaded in two steps with the load maintained for each step from 6 hours to 5 days.

If a test program were to use the proposed standard method, two piles would be prepared in a manner similar to that for unfrozen piles (ASTM D-1143) and temperatures would be measured along their lengths. A 100% of design load (adjusted for temperature) would be added to the first pile while a 200% of design load (adjusted for temperature) would be added to the second pile. Both loads would be maintained until a steady creep rate is obtained or for three days if a steady rate does not develop. Additional loads would then be added in order to fail the first pile in 6-12 hours and the second pile in 3-5 days. The results from these tests would be compared to a diagram similar to Figure 2.14 to determine if the design pile can sustain its design load throughout its service life.

If the Linell and Lobacz (1980) test loading procedure were used, one pile would be prepared in a manner similar to ASTM D-1143 and temperatures would be measured along its length. Incremental loads of 10,000 pounds would be added and maintained for 3 days (the recommended minimum). Incremental loading would continue until 1.5 inches of settlement (failure has occured) or a total load of 2.5 times the design load is obtained. A load determined to initiate pile failure could then be divided by a factor of

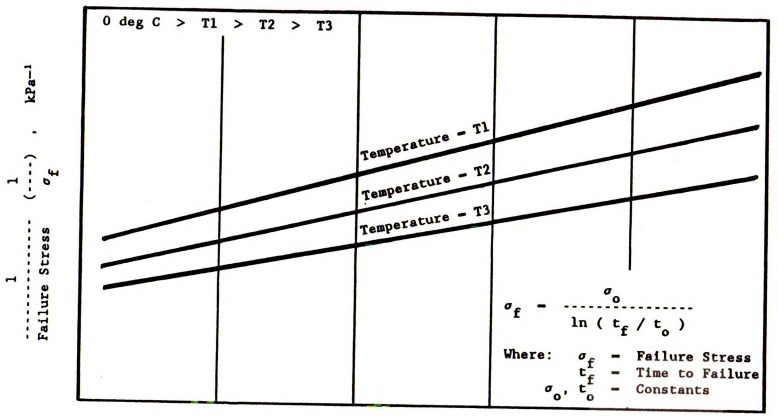

Figure 2.14. Vyalov relationship between failure stress and time (after Neukirchner, 1988).

saftey of at least 2.5, for dead load plus normal live load, or by a factor of saftey of at least 2.0, for dead load plus maximum live load. Although the loading periods are shorter than 3 days, Figure 2.15 illustrates how a failure load would be determined by this procedure.

Pile capacities based on pile tests or other preliminary work may be estimated by using previously established stress-strain-time relationships for frozen soils. Linell and Lobacz (1980) roughly estimated pile capacity by using soil temperature, soil type, and pile type to estimate sustainable adfreeze bonds on the pile's surface. In their examination of pile capacity estimation, Weaver and Morgenstern (1981b) considered compression piles to fail when the adhesive portion of the adfreeze bond between pile and soil was broken (resulting in large rapid settlements for relatively smooth straight piles) or when the frozen soils surrounding the pile deformed excessively (along the sides and at the end) during the design life of the pile.

Weaver and Morgenstern (1981b) used various estimates of soil cohesion (which they converted to pile/soil adhesion values as detailed in section 2.3.4) to create Figure 2.16. Constitutive equations that best fit a collection of uniaxial compression data and triaxial compression data (see section 2.1.4 for details) were incorporated into pile settlement equations based on creep

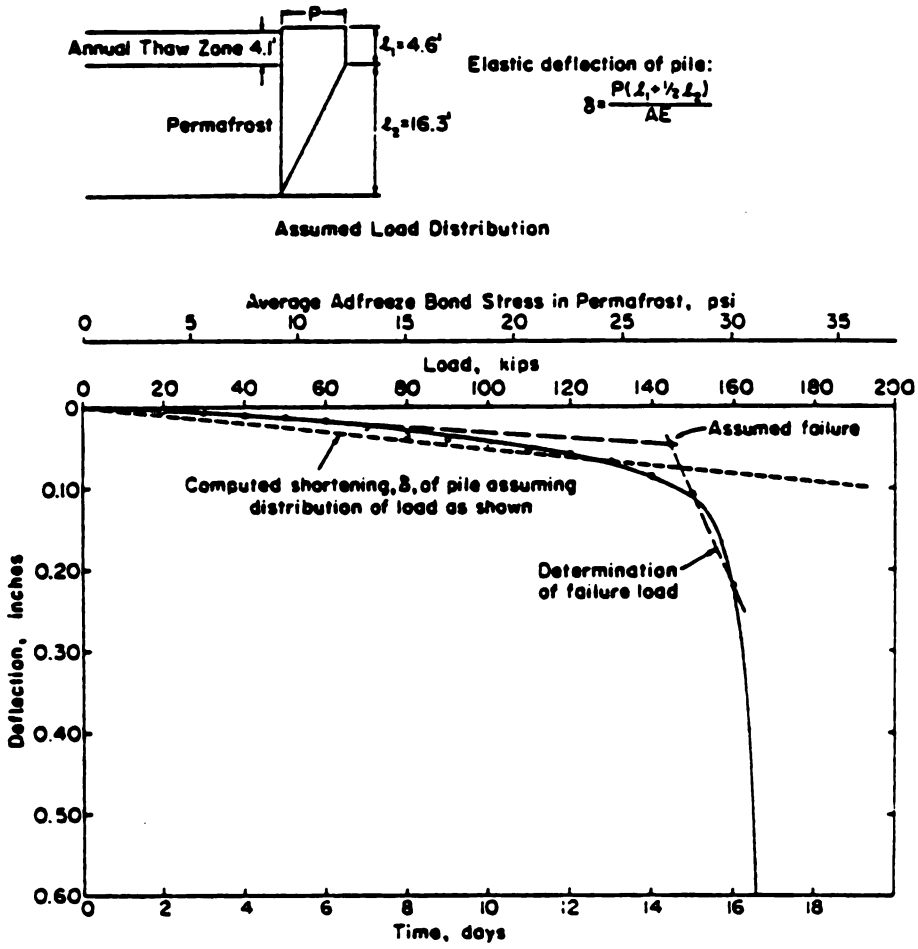

Pile type: 8-in. pipe, 36 lb/ft

Pile length: 20.9 ft

Length below surface: 20.4 ft

Embedment in frozen soil: 16.1 ft

Soil profile: 0-1 ft peat, 1-20.4 ft (bottom of pile) silt

Backfill around pile: silt-water slurry

Avg temp of frozen soil: 29.2°F

Test performed: July 1958

Loading schedule: 10-kip increments applied at 24-hr intervals. The deflection shown for an increment is that observed just prior to application of next increment.

Note: Pile not isolated from soil in thaw zone.

Figure 2.15. Load test of steel pipe pile (after Linell and Lobacz, 1980).

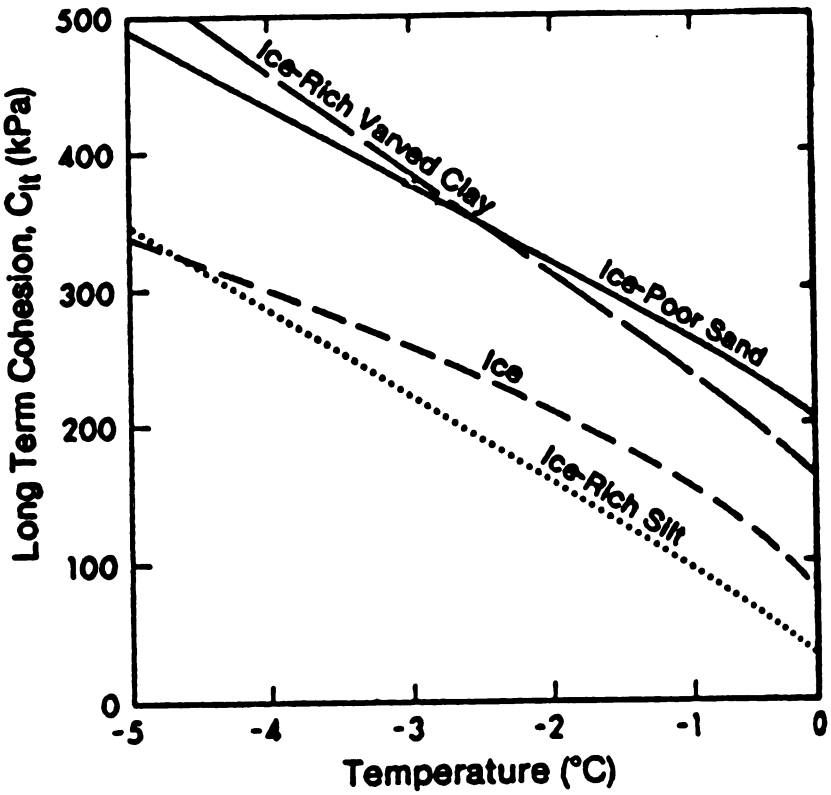

Figure 2.16. Long-term cohesion of frozen soils (after Weaver and Morgenstern, 1981b).

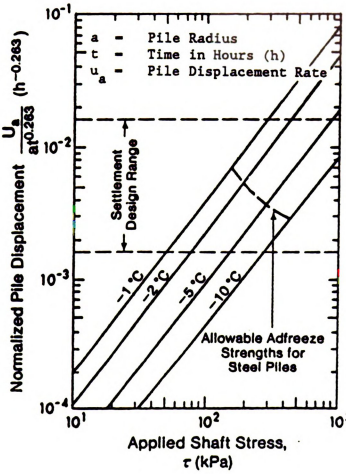

Figure 2.17. Design chart for friction piles in frozen Ottawa Sand (after Weaver and Morgenstern, 1981b).

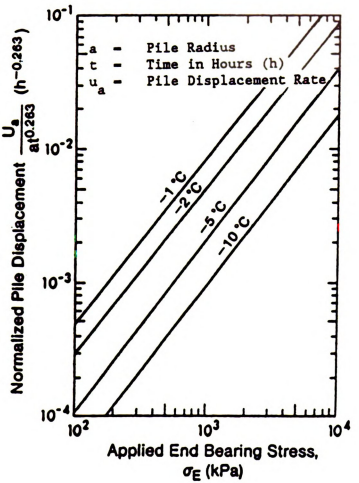

Figure 2.18. Design chart for friction end-bearing piles in frozen Ottawa Sand (after Weaver and Morgenstern, 1981b).

deformation theory (see section 2.5) to predict long term settlements. Normalized design diagrams were created to predict pile settlement from stress around the pile's shaft (Figure 2.17) and to predict pile settlement due to stress at the end of the pile (Figure 2.18) and each figure must be used with equal pile displacement values, U_a. The figures shown are for an Ottawa sand. Design diagrams for ice, Hanover clay, and Hanover silt are included in their paper but are not shown.

2.5. Pile Settlement Estimation Equations

2.5.1. Shear Deformation of Soil Along Pile Shaft

Johnston and Ladanyi (1972) found that rod anchors grouted into permafrost displayed typical creep behavior. The anchor behaved like a short pile and it displacement was described as

$$s(t) = s_i + \dot{s}(t) \qquad (2.30)$$

where s(t) is total displacement in terms of time, s_i is a fictitious instantaneous displacement, $\dot{s}$ is a constant displacement rate, and t is time. This equation is similar in form to the constitutive equation for secondary creep of frozen soils found in Equation 2.18. The assumptions made for this model include: a) Pile is cylindrical, b) Uniform shear stress along the pile surface, c) Uniform soil type, uniform temperature, and d) Neglect pile weight. End

bearing was nonexistent because the anchor was pulled upward.

It was assumed that shear stress at any distance from the pile's surface could be described by an equation from Nadai (1963) as

$$\tau = \tau_a \ (a / r) \tag{2.31}$$

where τ_a is shear stress at the pile surface, a is the pile radius, r is the distance from pile's center, and τ is shear stress at a distance. An expression for shear distortion rate, $\dot{\gamma}$ was used

$$\dot{\gamma} = \frac{- d(\dot{u})}{dr} \tag{2.32}$$

where $\dot{u}$ is the velocity of a soil element at distance r.

An equation from Odquist (1966) was used by Johnston and Ladanyi (1972) to describe an incompressible von Mises material in a general state of stress as

$$\dot{\varepsilon}_e = \dot{\varepsilon}_c \ [\frac{\sigma_e}{\sigma_{cu\theta}}]^n \tag{2.33}$$

where σ_e is equivalent stress, $\dot{\varepsilon}_e$ is equivalent strain rate, $\dot{\varepsilon}_c$ is a strain rate chosen for computation purposes, n is a creep parameter, and $\sigma_{cu\theta}$ is a temperature-dependant creep proof stress. This equation is a variation of Equation 2.13 (with b = 1) which best fit Nixon and

McRoberts (1976) uniaxial-creep-stress and strain-rate data for ice and ice-rich soil.

As a pile settles, a given soil particle will only move vertically and/or normally to the pile's surface, so that plane strain can be assumed. The stress [σ_1, σ_2 (= $\sigma_1/2 + \sigma_3/2$), σ_3] and strain rate [$\dot{\varepsilon}_1$, $\dot{\varepsilon}_2$ (= 0), $\dot{\varepsilon}_3$ (= $-\dot{\varepsilon}_1$) conditions for plane strain and constant volume were used to derive

$$\dot{\varepsilon}_1 = [\frac{\sqrt{3}}{2}]^{(n+1)} \dot{\varepsilon}_c [\frac{(\sigma_1 - \sigma_3)}{\sigma_{cu\theta}}]^n \qquad (2.34)$$

A horizontal normal force (lateral soil pressure) and a vertical shear force (resistance of soil to axial pile load) were thought (Johnston and Ladanyi, 1972) to develop simple shear in the frozen soil surrounding the pile. The stress, τ (= $\sigma_1/2 - \sigma_3/2$) and strain rate, $\dot{\gamma}$ (= $2\varepsilon_1$) conditions of simple shear are included in the plane strain equation so that

$$\dot{\gamma} = 3^{(n+1)/2} \dot{\varepsilon}_c [\frac{\tau}{\sigma_{cu\theta}}]^n \qquad (2.35)$$

Nixon and McRoberts (1976) suggest that pile behavior in ice and ice-rich soils are better described by a two term form of the previous equation so that

$$\dot{\gamma} = 3^{(n_1+1)/2} B_1 \tau^{n_1} + 3^{(n_2+1)/2} B_2 \tau^{n_2} \qquad (2.36)$$

After substituting Equations 2.31 and 2.32 into this

equation, integration of $d\dot{u}/dr$ between the boundry conditions ($u = \dot{u}_a$ and $\dot{\tau} = \tau_a$ at $r = a$ and $\dot{u} = 0$ at $r = \infty$) yields

$$\dot{u}_a = \frac{3^{(n_1+1)/2} \; B_1 \; \tau_a^{n_1} \; a}{n_1 - 1} + \frac{3^{(n_2+1)/2} \; B_2 \; \tau_a^{n_2} \; a}{n_2 - 2} \qquad (2.37)$$

This equation is valid only for the temperature used to evaluate its creep parameters. Other temperatures would each require a series of compression creep tests to determine additional sets of creep parameters.

Weaver and Morgenstern (1981b) assumed that a single term form of Equation 2.37

$$\frac{\dot{u}_a}{a} = \frac{3^{(n+1)/2} \; B \; \tau^n}{n - 1} \qquad (2.38)$$

was better able to describe pile behavior in ice or ice-rich soils. This equation was then used to determine pile capacity, P_s, thus

$$P_s = 2 \pi a L \; \tau$$

$$= 2\pi a L \; [\frac{\dot{u}_a}{a}]^{(1/n)} \; [\frac{n - 1}{3^{(n+1)/2}}]^{(1/n)} \; [\frac{1}{B}]^{(1/n)} \qquad (2.39)$$

Weaver and Morgenstern (1981b) described an equation that best fit uniaxial compression creep data for ice-poor

soils (Equation 2.25). This equation was similar in form to Equation 2.33 (for ice and ice-rich soils), hence the derivations used for pile displacement in ice and ice-rich soils (Equations 2.34 through 2.38) were used by Weaver and Morgenstern (1981b) with Equation 2.25 to give the displacement (u_a) for a pile in ice-poor soil, thus

$$\frac{u_a}{at^b} = \frac{3^{(c+1)/2} \quad D \quad \tau^c}{c - 1} \tag{2.40}$$

and pile capacity P_s, based on shaft shear stress τ_a, is given by

$$P_s = 2 \pi a L \tau_a$$

$$= 2\pi aL \left[\frac{u_a}{at^b}\right]^{(1/c)} \left[\frac{c-1}{3^{(c+1)/2}}\right]^{(1/c)} \left[\frac{1}{D}\right]^{(1/c)} \tag{2.41}$$

The relationship between pile capacity (applied stress), pile displacement, and temperature as determined by Weaver and Morgenstern for a pile frozen into Ottawa sand is shown in Figure 2.17.

2.5.2. Penetration Deformation of Soil at Pile Base

The theory of cavity expansion was first used by Bishop (1945) as a simple yet reasonably accurate model of deep indentation. Bishop, et al. (1945) and Hill (1950) believed the pressure that indents a deep hole in an elastic-plastic material to be related to the pressure that

expands a cavity of equal volume in a similar material. Johnston (1970) and Ladanyi (1966) approximated the volume (V_s) displaced by punch penetration (if penetration is less than the punch radius) as

$$V_s = \pi (r_{io})^2 s \tag{2.42}$$

where r_{io} is the punch radius and s is punch penetration. The volume (V_{io}) of the cavity before expansion is

$$V_{io} = \frac{2}{3} \pi (r_{io})^3 \tag{2.43}$$

By this theory, the volume (V_i) of the expanded cavity,

$$V_i = V_{io} + V_s \tag{2.44}$$

and a volume change ratio can be determined as

$$\frac{V_i}{V_{io}} = 1 + \frac{3 s}{2 r_{io}} = 1 + 3 \frac{s}{B} \tag{2.45}$$

Ladanyi (1972) described the axial steady state creep rate by an equation similar to Equation 2.33, thus

$$\dot{\varepsilon}_1(c) = \dot{\varepsilon}_c \left[\frac{\sigma_1 - \sigma_3}{\sigma_{cuo} \; f(\theta)}\right]^n \tag{2.46}$$

where $\dot{\varepsilon}_c$ is a creep rate selected for calculation purposes, n is a creep parameter, $f(\theta)$ is a function of temperature, and σ_{cuo} is the creep proof stress at a temperature close to the freezing point. If the instantaneous creep is

small, then this equation can be converted to a creep strain equation

$$\varepsilon_1^{(c)} = \left[\frac{\sigma_1 - \sigma_3}{\sigma_s}\right]^n \qquad (2.47)$$

where

$$\sigma_s = \sigma_{cuo}\ f(\theta)\ [\dot{\varepsilon}_c\ t]^{(-1/n)} \qquad (2.48)$$

is used for brevity.

For ice and ice-rich soils in a prefailure state (according to the von Mises criterion) that behave as described by the previous equation, the conditions of equilibrium are shown by Ladanyi and Johnston (1974) as

$$\frac{d(\sigma_r)}{dr} + \frac{2\sigma_r - \sigma_t}{r} = 0 \qquad (2.49)$$

where σ_r is the radial stress and σ_t is the circumferential stress. The solutions for this equation are given by Odquist and Hult (1962) and Hult (1966) as

$$\sigma_r = (\sigma_{re} - p_o)\ \left[\frac{r_e}{r}\right]^{(3/n)} + p_o \qquad (2.50)$$

and

$$\sigma_t = (\sigma_{re} - p_o)\ [1 - (3/2n)]\ \left[\frac{r_e}{r}\right]^{(3/n)} + p_o \qquad (2.51)$$

where radial stress σ_{re} at radius r_e can be found in the prefailure zone and p_o is the hydrostatic pressure. Ladanyi and Johnston (1974) describe the resulting

displacement (at radius, r) equation as

$$\frac{u}{r} = \frac{1}{2}\left[\frac{3\sigma_{re} - 3p_o}{2\,n\,\sigma_s}\right]^n \left[\frac{r_e}{r}\right]^3 \qquad (2.52)$$

Ladanyi and Johnston (1974) also approximated the relationship between the expanded cavity volume V_i and the initial cavity volume V_{io} as

$$\frac{V_i}{V_{io}} = [1 + u_i/r_{io}]^3 = [1 - u_i/r_i]^{(-3)} \qquad (2.53)$$

where r_{io} is the initial cavity radius, r_i is the expanded cavity radius, and u_i is the displacement of the cavity in the radial direction. A combination of Equations 2.45 and 2.53 yields

$$\frac{3s}{B} = [1 - u_i/r_i]^{(-3)} - 1 \qquad (2.54)$$

Combining this equation with Equation 2.52 yields

$$\frac{3s}{B} + 1 = \left\{ 1 - \frac{1}{2}\left[\frac{3p_i - 3p_o}{2\,n\,\sigma_s}\right]^n \right\}^{(-3)} \qquad (2.55)$$

when ($\sigma_{re} = p_i$) and ($r_e = r_i$).

According to Ladanyi and Johnston (1974), Hoff's elastic analogue allows the strain relationship of Equation 2.47 to be replaced by the steady state creep rate relationship of Equation 2.46. A derivation similar to those shown in Equations 2.49 through 2.51 yields a

displacement rate, $\dot{u}_i$ equation for ice and ice-rich soils as

$$\frac{\dot{u}_i}{r_i} = \frac{1}{2}\left[\frac{3p_i - 3p_o}{2\,n\,\sigma_s}\right]^n \qquad (2.56)$$

Weaver and Morgenstern (1981b) carried this equation further and showed a settlement rate equation,

$$\frac{\dot{u}_a}{a} = \frac{2}{3}\left\{1 - \frac{B}{2}\left[\frac{3\sigma_E}{2n}\right]^n\right\}^{(-3)} - \frac{2}{3} \qquad (2.57)$$

where σ_E is the pressure at the pile base and

$$B = \frac{1}{t\,\sigma_s^{\,n}} = \frac{\dot{\varepsilon}_c}{[\,\sigma_{cu\theta}\;\; f(\theta)\,]^n} \qquad (2.58)$$

Equation 2.57 is a rearrangement of equation 2.48 and is used for brevity. Equation 2.57 was simplified by Weaver and Morgenstern (1981b) to

$$\frac{\dot{u}_a}{a} = B\left[\frac{3\;\;\sigma_E}{2\;\;n}\right]^n \qquad (2.59)$$

This simplification allows easier (and reasonably accurate) estimation of pile end bearing in ice and ice-rich soils as

$$P_E = \left[\frac{\dot{u}_a}{D\;\;a}\right]^{(1/n)} \frac{2\,\pi\,n\;\;a^2}{3} \qquad (2.60)$$

For ice-poor soils, described by Ladanyi (1972) in Equation 2.23, Weaver and Morgenstern (1981b) reported that

the effect of confining pressure was limited (Ladanyi and Johnson, 1974) for pile end bearing and used Equation 2.25 to describe soil behavior. Equation 2.25 is similar to Equation 2.47, for ice and ice-rich soils, hence derivation of pile end bearing capacity was similar for both soil types. Weaver and Morgenstern (1981b) showed the pile displacement equation for ice-poor soils as

$$\frac{u_a}{at^b} = D \left[\frac{3 \sigma_E}{2 c}\right]^n \qquad (2.61)$$

where b and c are the creep parameters and D is shown in Equation 2.22. This equation was then converted to a pile end bearing capacity,

$$P_E = \left[\frac{u_a}{D \; at^b}\right]^{(1/n)} \frac{2 \pi n \; a^2}{3} \qquad (2.62)$$

Weaver and Morgenstern (1981b) created a design chart to show the relationships of pile end bearing capacity (applied end bearing stress), pile settlement, and temperature for a given pile frozen into Ottawa sand as shown in Figure 2.18. Weaver and Morgenstern (1981b) noted that adding a pile end bearing estimation to a pile (shear on side) capacity estimation is only approximate because peak end bearing capacity develops at a larger displacement than peak friction pile capacity, as shown in Figure 2.19.

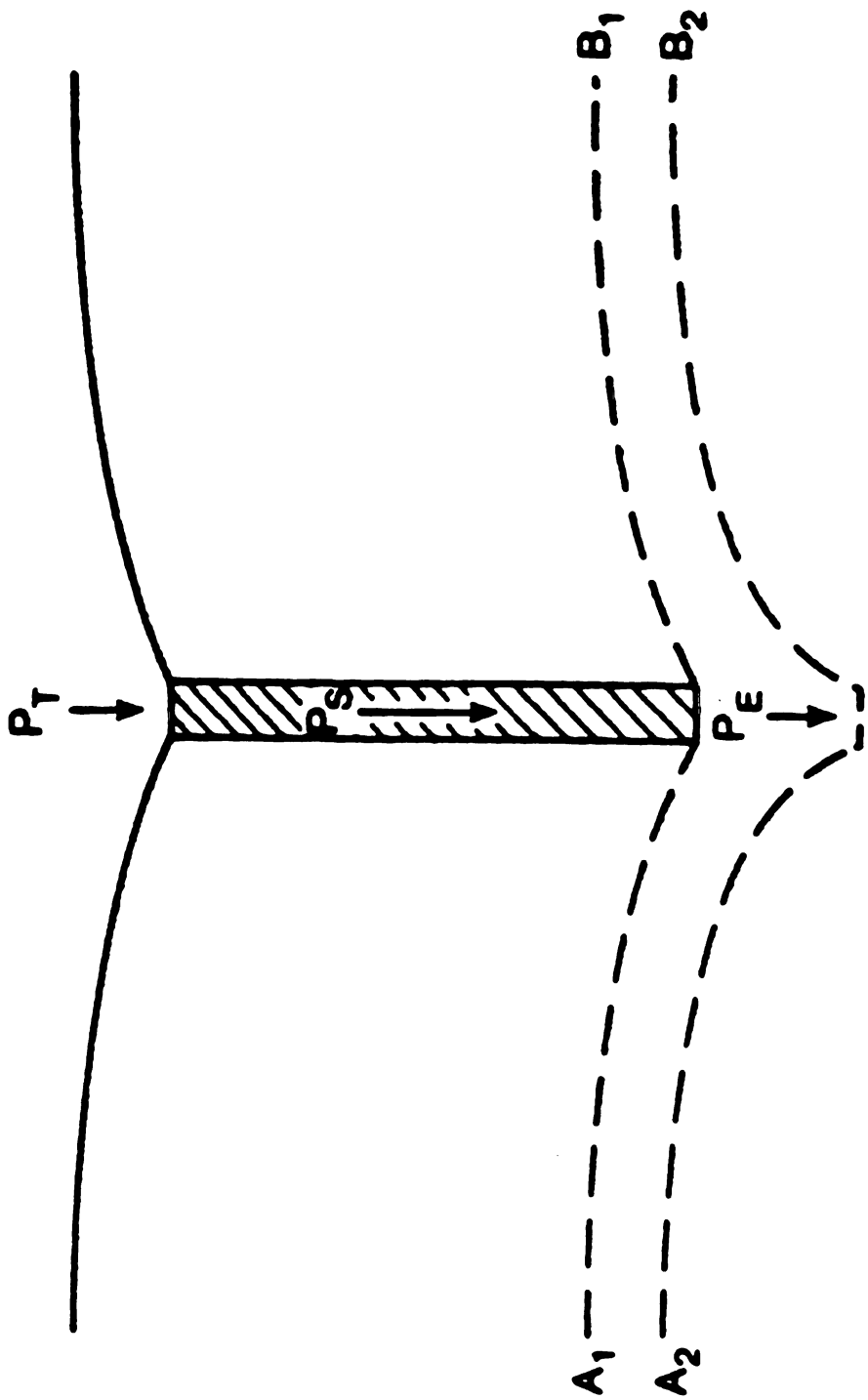

Figure 2.19. Uncoupling of effects due to pile shaft and base (after Weaver and Morgenstern, 1981b).

2.5.3. Expansion of a Cylindrical Cavity by Pile Settlement

As the pile shown in Figure 2.20 settles, it will push outward to expand the cavity in which the pile rests. Lateral pressure will increase along the pile surface, additional friction forces will develop, and the pile capacity will increase.

An equation for lateral pressure increase was used by Ladanyi and Johnston (1973) for analysis of pressuremeter data. It combined an equation for primary creep with Odquist's (1966) rate equation for creep cavity expansion. Ladanyi and Guichaoua (1985) rewrote this pressuremeter equation to describe the pressure created by movement of the pile (Figure 2.20) as

$$p_i - p_o = C \, [u_i / r_i]^{(1/n)} \qquad (2.63)$$

and

$$C = \sigma_{c\theta} \left(\frac{n}{\sqrt{3}}\right) t^{(-b/n)} \left\{ \left(\frac{2}{\sqrt{3}}\right) \left[\frac{b}{\dot{\varepsilon}_c}\right]^b \right\}^{(1/n)} \qquad (2.64)$$

where p_i is the pressure induced by soil expansion, p_o is the initial earth pressure, b and n are creep parameters, t is time, $\sigma_{c\theta}$ is the proof stress, and $\dot{\varepsilon}_c$ is the strain rate choosen for computation purposes. This expression for lateral pressure was then used to estimate frictional forces over the surface of the pile with

$$2\pi \bar{Q} = 2\pi \int_0^{L/\cos\alpha} (p_i - p_o) (\sin\alpha + \tan\alpha \cos\alpha) \, r_i \, dx \qquad (2.65)$$

using notations described in Figure 2.20. Pile settlement,

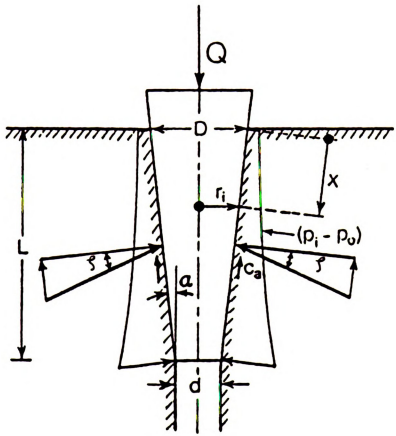

Figure 2.20. Notation for the theory of tapered piles (after Ladanyi and Guichaoua 1985).

s may be described as

$$u_i = s \tan\alpha \tag{2.66}$$

where u_i is the pile-cavity radial displacement, thus Equation 2.65 can be integrated to give

$$2\pi\bar{Q} = 2\pi C \frac{(1 + \tan\zeta)/(\tan\alpha)}{2 - (1/n)} \left[\frac{D}{2}\right]^2 * \\ * \left[\frac{1 - d/D}{L}\right]^{(1/n)} \{1 - [d/D]^{(2 - 1/n)}\} s^{(1/n)} \tag{2.67}$$

This equation may be shown more simply as

$$s = K \bar{Q}^n t^b \tag{2.68}$$

which can be rearranged and differentiated to become the pile settlement rate,

$$\dot{s} = b K Q^n t^{(b-1)} \tag{2.69}$$

2.6. Cyclic Loading of Piles and Pile Driving

Due to a lack of existing data for cyclic loading superimposed on statically loaded piles in frozen soils, information on pile driving has been reviewed. Schmid's (1969) study of model piles vibrated into unfrozen uniformly graded sand, showed several modes of vibration for the pile (Figure 2.22). The lowest mode, described as if the pile vibrated or moved as a rigid body with the

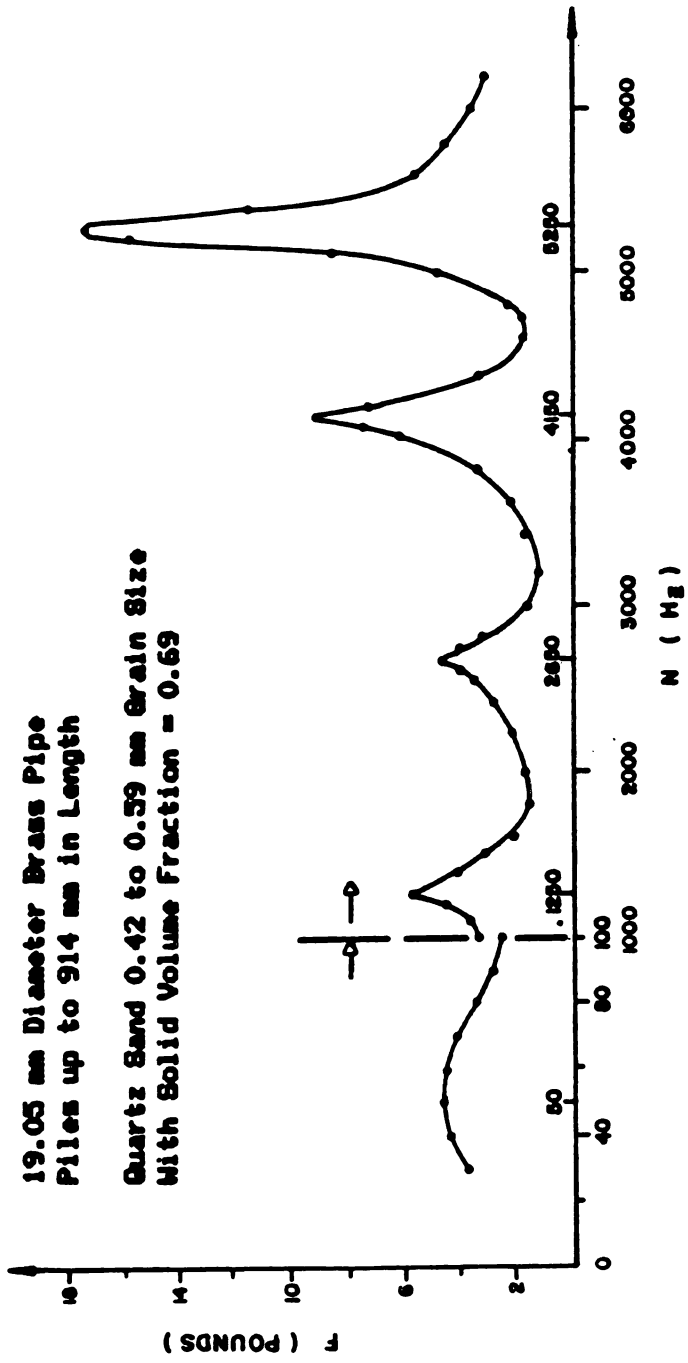

Figure 2.21. Vibratory frequency versus force amplitudes for model piles embedded in unfrozen sand (after Schmid 1969).

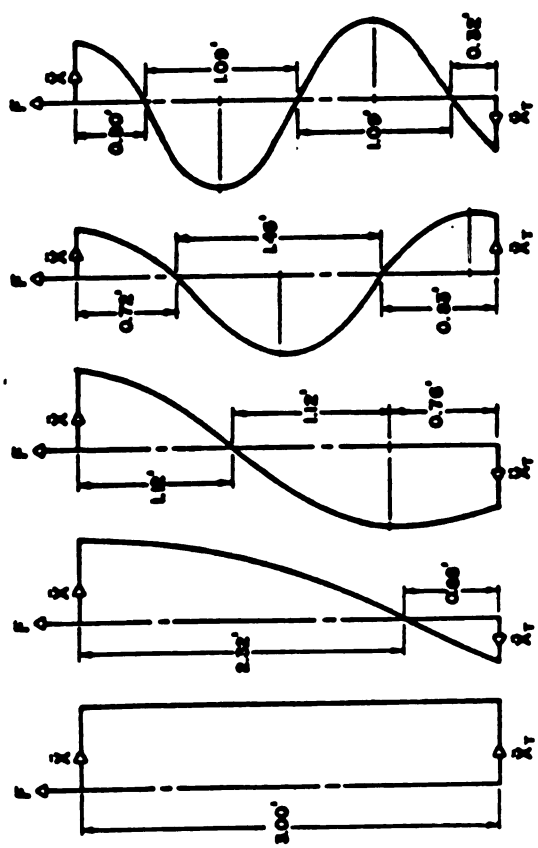

RESONANCE FREQUENCY N (Hz)	50	1250	2650	4150	5250
NUMBER OF NODES m	0	1	1	2	3
λ/L (APPROXIMATE)		3.00	1.50	1.00	0.75

Figure 2.22. Wave form of model piles at various resonance frequencies (after Schmid 1969).

soil, is shown as a wide flat peak in Figure 2.21. The maximum penetration velocity occured at this frequency of vibration. Schmid (1969) observed that most soil penetration resistance occured at the pile tip during the rapid tip impacts created by resonant vibration.

The lowered resistance along the pile shaft occurs (Kovacs and Michitti, 1970) when the relatively stiff pile moves in unison with the cyclic force, the soil/pile bond breaks, and individual soil grains tend to rearrange themselves. The pile/soil interface remains in a condition of reduced friction by the continued application of the cyclic force. This "fluidized" condition could not be achieved in a very dense sand and it was proposed that the lack of void space would not allow grain rearrangement (Kovacs and Michitti, 1970).

Pile driving in frozen soils has been observed to cause melting around the pile (Linell and Lobacz, 1980). Dufour et al. (1983) thought that the frozen soil yielded plastically at the driven pile tip and melting followed. The melting and rapid impacts associated with driving piles in permafrost may create conditions quite different from those associated with small cyclic loads.

Direct information on cyclic loading superimposed on piles in frozen soils is limited to data presented by Parameswaren (1982, 1984). A typical pile displacement-time curve (Parameswaren, 1984 shown in Figure 2.23)

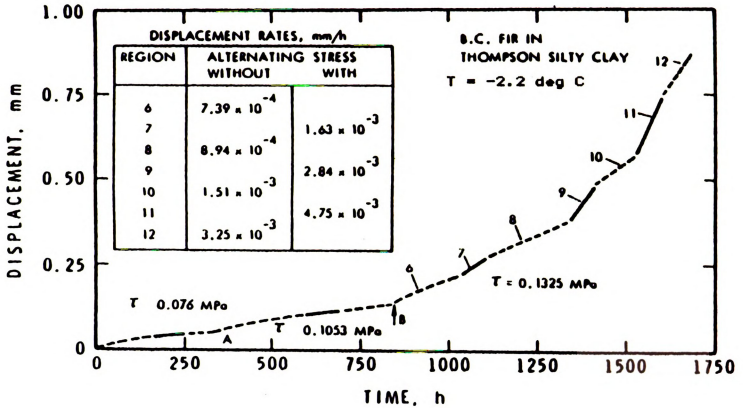

Figure 2.23. Typical creep curve showing the displacement of wood pile in frozen clay with time (after Parameswaren 1984).

represents a peak to peak cyclic load of nearly 5% of the static pile load superimposed on the model pile. The displacement rate for region 7 of this figure was more than doubled by the added cyclic loading. This increase in pile displacement (settlement) rate must be accounted for in determining the design load per pile. Suitable constitutive relations for predicting the increase in displacement rate as a function of cyclic loading (amplitude, frequency, etc) have not been available for frozen soils.

MATERIALS, SAMPLE PREPARATION, EQUIPMENT, AND TESTING PROCEDURES

3.1. Materials

Uniform soil samples were needed to examine the displacement behavior of model piles embedded in the frozen soil. Local differences within a frozen soil sample could, for a period of time, change a pile's displacement rate and distort data collected during that period. Comparisons of individual tests were more meaningful when samples were closely similar. Sand was used to produce uniform samples because it was not prone to develop ice lens during freezing, its unfrozen water content varied little, and its gradation could be controlled. Sand was also a good choice because it is commonly used in slurries that are frozen around field piles. A commercial washed silica sand (from Unimin Corporation, Oregon, Illinois) with subangular particles of specific gravity at 2.65, a gradation between 0.075 mm and 0.840 mm, and a D_{50} of 0.40 mm was readily available. Some samples used only that sand portion between 0.420 mm and 0.590 mm to improve local gradation control throughout each sample. Distilled water was used for all saturated frozen sand samples and all ice samples to reduce adfreeze bond variability due to water impurities (Alwahab, 1983).

The model piles needed to be stiff, strong, and have a constant surface roughness. The roughness of corrugated field piles (Thomas and Luscher, 1980) was simulated by

adding oversize protrusions, called lugs, to relatively smooth 9.52 mm diameter steel rods as shown in Figure 3.1. Lug heights ranged from 0.76 mm to 3.18 mm. Another surface roughness type tested used U.S. standard screw threads, fine (24 per inch) and coarse (16 per inch), machined into a 9.52 mm diameter steel rod. A variation of 72 threads per inch was specially cut into a third 9.52 mm diameter steel rod.

3.2. Sample Preparation

Density, freezing method, lateral stress on the pile, boundary interference with the pile, and pile alignment all influenced loaded pile behavior. Sample preparation methods which controlled these factors were developed and refined to provide closely similar samples.

A split mold was first clamped around the soil restraint plate. The lugged piles were cleaned using longitudinal strokes with a #400 (for metal) sandpaper followed by wiping the pile surface to a dull shine with a paper towel. A wire brush was used to dislodge any clinging materials from the threaded piles before wiping. Each model pile was then placed through a hole in the restraint plate, braced at its ends in a position normal to the plate, and sealed into this hole with a pliable putty. In some cases, plastic tubing was used to cover part of the pile. After the sample was frozen, this tubing was removed

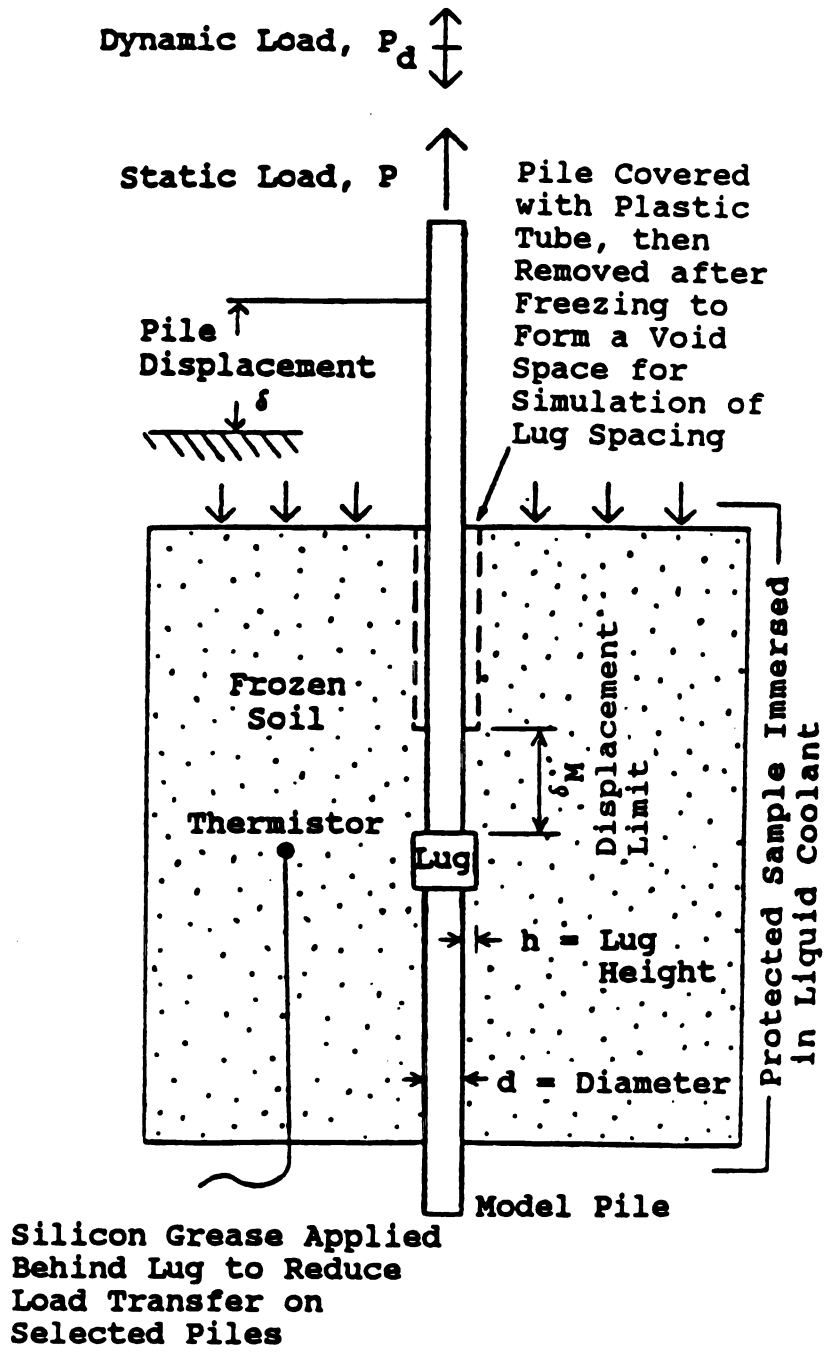

Figure 3.1. Model pile embedded in frozen sand. Lug provides controlled surface roughness.

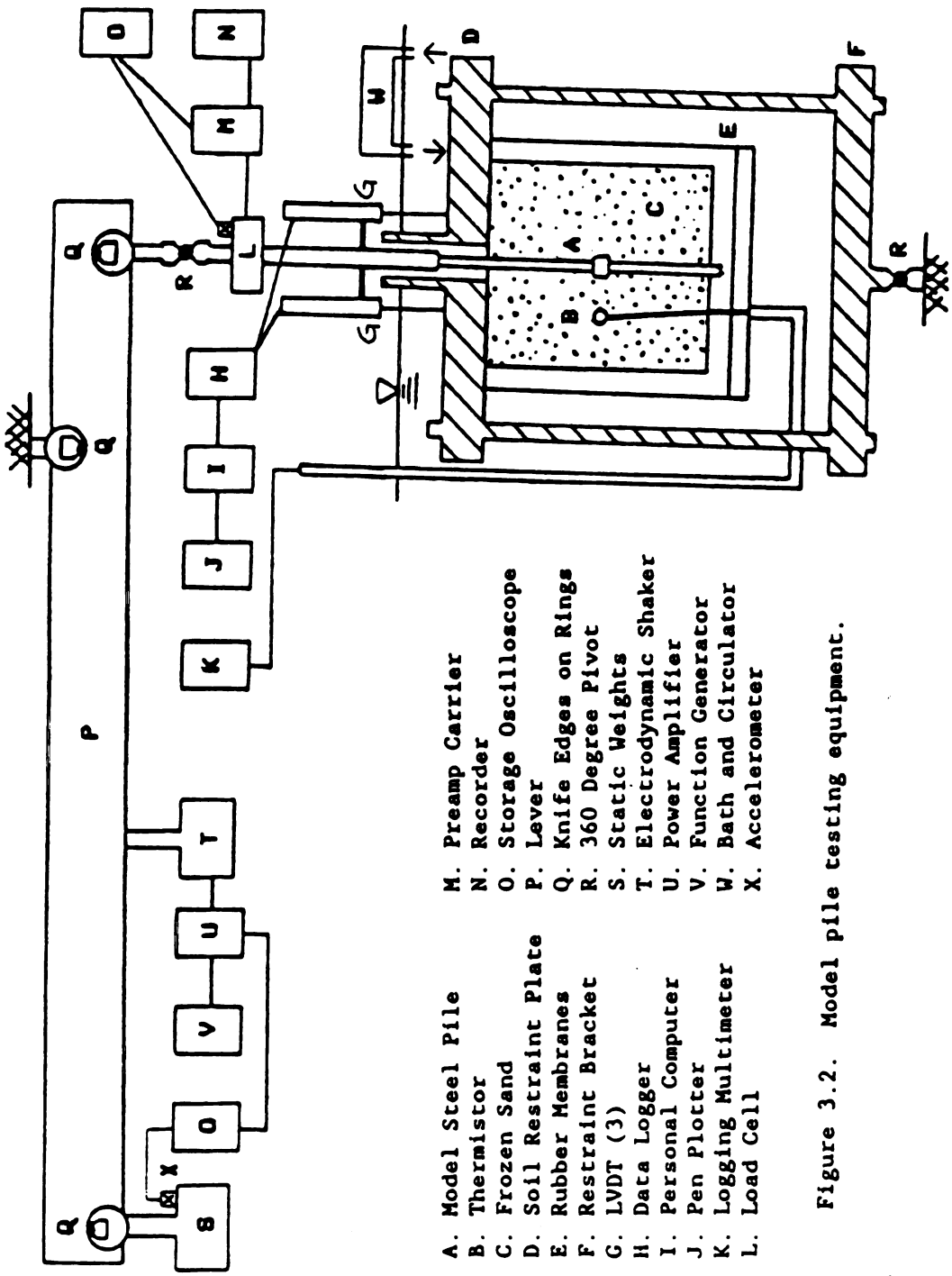

Figure 3.2. Model pile testing equipment.

to leave a void (with a diameter equal to that of the lug) ahead of the lug as shown in Figure 3.1. A thermistor was braced at a position within the mold that would avoid interference with sand displacement mechanisms involved with movement of the model pile, yet provide representative temperatures along the embedded model pile. The mold edges were sealed with pliable putty before placing the sample mold assembly in a top-opening freezer (Sears Kenmore 15) to chill at -14 deg C.

A layer of water was then placed into the mold. Sand was slowly poured from a small funnel through the standing water to settle lightly on the surface of the accumulating particles. As the sand's top surface increased within the mold, water was added as needed to maintain a level above the sand. Periodic tapping on the sides of the mold served to increase the density of some samples. The average solid volume fraction for loose sand was 0.58 and for dense sand samples was 0.64. The average ice matrix density for these samples was 0.89 Mg/m^3. These values are shown for each individual sample in Appendix B.

A different procedure was used to fill the mold for preparation of polycrystalline ice samples. Pans of distilled water were first frozen, then broken into pieces, and passed thru a chilled food processor (Cusinart). The finely chopped ice (average particle size approximately 1 mm) was sprinkled into a 1 cm layer of chilled water (near

0 deg C). After this water layer was saturated with ice particles, the mixture was stirred slowly to evenly distribute the ice particles and release any trapped air bubbles. Another 1 cm layer of chilled water was then slowly added to repeat this process until the mold was sufficiently filled. After insulating the mold (described in the next paragraph), chilled water would freeze around the ice particles to form a polycrystalline ice sample. The average ice density of these samples was 0.90 Mg/m^3. These procedures were followed for both ice and sand/ice samples.

To encourage longitudinal freezing along the pile axis and minimize lateral pile pressures due to freezing of trapped water, insulation was added around the mold so that the top was more heavily insulated than the sides. The bottom was uninsulated and left open to the -14 deg C freezer temperature. After 24 hours, the excess ice or frozen sand was scraped away from the frozen sample and the split mold halves were removed. The frozen sand was suspended below the reaction plate by adfreeze bonds with the model pile. Triple rubber membranes were placed around the sample to protect it from the ethylene glycol-water coolant and to help minimize effects of small temperature changes of the surrounding coolant. Open ends of these membranes were sealed with gaskets and hose clamps to the soil restraint plate and a lower circular plate. This

effectively sealed the bottom section of the pile and sample from the coolant. A small plastic tube, sealed into a hole thru the lower circular plate, allowed a thermistor lead wire to pass outside of the coolant tank.

The model pile, solidly frozen into the sample, extended through a hole in the soil restraint plate. A rubber hose, placed over this end of the model pile, was clamped to the soil restraint plate. The open end of this hose will later rise above the liquid coolant to allow the protruding pile end to be attached to the loading system. The hose protects the upper section of the pile (and sample) from the coolant while offering no restriction to pile movement.

The putty that sealed the opening between the 9.52 mm diameter pile and the 17.5 mm hole in the soil restraint plate during sample preparation was left in position because it remained pliable at test temperatures, offered little resistance to pile movement, and protected the frozen sample from small coolant leaks. Earlier tests with frozen sand samples under similar conditions showed no appreciable influence from the restraint plate (Alwahab, 1983) for a lugged pile, centered in a 152 mm by 152 mm sand sample. Preliminary tests during this study, using threaded piles in ice samples, showed no apparent change in pile behavior when additional putty was used to create a larger unsupported section at the restraint plate.

3.3. Temperature Control Equipment

The prepared sample was then transferred to a well insulated 58 liter coolant tank and attached to a restraint frame that could pivot in all directions (within limits) on a 31 kN capacity bearing (a Spherco rod end). The ethylene glycol-water coolant, colder than the test temperature, was then supplied by a circulating coolant bath (Forma Scientific 2425 Bath and Circulator) to fill the tank and quickly chill the testing equipment within the tank. The coolant bath was then adjusted to the warmer test temperature. Inflow from the coolant bath, colder than the outflow from the tank, was directed onto the top of the soil restraint plate to produce, as shown by preliminary tests (based on up to 6 internal sample temperature measurements), a nearly uniform temperature gradient along the pile's length.

The wire lead to the sample thermistor (Fenwal Electronics UUA35J84) was connected to a digital data logger (Hewlett-Packard 3467A Logging Multimeter). The internal sample temperature was checked to determine when coolant bath adjustments were needed. The thermistor had been calibrated earlier in an ice bath and had an accuracy of $\pm$ 0.1 deg C. The laboratory room temperature was maintained near constant to assist the coolant bath's temperature control.

3.4. Displacement Measurement Equipment

With the frozen soil and model pile in position and the coolant flow established, supports for the Linear Variable Displacement Transducers (Schaevitz 1000 HR-DC and 3000 HR-DC) were attached, through stiff connections, to the model pile. One or two LVDT's were used in earlier tests, but three LVDT's were used in later tests for greater measurement precision. These stiff connections minimized strains or displacements not associated with pile movement through the soil. Displacement was measured between the LVDT supports and the soil restraint plate.

The LVDT's were remotely powered by a DC source (Sola Electric 24VDC1.2A) and their resulting DC output was read and digitized by a data logger (Doric Minitrend 205). Earlier, each LVDT and the data logger had been carefully calibrated to $\pm$ 0.003 mm by a LVDT micrometer (Schavitz), Because of the relatively slow data logger response (approximately 1 second) measurements of cyclic displacements due to dynamic loading could not be directly recorded. The data recorded during these periods represents a sampling of the displacement data that could later be averaged. The digitized signals and their respective times were recorded by a personal computer (Hewlett-Packard 85B) on magnetic tapes. The recorded signals would later be run through a short program and plotted on a pen plotter (Hewlett-Packard 7470A).

Since automated data recording allowed a great number of data points to be collected, a simple data plotting program was used to connect consecutively recorded data points. Some graphs will appear as "stair steps" because the data, plotted point to point, was recorded at the limit of displacement transducer sensitivity. Gaps may appear in some curves between data files or when data was lost. Electrical interference caused some scatter of the plotted data recorded during precise measurements of threaded pile movement. Continuous recording at equal time intervals would have facilitated best fit curve plots and is recommended for future work.

3.5. Pile Loading and Load Measurement Equipment

Stiff connections, above the LVDT supports, were added to connect the 4.45 kN capacity load cell (Strainsert FL1U-2SGKT). This load cell was remotely powered (Sanborn 8805A Preamp Carrier) and its DC output was read from a strip chart recorder (Hewlett-Packard 7702B Recorder) or from the screen of a storage oscilloscope (Techtronix 564). Cyclic loading at 10 Hz was more accurately measured by the oscilloscope. The load cell, preamp carrier, recorder, and oscilloscope were calibrated together on a separate load frame using known weights.

A second pivoting connection was added above the load cell to connect the lever loading arm and to minimize

eccentric loading from this lever (Figure 3.2). Knife-edge type connections were used at the ends and fulcrum of this lever to minimize friction and maintain a nearly constant mechanical advantage of 4 times the static weight on the model pile. The static load weights and holder (suspended on a knife-edge connection) were temporarily supported by a hydraulic jack until testing began.

The electrodynamic shaker (APS 113) was connected to the lever arm so that 2 times the shaker force was added to the pile's static load. During some tests, the shaker was connected directly over the model pile in order to provide better-formed force waves. The pin-type connection between the shaker armature and the lever was rigid yet could rotate as the lever moved. This small amount of lever arm movement did not alter the dynamic force magnitude significantly during pile tests. A function generator (Zenith SG-1271) signaled waveform, frequency, and amplitude to the shaker's power amplifier (APS 114) which in turn supplied controlled power to the shaker. During some tests, an accelerometer (PCB 308B) was used to check the frequency and magnitude of accelerations at various locations on the loading system.

3.6. Testing Procedures

Once all connections were made and coolant flow was established, the coolant tank top was heavily insulated. A

very small load was applied (lever self weight) to bring all system connections into contact and check the load system alignment. Pivoting connections above and below the sample appeared to remove almost all eccentric loads from the pile. Force, temperature and displacement measurements were started and rechecked during a 18 hour waiting period. Consistant use of this waiting period, before adding test loads to the pile, was thought to stabilize temperatures and allow lateral pile pressures to diminish to similar levels. After checking the recording systems, the reaction force from static weights and their holder were slowly lowered onto the lever arm by the hydraulic jack to begin a pile test.

3.7. Model Pile Loading Procedures

Three different pile loading sequences were used to study the model pile's behavior. For the first case, load was maintained constant throughout the test as shown for a typical full duration load sequence labeled P_3, P_4, and P_5 in Fig. 3.3. Small variations in temperature, sand density, pile alignment, and other physical conditions altered pile displacement rates and made direct comparisons between full duration load tests less certain. Case P_2' and P_1'' (before load increase) were considered as full duration loads up until additional loads were added.

For the second sequence, loads were increased after

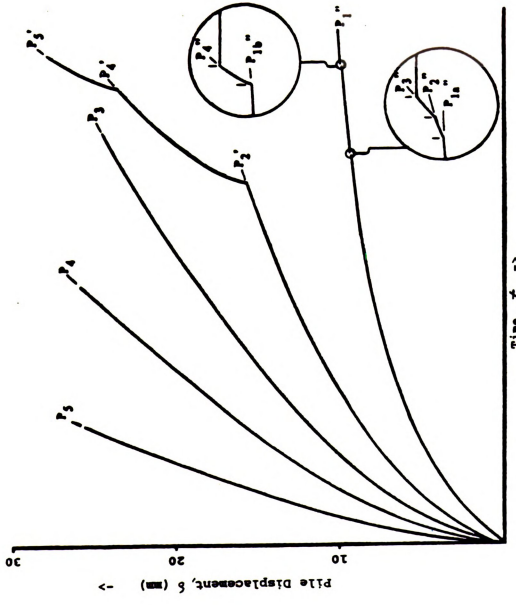

Figure 3.3. Typical model pile displacement curves.

periods of displacement as in the typical step loads labeled P_4', and P_5' in Fig. 3.3. Slight physical variations within samples effected comparisons between step loads. Step loads added after pile displacement rates reached nearly constant values appeared to yield more consistent results.

For the third sequence, a constant load was maintained until a nearly constant pile displacement rate was achieved. The load was next increased for a short duration, then reduced to its initial value. A nearly constant pile displacement rate was allowed to return before the next load increase. A short duration load is shown as P_4'' in Fig 3.3. The displacement rate resulting from a short duration load increase was compared to the displacement rate immediately before the short duration loading. This comparison normalizes the effect of physical variables and total pile displacement on pile displacement rates. Parameswaren (1984) used a similar technique to measure the effect of dynamic loading on a constantly-displacing model pile frozen in soil.

In a variation of the short duration loading sequence, more than one short duration load was added in succession (as shown by P_2'' and P_3'' in Fig. 3.3) before the load was reduced to its initial value. These multiple-short duration loads have the same advantages of the single loads and provide additional data.

3.8. Displacement-Time Data Plotting Techniques

To examine and emphasize data obtained during periods of nearly constant displacement rates, log (displacement) - log (time) plots were started at different points along the pile displacement. When similar (displacement) starting points were used to plot data for different tests, the creep curves could be compared. Three types of starting points will be described.

Point A on the linear displacement - linear time insert of Fig. 3.4 represents the initial time and initial displacement for a load increase on a model pile. The selection of an A-type starting point will affect the linearity of the initial portion of a log (displacement) - log (time) plot. Small data inconsistencies, such as elastic deformations and system seating errors, distort the initial portions of these plots.

Point C (Figure 3.4, insert) represents a data point at displacement $\Delta\delta_C$ after a load increase. Pile displacement data for different tests may be more closely compared when their data plots are started after a given displacement with a C-type starting point. As the curves approached nearly steady state conditions (after $\Delta\delta_C$ displacement), the variation of Δt_C between curves becomes less important. Typical log (displacement) - log (time) curves P_3, P_4, and P_5 (Fig. 3.4) are full duration loads (also shown in Fig. 3.3 by curves P_3, P_4, & P_5) with C-type initial points after

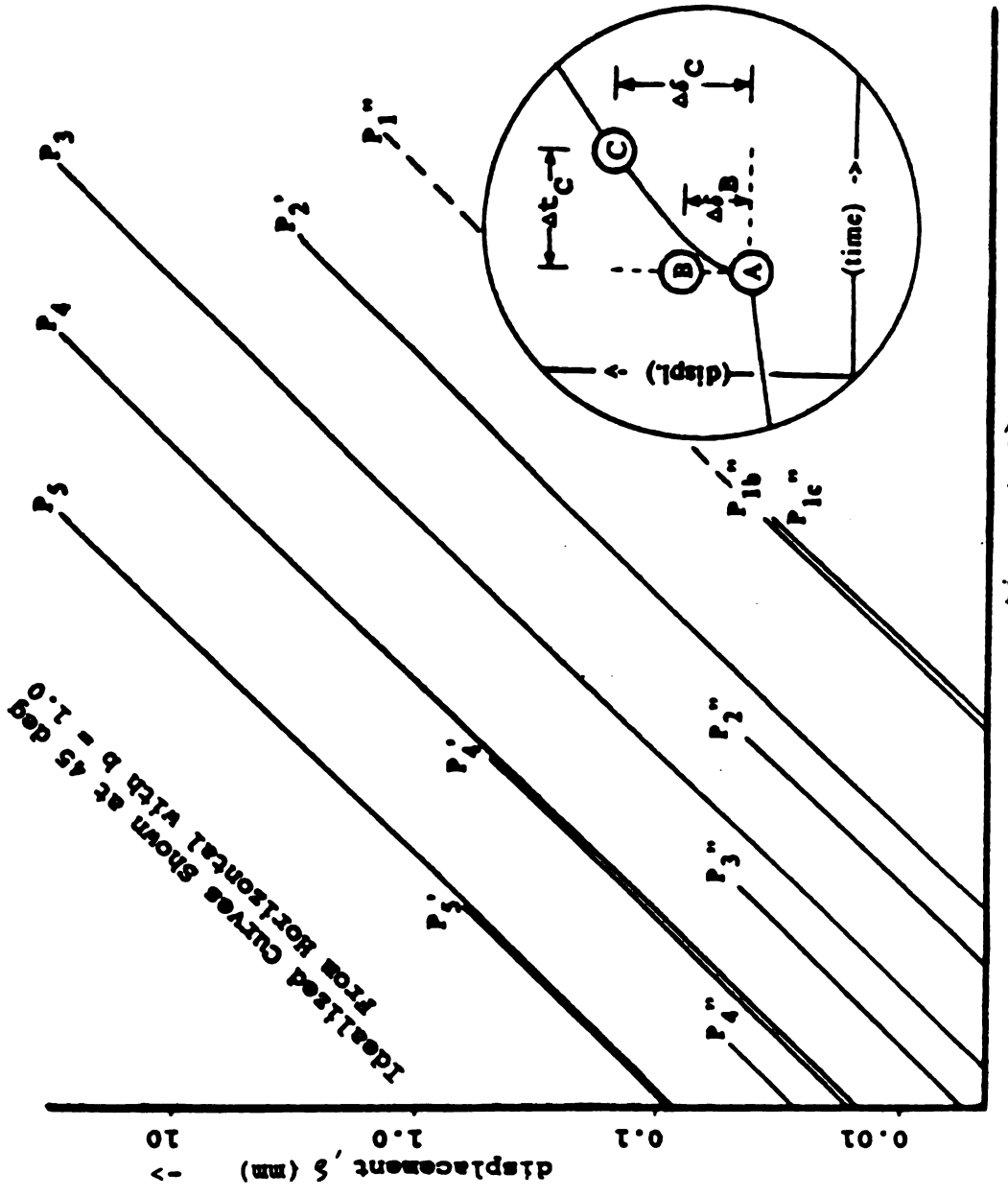

Figure 3.4. Typical log(time)-log(displacement) curves for model pile movement in frozen sand.

a given displacement. Curves P_4' and P_5' of Fig. 3.4 (also shown in Fig. 3.3 as P_4' and P_5') represent step loads plotted with C-type initial points.

Point B (Fig. 3.4, insert) remains at the initial time of load increase but is $\Delta\delta_B$ (a given displacement) after the increase. To compare load increases with a B-type starting point, a value of $\Delta\delta_B$ was arbitrarily chosen to produce the most linear, most parallel log (displacement) - log (time) curves as idealized by P_2'', P_3'', and P_4'' of Fig. 3.4 (also shown in Fig. 3.3 as P_2'', P_3'', and P_4''). The 2 curves labeled P_1'' (Fig. 3.4) use a C-type beginning at a time and displacement just before the short duration loads were added. The ratio of short duration load, P_4'' and the initial load, P_{1_b}'' may be compared with other short-duration/initial-load ratios or it may be used in equation 3.4. The multiple-short duration loads P_2'' and P_3'' may be directly compared using equation 3.4.

3.9. Determination of Pile Settlement Equation Parameters

Pile displacement - time equations, similar to the primary creep equations given by Ladanyi and Johntson (1974), can be written as

$$\delta = \left[\frac{\dot{\delta}_c}{b}\right]^b \left[\frac{P}{P_c}\right]^n t^b \qquad (3.1)$$

where δ is pile displacement, P is load, $\dot{\delta}_c$ is an arbitrary

displacement rate corresponding to a proof load P_c, t is time, n and b are exponents in the creep equation. These equation parameters may be determined graphically as in Figure 3.5.

Differentiating Eq. 3.1 with respect to time gives

$$\dot{\delta} = [\frac{\dot{\delta}_c}{b}]^b \quad [\frac{P}{P_c}]^n \quad bt^{(b-1)} \tag{3.2}$$

where $\dot{\delta}$ is the pile displacement rate. Taking a ratio of 2 displacement rates, as described by equation 3.2, gives

$$\frac{\dot{\delta}_2}{\dot{\delta}_1} = [\frac{P_2}{P_1}]^n \quad [\frac{t_2}{t_1}]^{(b-1)} \tag{3.3}$$

For $t_2 = t_1$ and/or $b = 1$, equation 3.3 reduces to

$$\frac{\dot{\delta}_2}{\dot{\delta}_1} = [\frac{P_2}{P_1}]^n \tag{3.4}$$

When displacement rates are nearly constant, $b = 1$ can be assumed. Using n determined by equation 3.4 and assuming $b = 1$, a value for $\dot{\delta}_c$ can be arbitrarily chosen and P_c may be determined.

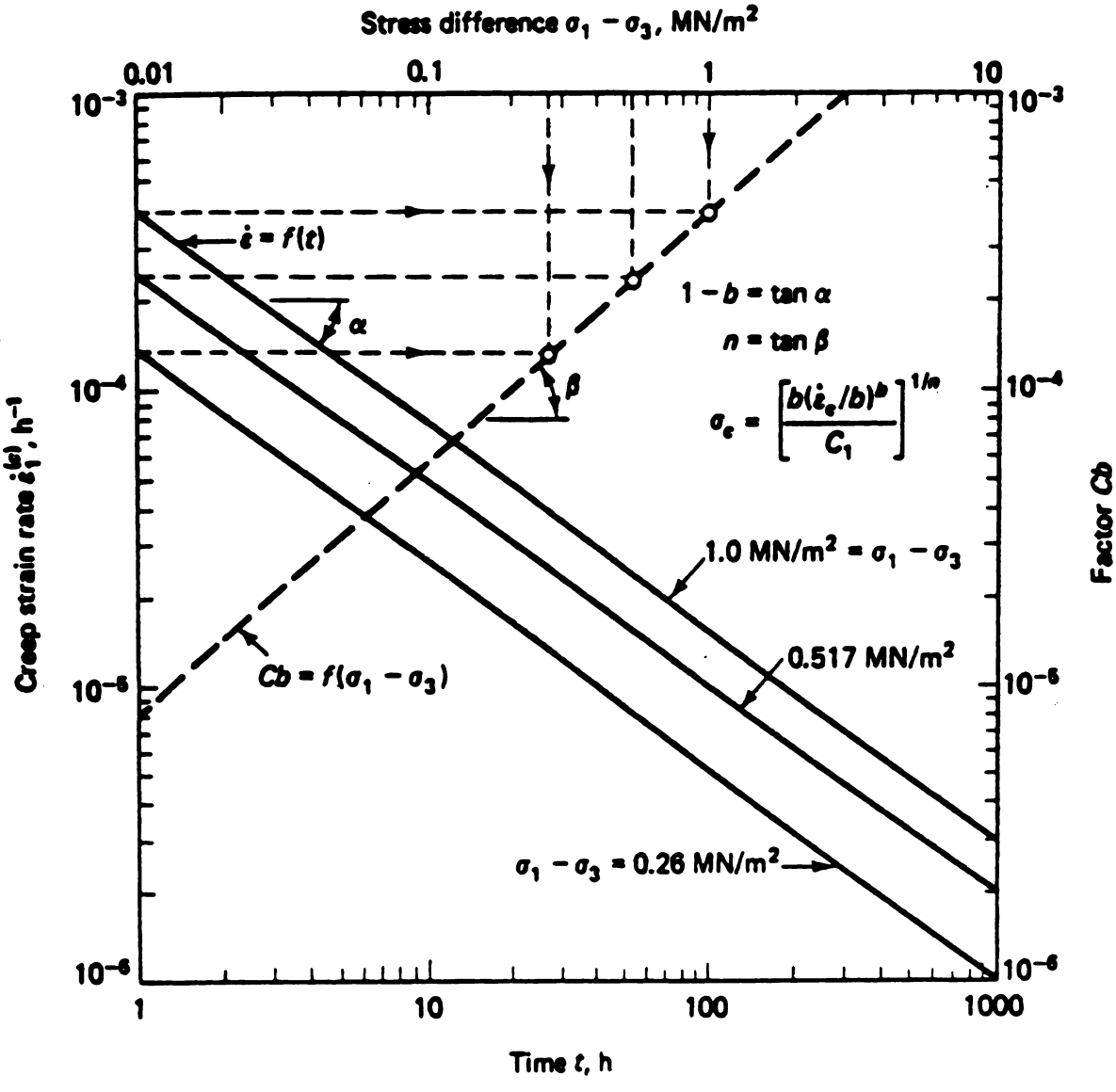

Figure 3.5. Primary-creep parameters from time-creep-strain data. (after Andersland, et al. 1978).

EXPERIMENTAL RESULTS

Prediction of pile settlement due to superimposed cyclic loads first required information on pile behavior under constant loads and after static load increases. The results from static load tests on various model piles provided examples of typical model pile performance. Use of new interpretation techniques with time versus displacement data allowed detailed analysis of this pile behavior. These techniques also provided a better understanding of pile displacement rate increases from static load increases. With this knowledge of static pile behavior, changes due to cyclic loads for various load magnitudes and frequencies could be studied. Comparisons between static load increases and superimposed cyclic loads allowed the effects of cyclic load variables (frequency and magnitude) to be quantified.

4.1 Sample Inspection After Testing

The frozen soil and model piles were examined after each test for contamination, sample imperfections and information on soil-pile interaction. Shallow grooves cut parallel to the model pile on opposite sides of the frozen soil allowed the sample to be split cleanly into 2 parts.

Changes in color and the presence of crushed particles in front of the lug were noted in the otherwise uniformly-

colored, uniformly-graded sand. The compacted sand and ice formed a wedge with close to a 45 deg angle in front of the lug. An open void always formed behind the lug after pile displacement thru frozen sand and ice. This void, although impossible to measure precisely because of sample disturbance during equipment disassembly, was nearly equal to the pile displacement measured during the test. Almost all pile displacement resulted from relative movement between the pile and the surrounding frozen soil.

When a void, created ahead of a lug, was used to simulate one lug in a series of lugs (Figure 3.1), a cylinder of frozen sand was sheared off and pushed ahead of this lug before the lug reached the void. Pile displacement rates increased just before this failure in shear. The outside diameter of this cylinder of sand equalled the lug diameter, the inside diameter equalled the pile shaft diameter, and the length was observed to be slightly less than the displacement remaining at the start of pile failure. For example, all 0.79 mm height lugs tested in this manner were observed with 4 to 6 mm frozen soil pushed ahead of their lugs while 8 to 17 mm was pushed ahead of the 3.18 mm height lugs. These cylinder lengths are given for each sample in Appendix B.

A void was also observed after pile displacement through polycrystalline ice samples. A white, possibly crushed ice zone (vs clear for undisturbed ice) was found

ahead of the lug. In regions where rapid lug displacement had occured, the white zones extended radially outward into the sample suggesting a larger fracture zone.

Changes in sand color and the presence of some crushed particles were found along the length of threaded rods frozen in sand. Some particles remained wedged between the threads but between many threads only bits of ice were found. The slip surface occured at the outer edge of the pile threads. A number of loose sand grains were found between the pile and the adjacent discolored sand/ice solid.

The threaded-rod/polycrystalline-ice samples showed a white zone along the length of the pile at the pile/ice interface. The slip surface occured between the inner edge of this zone and the outer edge of the pile threads. It was common to find ice, initially frozen between two threads, had been displaced so that only a fraction of it remained wedged between ice slip surface and the top of the trailing lug.

It appears that pressure melting of ice, movement of unfrozen water to adjacent areas with lower pressures, and refreezing describes part of the process responsible for pile creep displacements.

4.2 Full Duration Loads on Lugged Model Piles

Full duration loads on lugged model piles frozen in

loose sand are shown in Figure 4.1. A void space, beginning at 25.4 mm ahead of the pile lug's leading edge and equal in diameter to the lug, limited the amount of direct pile to frozen sand contact area and served to simulate the condition of one lug in a series of lugs. Limiting the lug displacement in this way caused these piles to increase their displacement rates and begin to fail after 8 to 9 mm of total displacement. Little or no secondary creep (constant displacement) was observed during these pile load tests. Plotting the test data with log(displacement)-log(time) coordinates usually transformed these results into relatively straight lines that were overly effected by small aborations during initial pile displacements. Starting each pile test plot after a given displacement reduced plot variations and provided better comparisons between pile test results.

Various C-type starting points (Figure 3.4) have been used in plots of a single pile test in Figures 4.2a, 4.2b, and 4.2c (Pile Tests #105, #114, and #111 respectively). The differences between the 0 mm and the 1 mm C-type starting point plots in these figures are apparent. Changes are smaller between larger C-type starting point plots (such as 4.75 mm and the 6.00 mm C-type starting point plots) shown in figures 4.2b and 4.2c. The displacement rates of these piles are clearly displacement dependent.

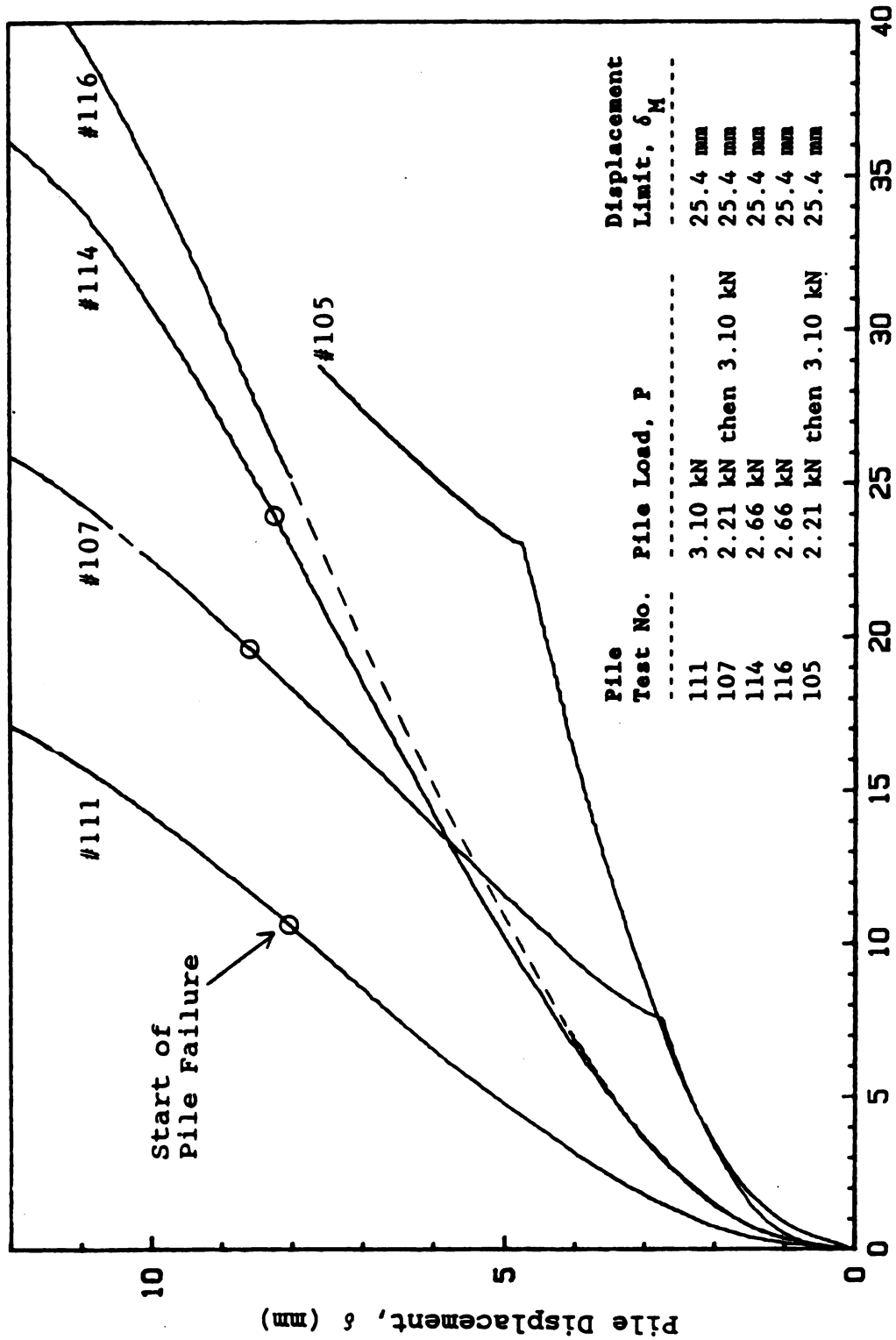

Figure 4.1. Time-displacement curves for model steel piles with 3.18 mm lug heights in frozen sand.

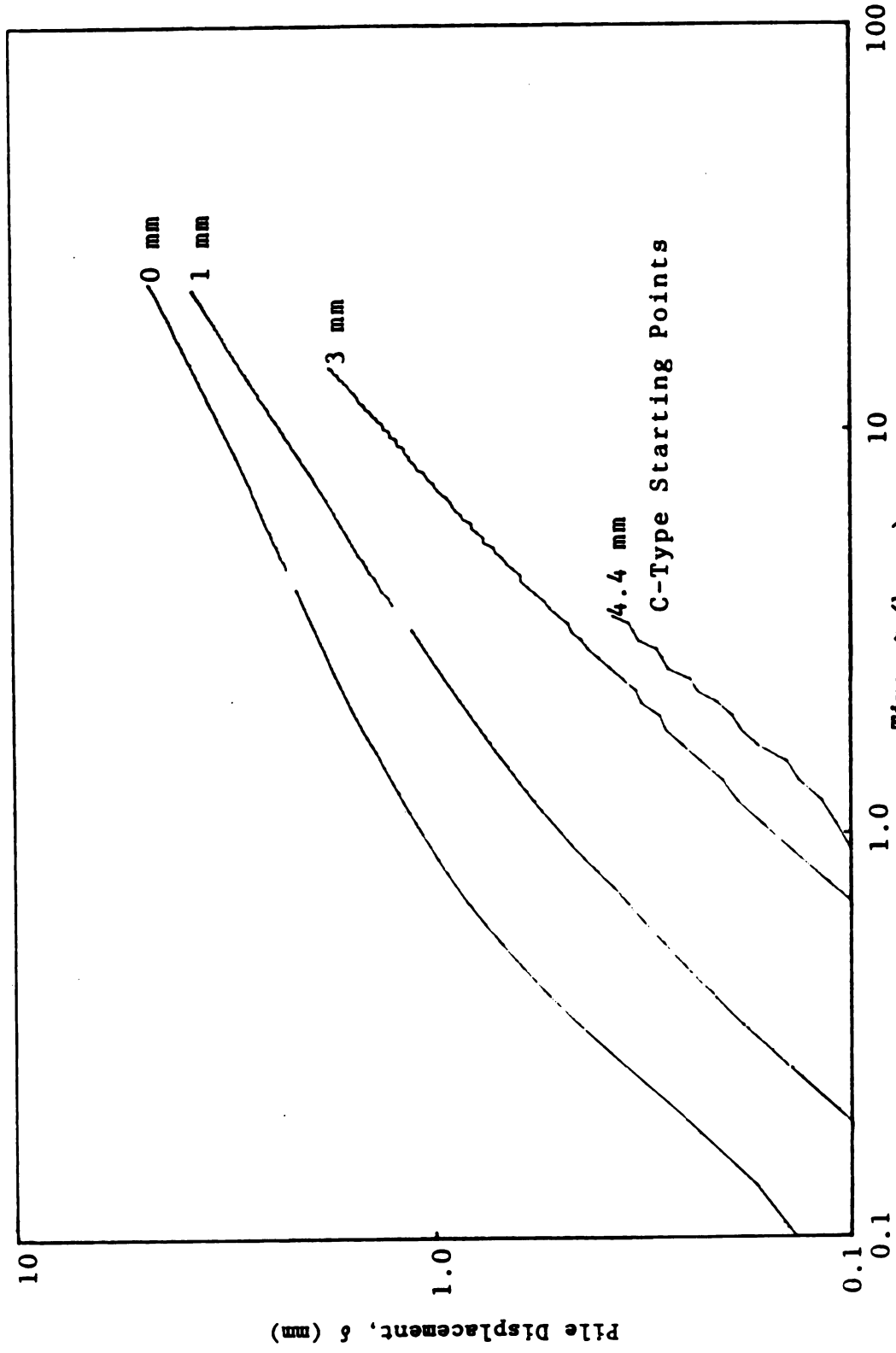

Figure 4.2. Log(time)-log(displacement) curves for a pile test using various C-type starting points. (a) Test #105.

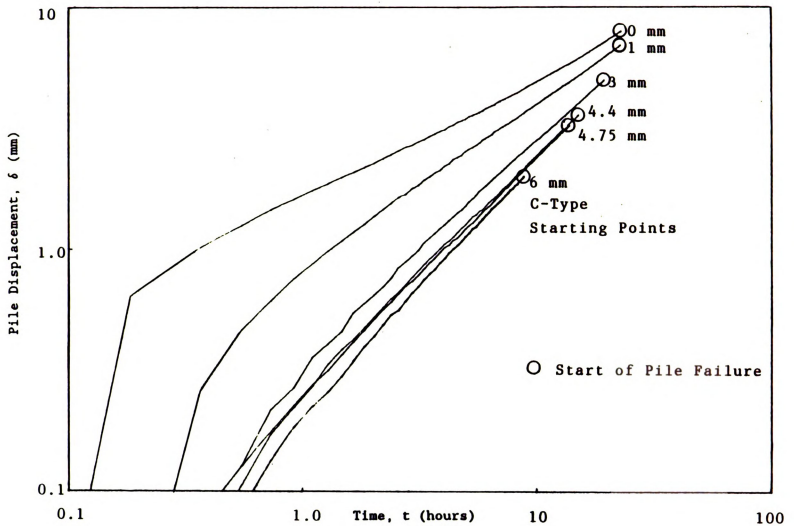

Figure 4.2b. Log(time)-log(displacement) curves for Test #114 with various starting points.

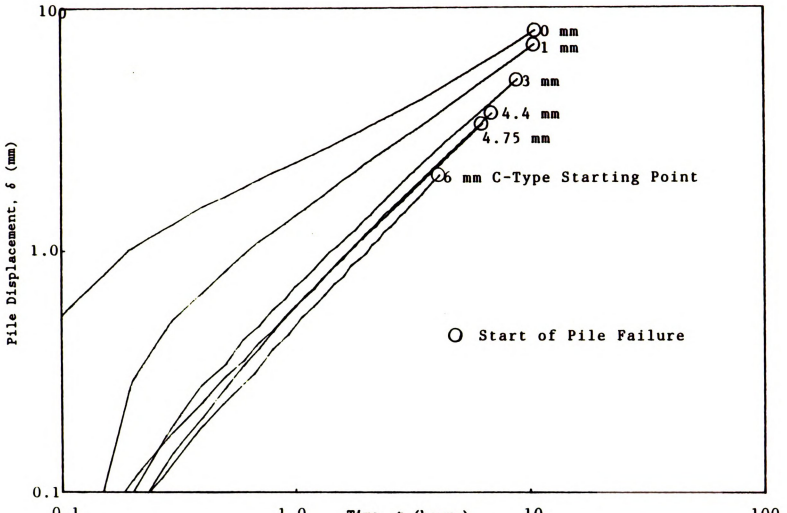

Figure 4.2c. Log(time)-log(displacement) curves for Test #111 with various starting points.

Pile Tests #105, #114, and #111, plotted with equal C-type starting points, are shown in Figures 4.3a through 4.3e. The beginning portions of these curves, (particularly the 0 mm starting point curves in Figure 4.3a) are sometimes erratic as shown by the high sensitivity of the log coordinate system at its lower end. This portion of each curve (the initial 1 mm or less) was neglected when fitting parallel straight-lines for each group of curves shown in Figures 4.3a through 4.3e.

Parallel straight-line-approximations can then be treated, as Andersland et al. (1978) did with unconfined compression of frozen soils shown in Figure 3.5, to determine the material creep parameter b (dimensionless), n (dimensionless), and σ_c (proof compression stress at an arbitrarily chosen strain rate $\dot{\varepsilon}_c$). Since pile loads will be analyzed instead of compression stresses, P_c (model pile proof load) is substituted for σ_c and $\dot{\delta}_c$ (arbitrary reference pile displacement rate) for $\dot{\varepsilon}_c$ as shown on Figures 4.3a through 4.3c.

These parameters can then be used in the pile creep equation (3.1)

$$\delta = (\dot{\delta}_c / b)^b \ (P / P_c)^n \ t^b \qquad (3.1)$$

to predict pile displacement. Note that creep equation parameters derived from curves with C-type starting points other than 0 mm, can only predict pile displacement beyond

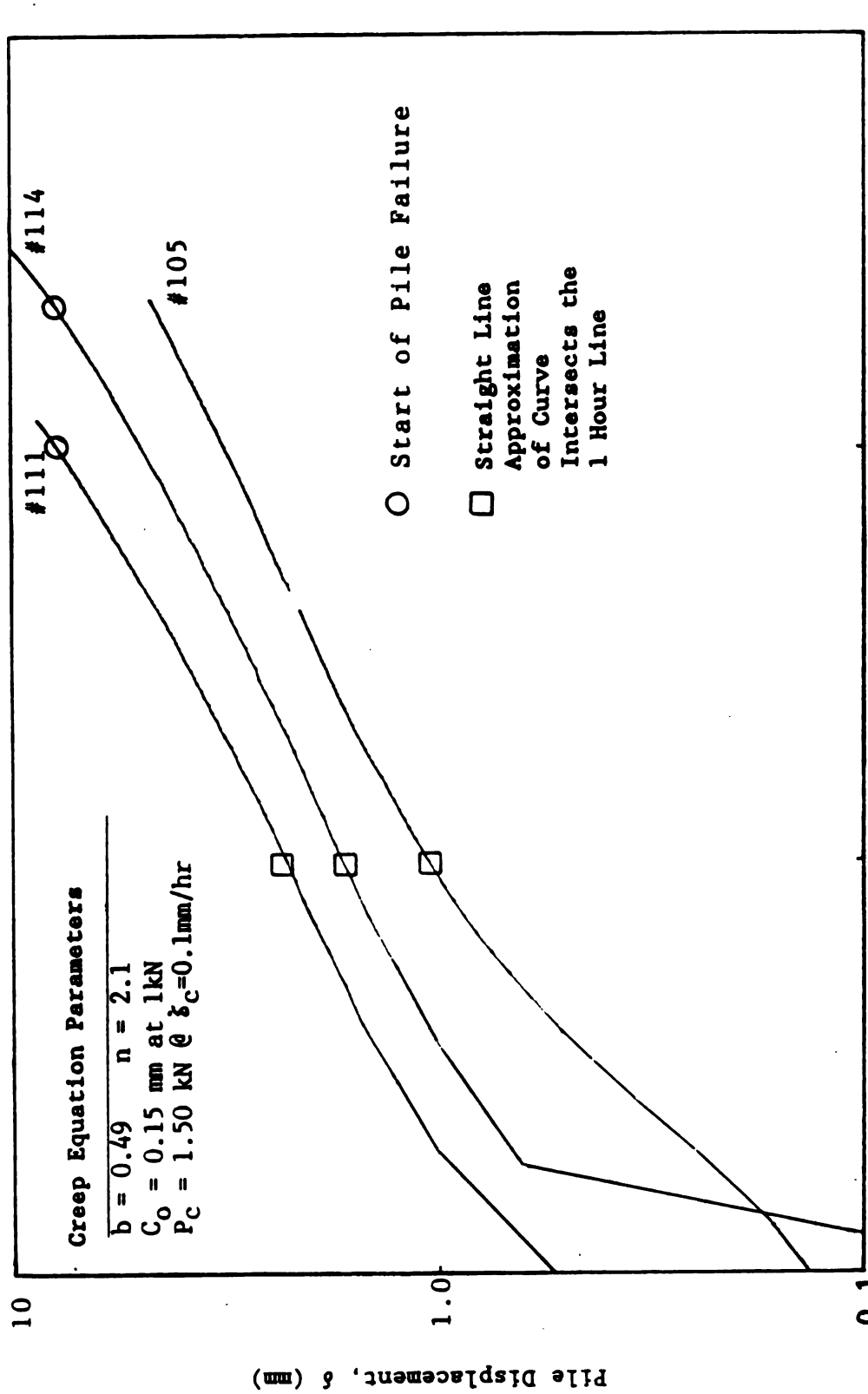

Figure 4.3. Time-displacement curves for model piles with 3.18 mm lug heights in frozen sand @ -3 • C and 25.4 mm displacement limits. (a) With 0 mm C-type starting points.

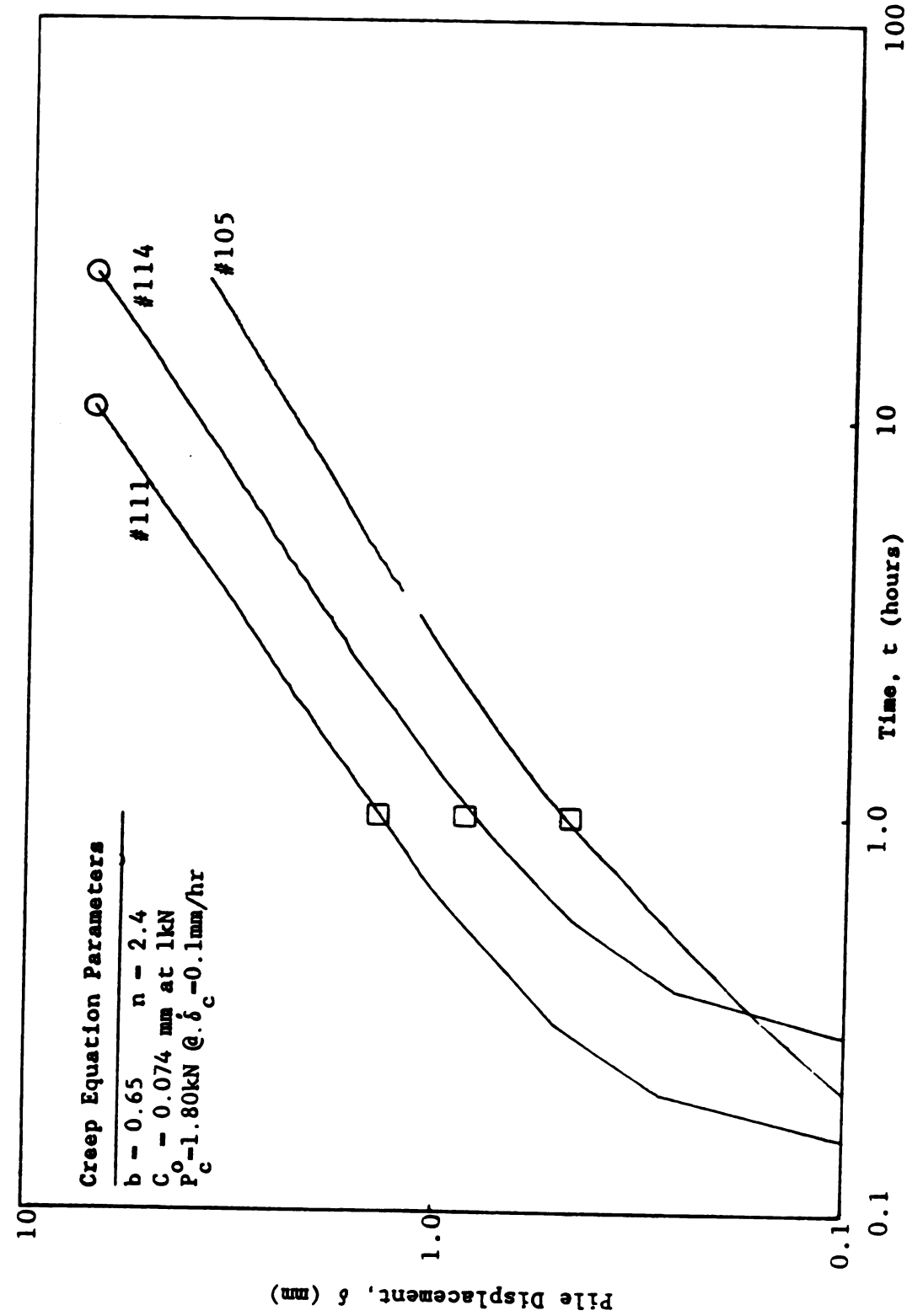

Figure 4.3b. With 1 mm C-type starting points.

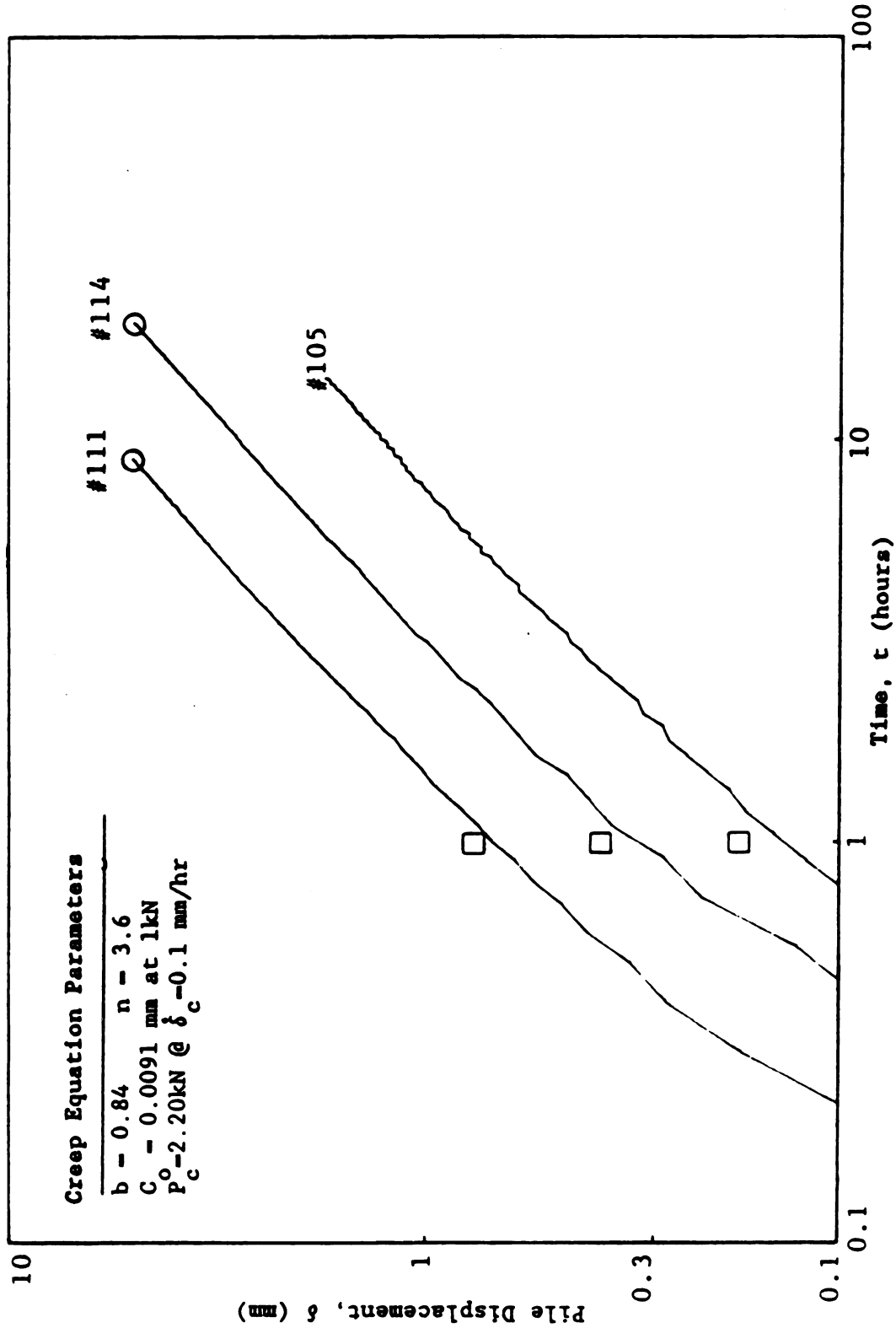

Figure 4.3c. With 3 mm C-type starting points.

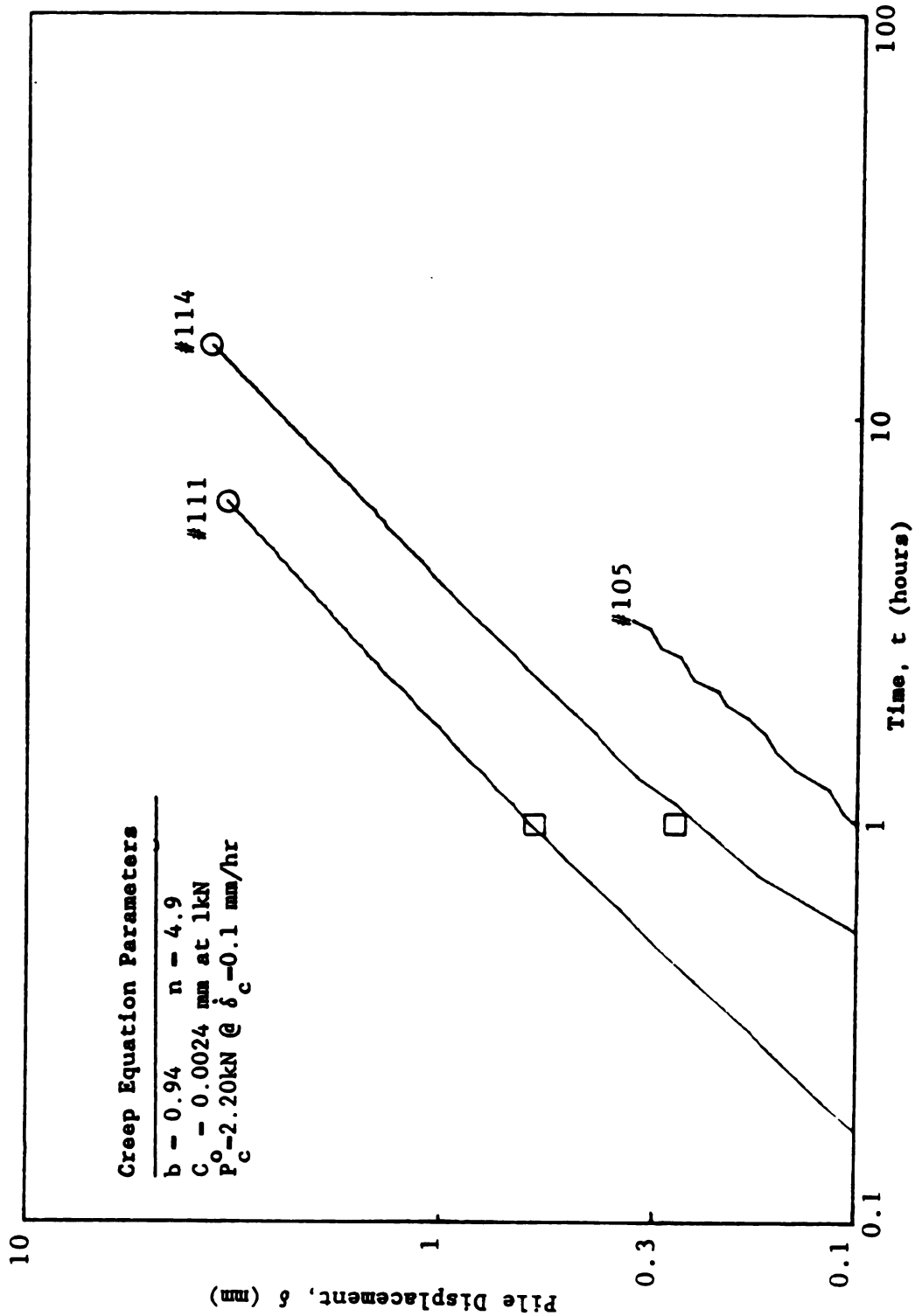

Figure 4.3d. With 4.4 mm C-type starting points.

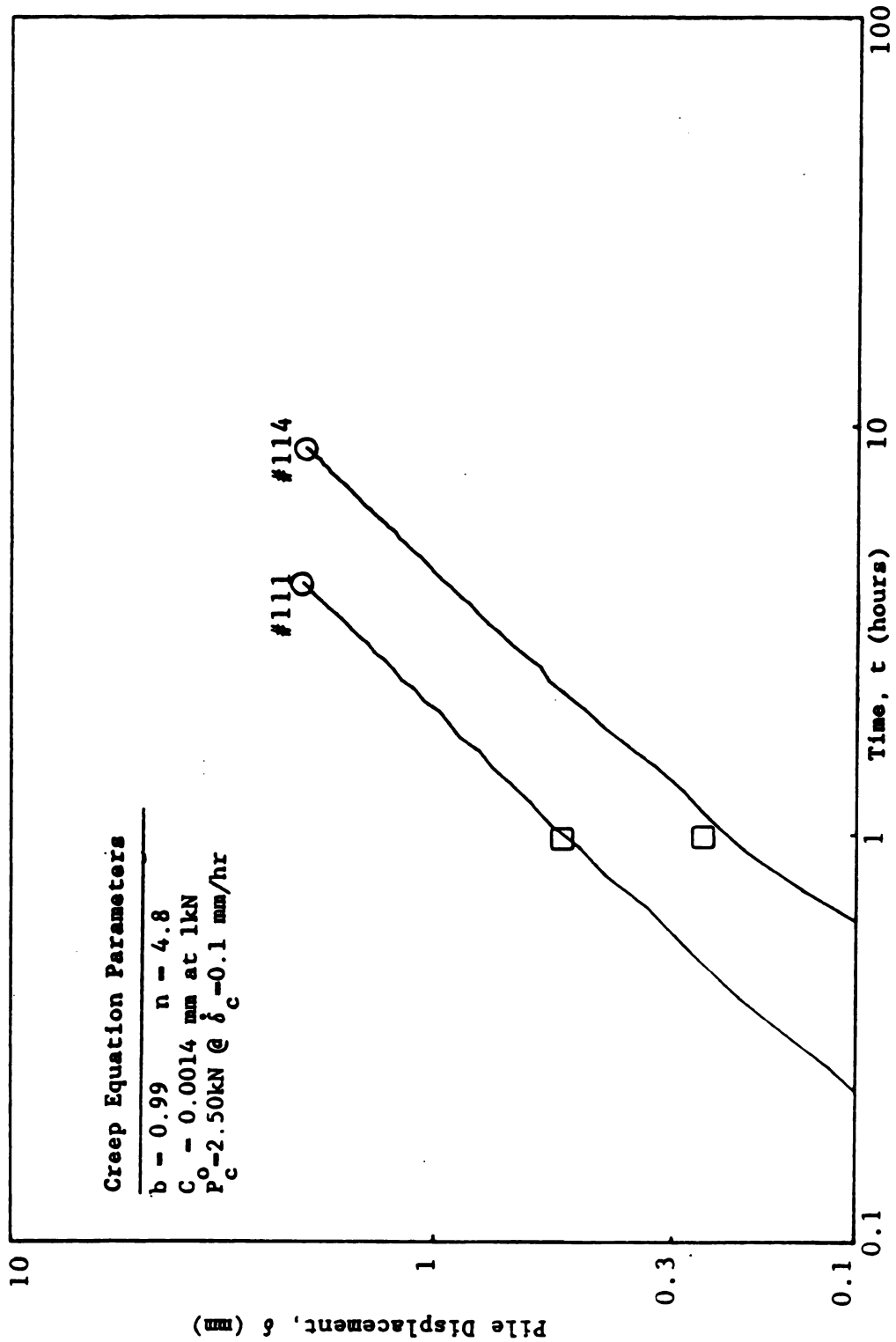

Figure 4.3e. With 6 mm C-type starting points.

their respective starting points. However, the parameters obtained from curves started at C-type points other than 0 mm can be used to compare pile types, soil types, and other test variables.

Full duration load tests for 6 model pile types are plotted with various C-type starting points in Appendix A. The creep parameters obtained from these figures are included with those from Figures 4.3a through 4.3e and are included in Table 4.1. At this time note that most model piles with C-type starting points of 3 mm and greater, have b values nearly equal to 1.0. Straight line approximations of these curves represent nearly constant displacement rates.

Full duration pile load tests demonstrate pile behavior and failure displacement in the most reliable manner, but are time consuming since more than one pile test is needed to describe general pile behavior. Adding incremental loads to a pile's initial load allows comparisons to be made during a single pile test.

4.3 Step Loads on Lugged Model Piles

Displacements for 2 similar piles, shown in Figure 4.1, are very similar to those in Figure 4.4. After a pile displacement of 2.75 mm, the pile load was increased during Pile Test #107. This same load increase was applied,after a pile displacement of 4.75 mm, to Pile Test #105 . In

Table 4.1. Creep Equation Parameters from Full Duration Tests of Lugged Piles.

Lug Size mm	Fig. No.	Avg. Embedment Ahead/Behind Lug mm / mm	C-type Start Pt. = 0 mm b	n	C_o mm &	P_c Kn &	C-type Start Pt. = 1 mm b	n	C_o mm &	P_c Kn &	C-type Start Pt. = 3 mm b	n	C_o mm &	P_c Kn &	C-type Start Pt. = 5 mm b	n	C_o mm &	P_c Kn &	C-type Start Pt. = 6 mm b	n	C_o mm &	P_c Kn &
0.79	A.15	76 / 63 @+	0.84	7.2	0.23	0.89	0.81	7.2	0.20	0.81	0.82	7.5	0.17	0.93					1.0	8.0	.10	1.00
	A.12	76 / 63 @*	0.50	5.6	0.30	1.08	0.67	7.4	0.088	1.17	0.94	15 ?	0.0021	1.31					1.0	17 ?	.00072	1.33
	A.10	24.1/ 61 @	0.73	5.5	0.78	0.80	0.86	6.3	0.48	0.84	0.97	7.2	0.28	0.88					1.0	7.4	0.22	0.90
1.59	A.8	76 / 63 @	0.54	3.6	0.13	1.38	0.73	5.5	0.014	1.66	0.97	7.0	0.0028	1.68	1.0	7.3	0.0019	1.72				
	A.6	25.4/ 64 @	0.56	4.4	0.16	1.21	0.73	5.6	0.053	1.30	0.81	6.1	0.027	1.37					0.92	6.8	0.012	1.42
	A.6	17.8/ 63 @	0.47	1.8	1.0	0.66	0.63	2.5	0.48	0.86	0.81	3.6	0.12	1.12					1.0	6.1	0.012	1.42
3.18	A.4	76 / 29 @	0.49	2.1	0.20	1.50	0.65	2.4	0.074	1.76	0.84	3.6	0.0091	2.21	0.96	4.0	0.0041	2.30				
	4.2	25.4/ 62 @	0.50	2.4	0.15	1.56	0.65	2.9	0.053	1.82	0.87	4.3	0.0058	2.13					0.98	5.0	0.0017	2.30
	A.2	19.0/ 62 @	0.47	2.8	0.10	1.76	0.65	4.0	0.015	2.11	1.0	5.7	0.0010	2.22								

& C_o measured at 1 KN, P_c determined from C_o and $\dot{\delta}_c$=0.1 mm/hr

@+ 0.074 to 0.84 mm sand at -2 deg C

@* 0.074 to 0.84 mm sand at -3 deg C

@ 0.42 to 0.59 mm sand at -3 deg C

? Questionable results

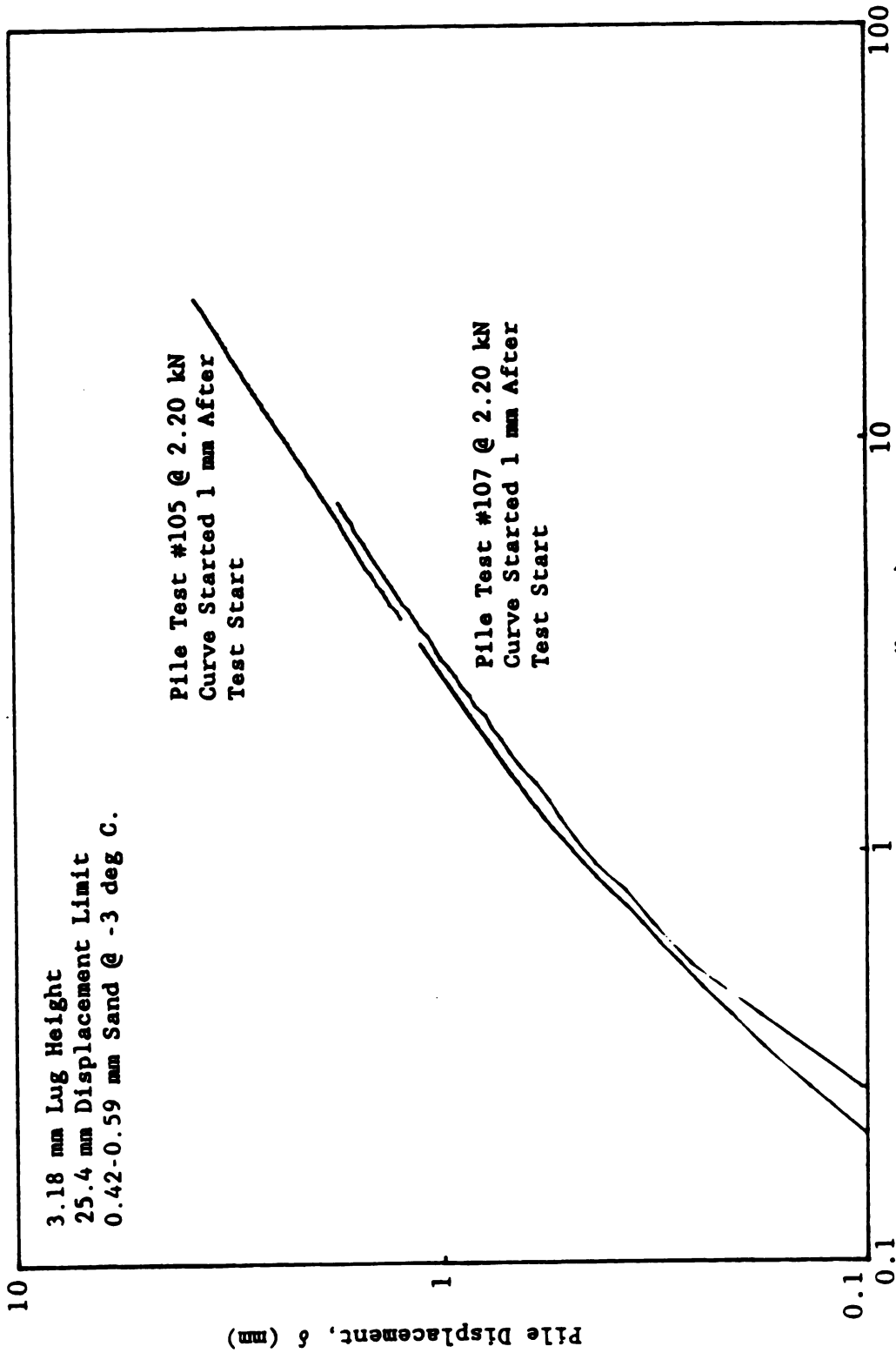

Figure 4.4. Time-displacement behavior of similar piles subjected to similar loads in frozen sand using a 1 mm C-type starting point.

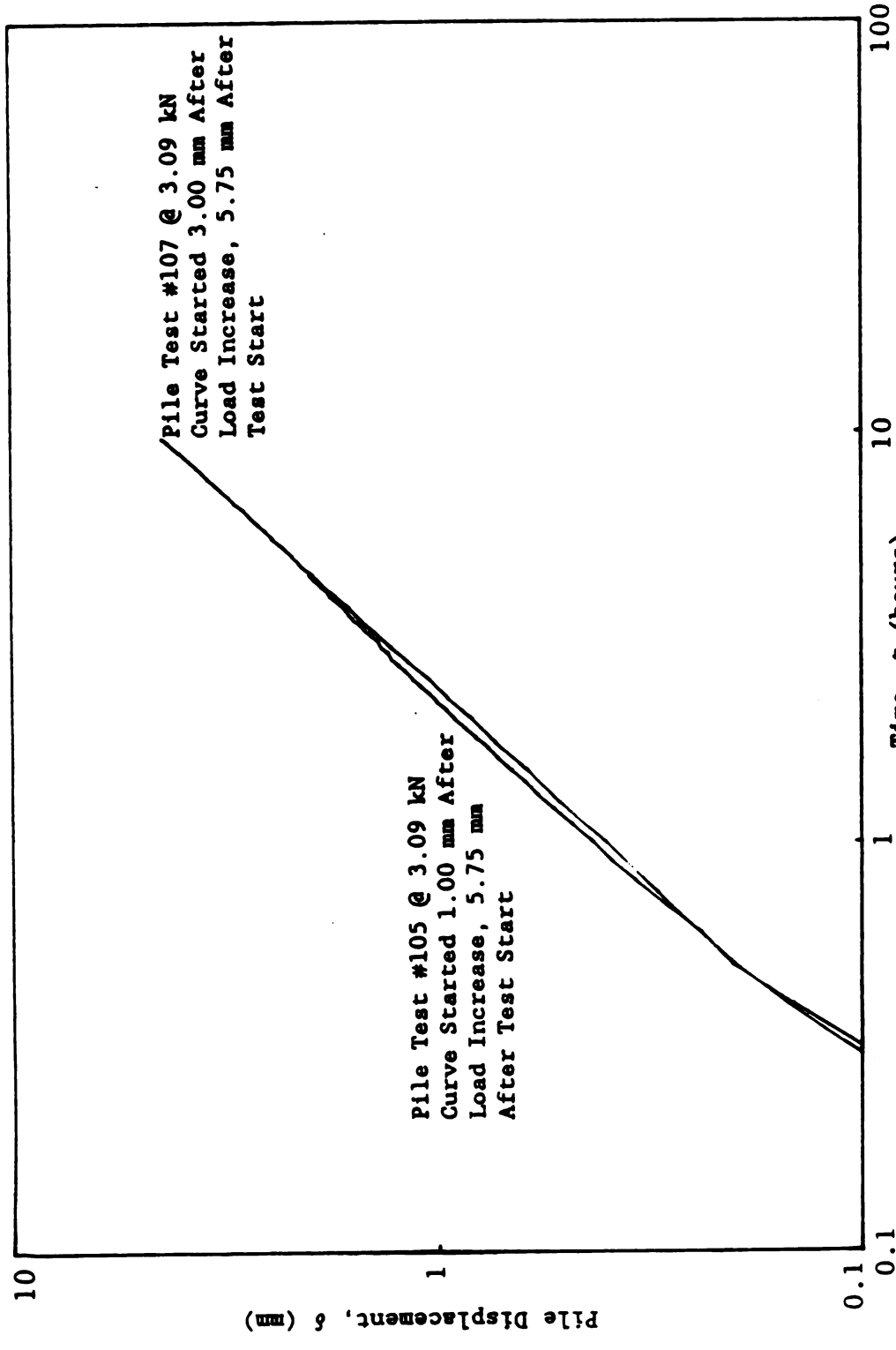

Figure 4.5. Time-displacement behavior of two similar model piles in frozen sand subjected to similar load increases. Plots used 5.75 mm C-type starting points.

Figure 4.5, displacement data from #107 is shown using a C-type starting point of 5.75 mm (3 mm after after the load increase). Based on our knowledge of full duration pile behavior after a 3 mm displacement, Pile Test #107 can be assumed to be close to the steady state creep rate condition. Pile Test #105, plotted in Figure 4.5 using a 5.75 mm C-type starting point (1 mm after its load increase) nearly matches Pile Test #107's behavior. A comparison of plots in Figure 4.5 with Pile test #111 (a full duration test plotted with a 6 mm C-type starting point) in Figure 4.3e would show all three to be similar and would appear to represent general pile behavior.

The log (time) - log (displacement) curves for a model pile, started 1 mm before and 1 mm after a load change, are shown in Figure 4.6a and 4.6b. Pile Test #107's load increase at 2.75 mm produced plots that are less similar and more unsteady than the plots produced by the load increase on Pile Test #105 at 4.75 mm. Straight line approximations are more easily made for Pile Test #105 in Figure 4.6b and these approximations are similar to those from full duration loads (with 6 mm C-type starting points) shown in Figure 4.3e. The load increase at 4.75 mm produced better and more consistent results.

To closely observe pile displacement after a load increase, data from Pile Test #105 has been plotted (Figure 4.7a) using various C-type starting points after the load

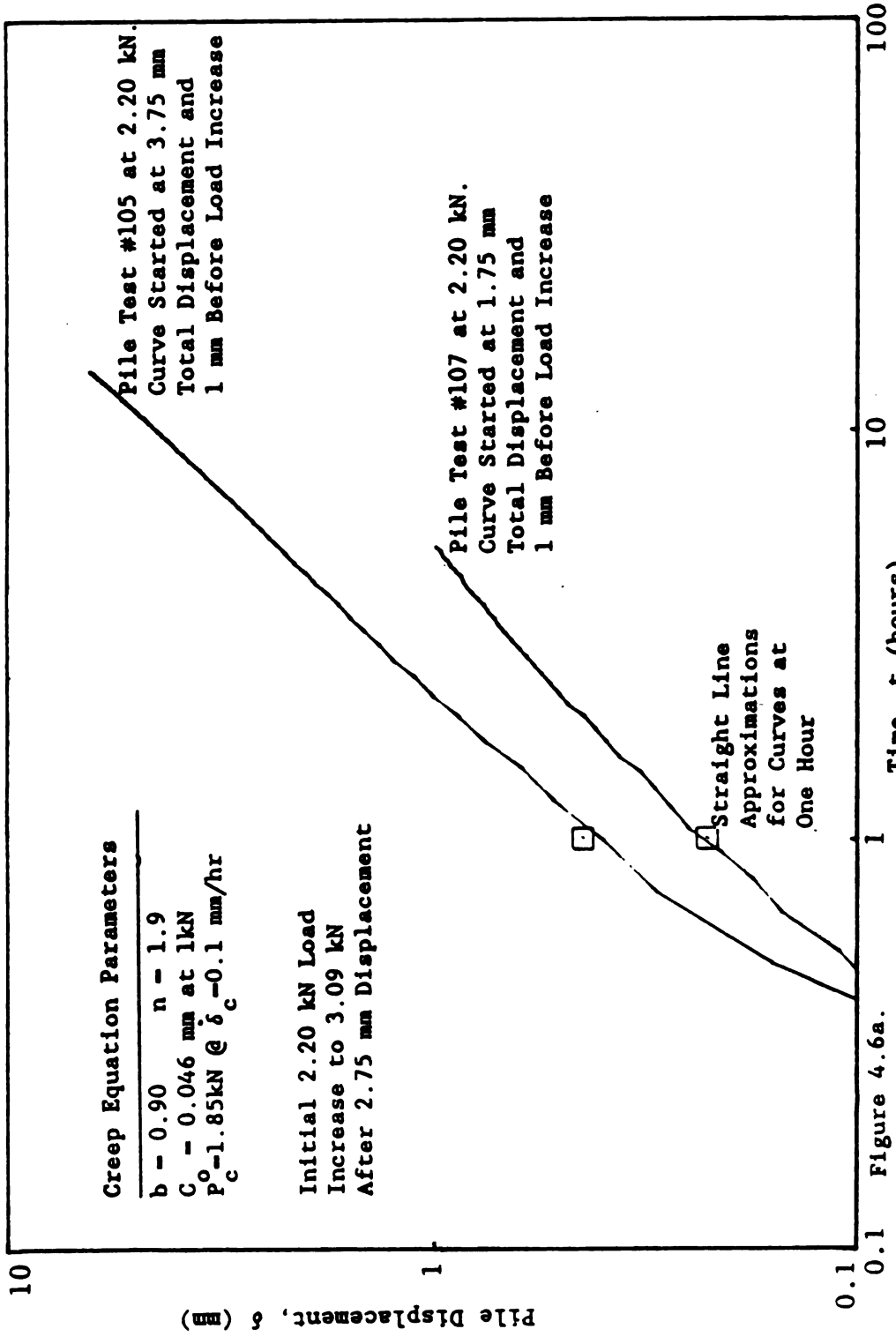

Figure 4.6a.

Figure 4.6. Time-displacement behavior of a model pile before and after a load increase.
(a) Load increased after a relatively small pile displacement.

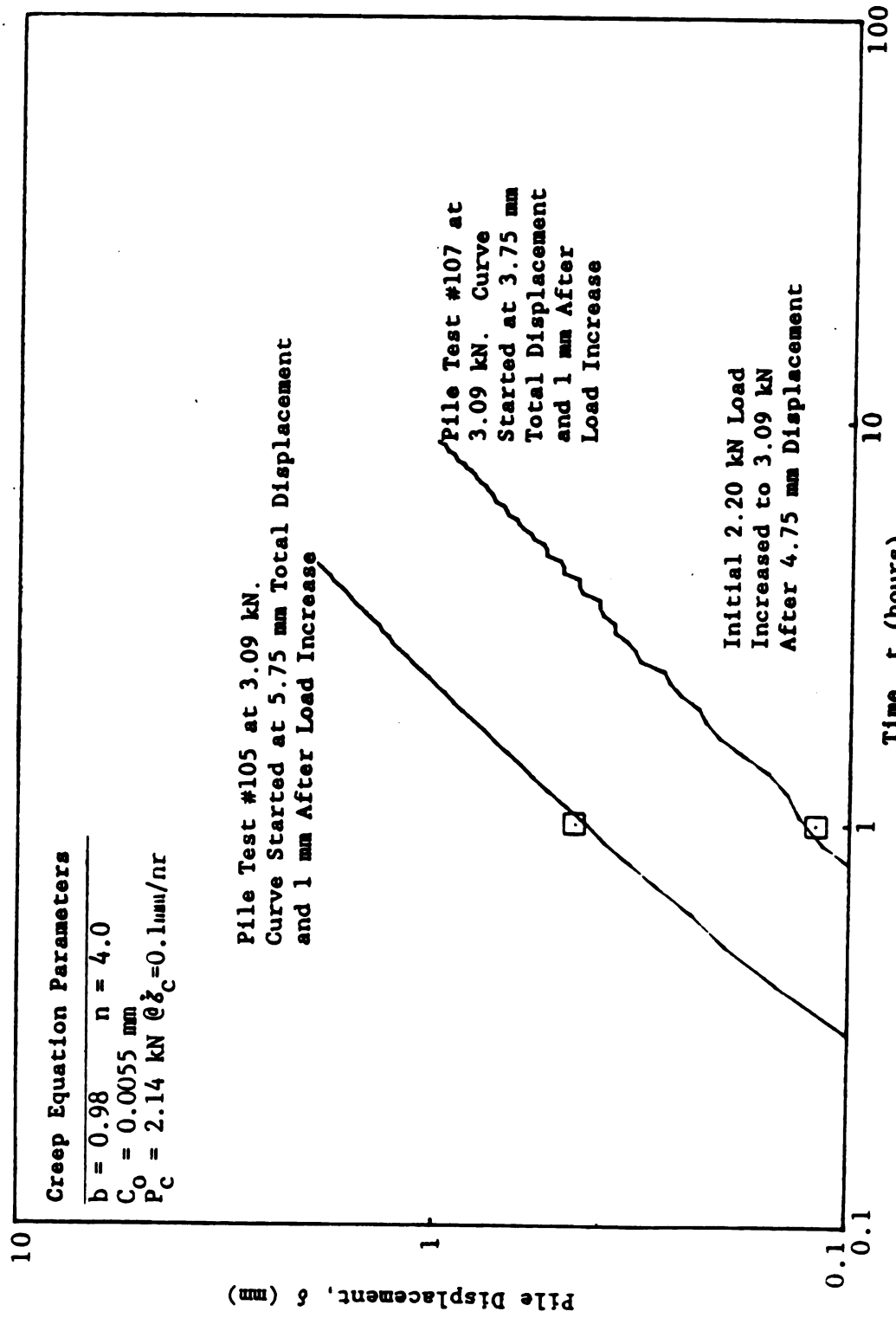

Figure 4.6b. Load increased after a relatively large displacement.

increase. A pile at a constant displacement rate would be parallel to the dashed line in Figure 4.7a. Nearly constant displacement rates can be observed between the asterisk marks of the curves started at 1.0 mm and 0.065 mm after the load increase. Constant displacement rates can be estimated for those portions between asterisk marks. The displacement rate estimated from the 0.065 mm C-type curve does not represent general pile behavior but can be compared to other load increases plotted at 0.065mm C-type starting points. The relatively-short total displacement (0.65 mm) of the 0.065 mm C-type curve is an advantage that will be used later.

Various B-type starting points (also shown in Figure 3.4) are used for plots of Pile Test #105 in Figure 4.7b. The plot, started at 0.2 mm more than the displacement at the time of load increase, is similar to the C-type plot in Figure 4.7a started 1.0 mm after the load increase. The displacement rates between asterisk marks of these two curves are approximately the same. The 1.0 mm B-type starting point distorts the log (time) - log (displacement) curve to a point where it is no longer useful. The 0.065 mm C-type and the 0.065 mm B-type curves of Figure 4.7a and 4.7b, respectively, are nearly the same at this displacement transducer sensitivity. In general, B-type starting point plots would allow displacement rate estimation after shorter total pile displacements.

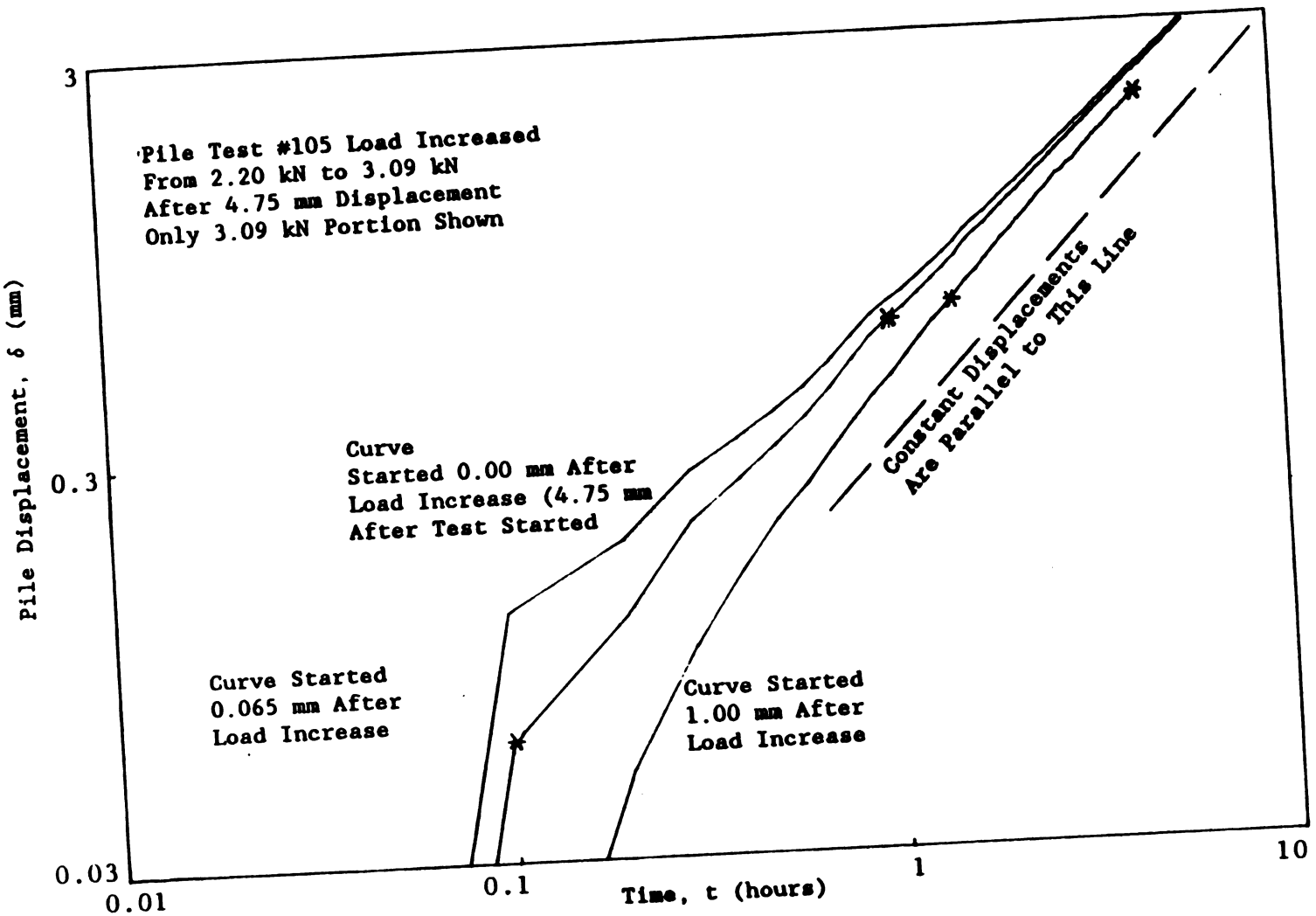

Figure 4.7. Time-displacement curves of a single pile test in frozen sand after a load increase. (a) Using C-type starting points.

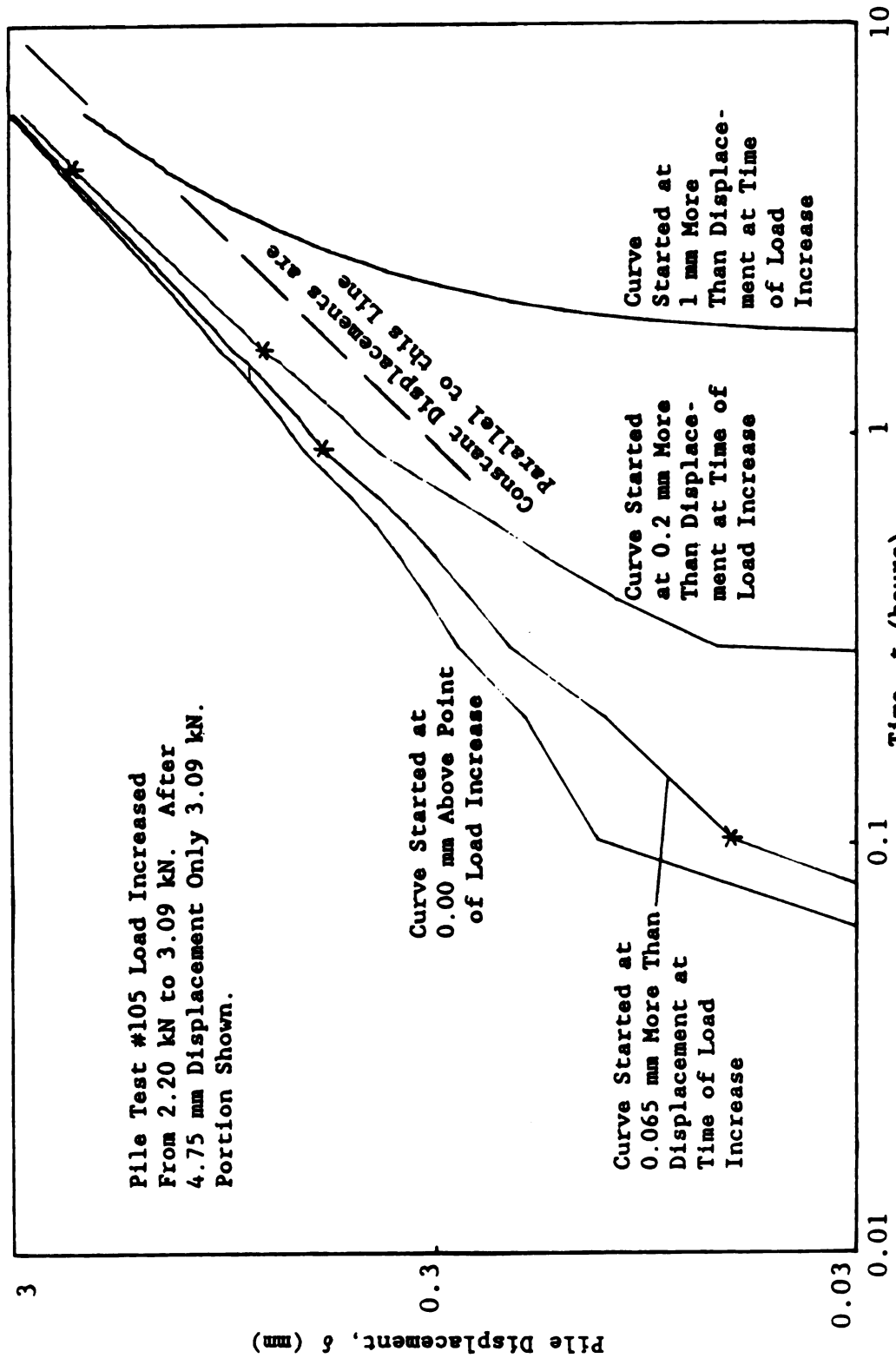

Figure 4.7b. Using B-type starting points.

4.3.1 Step Load Increase Magnitudes

These comparisons involve model piles with a 0.76 mm high tapered lug embedded in frozen low density (loose) sand. This lug pushes the frozen sand outward instead of forming a compacted sand wedge to displace the surrounding frozen sand, as described in Section 4.2 for a square-edged lug. The pile in Figure 4.8 moved very slowly for the first 4 hours. This behavior was not unique to this lug and was sometimes seen at the beginning of tests of pile with square-edge lugs. Piles that showed this behavior had small lugs (0.76 to 0.79 mm) and in at least one case (Pile Test #25) was found to be slightly out of alignment. After a few millimeters displacement, typical pile movement resumed so that the step load at 9.73 mm can be considered to be uneffected by this initial failure.

Three step loading sequences are shown in Figure 4.8. A static load has a small cyclic load superimposed which is followed by a static load increase. The displacement rates of the static load before cyclic loading and the displacement rates of the static load increases are shown for each step load in Figures 4.9a through 4.9c. The creep equation parameters determined from these step loads are included in Table 4.2. The cyclic loads were relatively small and applied for relatively short periods of time. They were assumed to have little or no effect on the succeeding load increase and will be considered in the

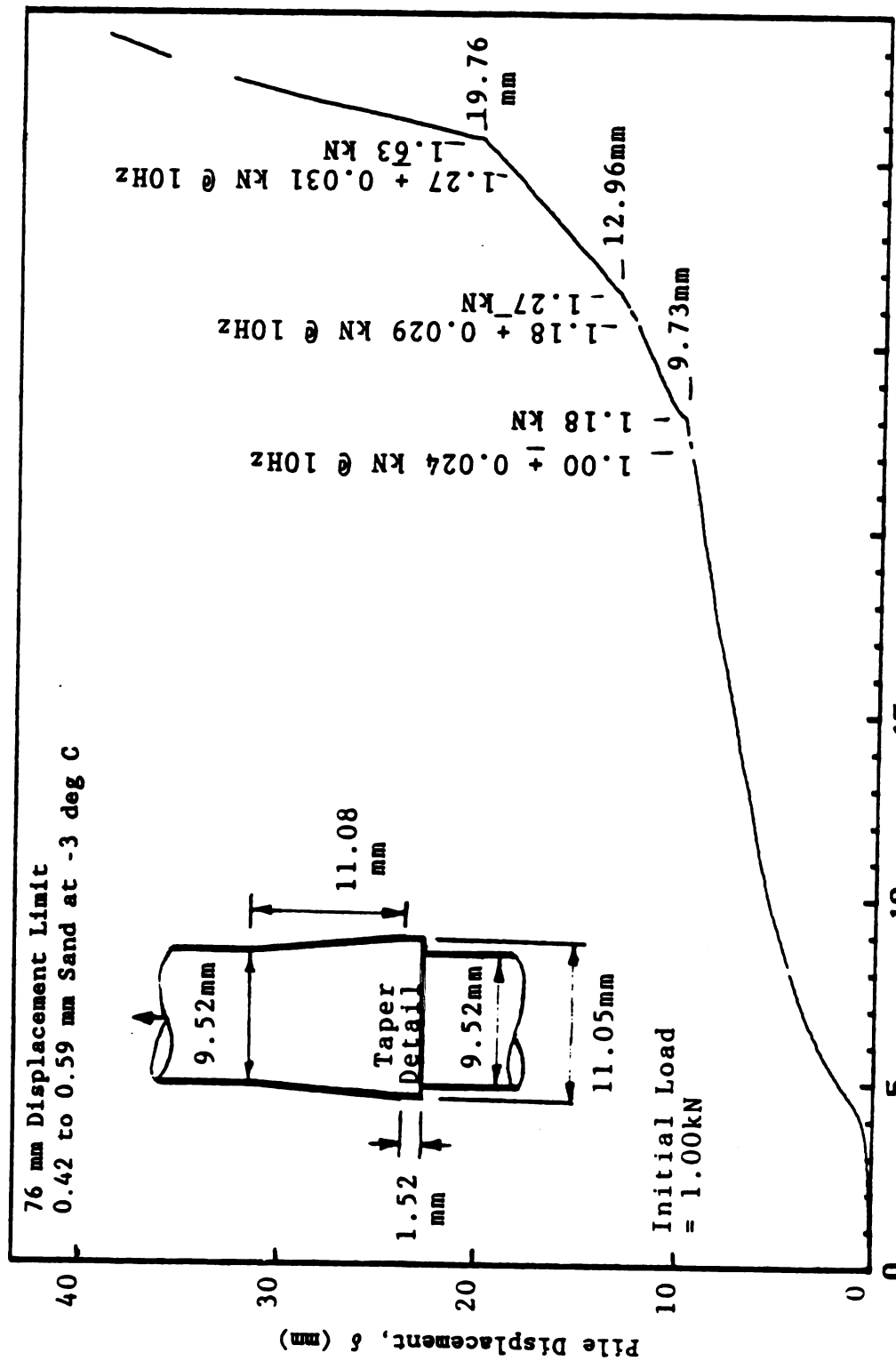

Figure 4.8. Time-displacement behavior of a tapered-lug model pile (Test #60) loaded by several steps including a superimposed dynamic load.

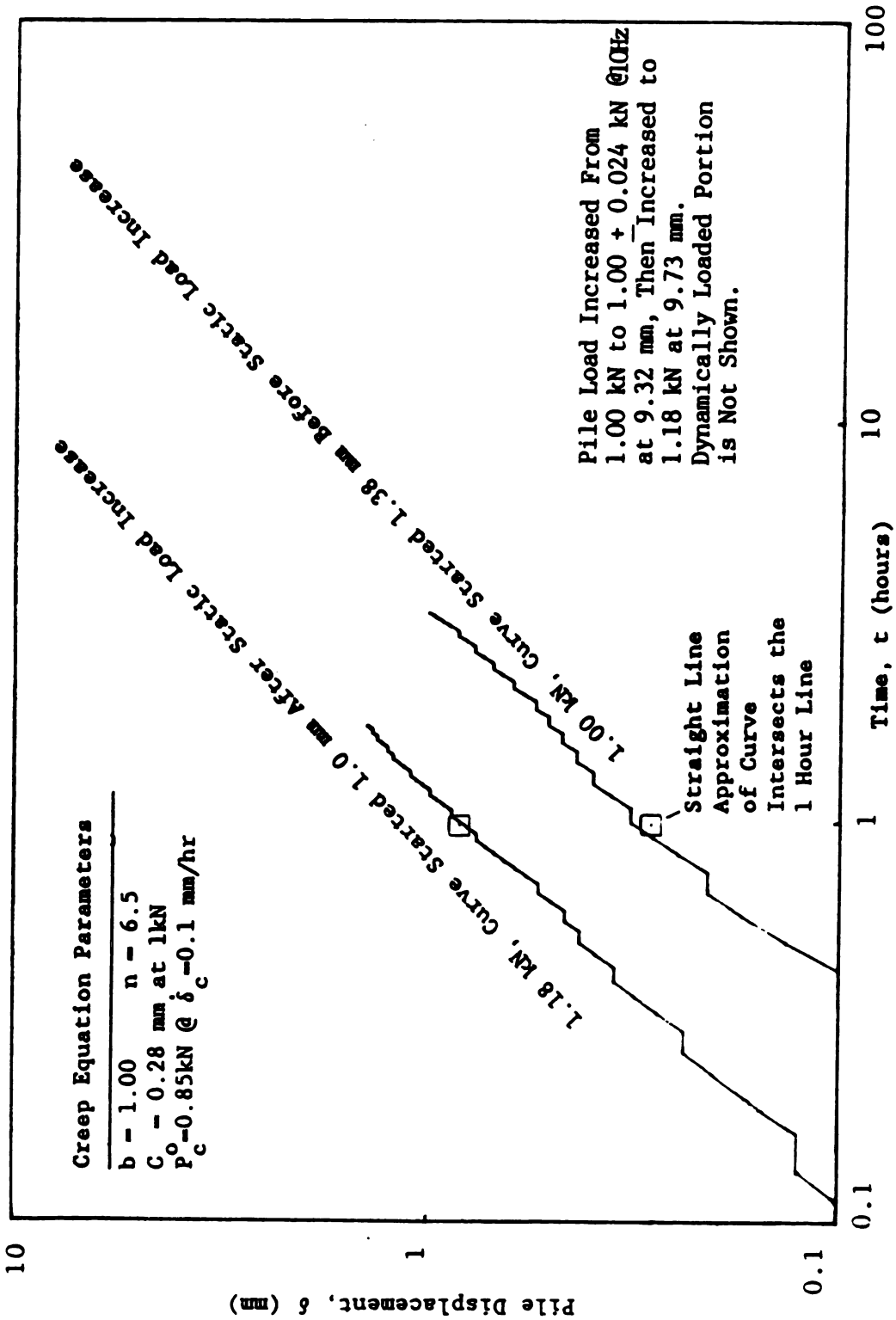

Figure 4.9. Time-displacement of a tapered-lug model pile before and after loading. (a) Static load increase at 9.73 mm displacement of Test #60.

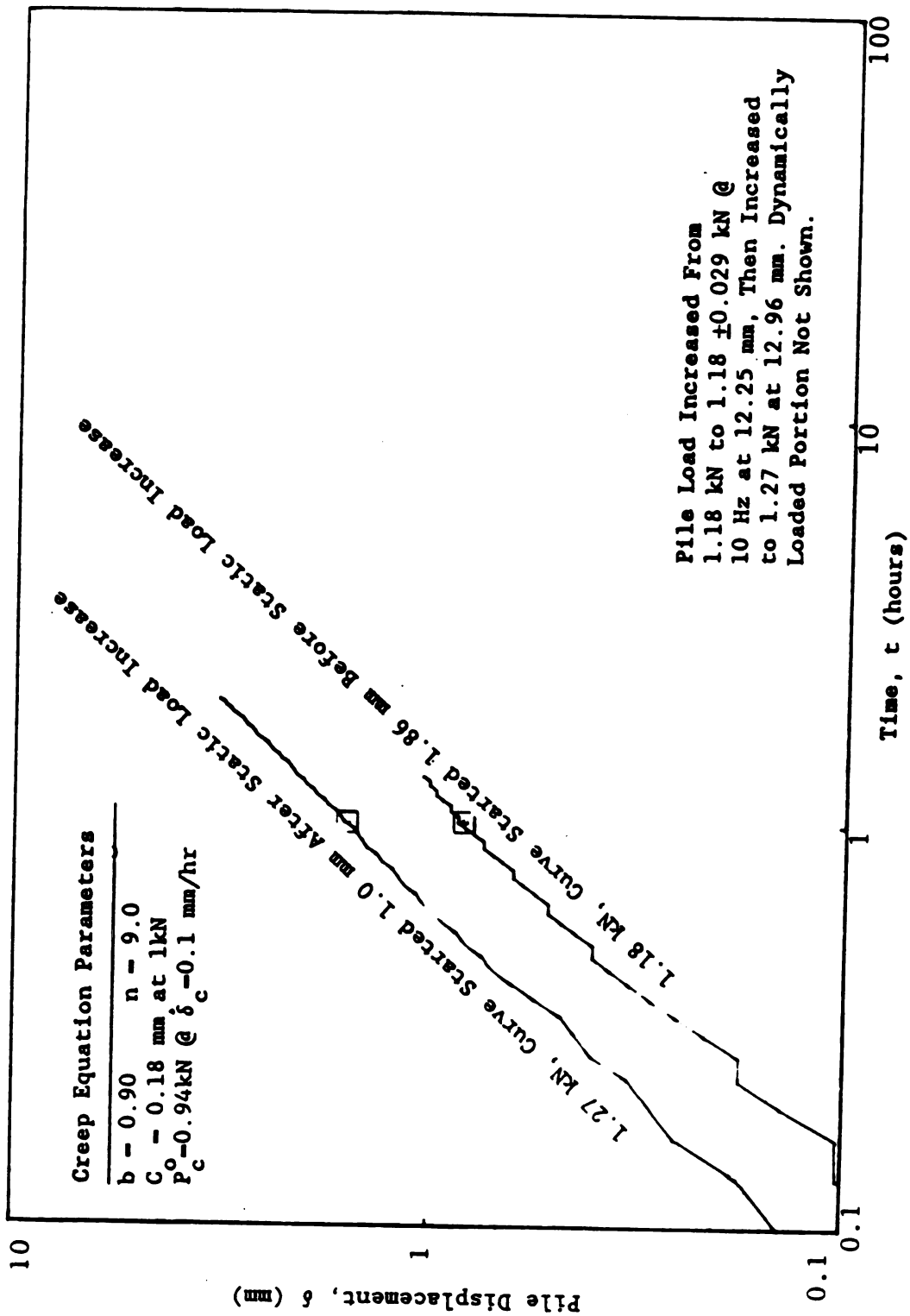

Figure 4.9b. Static load increase at 12.96 mm displacement of Test #60.

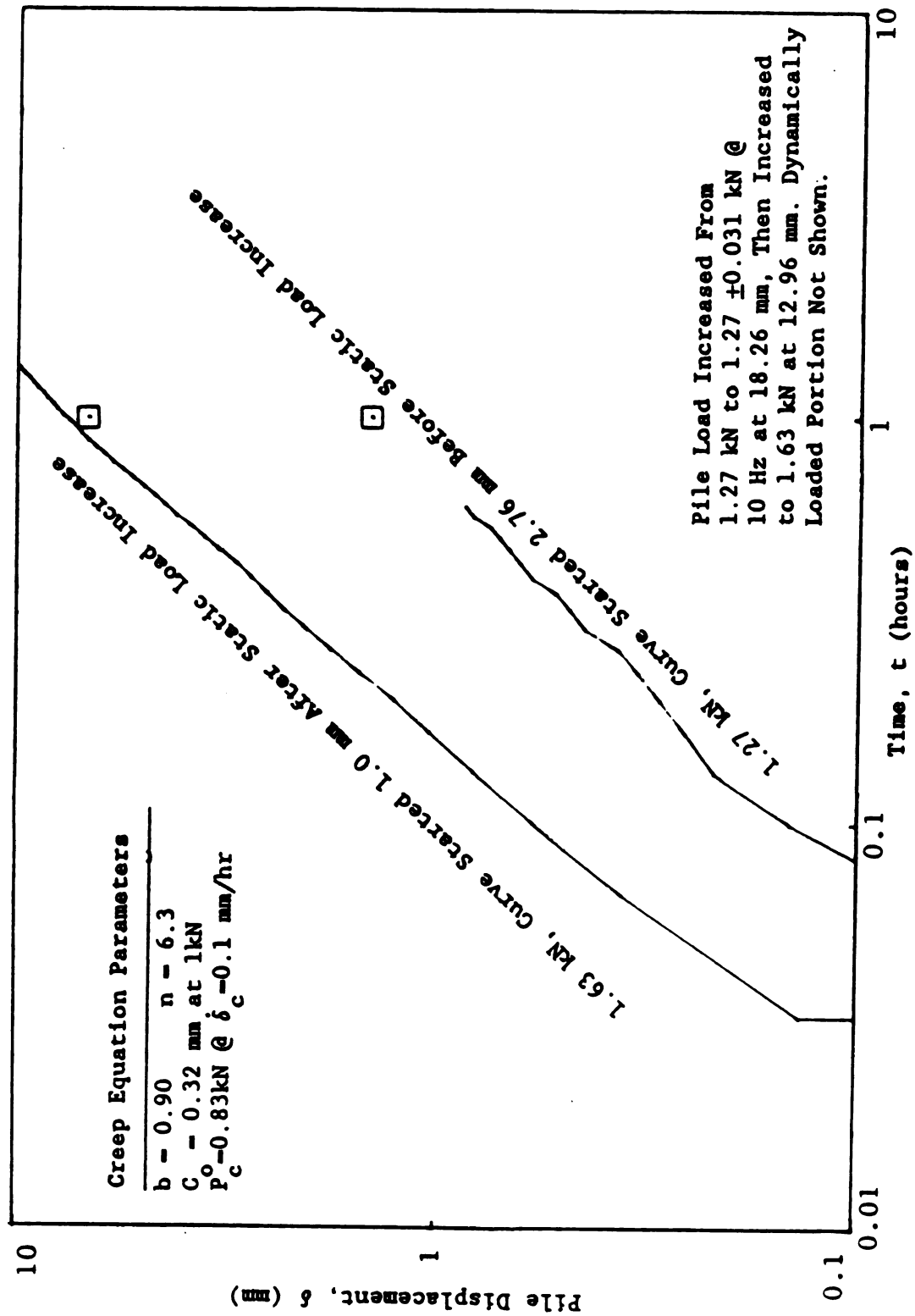

Figure 4.9c. Static load increase at 19.76 mm displacement of Test #60.

Table 4.2 Creep Equation Parameters for Lugged Piles from Step Loads.

Pile Test No.	Test Temperature deg C	Sand Size Range mm-mm	Solid Volume Fraction %	Pile Lug Size mm	Embedment Ahead/Behind Lug mm/mm	Displacement at Increase mm	Initial Load Kn	Load Increase %	Creep Equation Parameters b	n	P_c Kn*p
22	-2	.07-.84	58.1	0.79	76/57	31.52	1.31	13.6	1	7.7	1.00
23	-3	.07-.84	58.2	0.79	76/62	8.16	1.38	32.2	1	6.1	1.24
24	-3	.07-.84	59.0	0.79	76/64	2.97	0.885	30.7	1	4.7	1.08
						25.72	1.16*	12.9	1	8.2	1.17
						33.12	1.31*	18.9	1	6.3	1.16
25*a	-3	.07-.84	58.3	0.79	76/61	2.16	1.56	28.4	1	9.3	1.59
26*1	-3	.07-.84	58.0	0.79	76/62	26.29	1.56*	8.0	1	4.0	0.82
27	-3	.07-.84	57.6	0.79	76/60	11.54	1.38*	17.2	1	9.1	1.20
28	-3	.07-.84	58.1	0.79	76/67	2.38	1.11	40.0	1	5.5	1.24
						11.25	1.56*	14.0	1	4.5	1.27
29	-3	.07-.84	58.0	0.79	76/60	2.27	1.12	31.9	1	5.3	1.22
						10.86	1.38	24.2	1	5.3	1.10
32	-3	.07-.84	63.4	0.79	76/62	9.97	1.72*	9.9	1	3.9	1.45
						11.76	1.90*	22.6	1	8.3	1.69
						18.74	2.37*	17.1	1	6.3	1.53
33	-3	.07-.84	64.5	0.79	76/62	2.38	1.63	6.8	1	6.2	1.56
	-3					7.40	1.74	30.9	1	10	1.76
	-3,-2					9.51	2.28	14 *n	1	10*n	---
	-2					32.90	2.28	15.2	1	9.2	1.49
34	-3	.07-.84	63.8	0.79	76/64	1.15	1.29	27.6	1	7.9	1.70
	-3,-2					3.57	1.65*	25 *n	1	8*n	----
	-2					16.55	1.65*	26.2	1	8.7	1.38
35	-3	ice, 0.90g/cc		0.79	76/76	32.85	0.56	32.0	1	4.6	0.22
38*g	-3	ice, 0.89g/cc		0.79	76/76	15.83	0.44*	40.0	1	4.4	0.18
						28.88	0.62*	12.1	1	4.0	0.16
39*g	-3	ice, 0.90g/cc		0.79	76/76	16.88	0.44*	26.3	1	3.9	0.20
						27.10	0.56*	43.2	1	4.9	0.24
44	-3	ice, 0.90g/cc		0.79	76/76	20.15	0.56*	31.2	1	6.2	0.33

Table 4.2 (cont.)

46	-3	ice, 0.89g/cc	0.79	76/76	28.96	0.56*	8.0	1	6.0	0.26
					41.24	0.60*	5.2	1	7.5	0.32
48	-2	ice, 0.90g/cc	0.79	76/76	29.35	0.56*	7.1	1	9.1	0.36
49	-3	ice, 0.90g/cc	0.79	76/76	7.57	0.56*	32.0	1	7.6	0.41
55	-3	.42-.59	57 *v	0.79	76/64	3.88	1.55	5.8	1	5.7	0.84
60*t	-3	.42-.59	57 *v	0.76	76/62	9.73	1.00	18.2	1	6.5	0.85
						12.96	1.18	7.5	1	9.0	0.94
						19.76	1.27	28.3	1	6.3	0.83
78*g	-3	.42-.59	57 *v	3.18	76/32	2.51	1.56	94.3	0.90	3.1	1.98
82*g	-3	.42-.59	57 *v	1.59	76/63	2.26	0.93	68.8	0.87	3.7	1.47
105	-3	.42-.59	57 *v	3.18	25/63	4.75	2.20	40.0	0.98	4.0	2.14
107	-3	.42-.59	57 *v	3.18	25/61	2.75	2.20	40.0	0.90	1.9	1.85

& P_c determined at δ_c =0.1 mm/hr
* Estimated at [static load + 0.5(dynamic load amplitude)]
*a Pile out of alignment
*f Test appears to be "fast" and have a low P_c value
*g silicon grease applied to pile and lug surface to reduce bond
*n In Pile Test #33, if n = 10 is assumed, the -3 to -2 deg C increase is equivalent to a 14% (-3 deg C constant temperature) increase
In Pile Test #34, if n = 8 is assumed, the -3 to -2 deg C increase is equivalent to a 25% (-3 deg C constant temperature) increase
*t Leading edge of lug is tapered instead of square-edged
*v Estimated from the average of similar tests

short duration load section (4.4) of this chapter.

Log (time) - log (displacement) plots for load increases are started at the time of increase and 1 mm after the increase are shown in Figure 4.10. The difference between curves for the 7.5% load increase is notably smaller than the difference between curves for the 28.3% load increase. The 7.5% curve, started at the time of load increase, was nearly straight. After the smaller load increase, the pile quickly regained its load/displacement equilibrium.

4.3.2 Repeated Step Load Increases

A model pile with three step loads is shown in Figure 4.11. Log (time) - log (displacement) plots for this load increase (Figure 4.12b) were started 2.0 mm before the load increase, 1.0 mm before the load increase, at the time of load increase, and 1.0 mm after the load increase. The plot started at the 24.2% load increase (at 10.86 mm), is similar to the plot started 1.0 mm after this load increase (at 11.86 mm).

In contrast to the relatively steady creep rate observed around 10.86 mm, Figure 4.12a shows the 31.8% load increase at 2.31 mm to cause a larger readjustment in pile displacement rates. While the slow initial pile displacement (similar to the initial displacement in Figure 4.8) may have worsened this situation, unsteady conditions

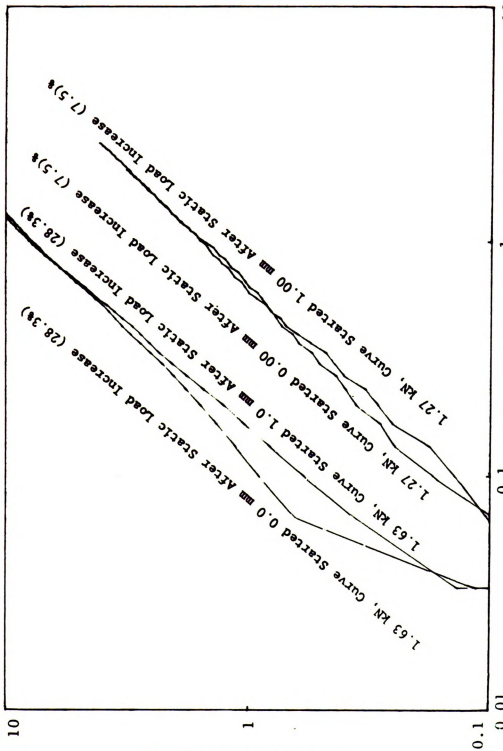

Figure 4.10. Comparison of load increases on a model pile (Test #60) using C-type starting points.

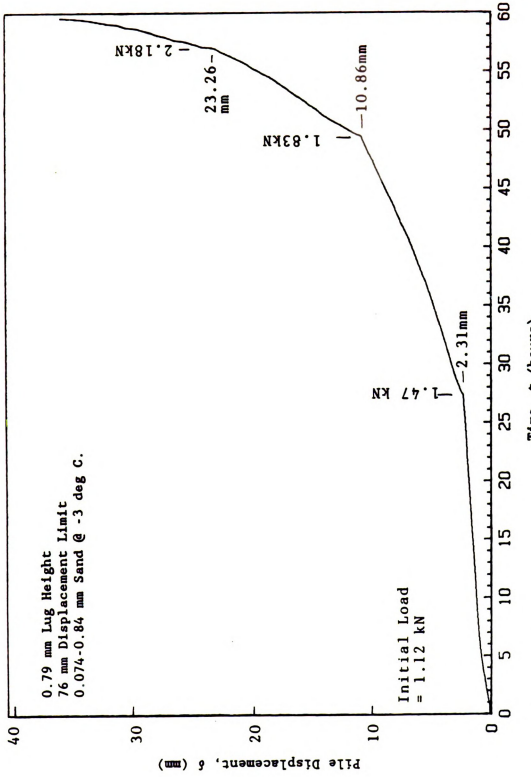

Figure 4.11. Time-displacement behavior of a model steel pile (Test #29) loaded by several steps.

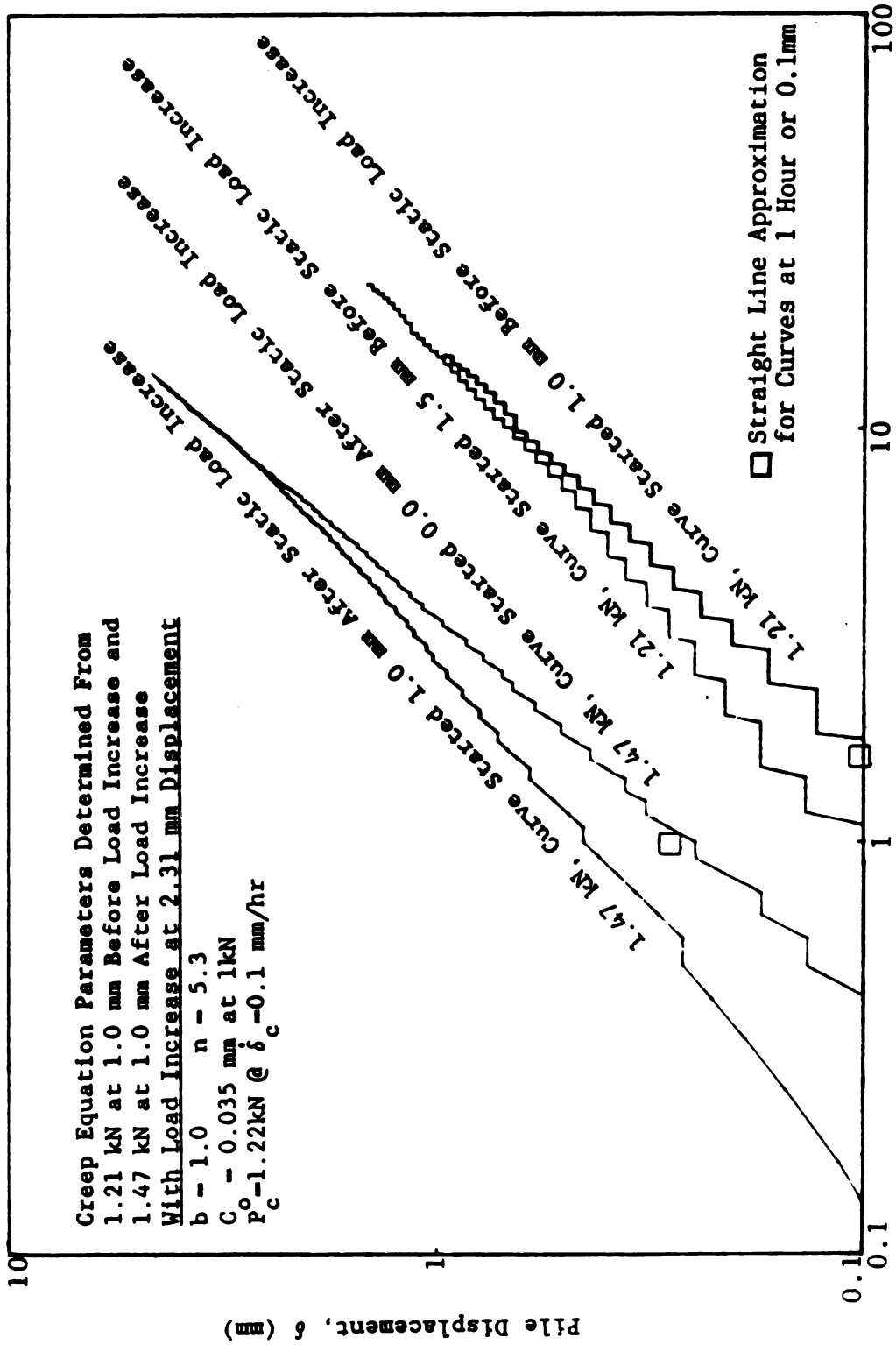

Figure 4.12. Time-displacement behavior of a model steel pile before and after loading.
(a) First step load during Test #29.

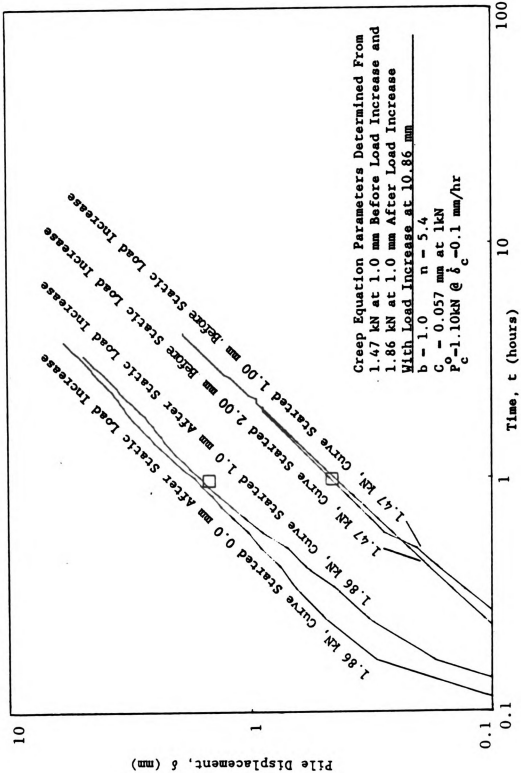

Figure 4.12b. Second step load during Test #29.

are generally found at pile displacements of less than 3 mm.

4.4.3. Rapid Adjustment to a Nearly Steady State

The time-displacement behavior for a model pile frozen in dense sand is illustrated in Figure 4.13. Step loads are shown at 2.38 mm and 7.40 mm of displacement and a temperature increase was started at 9.51 mm of displacement. Note the relatively sharp displacement rate change at 7.40 mm. The displacement rate change at 2.38 mm is equally sharp but difficult to see in Figure 4.13. The log (time) - log (displacement) plots in Figure 4.14a and 4.14b are relatively straight and parallel to each other even though the increased-load curves were started at the time of load increase. The ratio of displacement rates shown in Figure 4.13 is almost the same as the ratio determined from straight line approximations in Figure 4.14b.

The data plot shown in Figure 4.14c started 1.0 mm before the coolant bath temperature was increased and the second plot was started after the pile displacement had stabilized in the higher temperature frozen soil. Temperature stabilization required more than one hour and 4.43 mm of displacement. The curve at -2 deg C was started 4.43 mm after the temperature bath surrounding the pile and the sample had been increased. Despite the large

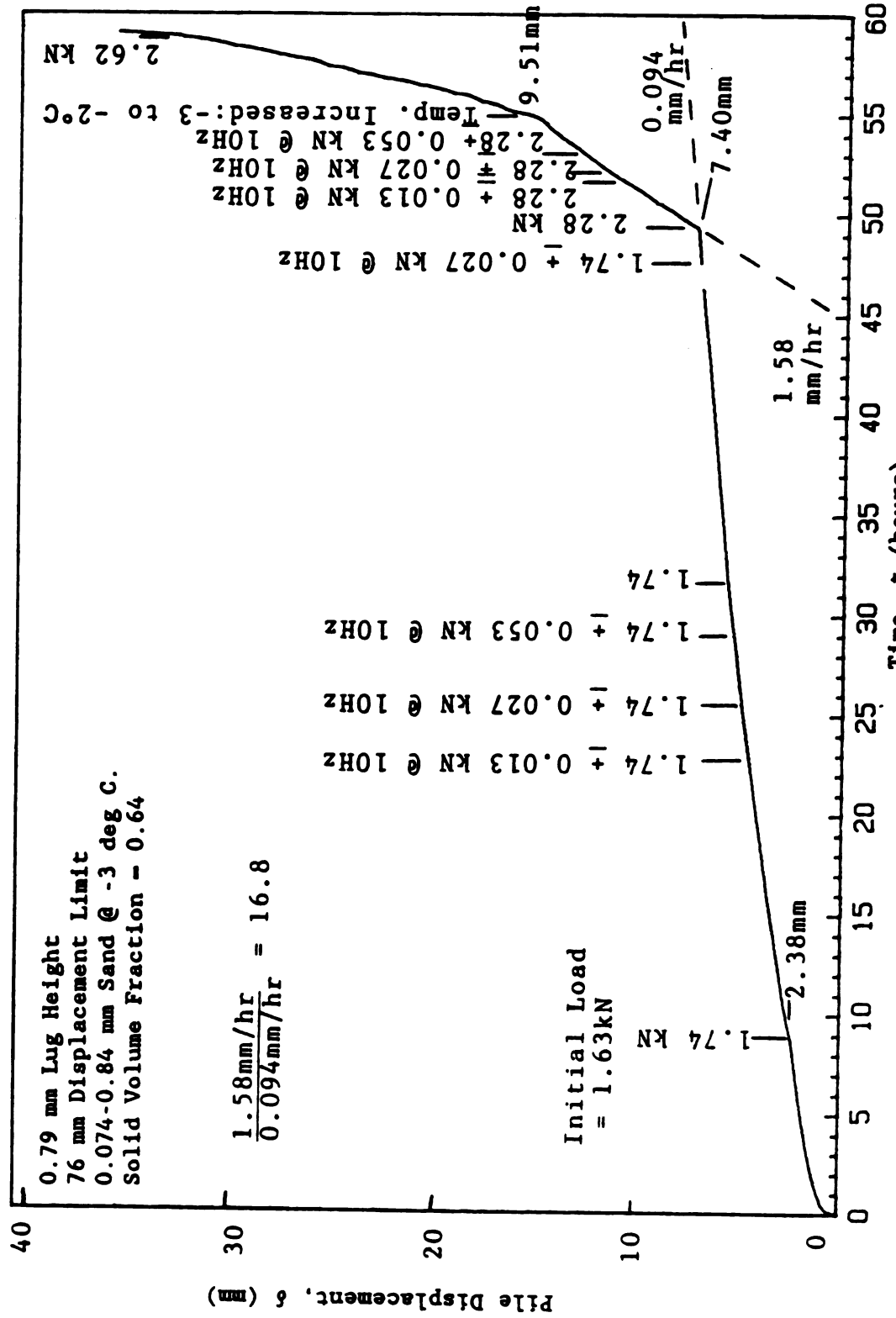

Figure 4.13. Time-displacement behavior of a model pile (Test #33) frozen in a dense sand and loaded by steps including a superimposed dynamic load.

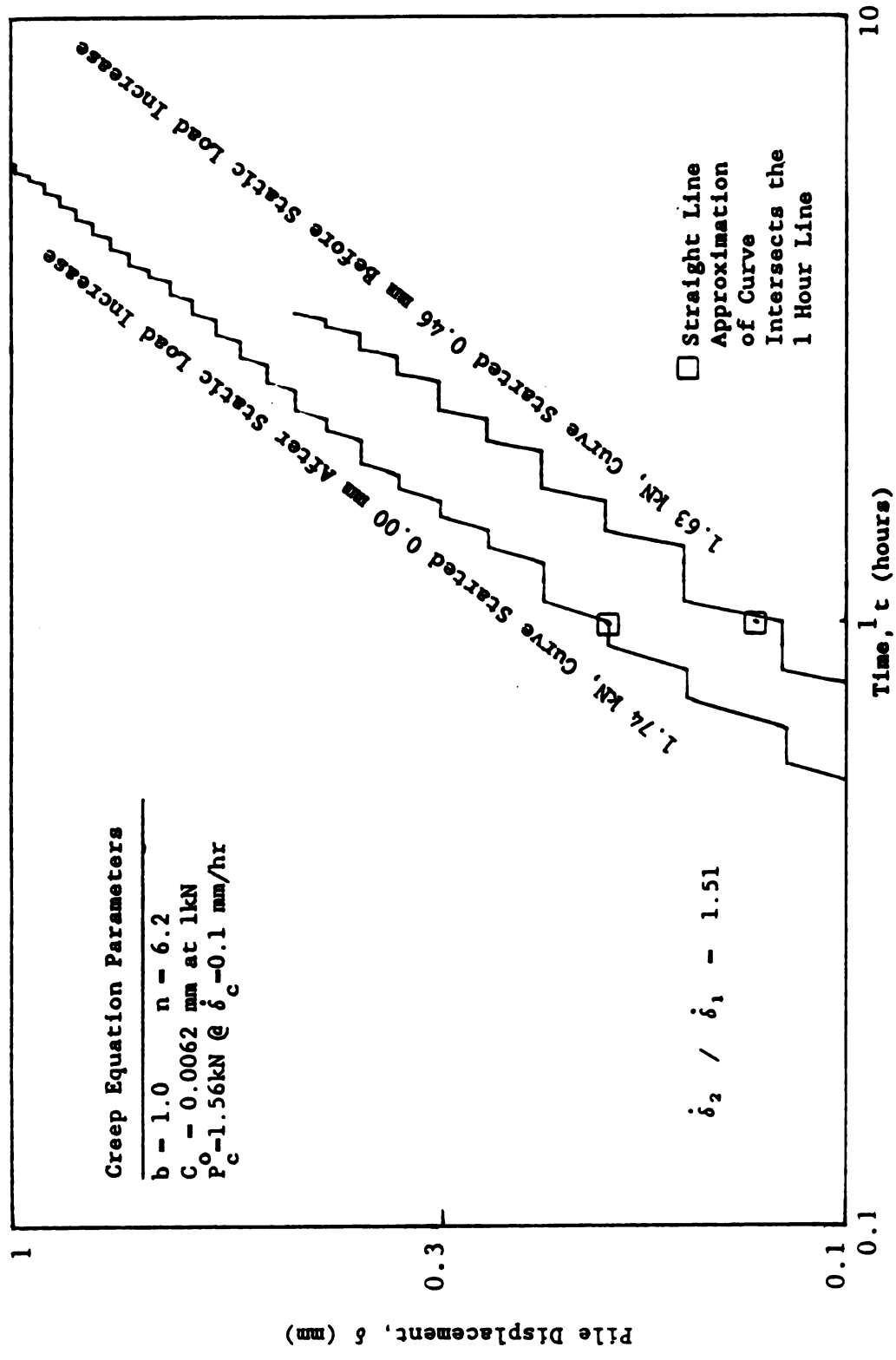

Figure 4.14. Time-displacement behavior of a model pile (Test #33) in dense sand before and after a load increase. (a) Step load 2.38 mm after beginning of Test #33.

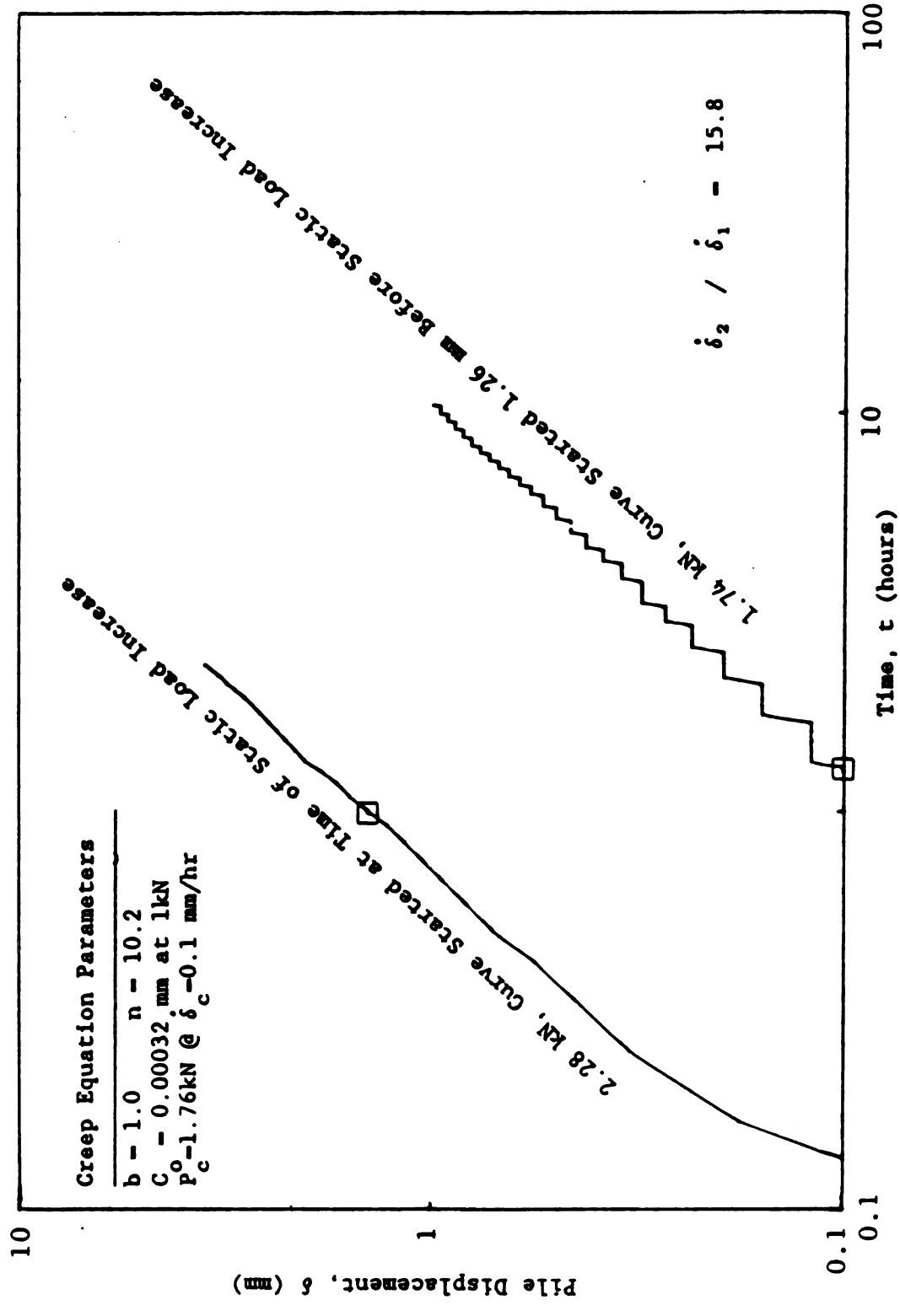

Figure 4.14b. Step load added at 7.46 mm after beginning of Test #33.

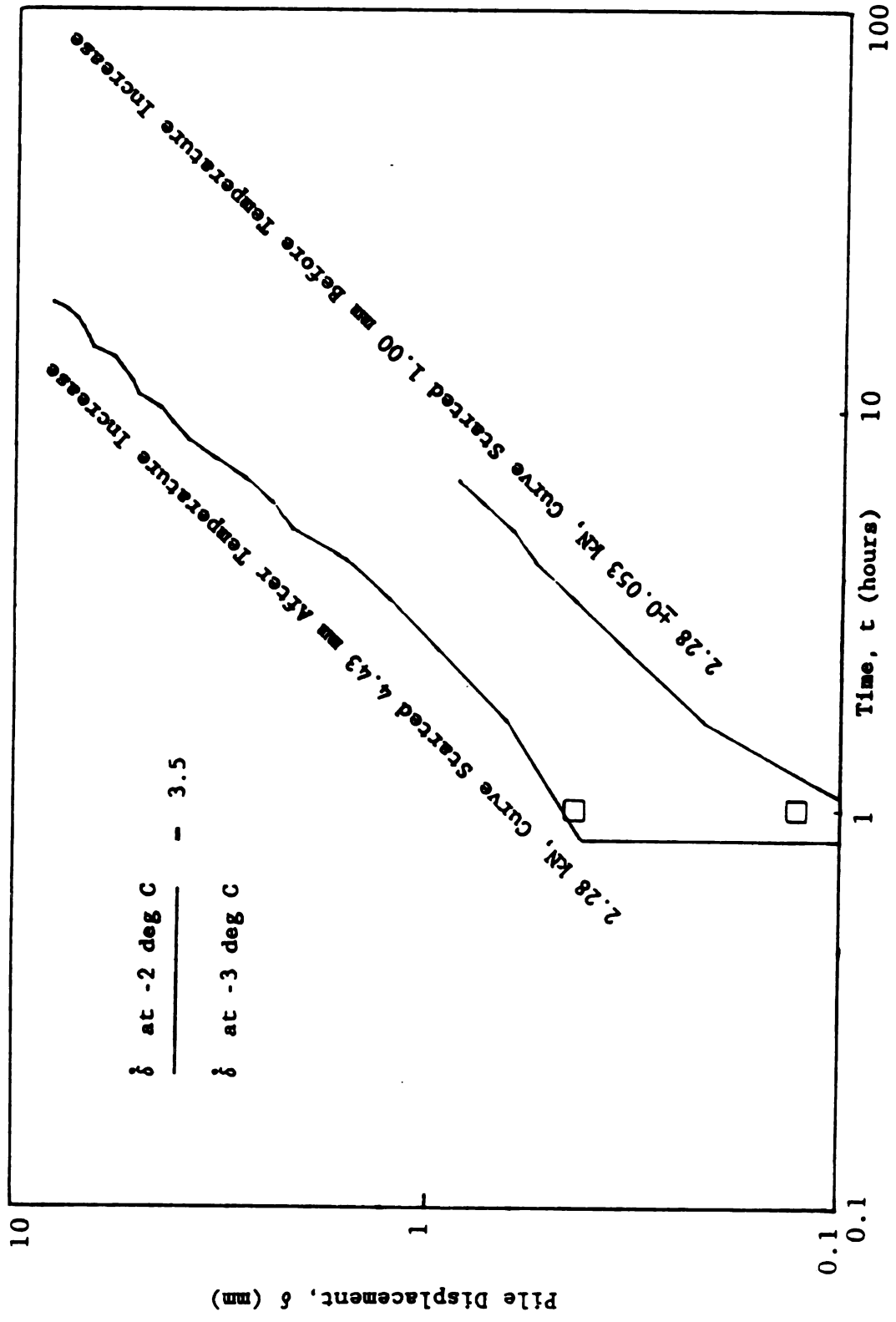

Figure 4.14c. Temperature increased from - 3 deg C to -2 deg C at 9.51 mm after the beginning of Test #33.

difference between starting points of the plots (5.43 mm), a good comparison may still be obtained if the pile's behavior is relatively steady within this range of displacement.

The behavior of a lugged pile frozen in polycrystalline ice is shown in Figure 4.15. The relatively large initial load (1.53 kN) was removed after approximately 14 mm of displacement to prevent further rapid failure. The initial rupture of ice adhesion is shown in Figure 4.15's insert. After the ice adhesion rupture and removal of the large initial load, the pile continued to displace with a smaller static load. Dynamic loads were later superimposed on this small static load. A relatively sharp change in displacement rate can be seen after a static load increase at 32.85 mm. The ratio of the straight line estimates of displacement rates before and after 32.85 mm is shown on Figure 4.15.

The log (time) - log (displacement) plots are not shown for this type of sample because the effect of the initial rapid displacement on the pile's general behavior is not known. The displacement rate ratio, determined from the relatively straight lines of the time-displacement plot, can be used to compare the rate changes due to various load increases.

Parameters determined from various step loads are listed in Table 4.2. The creep equation parameters show

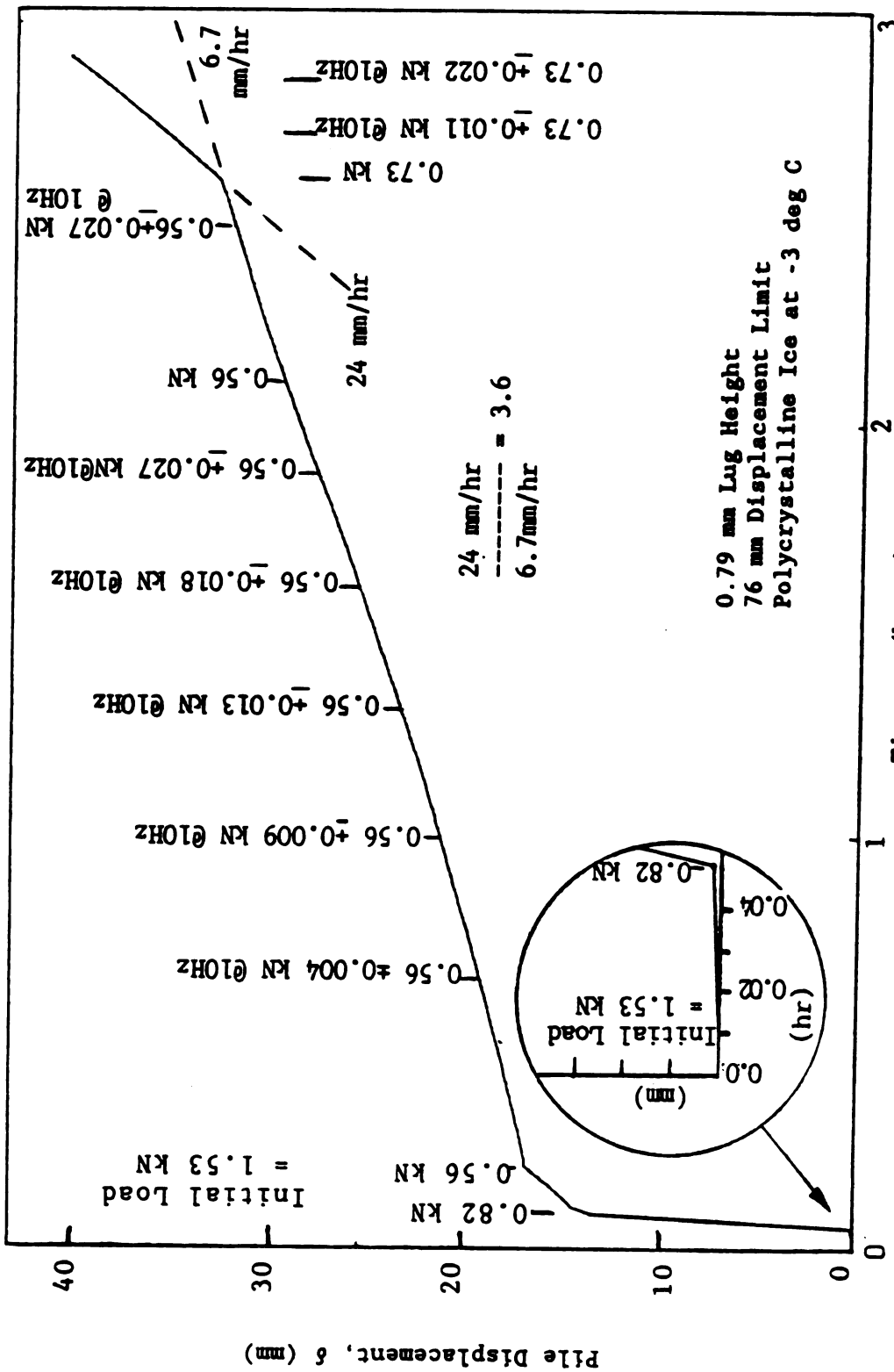

Figure 4.15. Time-displacement behavior of a lugged pile (Test #35) shown with several superimposed dynamic loads and one static load increase.

considerable variability even when derived from a single sample. Sample material variability and slight temperature changes during a step load may have contributed to variations of creep equation parameters. The short duration loads shown next will shorten the periods of test data collection to reduce displacement rate variablility and allow more comparisons during one pile test.

4.4 Short Duration Loads on Model Lugged Piles

Data from a model pile test with a slowly increasing displacement rate is shown in Figure 4.16. A group of similar piles with very dissimilar displacement behavior is shown in Figure A.13 (Appendix A). Creep equation parameters determined from these plots for full duration loads (or from load increases on them) would be questionable. However, if a very short section from any one of these curves is considered, a nearly constant displacement rate would be observed. A short duration load takes advantage of this short term consistency.

The short duration loading was convenient for applications of cyclic loads to model piles. Superimposed cyclic loading could be carefully monitored during the entire short duration period and a constant loading condition could be maintained. Performing many short duration loads on one sample allowed a range of frequencies and amplitudes to be tested. Short duration static load

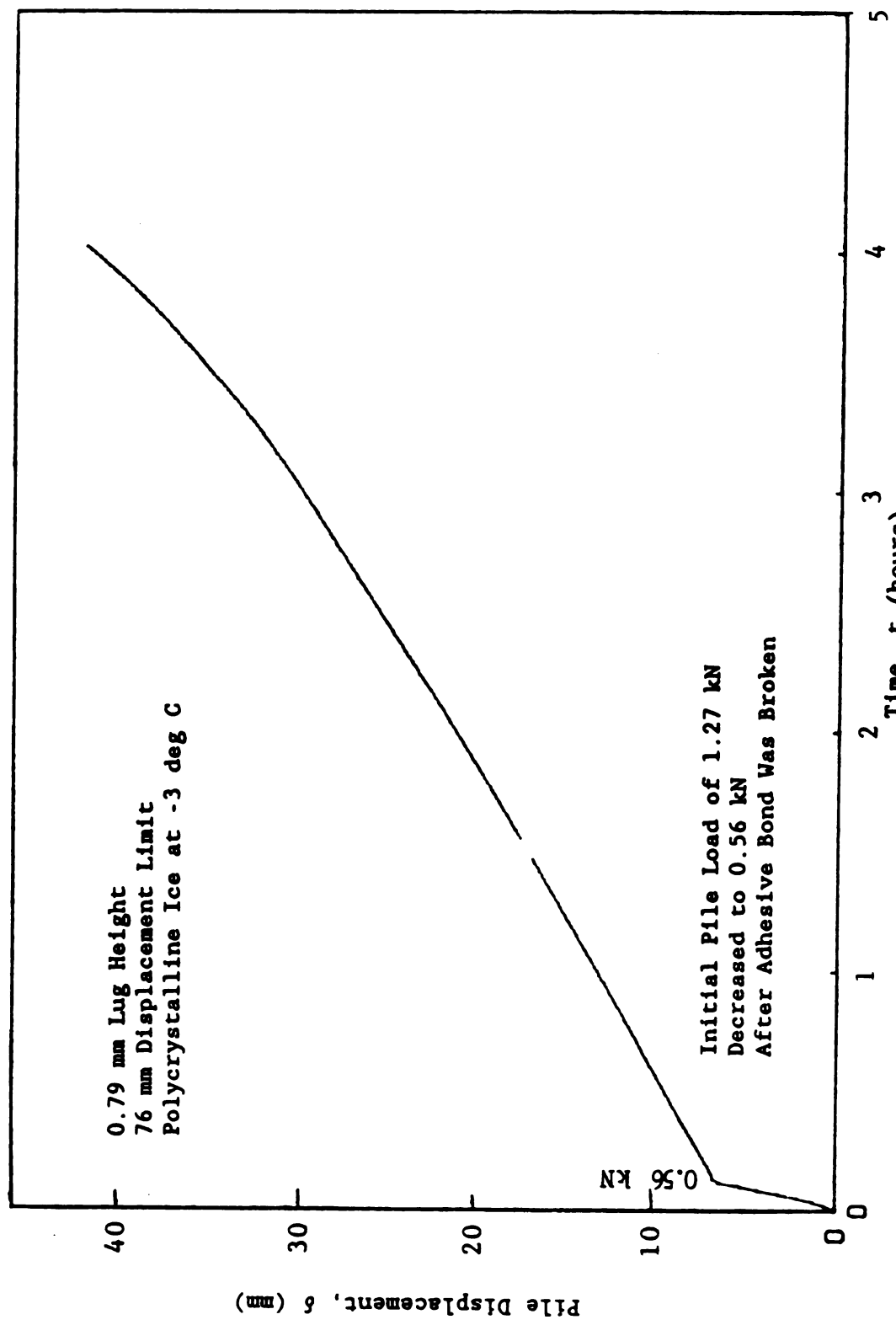

Figure 4.16. Time-displacement behavior of a lugged pile (Test #51) in polycrystalline ice with a constant load.

increases were also included to allow comparisons with dynamic short duration load increases.

The time-displacement plot of Pile Test #92 is shown in Figure 4.17. The three periods for lever arm adjustment are shown. The log (time) - log (displacement) behavior after reloading is shown in Figure 4.18. The typical decreasing displacement rate was disturbed by the arm adjustment process so that these three displacement rates, determined after different total displacements, are nearly the same. After each arm readjustment, the pile was allowed to reach a nearly constant rate before short duration loads were again added.

A series of short duration loads (static load increases and superimposed cyclic loads) are shown in Figure 4.19. After each load increase, the initial pile load was reapplied and maintained until a nearly constant displacement rate was re-established. At this point, another short duration load was added. Slopes of the initial displacement rates, illustrated in Figure 4.20, vary slightly between short duration loads. Slight variations were normalized when displacement rate ratios were used for comparisons.

With each short duration load increase, the time displacement curves often show small (0.02 mm for Test VIII in Figure 4.20) periods of rapid displacement (believed due to material and/or loading system characteristics). These

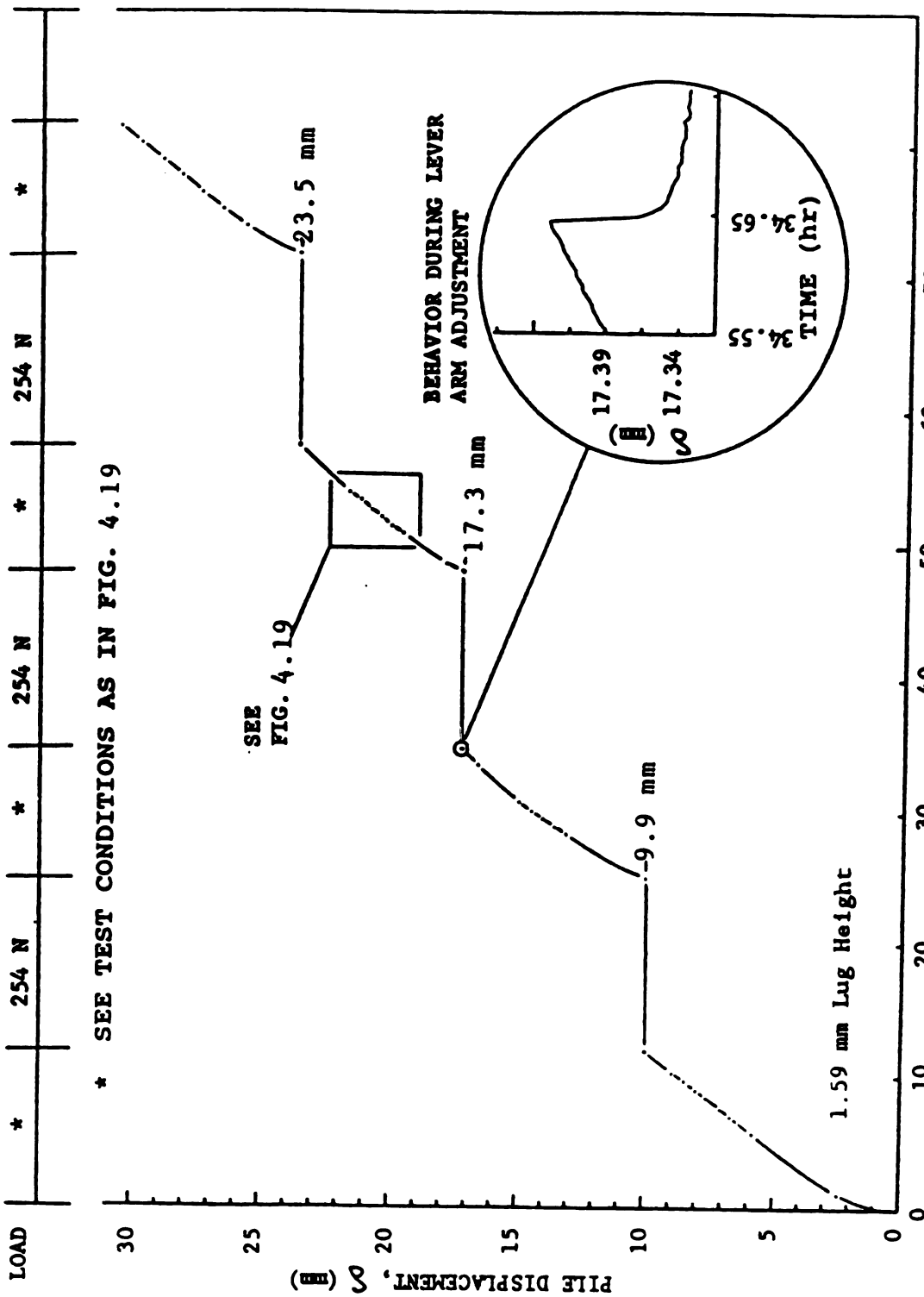

Figure 4.17. Time-displacement curves for a model pile in frozen sand at -3 deg C with periods of unloading.

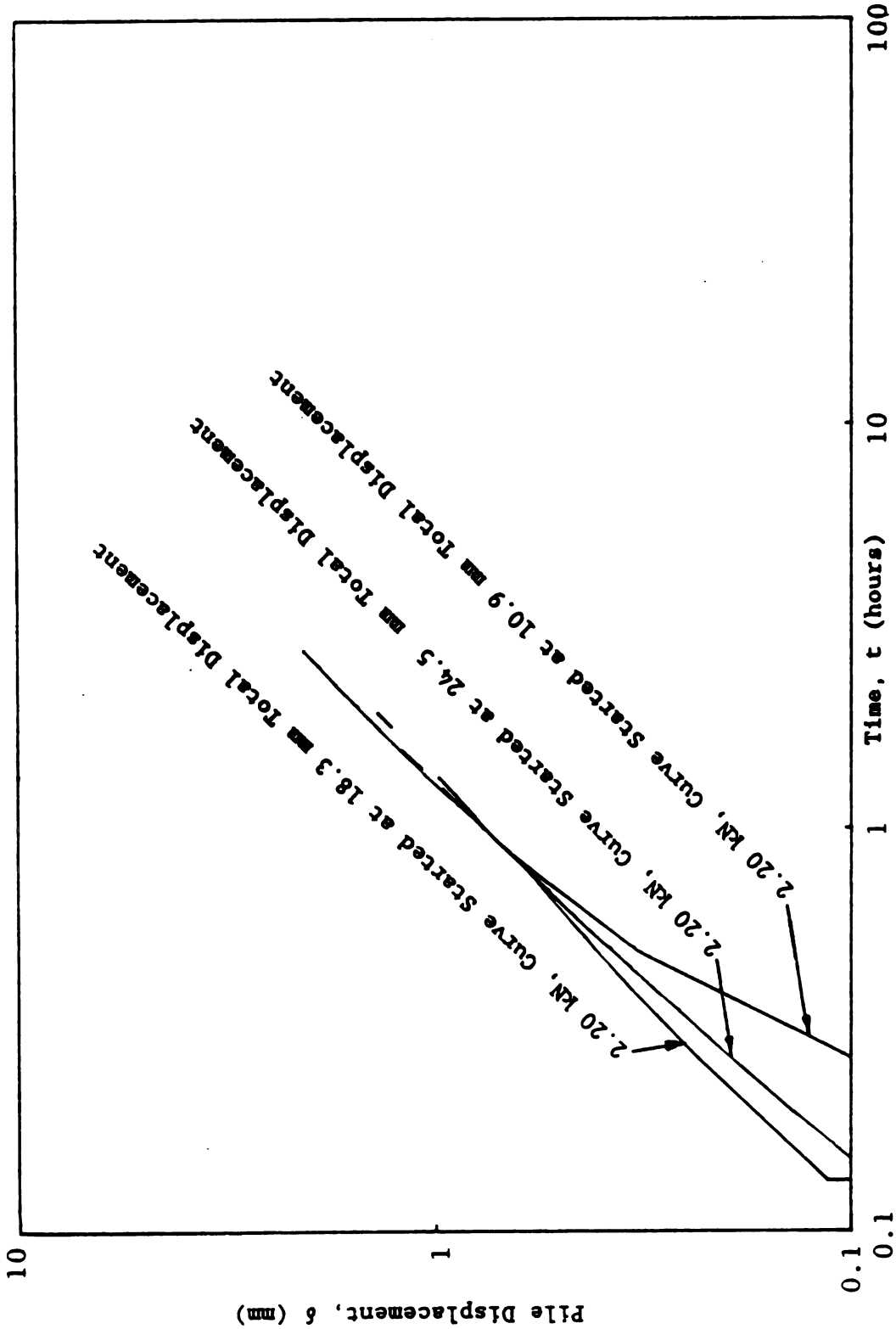

Figure 4.18. Time-displacement behavior of a single pile (Test #92) shown 1 mm after restoration of the static pile load.

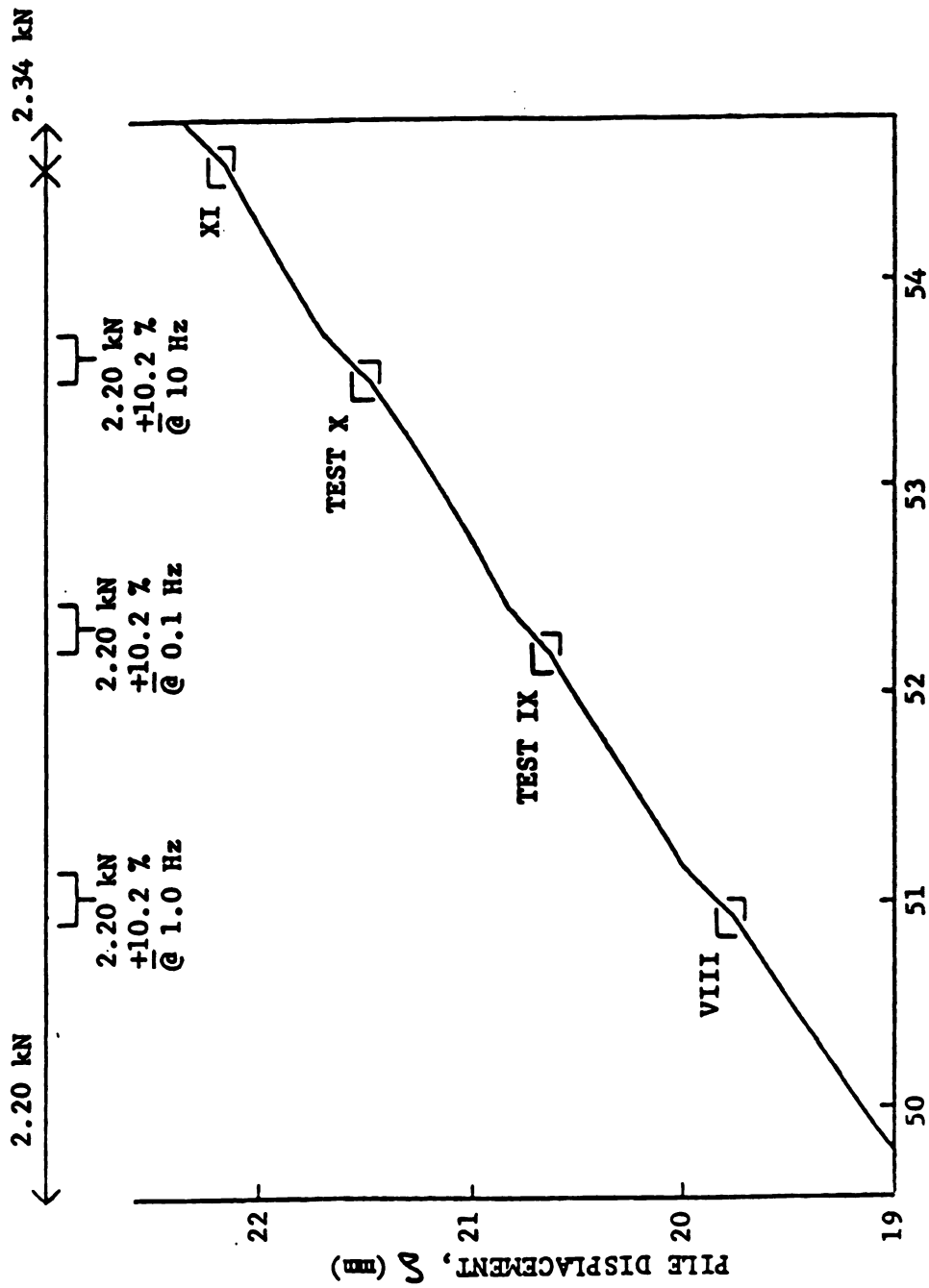

Figure 4.19. Time-displacement curve for a model pile in frozen sand showing the relationship for short duration load increases VIII through XI of Test #92.

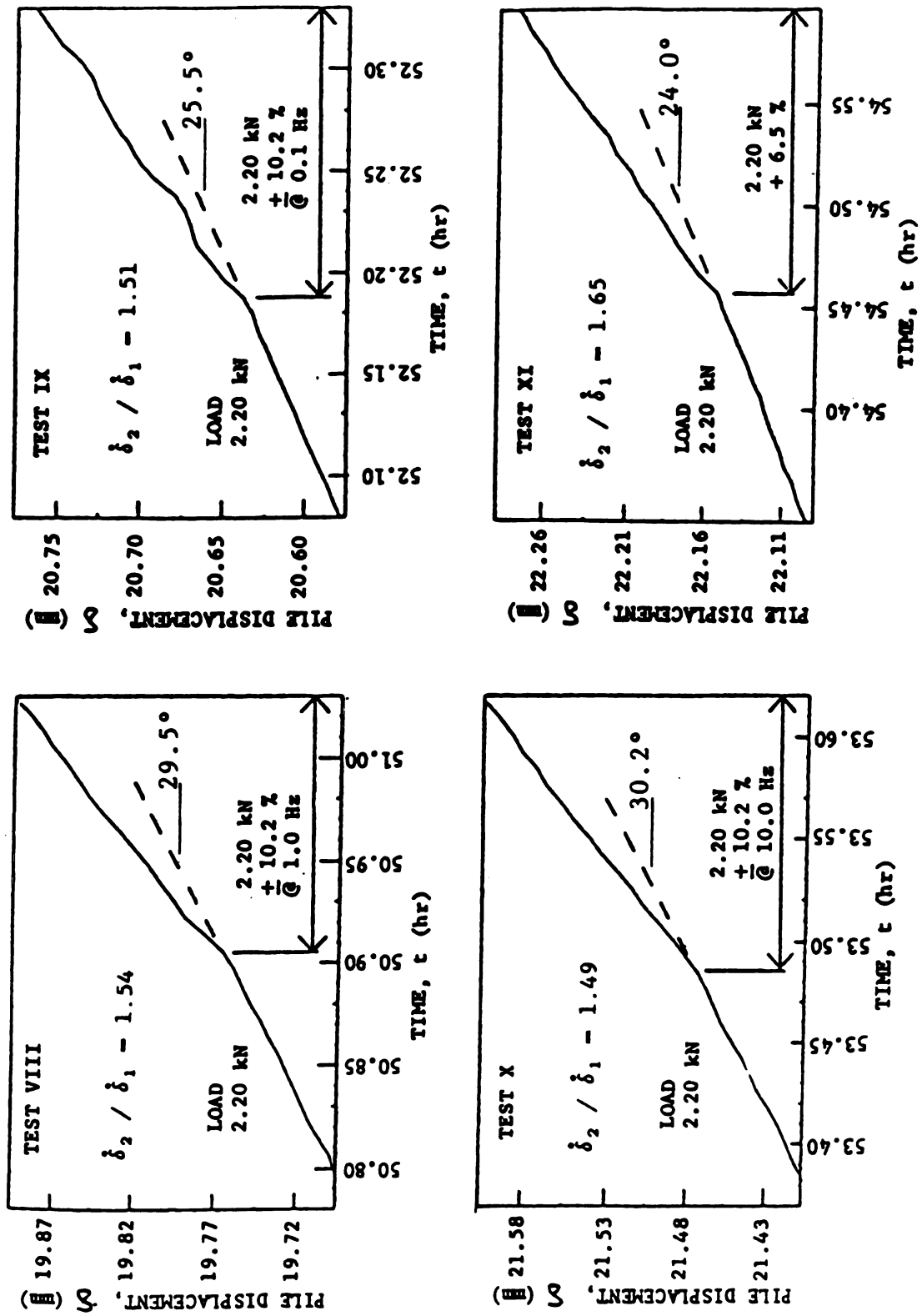

Figure 4.20. Short duration time-displacement curves for a model pile in frozen sand, load increases VIII Through XI of Sample #92.

are followed by slowly decreasing displacement rates, (seen as fairly steady in Figure 4.20) which could often be approximated by straight lines. The displacement rates before short duration loading can be estimated in this way.

Note that the displacement rate during short duration loading can be considered as relatively steady over a small range of displacement. This was shown earlier for a portion of the 0.065 mm C-type curve in Figure 4.7a between asterisks. The displacement rate during a short duration loading does not represent general pile behavior. However, the relatively fast displacement rates from short duration loads can be compared with each other.

For better comparisons, the displacement rate estimated during short duration loading can be divided by the displacement rate estimated before the load increase to provide a displacement rate ratio for each test. These ratios are shown in each part of Figure 4.20. Displacement rate ratios tend to normalize any differences preceeding the short duration load increases and clearly provide the magnitude of change (displacement rate increase) produced by adding a given load variable. The effect of a dynamic load increase can be compared with the effect of a static load increase

Data from tests where cyclic loads were superimposed on lugged piles with approximately the same lug heights and tested at the same temperature are shown in Figures 4.21a

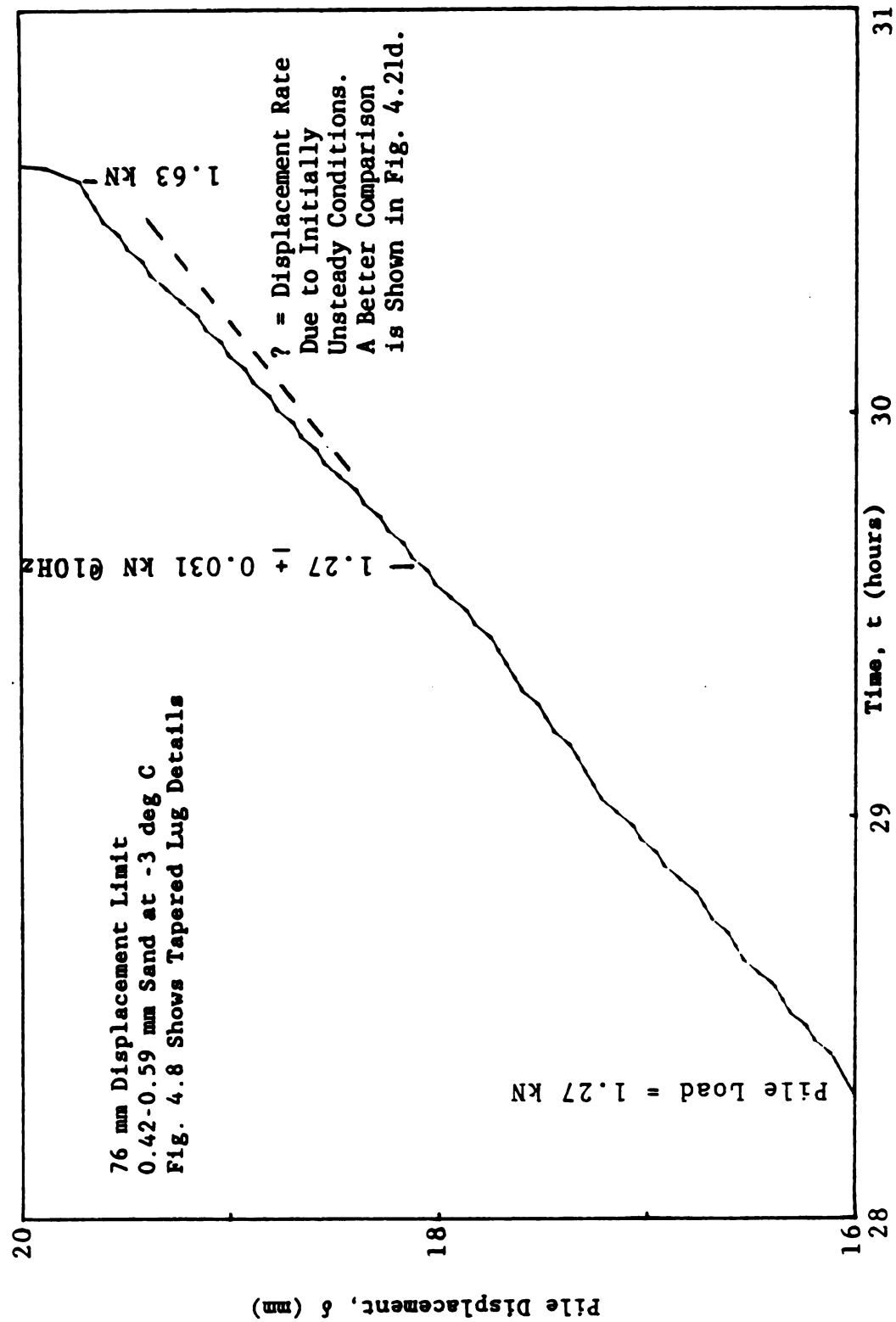

Figure 4.21. Time-displacement behavior of model piles subjected to superimposed dynamic loads. (a) Curve of tapered lug pile (Test #60) in loose sand at -3 deg C.

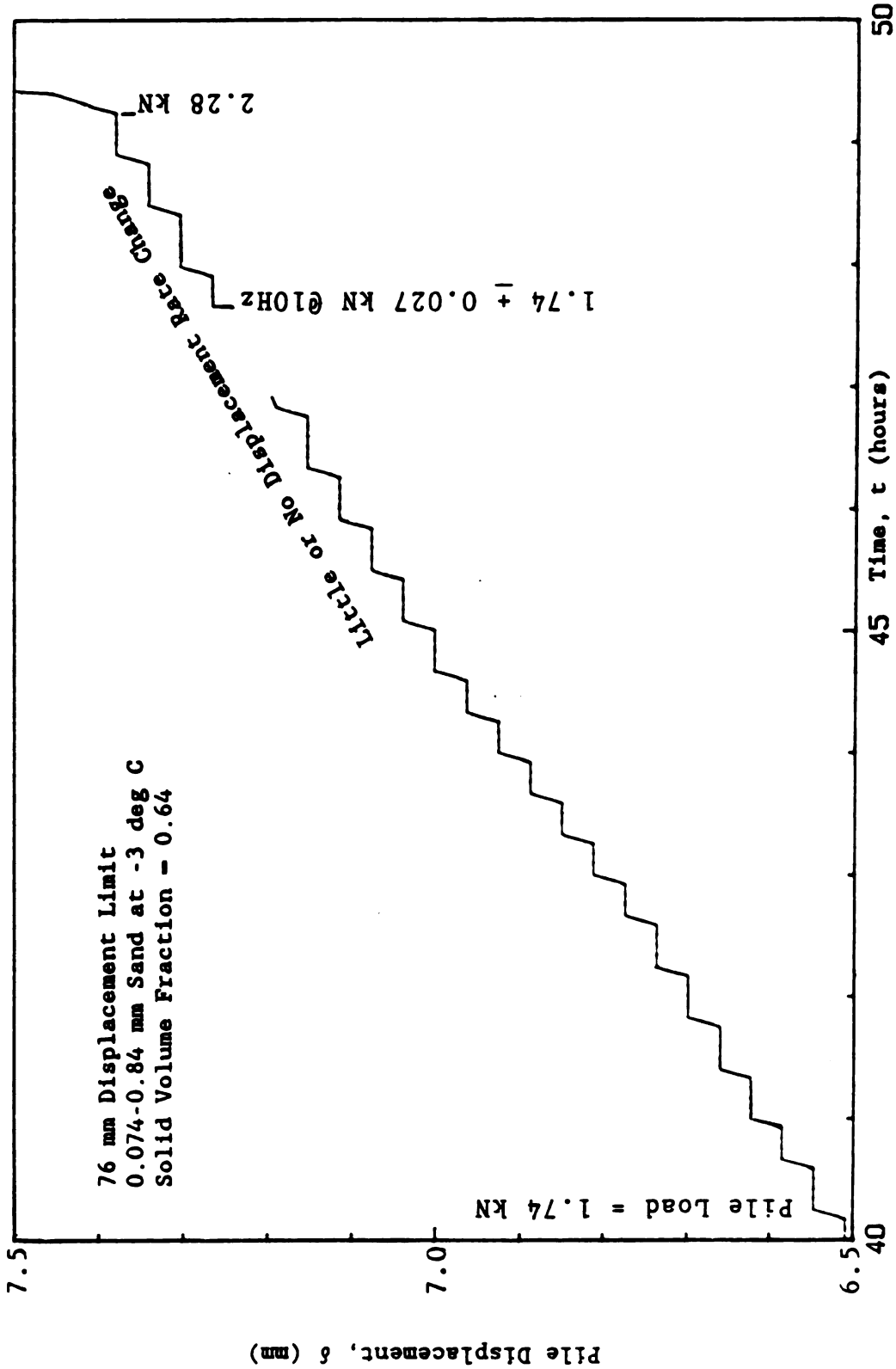

Figure 4.21b. Curve of 0.79 mm lug in dense sand (Test #33) at -3 deg C.

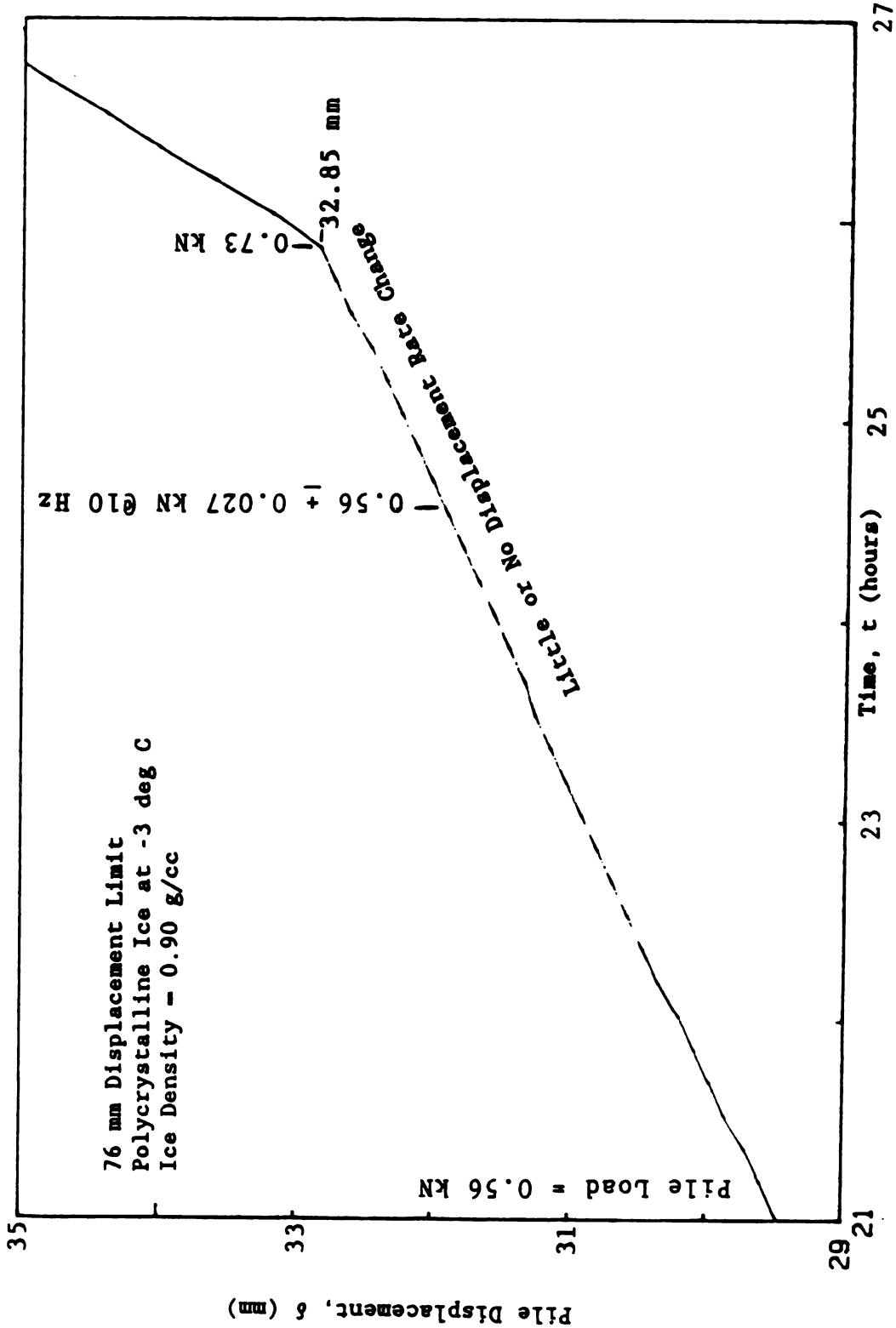

Figure 4.21c. Curve of 0.79 mm lug in polycrystalline ice (Test #35) at -3 deg C.

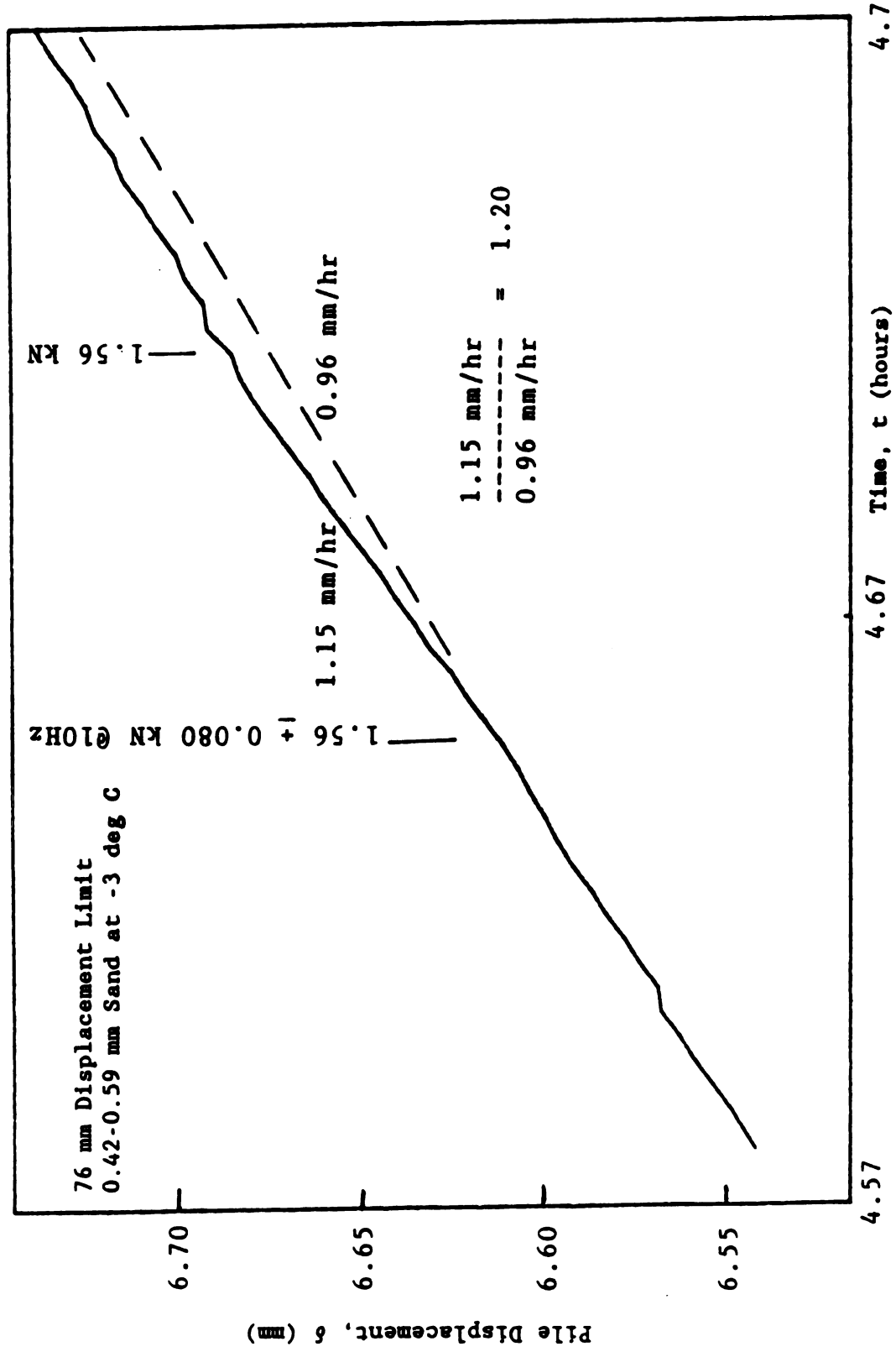

Figure 4.21d. Curve of 0.79 mm lug in loose sand (Test #88) at -3 deg C.

Table 4.3 Displacement Rate Increases from Short Duration Load Increases on Lugged Piles.

Pile Test No.	Test Temperature deg C	Sand Size Range mm-mm	Solid Volume Fraction %	Pile Lug Size mm	Embedment Ahead/Behind Lug mm/mm	Initial Load Before Increase kn	Percent Load Increase and Frequency % / Hz	Displacement at the Time of Load Increase mm	Displacement Rate Before Load Increase mm/hr	Percent Displacement Rate Increase %	Creep Parameter n
33	-3	.07-.84	64.5	0.79	76/62	1.27	± 1.5/10	7.27	0.090	?	-
35	-3	ice, 0.90g/cc	0.79	76/76	0.56	± 4.8/10	31.90	6.7	?	-	
60*t	-3	.42-.59	57 *v	0.76	76/62	1.74	± 2.4/10	18.08	1.57	?	-
78*g	-3	.42-.59	57 *v	3.18	76/32	1.56	± 5.1/.2*v	2.45	0.042	43	7.2
81*g	-3	.42-.59	57.8	0.79	76/62	0.88	± 8.7/.1*v	3.85	0.190	25	2.7
82*g	-3	.42-.59	57 *v	1.59	76/63	1.56	± 5.1/10	5.70	0.112	5	1.0
						1.56	± 1.7/10	7.80	0.102	3	1.8
						1.56	+3.4static	8.25	0.093	19	5.2
						1.56	+3.4static	8.35	0.104	18	4.4
						1.56	+6.9static	8.47	0.099	38	4.9
87	-3	.42-.59	56.4	1.59	76/64	1.55	± 5.2/ 1	2.98	0.038	52	8.3
						1.55	± 5.2/ 1	3.21	0.038	50	8.0
						1.55	± 5.2/ 1	3.90	0.027	58	8.8
88	-3	.42-.59	58.6	0.79	76/61	1.56	± 5.1/ 1	6.61	0.96	20	3.7
						1.56	± 5.1/ 1	7.65	1.10	25	4.5
						1.56	± 5.1/ 1	11.29	0.78	24	4.3
						1.56	± 1.7/ 1	12.76	1.00	6	3.5
89	-3	.42-.59	56.7	1.59	76/64	3.09	± 2.6/ 1	9.30	5.0	11	4.1
						3.09	± 5.2/ 1	11.12	5.3	28	4.9
						3.09	± 5.2/ 0.1	14.02	4.8	6	1.2
92	-3	.42-.59	57.8	1.59	76/64	2.20	± 2.5/ 1	6.76	0.64	10	3.9
						2.20	± 2.5/ 0.1	7.71	0.68	5	2.0
						2.20	± 2.5/10	8.57	0.73	8	3.1
						2.20	+1.6static	9.49	0.87	14	8.2
						2.20	± 5.1/ 1	13.55	0.87	26	4.6
						2.20	± 5.1/ 0.1	14.57	0.68	19	3.5
						2.20	± 5.1/10	15.54	0.69	20	3.7
						2.20	±10.1/ 1	19.76	0.66	54	4.5
						2.20	±10.1/ 0.1	20.64	0.57	51	4.3
						2.20	±10.1/10	21.47	0.69	49	4.1
						2.20	+6.5static	22.15	0.54	65	8.0
						2.20	+3.2static	26.92	0.66	28	9.6
						2.20	± 4.0/ 0.3	27.64	0.58	12	2.9
						2.20	± 4.7/ 0.3	28.38	0.62	19	3.8
						2.20	±10.1/ 0.3	29.18	0.65	51	4.3
						2.20	± 5.1/ 3	30.01	0.67	19	3.5

Table 4.3 (cont.)

93	-3	.42-.59	57.9	1.59	76/62	2.20	±10.1/10	6.94	0.68	42	3.6
						2.20	±10.1/ 1	7.52	0.68	67	5.3
						2.20	±10.1/ 3	8.10	0.67	43	3.2
						2.20	±10.1/ 2	8.71	0.73	47	4.0
						2.20	±10.1/ 0.8	12.64	0.52	55	4.6
						2.20	±10.1/ 0.3	13.03	0.52	51	4.3
						2.20	±10.1/ 3	13.44	0.47	51	4.3
						2.20	±10.1/ 1	13.89	0.41	73	5.7
						2.20	±10.1/ 1.3	14.20	0.37	53	4.4
						2.20	± 5.1/ 0.3	16.56	0.56	25	4.5
						2.20	± 5.1/ 3	16.99	0.45	24	4.3
						2.20	± 5.1/ 1	17.35	0.42	32	5.6
						2.20	± 2.5/ 0.3	17.80	0.41	10	3.9
						2.20	± 2.5/ 3	18.14	0.40	14	5.3
						2.20	± 2.5/ 1	18.51	0.43	20	7.4
						2.20	±10.1/ 0.3	21.35	0.49	59	4.8
						2.20	±10.1/ 3	21.72	0.49	58	4.8
						2.20	±10.1/ 1	22.04	0.40	73	5.7
						2.20	±10.1/ 1.3	22.33	0.38	67	5.3
						2.20	±10.1/ 6.2	23.06	0.36	80	6.1
						2.20	±10.1/ 3	23.33	0.37	63	5.1
						2.20	±10.1/10	23.60	0.31	68	5.4
						2.20	±10.1/ 1	23.89	0.40	65	5.2
						2.20	±10.1/ 0.3	25.50	0.45	64	5.1
						2.20	±10.1/ 1	25.84	0.43	91	6.7
						2.20	±10.1/ 3	26.17	0.37	64	5.1
						2.20	±10.1/ 6	26.42	0.35	74	5.8
						2.20	±10.1/10	26.68	0.35	71	5.6
94	-3	.42-.59	57.8	1.59	76/64	1.95	± 2.5/ 0.3	5.61	0.22	10	3.7
						1.95	+1.4static	6.05	0.20	18	12.0
						1.95	± 5.0/ 0.3	6.40	0.169	26	4.7
						1.95	+2.7static	6.65	0.21	23	7.6
						1.95	±10.0/ 0.3	6.90	0.171	65	5.2
						1.95	±10.0/ 3	7.19	0.195	46	3.9
						1.95	±10.0/ 0.1	7.47	0.20	47	4.0
						1.95	+2.7static	7.72	0.20	31	10.0
						2.00	+2.7static	7.77	0.27	13	4.5
						1.95	±10.0/ 0.1	10.26	0.186	61	5.0
						1.95	±10.0/ 3	10.54	0.147	52	4.4
						1.95	+4.6static	10.82	0.153	53	9.5
						1.95	+2.3static	11.05	0.161	28	11.0
						1.95	± 5.0/ 0.1	11.20	0.166	39	6.7
						1.95	± 2.5/ 0.1	11.40	0.169	6	2.4
						1.95	+1.1static	11.63	0.164	11	9.4
						1.95	+13.static	14.33	0.172	182	8.5
						2.20	± 2.2/ 0.1	15.39	0.39	9	4.1
						2.20	± 2.5/ 3	15.82	0.39	16	5.8
						2.20	± 2.5/ 0.3	16.33	0.47	11	4.1
						2.20	+1.2static	16.69	0.37	13	10.1
						2.20	± 5.0/ 0.3	17.02	0.41	24	4.4

Table 4.3 (cont.)

						2.20	+2.4static	17.42	0.38	19	7.3
						2.20	±10.1/ 0.3	17.73	0.35	64	5.1
						1.95	+13.static	20.32	0.171	176	8.3
						2.20	±10.1/ 0.3	21.03	0.42	64	5.2
						2.20	±10.1/ 3	21.34	0.41	46	3.9
						2.20	±10.1/10	21.64	0.35	55	4.6
						2.20	+4.0static	21.92	0.33	50	10.3
						2.20	±10.1/ 0.1	22.17	0.33	76	5.9
						2.20	+4.0static	22.45	0.36	25	5.7
						2.20	+4.0static	23.24	0.36	28	6.3
						2.20	±10.1/10	23.57	0.38	63	5.1
						2.20	± 5.0/10	23.83	0.40	27	4.9
						2.20	± 5.0/10	24.10	0.36	32	5.6
						2.20	+2.0static	24.36	0.40	19	8.6
						1.95	+26.static	27.38	0.185	450	7.3
						2.46	+3.6static	28.24	1.10	30	7.3
						2.46	± 9.0/10	28.68	1.03	58	5.3
						2.46	±10.1/ 0.1	29.06	1.01	43	3.7
						2.46	± 3.8/ 0.3	29.41	0.99	13	3.4
						2.46	±10.1/ 0.3	29.72	1.03	53	4.4
						2.46	±10.1/10	30.18	1.14	67	5.3
						2.46	+1.8static	30.58	1.14	15	7.7
						2.46	± 5.1/ 0.1	30.94	1.08	12	2.3
						2.46	± 5.1/ 0.3	31.29	1.09	14	2.7
						2.46	± 5.1/10	31.75	1.09	22	4.1
						2.46	+0.9static	32.13	1.08	9	9.5
						2.46	+1.8static	32.46	1.05	24	6.0
						2.46	+3.6static	32.77	0.98	52	11.8
						1.95	±14.0/10	37.48	0.34	90	4.9
						1.95	±10.0/10	37.80	0.27	64	5.2
						1.95	+4.6static	38.07	0.30	52	9.3
						1.95	±10.0/10	38.33	0.27	63	5.1
						1.95	+4.6static	38.58	0.28	54	9.6
						2.04	+8.1static	38.66	0.43	69	6.7
						2.20	+4.0static	39.22	0.71	24	5.3
						2.20	±10.1/10	39.52	0.70	61	4.9
						2.20	±10.1/10	39.86	0.76	48	4.1
						2.20	+4.0static	40.21	0.72	26	5.9
						2.29	+7.4static	40.28	0.91	82	8.4
						2.46	+3.6static	40.63	1.47	43	9.9
						2.46	±10.1/10	41.63	1.35	59	4.8
						2.46	±10.1/10	42.01	1.25	53	4.4
						2.46	±10.1/10	42.44	1.26	48	4.1
						2.46	+3.6static	43.05	1.31	25	6.3

? Displacement rate increases can't be measured accurately but seem to be small

*g Silicon grease applied to pile and lug surface to reduce bond

*t Leading edge of lug is tapered instead of square-edged

*v Estimated from the average of similar tests

*w Square wave form used

through 4.21d. The major difference involves the material in which each pile was frozen. The larger displacement rate increases are obtained for loose frozen sand as shown in Figures 4.21a and 4.21d. The dense sand, Figure 4.21b, and the polycrystalline ice, Figure 4.21c, show little or no displacement rate increases. These and other results from short duration loads are summarized in Table 4.3.

4.5. Multiple Short Duration Loads on Lugged Model Piles

The short duration load technique can be repeated on the same frozen sand sample in order to provide much more data. The time-displacement behavior for this type of loading sequence is shown in Figure A.3 (Appendix A) on Pile Test #123. After an extended period of displacement at the initial pile load of 3.10 kN, the load was increased 0.12 kN (5.2%) for a 90 minute period. Two additional 0.16 kN pile load increases were added during subsequent 90 minute intervals. The last 0.16 kN increase (3.74 kN total pile load) remained for more 90 minutes. An alternative loading sequence might have restored the load to 3.10 kN after the last addition. The log(time)-log(displacement) curves from these load increases, using 0.1 mm B-type starting points, are shown in Figure 4.22.

Curves B, C, D, and E in Figure 4.22 show a relatively faster displacement during periods of (primary behavior) compared to the nearly constant, late primary-secondary

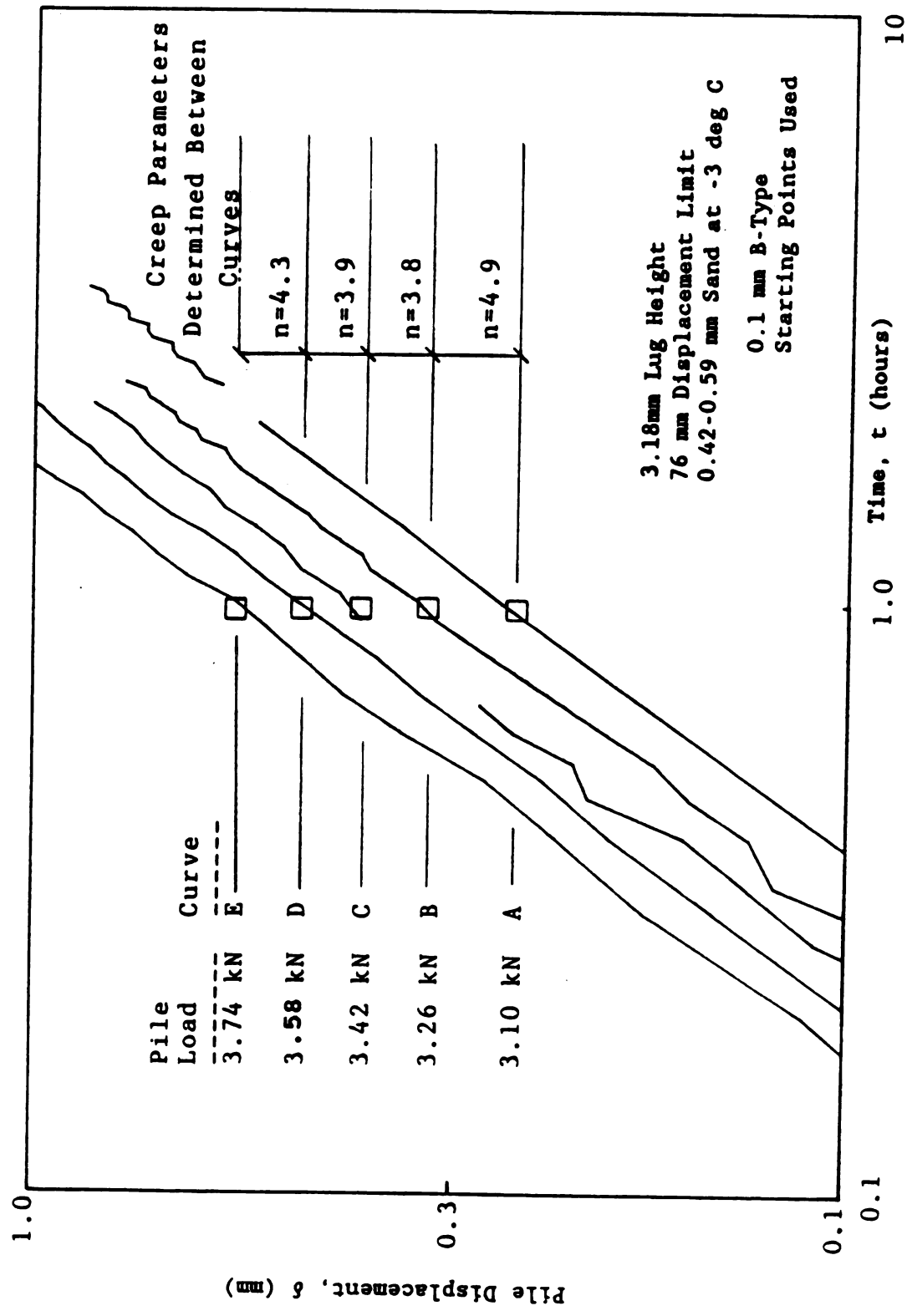

Figure 4.22. Time-displacement behavior of a single pile (Test #123) loaded by successively larger loads during a short total duration.

Table 4.5. Displacement Rate Increases from Multiple Short Duration Loads on Lugged Piles.

Pile Test No.	Test Temperature deg C	Sand Size Range mm-mm	Solid Volume Fraction %	Pile Lug Size mm	Embedment Ahead/Behind Lug mm/mm	Initial Load Before Increase Kn	Percent Load Increase and Frequency % / Hz	Creep Parameter n	Displacement at the Time of Load Increase mm	Displacement Rate Before Load Increase mm/hr	Displacement Rate After Load Increase mm/hr
123	-3	.42-.59	57.3	3.18	76/20	3.10	-	-----	-	0.30	-
								4.9			
							5.2/static	-----	16.10	-	0.33
								3.8			
							5.2/static	-----	16.86	-	0.39
								3.9			
							5.2/static	-----	17.80	-	0.47
								4.3			
							5.2/static	-----	18.93	-	0.57

behavior of curve A. Curves B, C, D, and E would move closer to curve A (by slowing down) if each curve was extended, but any comparisons between them would extend over a larger range of total displacement and thus complicate these comparisons. Curves B through E can not be readily compared to the nearly-steady Curve A, but can be compared with each other since they were drawn during the same early stage and are within a relatively small range of total displacement. Data comparisons are also improved because no pile unloading period was allowed to complicate conditions during the test.

With parameter b = 1, equation 3.4 written in the form

$$(\dot{\delta}_2 \; / \; \dot{\delta}_1) \quad = \quad (P_2 \; / \; P_1)^n$$

was used to compute n values shown in Figure 4.22. These n values, computed between curves B, C, D, and E, are similar to the value of n = 4.0 computed from the full duration loads (at C-type starting points of 5 mm) in Table 4.1.

4.6 Threaded Rods as Model Piles

Each thread of a threaded rod can be considered as a lug and the entire pile as a series of closely spaced lugs. Pile test data for a single size thread (24 per inch with a 1.06 mm peak to peak distance) in a frozen loose sand is shown in Figure 4.23. Note that pile failures (Tests #91 and #86) began at approximately 1.0 mm which is nearly

Table 4.4. Threaded Pile Test Results

Type of Load Duration	Thread to Thread Length	Pile Test No.	C-Type Starting Point	Sand or Ice&	Test Temperature	Solid Volume Fraction	Initial Load	Load Increase	Displacement at Load Increase	Displacement Rate at Increase	Creep Parameters b	n	r_c
	mm		mm		deg C	%	MPa	% / Hr	mm	mm/hr			MPa
Full	1.06	91	0.14	sand	-3	58.3	2.03	constant	-	-	0.80	3.2	2.18
		86	0.14			57.8	2.02	constant					
		69	0.14			57*	1.34	constant					
		67	0.14			57*	0.59	constant					
Full	1.06	91	0.30	sand	-3	58.3	2.03	constant	-	-	0.95	6.8	1.85
		86	0.30			57.8	2.02	constant					
		69	0.30			57*	1.34	constant					
		67	0.30			57*	0.59	constant					
Full	1.59	120	0.0	sand	-3	56.5	2.04	constant	-	-	0.64	2.0	0.95
		90				53.1	1.71	constant					
Full	1.59	120	0.14	sand	-3	56.5	2.04	constant	-	-	0.86	2.8	1.30
		90				53.1	1.71	constant					
Full	1.59	120	0.3	sand	-3	56.5	2.04	constant	-	-	0.90	3.5	1.43
		90				53.1	1.71	constant					
Full	1.59	120	0.7	sand	-3	56.5	2.04	constant	-	-	1.0	5.2	1.65
		90				53.1	1.71	constant					
Step	1.06	67	0.1	sand	-3	57*	0.59	+100static	0.193	0.0038	1.0	3.2	1.65
Step	1.06	69	0.1	sand	-3	57*	1.34	+ 70static	0.66	0.0077	1.0	4.4	2.40
Step	1.06	80	0.1	sand	-2	57.1	0.97	+ 42static	0.23	0.072	1.0	2.8	1.10
Short	1.06	79	0.02	sand	-3	51.1	1.11	+ 68static	0.125	0.087	-	3.2	-
Short	1.06	86	0.01	sand	-3	57.8	2.02	±2.6/ 1	0.227	0.24	-	2.5	-
							2.02	±5.2/ 1	0.450	0.184	-	2.5	-
							2.02	±5.2/ 1	0.659	0.152	-	3.5	-
							2.02	±5.2/ 1	0.950	0.148	-	3.0	-
Short	1.06	63	0.01	ice	-3,0.90g/cc	0.60	+ 52static	?	0.0041	-	4.1	-	
Short	1.06	64	0.01	ice	-3,0.90g/cc	0.41	+ 27static	?	0.0050	-	3.3	-	
						0.41	±5.0/ 10	?	0.0087	-	4.8	-	

& P_c determined at $\dot{\delta}_c$ = 0.1 mm/hr

@ Sand is graded 0.42 to 0.59 mm, ice is polycrystalline

*v Estimated from the average of similar tests

? Displacement rates measured after large jumps in total displacement

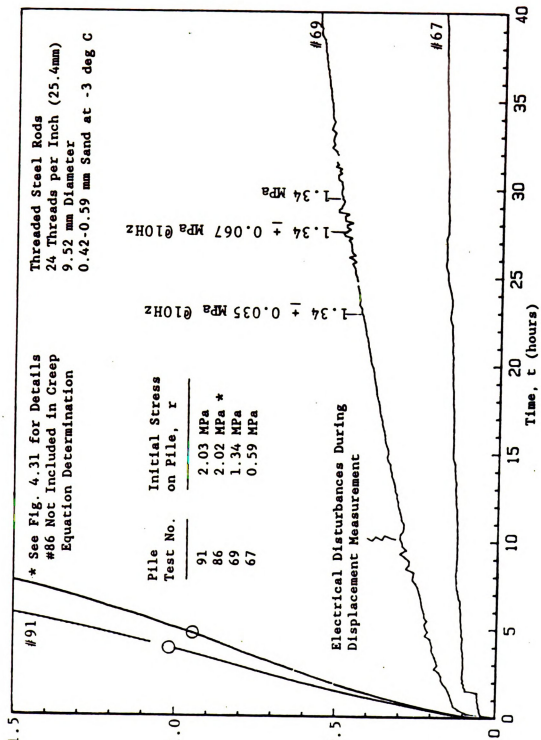

Figure 4.23. Time-displacement of threaded rods in frozen sand.

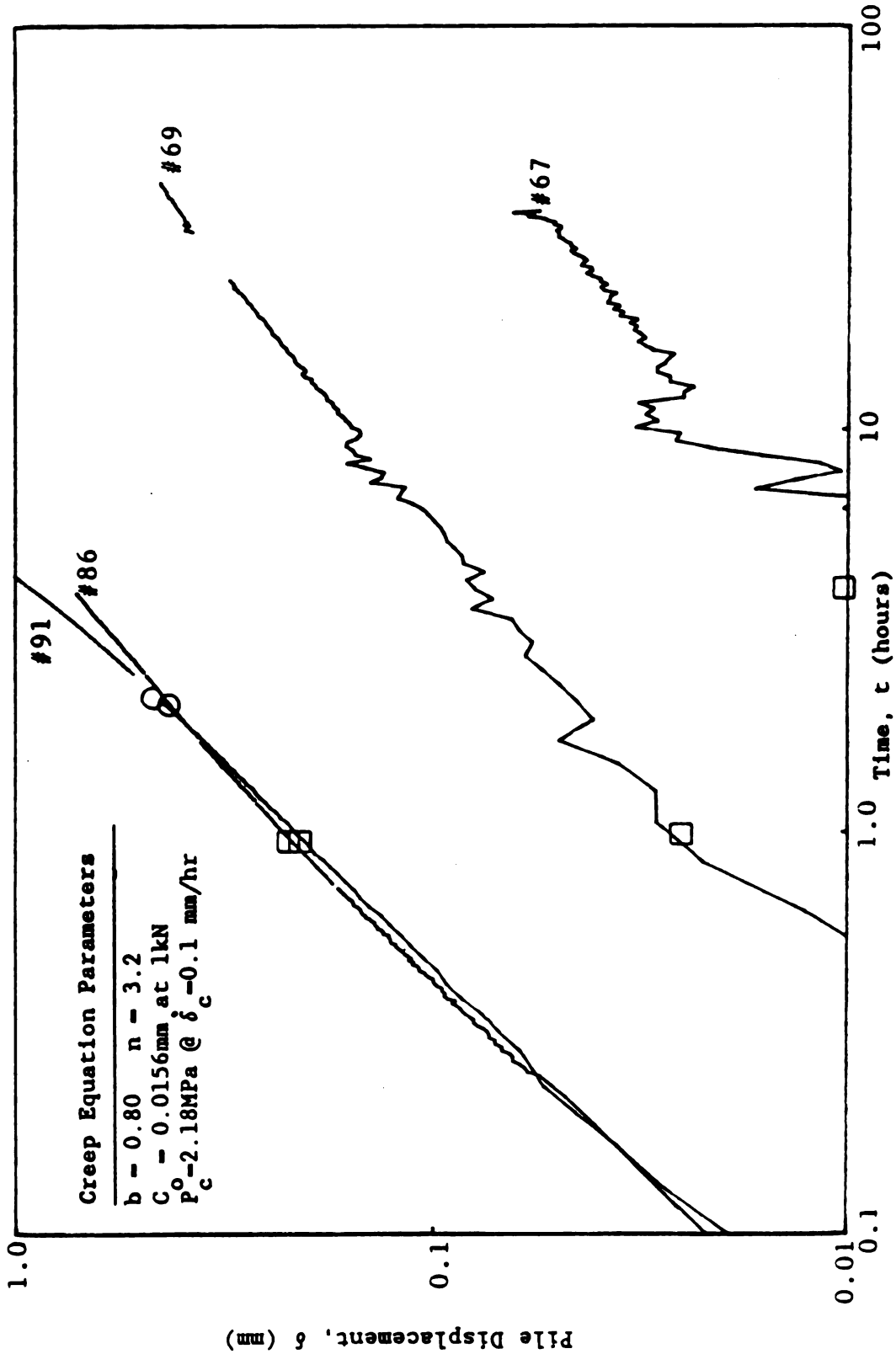

Figure 4.24. Time-displacement behavior of threaded rods in frozen sand. (a) Threaded rod time-displacement curves started 0.14 mm after initial loading.

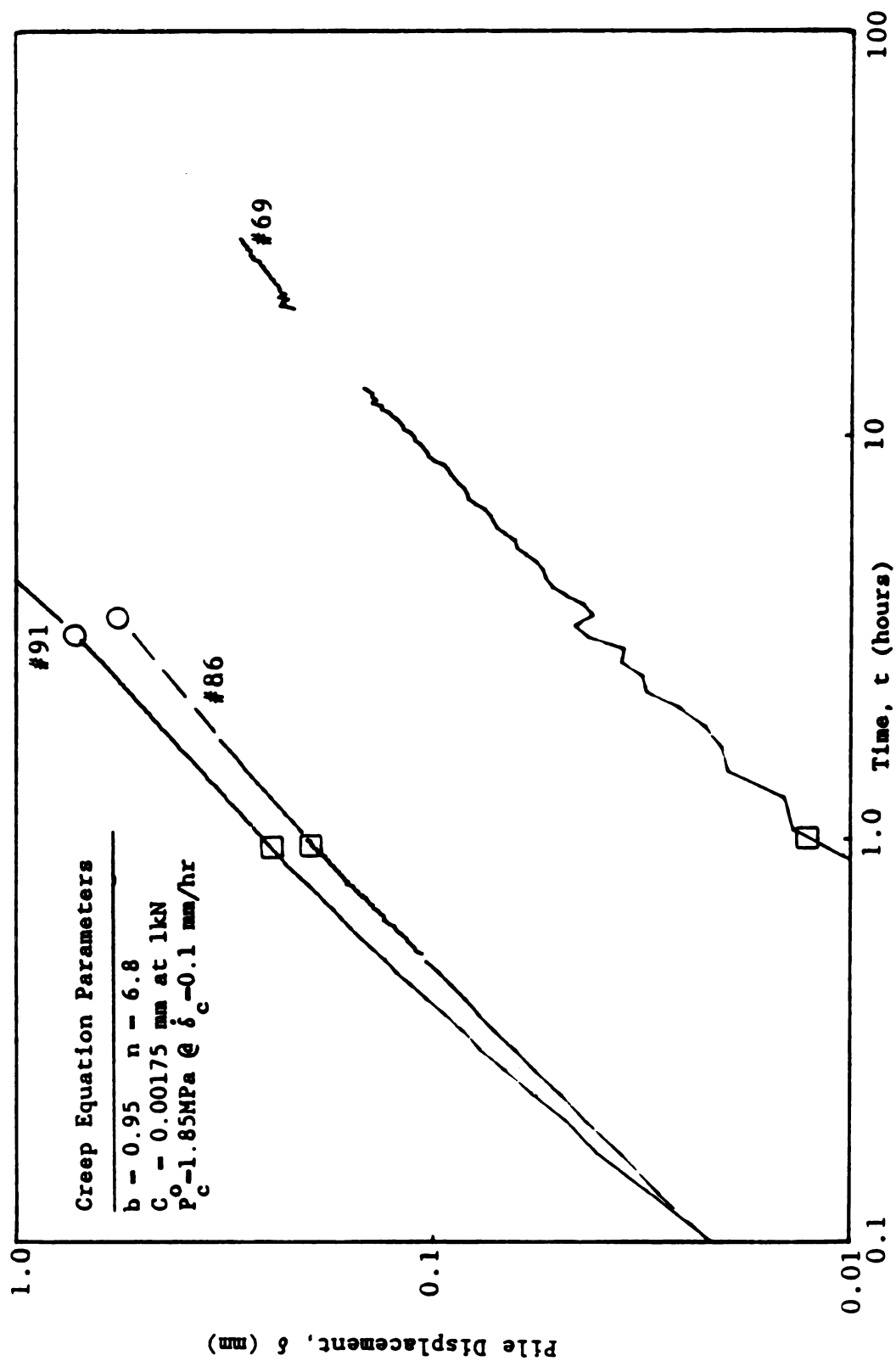

Figure 4.24b. Threaded rod time-displacement curves started 0.3 mm after initial loading.

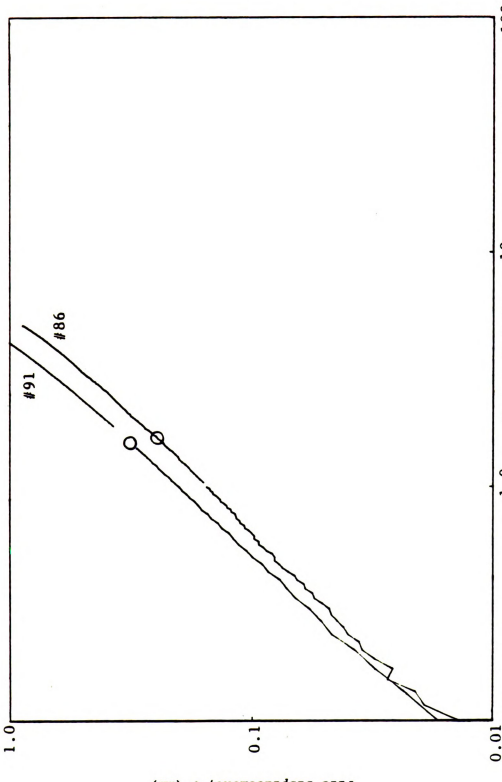

Figure 4.24c. Threaded rod time-displacement curves started 0.7 mm after initial loading.

equal to the peak to peak distance.

Figures 4.24a through 4.24c show log (time) - log (displacement) behavior for the pile tests shown in Figure 4.23. While measurements for these relatively small displacements are more subject to system errors as compared with the lugged pile data, it is clear that these piles achieved nearly steady rates at much smaller displacements than the lugged piles.

A time-displacement curve for a model pile with larger threads (16 threads per inch and a peak to peak distance of 1.59 mm) in frozen loose sand is shown in Figure 4.25. Pile failure for Test #90 appears to begin, with some initial oscillation, at 1.5 mm which is nearly equal to the thread to thread distance.

The behavior of a model pile with small threads (72 per inch and 0.35 mm peak to peak distance) in frozen loose sand (particle size of 0.42 to 0.59 mm size) is shown in Figure 4.26. In this case failure occured at about 0.14 mm displacement. In polycrystalline ice this same pile failed at 0.17 mm (Figure 4.27), compared to an apparent pile failure of 0.14 mm in frozen loose sand. Any interaction between sand and threads may have been prevented by the small size threads which limited failure to ice at the soil/pile interface.

Time - displacement data for the 24-threads per inch piles, frozen and loaded in polycrystalline ice, are shown

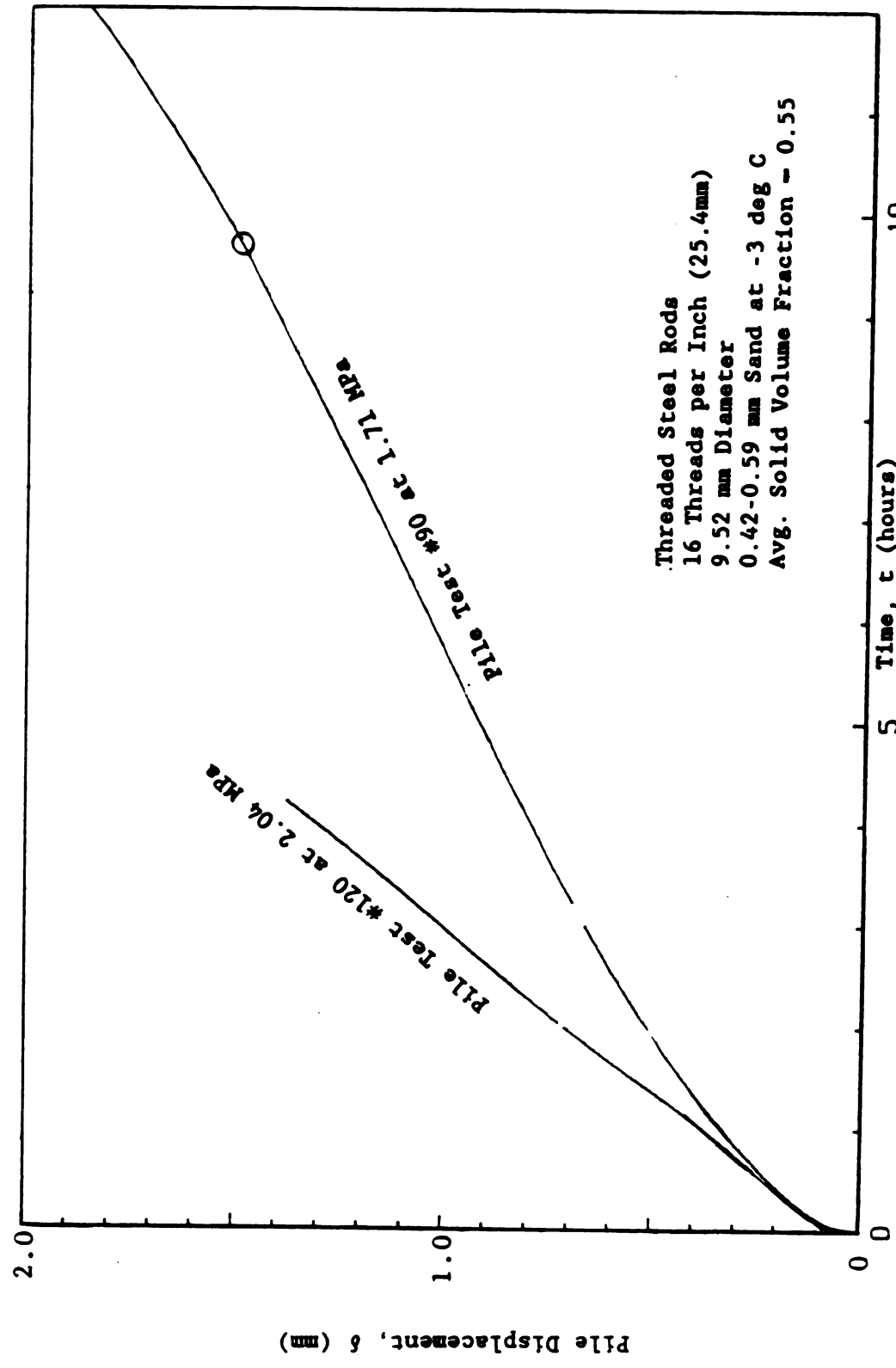

Figure 4.25. Time-displacement behavior for 16 thread per inch piles embedded in frozen sand.

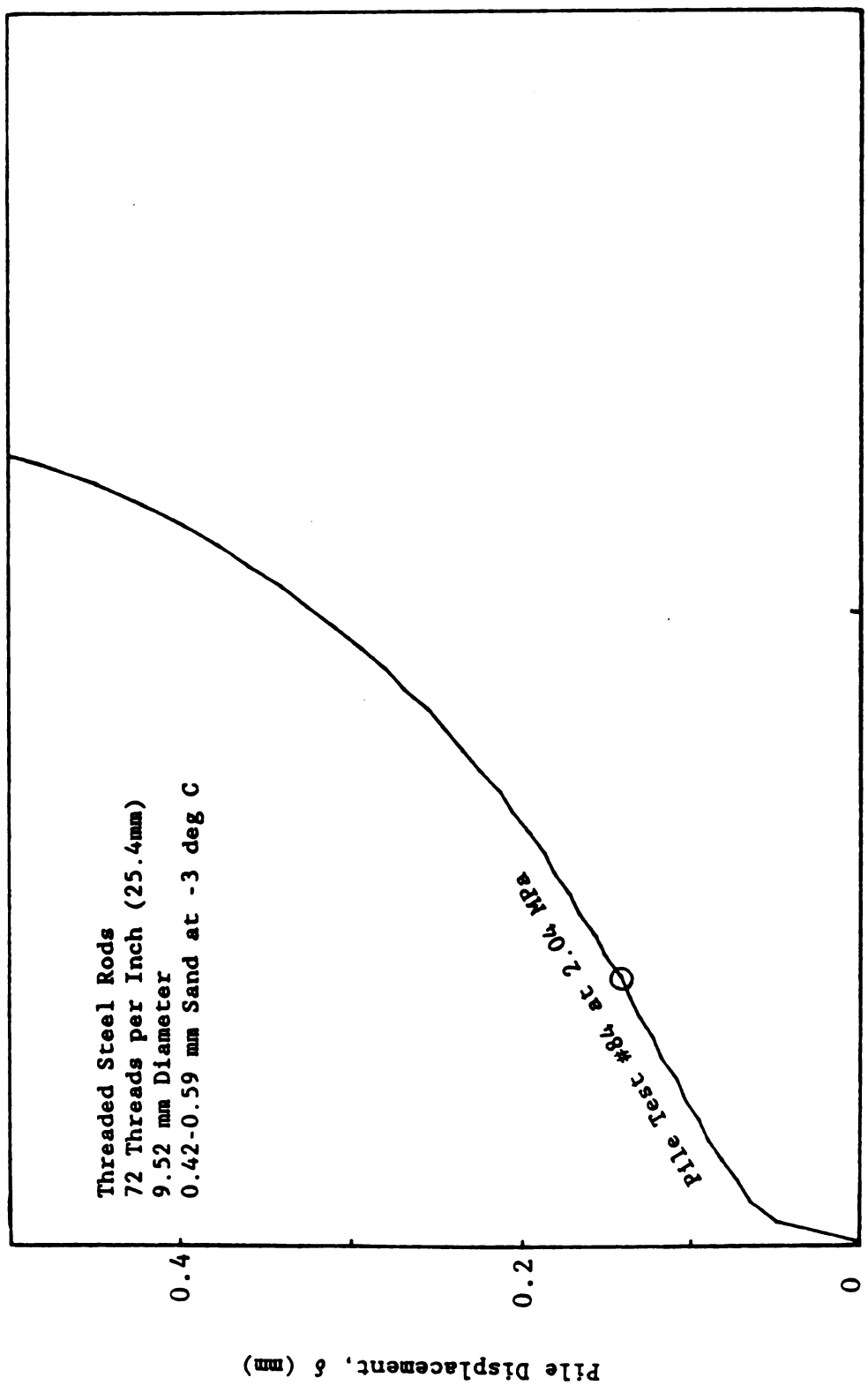

Figure 4.26. Time-displacement behavior for 72 thread per inch piles embedded in frozen sand.

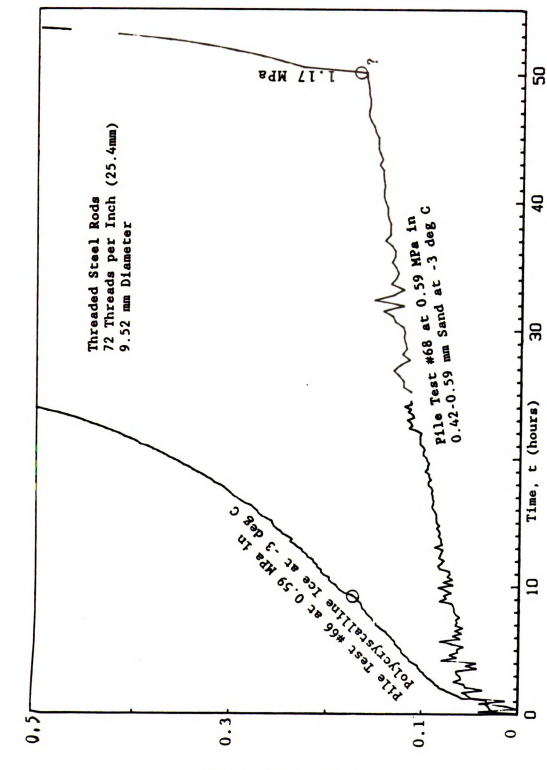

Figure 4.27. Time-displacement behavior of a 72 thread per inch pile embedded in polycrystalline ice and sand.

in Figure 4.28. Initial failure begins at about 0.19 mm. This is close to the failure displacement shown in Figure 4.27 for the 72 thread per inch pile. Additional tests are needed to show if the failure displacement in polycrystalline ice is totally independent of thread size.

Pile displacement data, summarized in Figures 4.29a and 4.29b, was obtained using 2 displacement transducers positioned on opposite sides of the model pile. This arrangement recorded large displacements at the start of each load increase. Later, a third displacement transducer was added and all three displacement transducers were repositioned evenly around the model to provide more reliable results. Although the total displacements shown in Figure 4.29a and 4.29b are questionable, the displacement rates shown after each displacement jump appear to be reasonable. Straight lines were used to approximate the displacement rates of these piles during given periods. Ratios for these displacement rate changes are shown on each figure.

An enlarged portion of the data from Figure 4.29b is shown in Figure 4.30. Pile Test #86, reported earlier in Figures 4.23 and 4.24, is shown in more detail in Figure 4.31 and Figure 4.32 with the displacement rate increase approximated by straight lines.

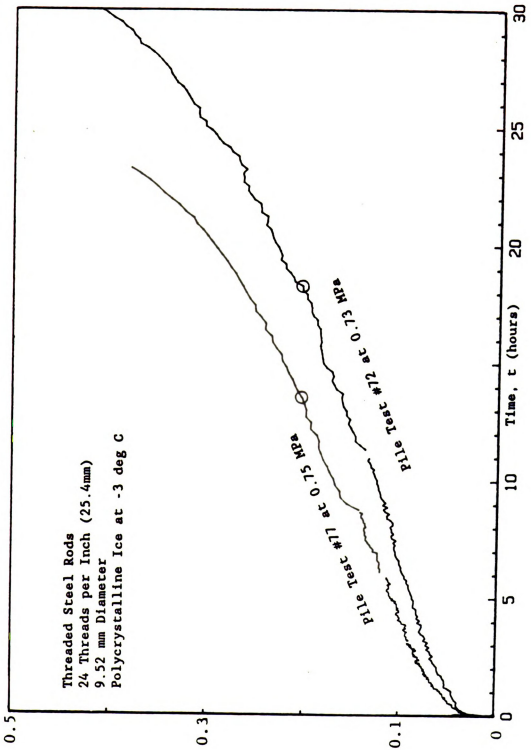

Figure 4.28. Time-displacement behavior for a 24 thread per inch pile embedded in polycrystalline ice.

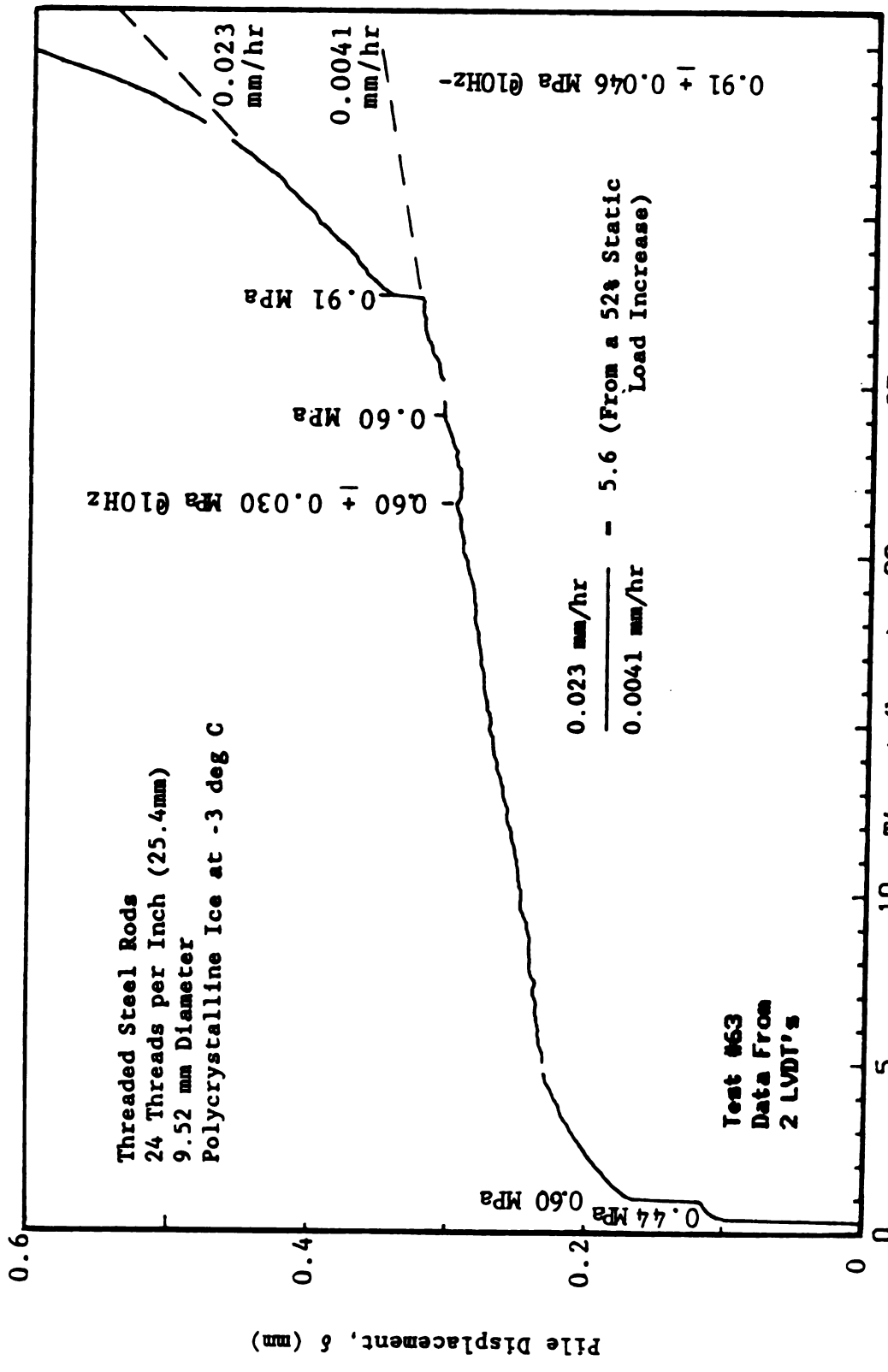

Figure 4.29. Time-displacement behavior for a 24 thread per inch pile embedded in polycrystalline ice. (a) Static load increase of 52%.

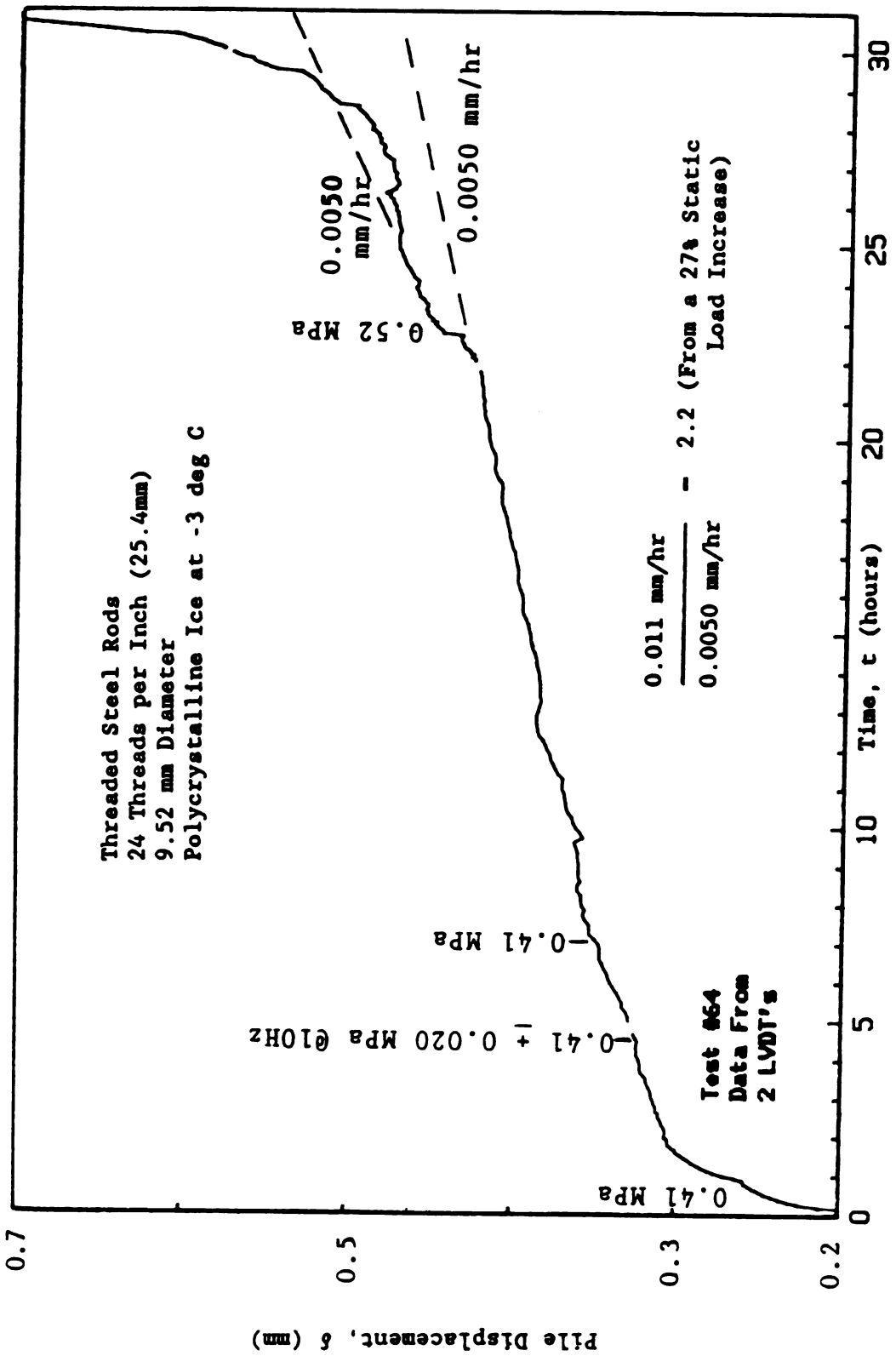

Figure 4.29b. Static load increase of 27%.

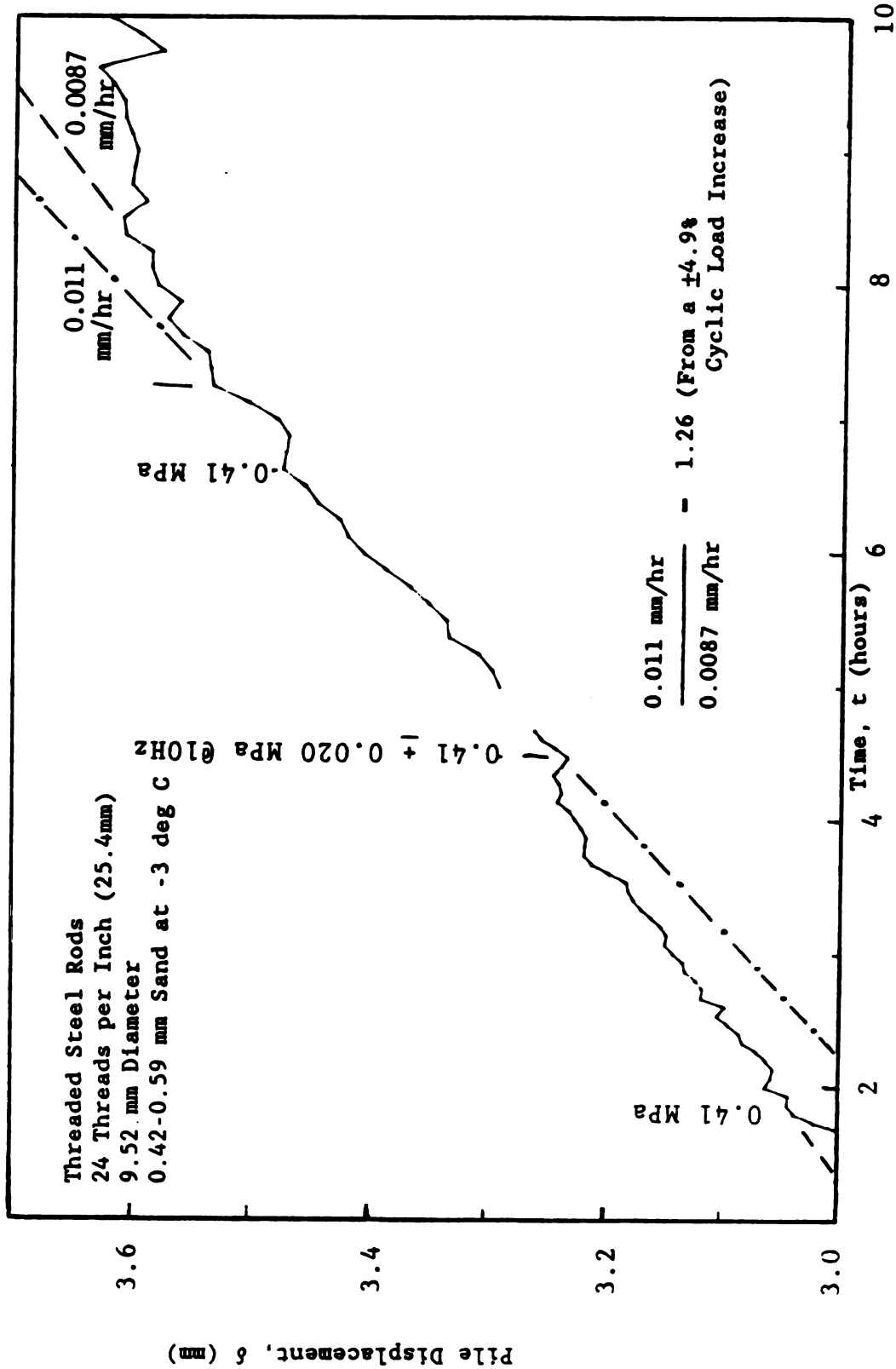

Figure 4.30. Enlarged time-displacement behavior for a 24 threaded per inch pile (Test #64) in polycrystalline ice showing a displacement rate increase from a cyclic load.

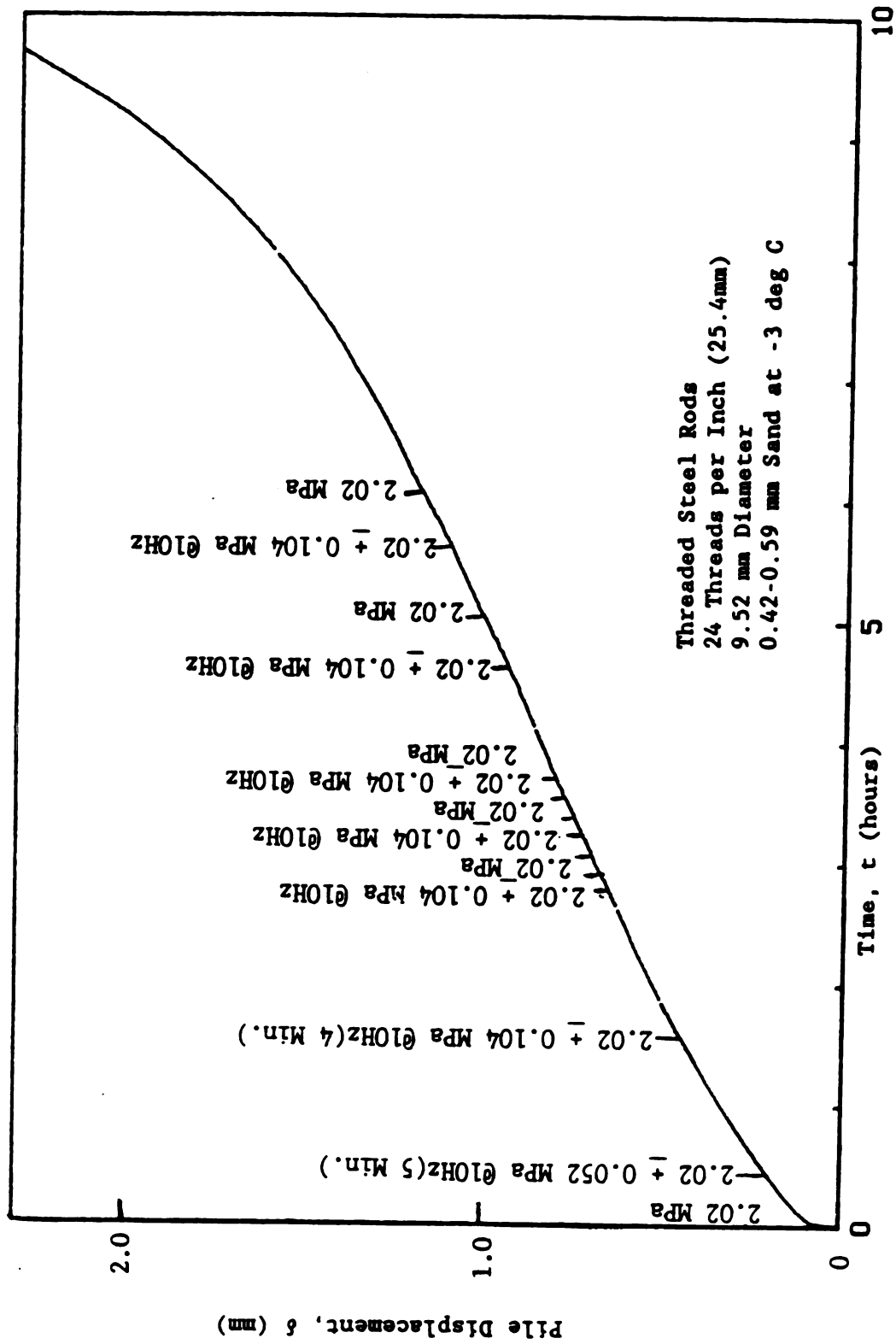

Figure 4.31. Time-displacement behavior for a 24 thread per inch pile (Test #86) in loose frozen sand with periods of superimposed cyclic loads.

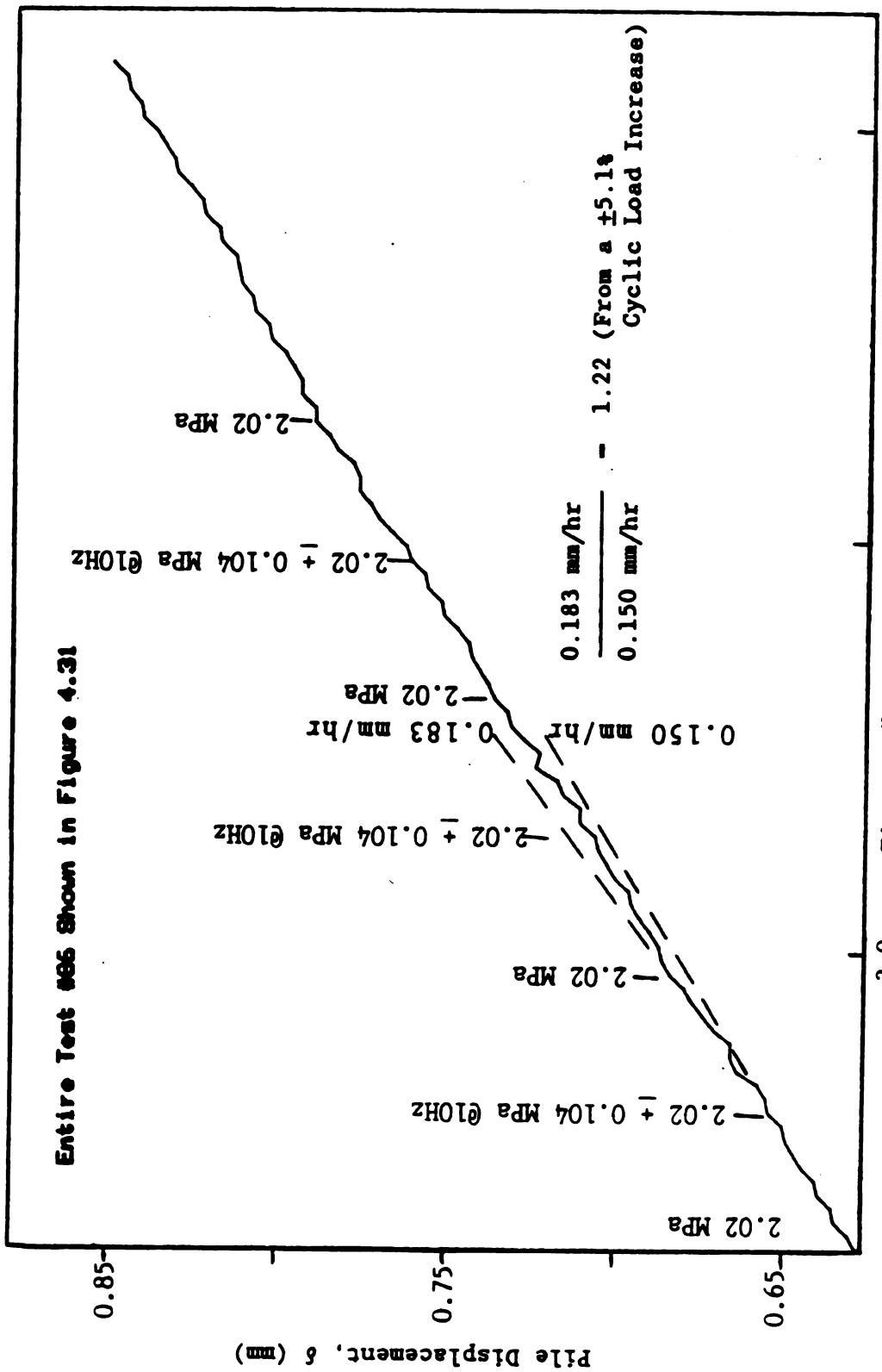

Figure 4.32. Enlarged due to a superimposed cyclic load.
(a) Time-displacement behavior after 0.65 mm displacement.

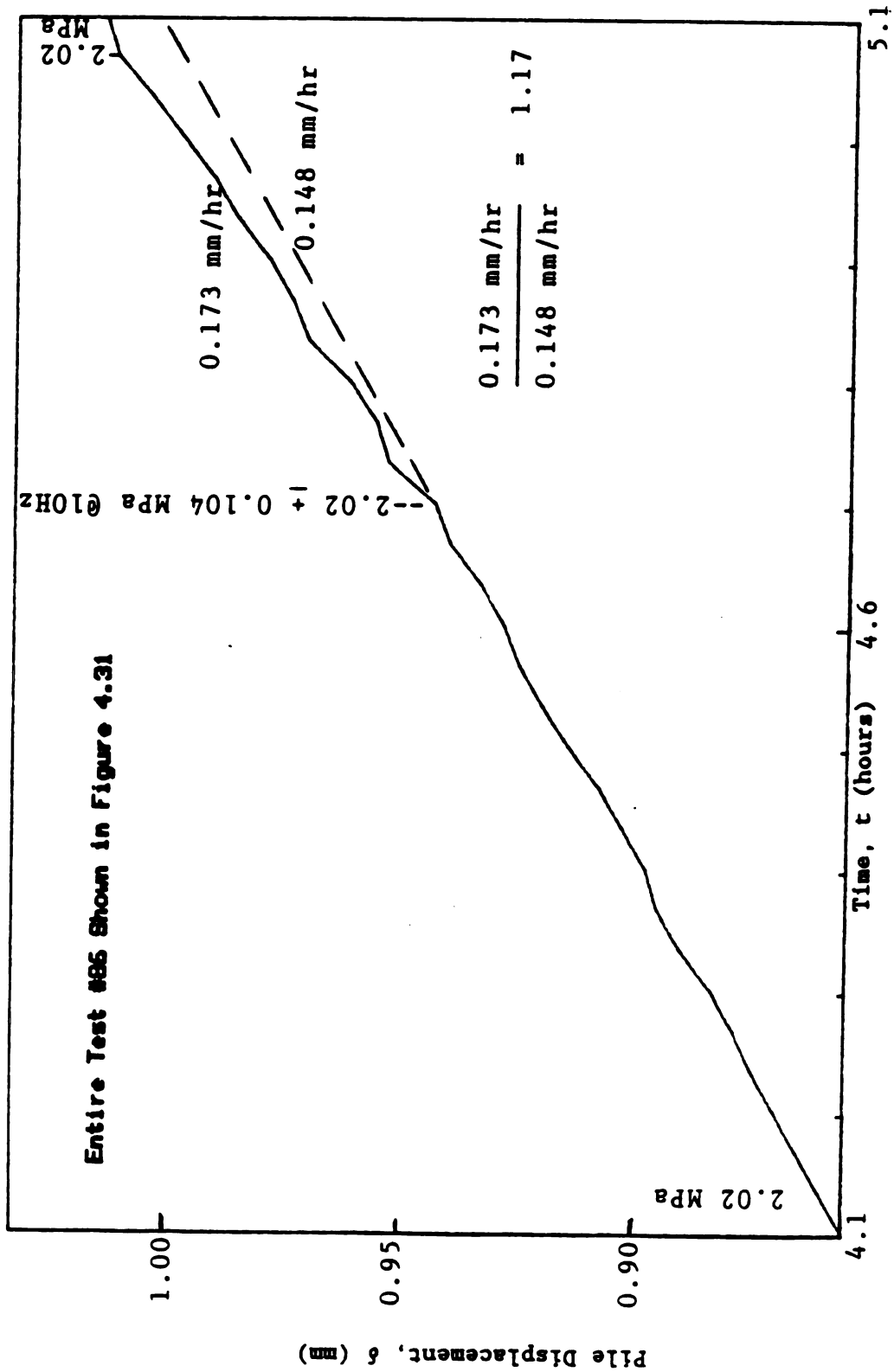

Figure 4.32b. Time-displacement behavior after 0.95 mm Displacement.

DISCUSSION AND APPLICATIONS

5.1. Creep Equation Parameters from Static Loads

The results from full duration model pile tests, summarized in Table 4.1, may be analyzed to better illustrate general pile behavior. The parameters n, b, and P_c are shown for 3 model pile types in Figures 5.1, 5.4, and 5.8. The piles represented in these figures are similar in all ways except for their lug size (3.18, 1.59, and 0.79 mm).

In figure 5.1, the b values for each lug size approach a value of 1, which represents a constant displacement rate. The b values for the smallest size lug approached this constant value more quickly than the larger lug sizes. Values for the 1.59 mm lug at 3 mm and 6 mm (Figure 5.1) appear to be low because other b values for this lug height are higher in Table 4.1. As a smaller lug advances through the frozen soil, fewer particles are moved, compacted, and displaced around the front of the advancing lug. The smaller volume of sand grains and ice ahead of the smaller lug should accumulate with less pile displacement. A two-dimensional approximation of what these zones of compacted sand might look like is shown in Figure 5.2.

Ladanyi (1976) showed a compacted soil condition for a a flat cylindrical punch (Figure 5.3a) after it had penetrated a frozen soil and reached a relatively constant

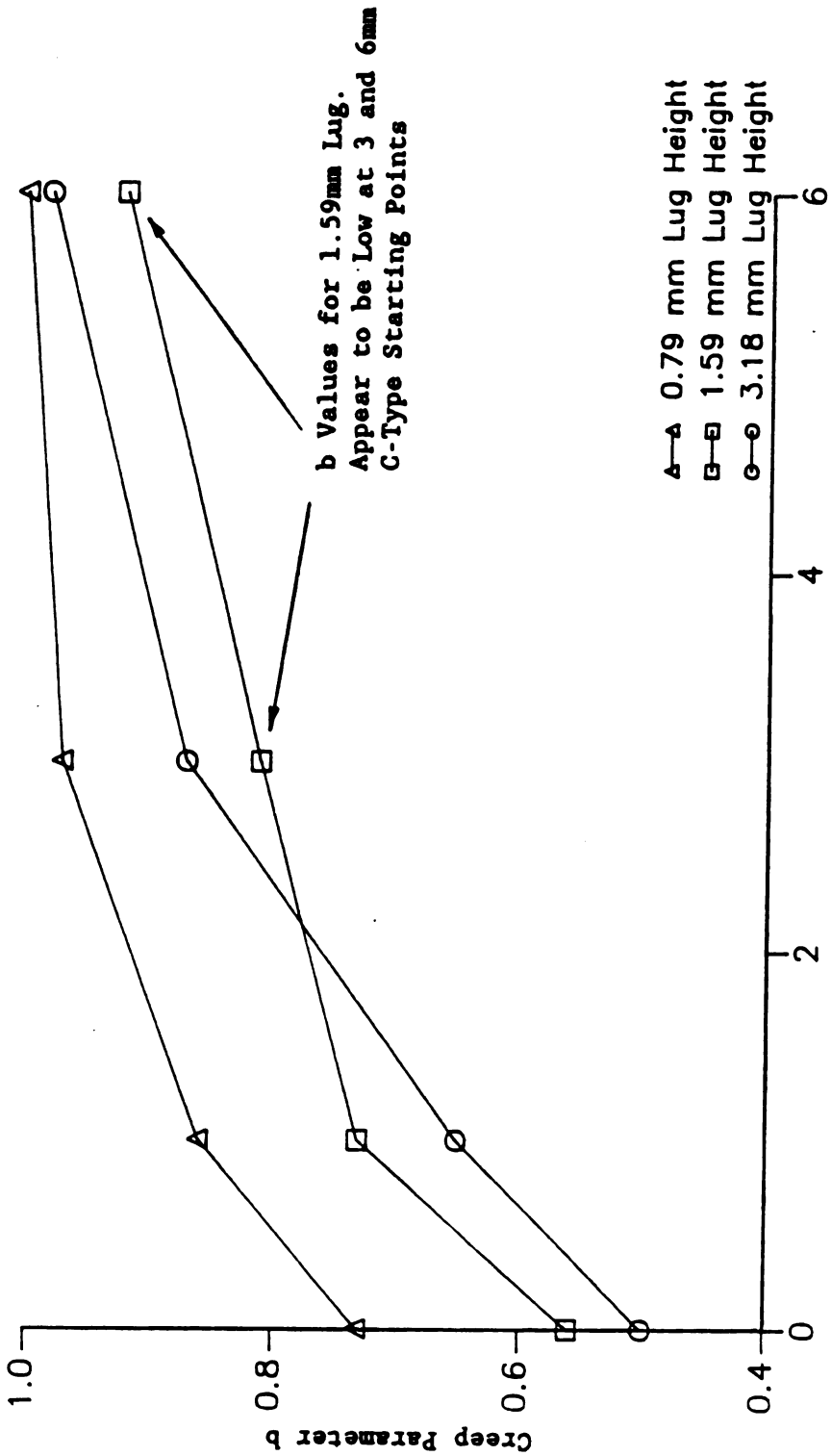

Figure 5.1. Piles with different lug sizes approach steady state (b=1) at various rates.

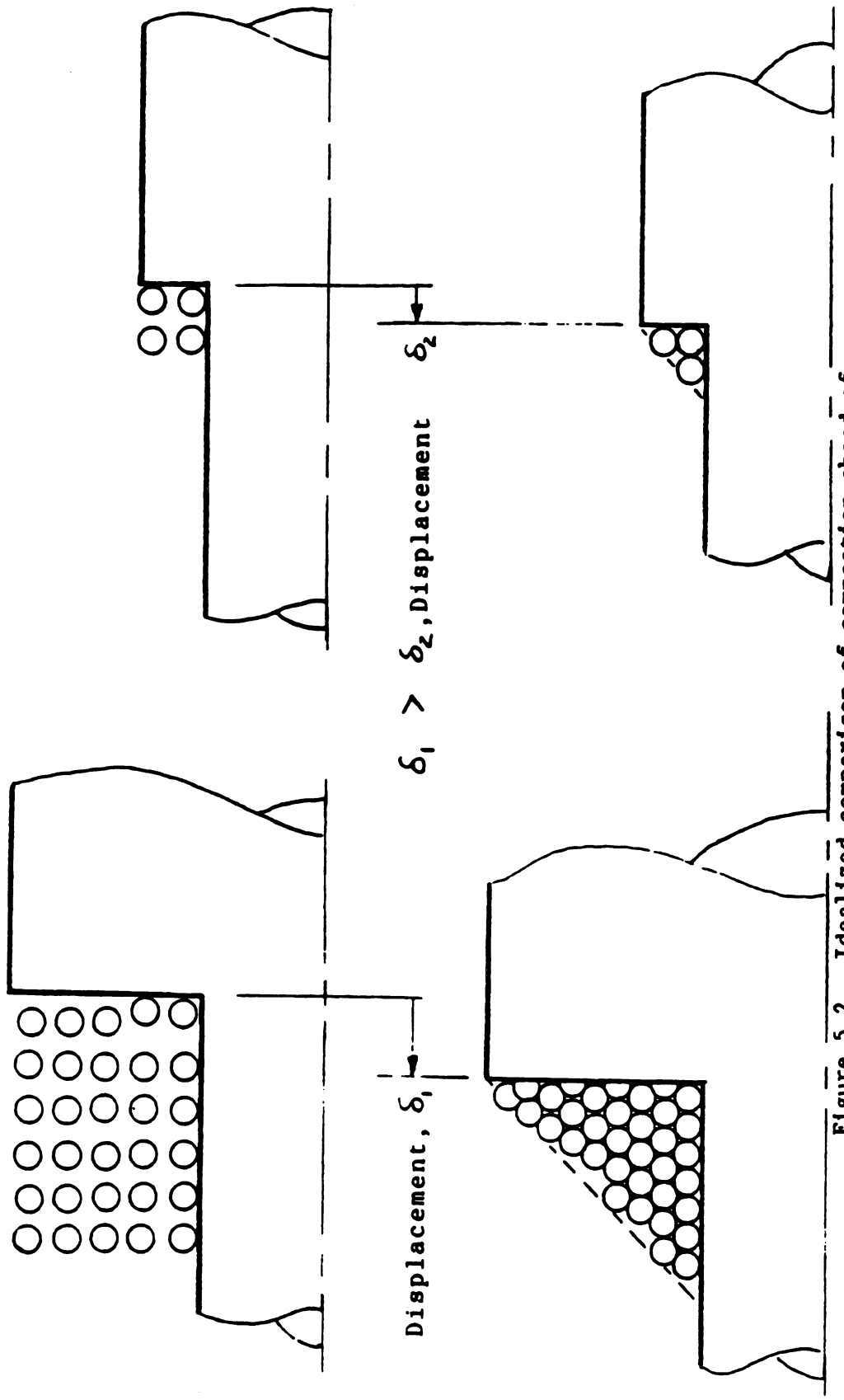

Figure 5.2 Idealized comparison of compaction ahead of pile lugs having different lug heights.

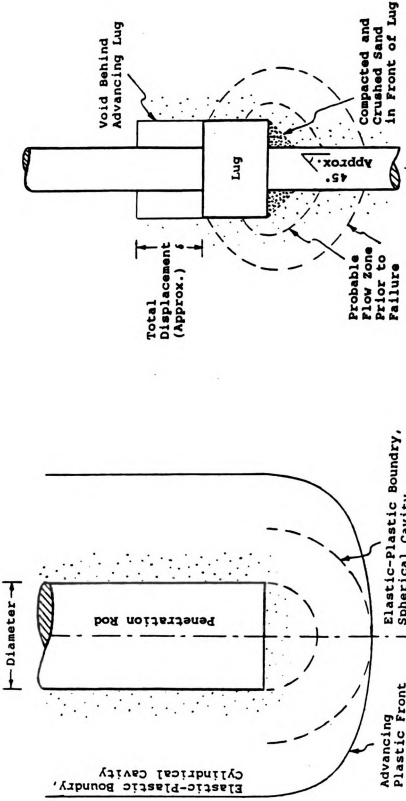

Figure 5.3. Comparison between penetration tip and pile lug. (a) Cavity expansion model (after Ladanyi, 1976). (b) Region of increased pressure around pile lug.

displacement rate. The region just ahead of the flat tip (half sphere of radius a) would correspond to the region of compressed sand shown in Figure 5.2. In Figure 5.3a, the region labeled as "advancing plastic front" illustrates where frozen soil plastically deforms around the advancing lug. A compressed zone of ice and sand ahead of the advancing pile lug and flow of sand and ice around the pile lug are shown in Figure 5.3b. After the lug has passed by, a void remains. Figure 3.1 shows a void ahead of the pile lug, created during sample preparation in order to simulate lug spacing on a multiple lugged pile. As shown later, piles with these displacement limits reach a critical displacement when each pile begins to accelerate. This pile failure involves shearing of frozen soil ahead of the lug.

The proof load P_c in Figure 5.4 represents the pile load at an arbitrary pile displacement rate of 0.1 mm/hr. This load tended to approach a constant value for each lug size as the plot starting point was increased. At this displacement rate, the resistance along each piles smooth shaft should be constant (for equal lengths) so that the difference between P_c values can be attributed to variation in lug size.

5.2. Pile Capacity For A Straight Shaft

A more complete picture of pile lug behavior in frozen

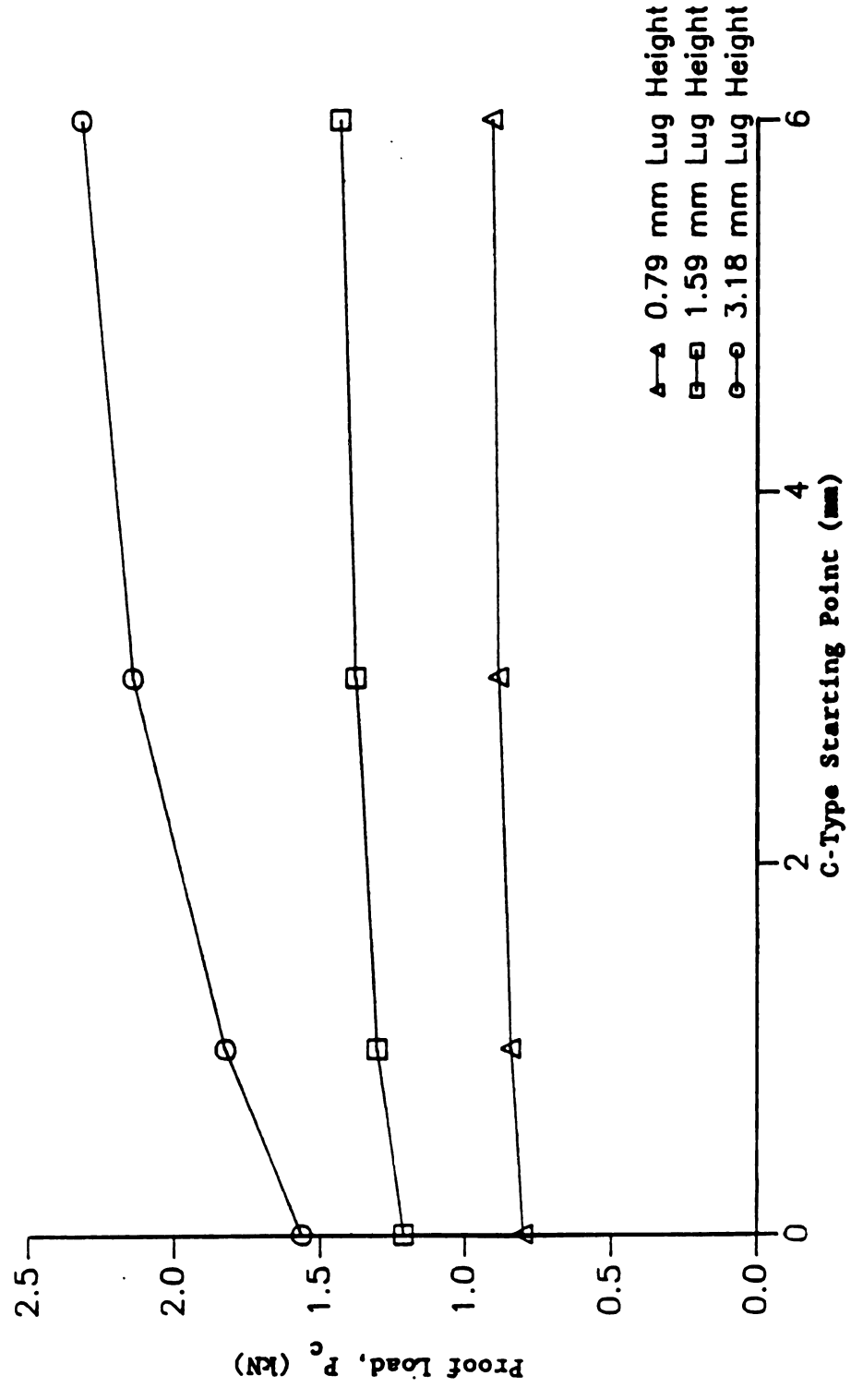

Figure 5.4. Difference in creep equation proof load results from difference in pile lug size.

sand is obtained by considering resistance to pile displacement along the straight shaft of a pile. With this knowledge, model pile capacity can be separated into a shaft resistance component and a pile lug resistance component.

To determine that portion of the total load attributed to a pile's straight shaft, silicon grease was applied on some piles to eliminate or greatly reduce adhesion, mechanical interaction, and friction at this interface. A direct comparison between partly greased and ungreased piles is shown im Figure A.1. Note that the behavior for Pile Test 99 (partly greased and loaded to 2.21 kN) is very similar to Pile Test 112 (an ungreased pile loaded to 2.66 kN). The difference between these loads is 0.45 kN (shear stress close to 240 kPa) and appears to be representative of the adfreeze strength at the section of pile behind the advancing lug. The pile sections in front of the lug were influenced by pressures developed on the lug and have, most likely, a higher level of adfreeze strength.

Another comparison can be made using creep parameters for the 1.59 mm lug height piles in Figure 5.5. Piles with an average embedment ahead and behind the lug of 76 mm and 63 mm (139 mm total) can be compared to piles with 25.4 mm and 64 mm embedments (89.4 mm total). The difference in total embedment (49.6 mm) corresponds to the difference in

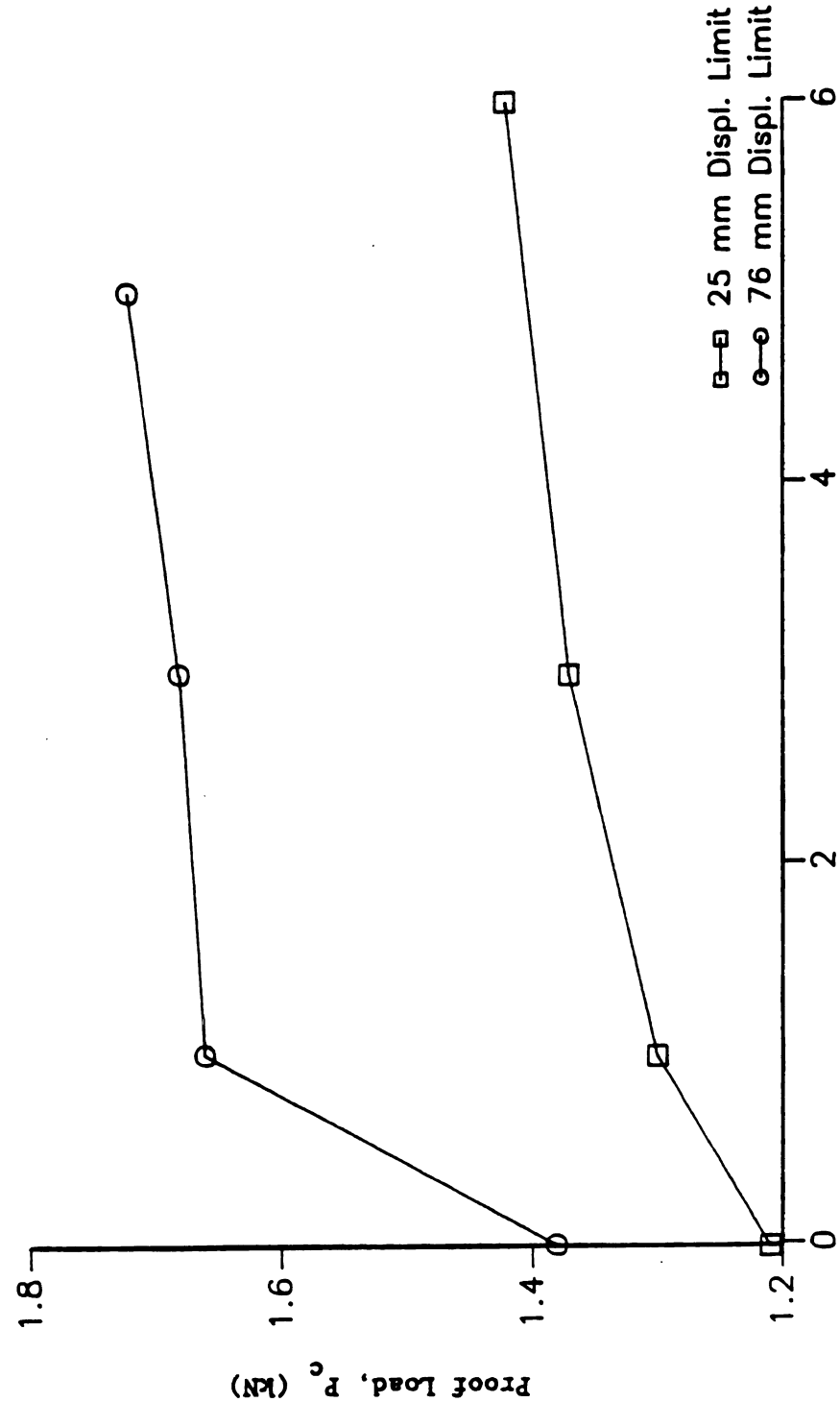

Figure 5.5. Difference in creep equation proof load shown for lugged pile with different embedments along their straight shaft portions.

proof load values, P_c, shown in Figure 5.5. This difference, about 0.3 kN for the 49.6 mm embedment difference along this portion of pile can be converted to approximately 200 kPa.

Earlier attempts to measure this resistance (Alwahab, 1983) using straight shaft piles and constant loads, lead to sudden failures after very small initial displacements. The load capacity of the ice adhesion bond is much greater than the residual capacity remaining after this break. The constant rate tests by Alwahab (1983) probably better represent long term conditions for straight shaft piles since they did not allow rapid pile displacements to occur.

A plot of data from 4 of Alwahab's (1983) constant rate pile tests is shown in Figure 5.6. The initial peaks vary greatly and are dependent on the displacement rates applied. A plot of peak pile capacity versus displacement rate (similar to those shown by Alwahab, 1983) gives an n parameter of approximately 5 in Figure 5.5. This parameter is typical for frozen soil creep processes at this temperature. After the short initial displacement required to rupture the pile/frozen sand adhesion, all residual pile capacity is derived from mechanical interaction and/or friction. The estimated residual pile capacities, after approximately 0.56 mm of displacement, are plotted against their respective displacement rates in Figure 5.7. Note that a descriptive creep equation (equation 3.4) for a best

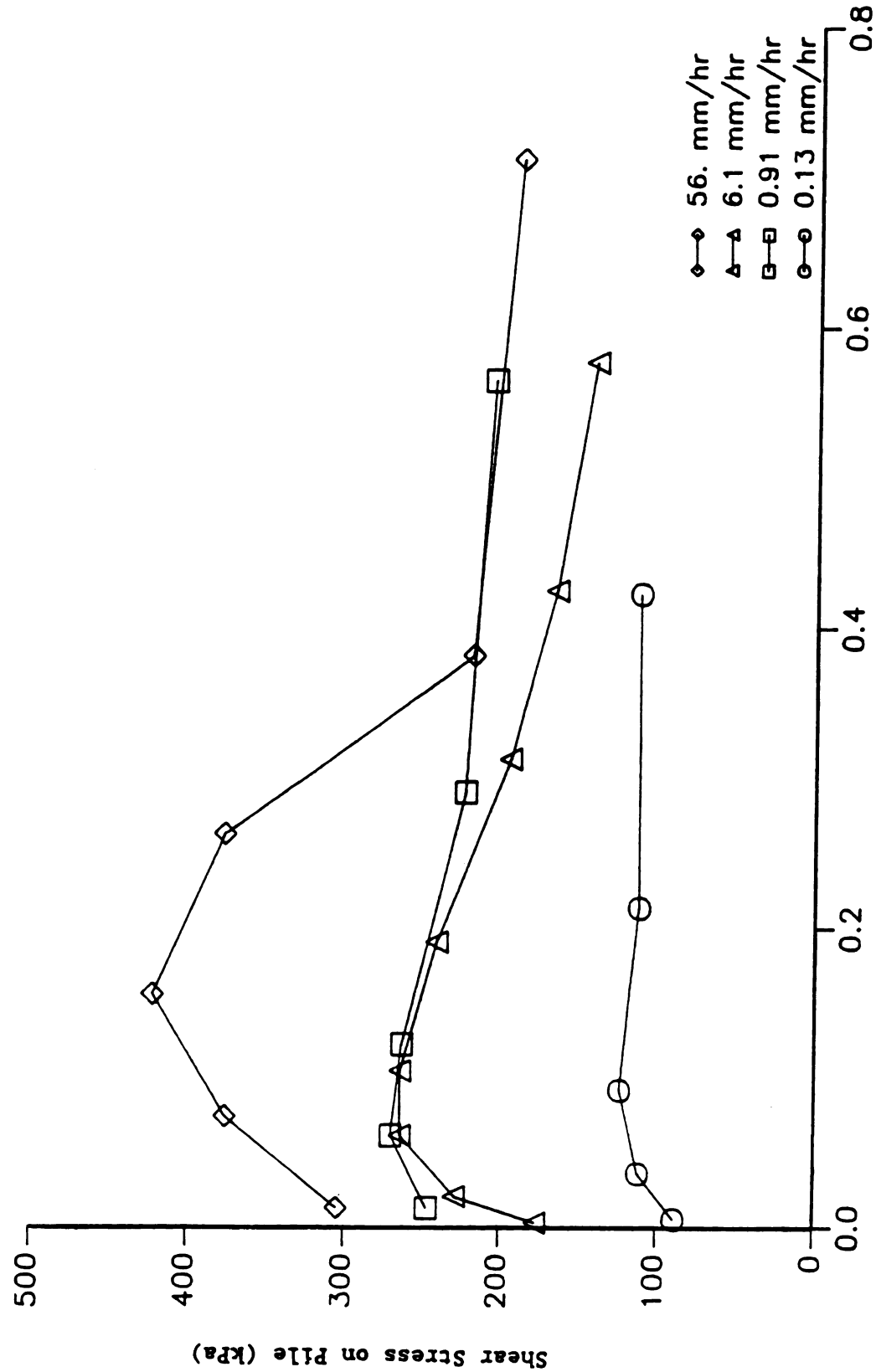

Figure 5.6. Comparison of straight-shaft pile behaviors at various constant displacement rates.

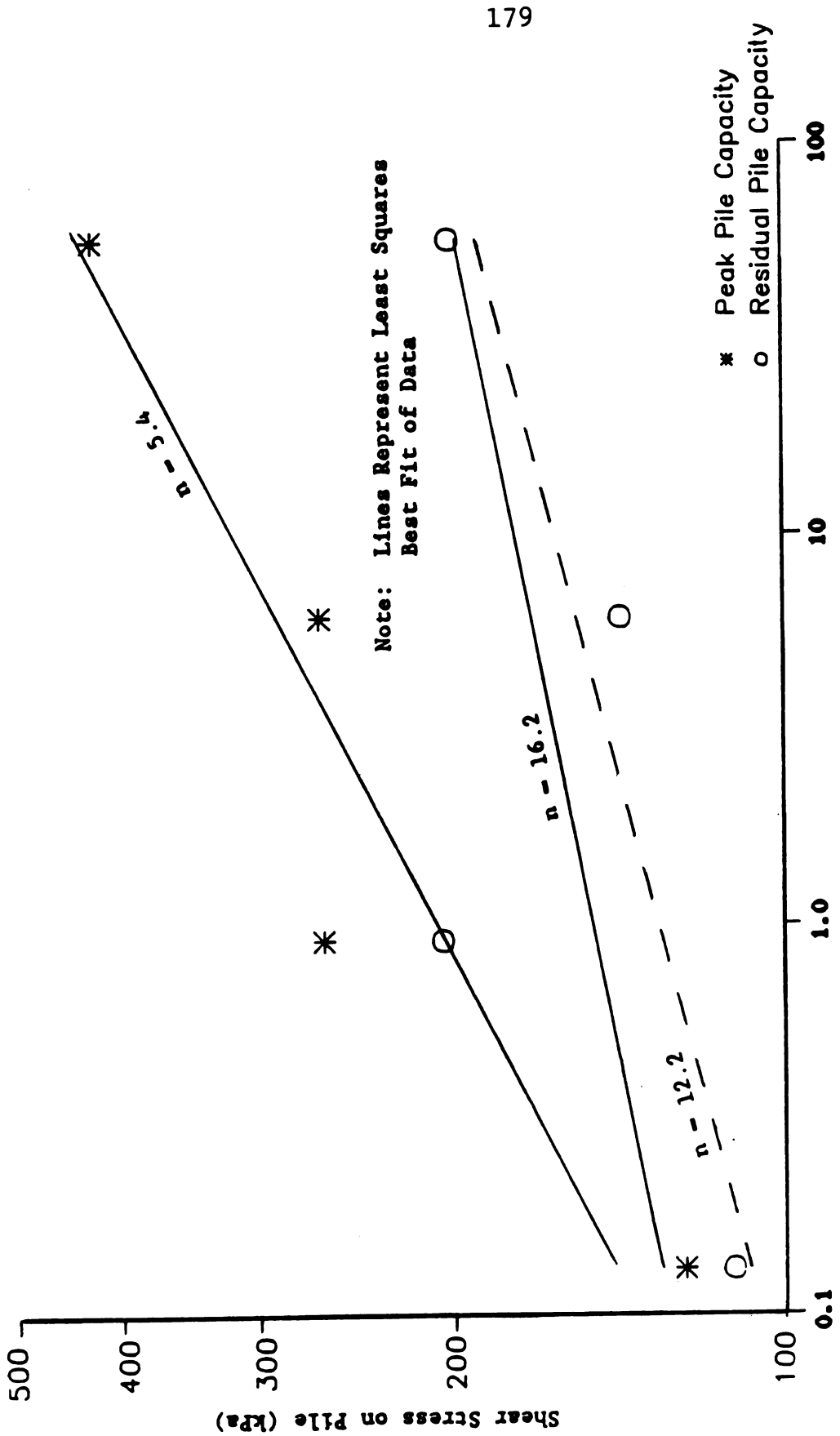

Figure 5.7. Best fit lines are shown to generalize peak capacity and residual capacity of straight-shaft piles (data from Figure 5.6).

fit straight line through this data has a relatively large n parameter power term (n = 16). The dashed line in this figure is best fit to this data excluding the 0.91 mm/hr displacement rate test (which is different from the other data) to produce another relatively large n value of 12. Alwahab's (1983) tests at -6 deg C did not show the relatively small peaks (especially in the 0.13 mm/hr test) observed during the tests at -2 deg C. Experimental limitations prevented Alwahab (1983) from testing at slower rates which may have produced tests with relatively small peaks at -6 deg C.

At warm temperatures and slow constant displacement rates, little or no peak may result as the ice adhesion bond shears at the smooth pile surface. Gradual changes during adhesion failure would allow sand grains to remain intact in the frozen sand matrix. If the pile were smooth, relative to the sand particle size, very little rearrangement of sand grains adjacent to the pile surface will occur and the pile's capacity due to this mechanical interaction will be small. Dilation of sand grains, at very small pile surface irregularities, could increase the pile to sand grain contact pressures and thereby increase friction along the interface. Pressures at the interface would eventually approach equilibrium with lateral soil pressures around the pile. Residual pile capacity derived from frictional forces would in turn be dependent on the

creep process of frozen sand surrounding the pile. Load capacities for these piles should approach and remain at a constant value for these circumstances.

Initial displacement behavior of a straight shaft pile, at the time it is first loaded, is influenced by creep behavior of the ice which carries much of the pile's load. A creep equation describing this initial behavior contains the n parameter characteristic of the creep process. Once the ice bond at the pile surface is broken, other materials at this interface (steel and sand) are less effected by time. A small increase in pile load will be accompanied by a large displacement rate increase. A creep equation descriptive of this behavior should have a larger n parameter. However, the load-displacement behavior following the adhesion break should retain some time dependance because pressures at the pile and sand grain interface are dependant on creep processes of the surrounding frozen sand. The point of this discussion is that creep behavior and its n parameter can change with increasing displacement rate when certain pile types, soil types, and loading conditions are combined.

The sequence of events described requires a slow displacement rate as the ice adhesion bond at the pile surface is gradually sheared. Constant load tests with straight shaft piles generally rupture the adhesion bonds which permits a rapid pile displacement. The residual pile

capacity following this break is usually very small. As the adhesion bond breaks on a lugged pile, a portion of the pile load will be transfered to the pile lug. This transfer helps maintain a residual load on the straight portion of the pile. The mechanisms involved are not fully understood.

Values of 200 kPa and 240 kPa shear resistance observed at -3 deg C for the straight shaft portion of lugged piles will be averaged to 220 kPa. This value is approximate, since it was based on limited data and was determined indirectly. It will allow comparisons between pile capacity components in subsequent sections.

5.3. Load Capacity From Pile Lugs

The n parameters for 3 lug sizes, summarized in Table 4.1, are plotted relative to their respective C-type starting points in Figure 5.8. The n values for each pile type approach a constant value and increase with decreasing lug size. However, this graph does change when pile shaft resistance is accounted for.

Creep equation parameters in Table 5.1 are listed as they appeared in Table 4.1 and again after each pile's resistance was estimated (220 kPa behind the advancing lug) and subtracted from the parameter calculations. The 25.4 mm straight pile portion ahead of the lug may develop a higher resistance due to higher lateral pressures around

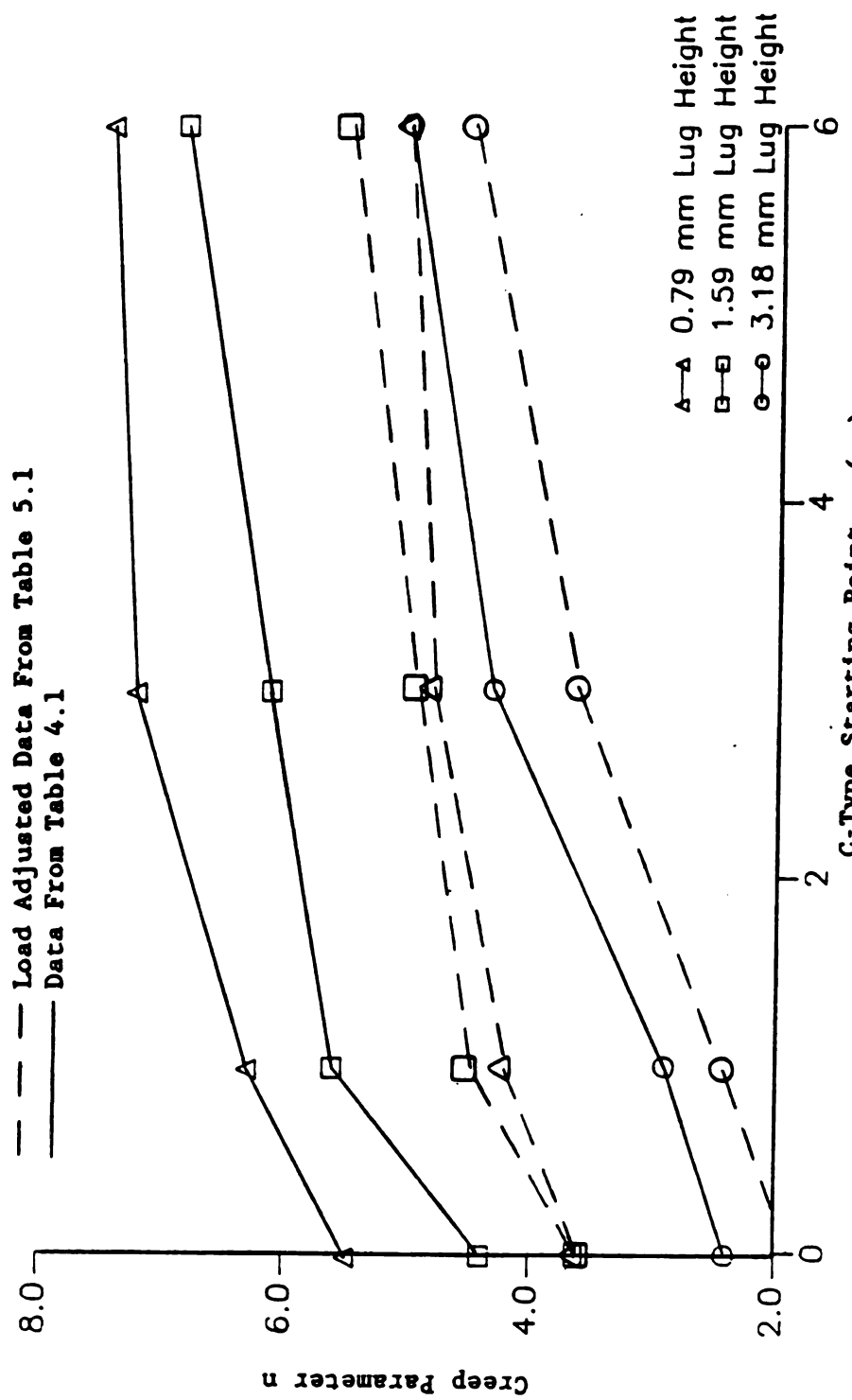

Figure 5.8. Creep parameter n increases with decreasing lug size.

Table 5.1. Creep Equation Parameters from Full Duration Tests of Lugged Piles With and (Estimated) Without Resistance on Shaft Behind Lug.

Lug Size mm	Fig. No.	Avg. Embedment Ahead/Behind Lug mm / mm	C-type Start Pt. = 0 mm b	n	C_o mm &	P_c Kn &	C-type Start Pt. = 1 mm b	n	C_o mm &	P_c Kn &	C-type Start Pt. = 3 mm b	n	C_o mm &	P_c Kn &	C-type Start Pt. = 6 mm b	n	C_o mm &	P_c Kn &	C-type Start Pt. = 12 mm b	n	C_o mm &	P_c Kn &
0.79	A.10	24.1/ 61 @	0.73	5.5	0.78	0.80	0.86	6.3	0.48	0.84	0.97	7.2	0.28	0.88	1.0	7.4	0.22	0.90	1.0	7.3	0.23	0.90
		24.1/ 0 @-	0.73	3.6	5.2	0.42	0.86	4.2	4.3	0.46	0.97	4.8	3.4	0.49	1.0	5.0	2.9	0.51	1.0	4.9	3.0	0.50
1.59	A.6	25.4/ 64 @	0.56	4.4	0.16	1.21	0.73	5.6	0.053	1.30	0.81	6.1	0.027	1.37	0.92	6.8	0.012	1.42				
		25.4/ 0 @-	0.56	3.6	0.69	0.85	0.73	4.5	0.33	0.93	0.81	4.9	0.19	0.99	0.92	5.5	0.101	1.05				
3.18	4.2	25.4/ 62 @	0.50	2.4	0.15	1.56	0.65	2.8	0.053	1.82	0.87	4.3	0.0058	2.13	0.98	5.0	0.0017	2.30				
		25.4/ 0 @-	0.50	1.9	0.37	1.11	0.65	2.4	0.13	1.42	0.87	3.6	0.021	1.72	0.98	4.5	0.0061	1.89				

& C_o measured at 1 KN, P_c determined from C_o and $\dot{\delta}_c$=0.1 mm/hr

@ 0.42 to 0.59 mm sand at -3 deg C

@- 0.42 to 0.59 mm sand at -3 deg C without 2.2 kPa resistance behind lug

the lug. This effect was not estimated or accounted for in the calculations. Experimental limitations prevented determination of pressures on the lug. The recalculated n values for the lug and the pile portion just ahead of the lug are all approximately equal to 5 (see Figure 5.8) and appear to be independant of lug size once steady state creep (b = 1) conditions are approached.

5.4. Temperature Dependance of Pile Capacity

Proof load P_c values are used to illustrate the effect of temperature on pile behavior in frozen sand. Values of P_c from Tables 4.1 and Table 4.2 are summarized in Figure 5.9. A variation of the temperature dependance equation 2.7 can be used with the proof load $P_{c\theta}$ (at temperature θ) values obtained from Figure 5.9 as :

$$P_{c\theta} = P_{co} \left(1 + \frac{\theta}{\theta_c} \right)^{\omega} \qquad (5.1)$$

where θ_c = 1 deg C, θ = 0 deg C - T(deg C) the absolute value of the test temperature, and P_{co} is the proof load at a temperature near 0 deg C. Rearrangement of this relationship yields:

$$P_{co} = P_{c\theta} \left(1 + \frac{\theta}{\theta_c} \right)^{-\omega} \qquad (5.2)$$

which is a constant. Equating these relationships at temperatures of -2 deg C and -3 deg C yields:

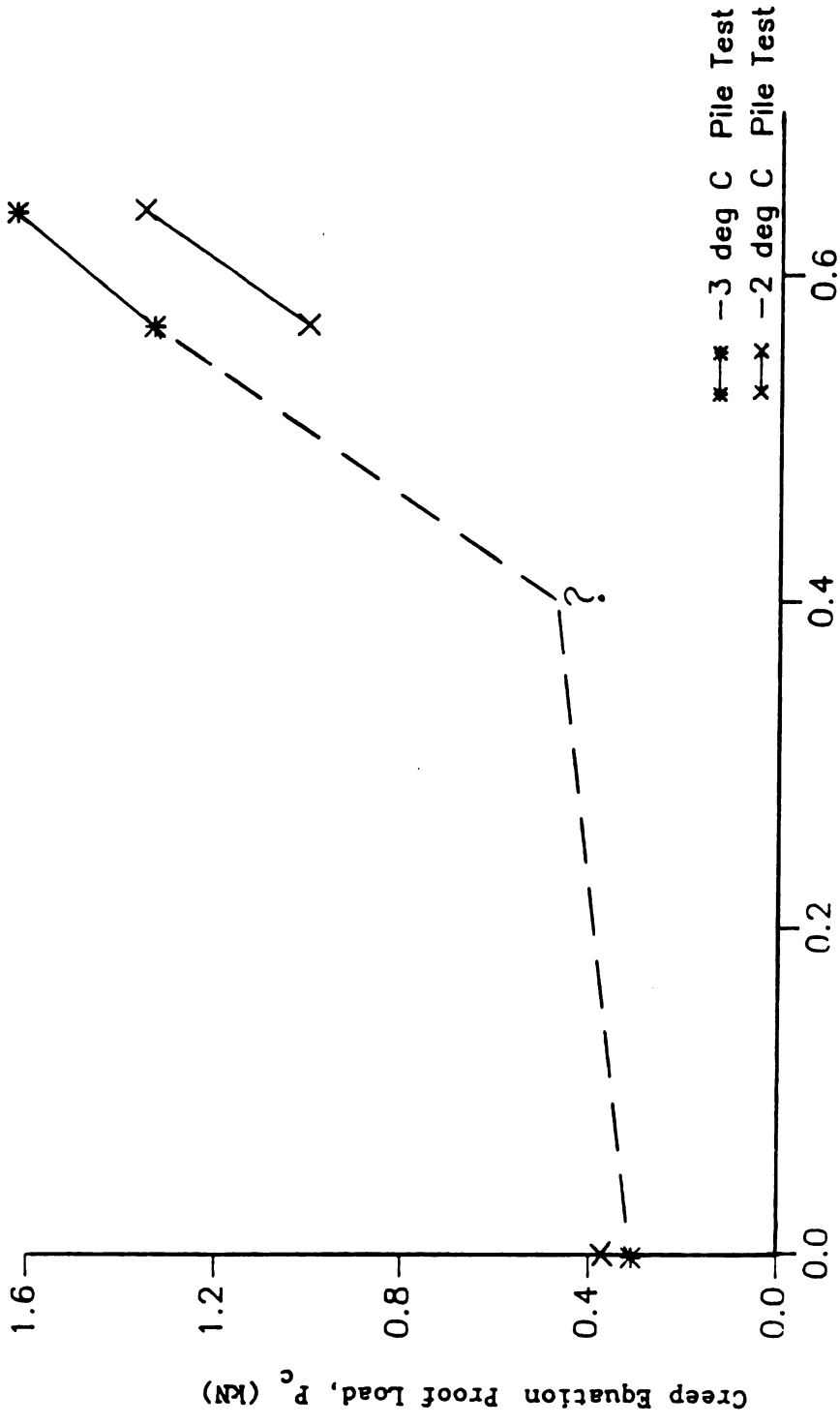

Figure 5.9. Load capacity of lugged model piles based on step-load test.

$$(1 + \frac{3}{1})^{-\omega} \; P_{c(3)} = (1 + \frac{2}{1})^{-\omega} \; P_{c(2)} \qquad (5.3)$$

These proof loads, the sample solid volume fractions, and the computed ω values are summarized in Table 5.2. These ω values are similar to the value (ω = 0.64) determined by Alwahab (1983) for model piles in frozen sand. The step temperature increases from -3 to -2 deg C appears to allow determination of the ω parameter.

5.5. Dynamic Effects on Model Pile Load Capacities

Experimental data, summarized in Figure 5.10, shows that model pile displacement rates in frozen sand were essentially independent of frequency in the range of 0.1 Hz to 10 Hz. This behavior is in agreement with work reported by Schmid (1969) for model brass piles embedded in dry, uniformly graded, unfrozen quartz sand with the same particle size range. Schmid (1969) reported a pile-soil resonance at about 50 Hz with a small peak in his load versus frequency curve (Figure 2.21. This curve was relatively flat at frequencies above and below resonance. The smaller model steel pile and stiff frozen sand used in this study should have a higher natural frequency and pile displacement should be relatively frequency independent for 0.1 Hz to 10 Hz. Observed resonant frequencies close to 1.0 Hz and 6.2 Hz were clearly due to the loading system since they could be altered by changing the loading arm

Table 5.2. Determination of Temperature Dependent Creep Equation Exponents. (Data From Table 4.2)

Average Solid Volume Fraction.....	0.58	0.64
Average Creep Equation Proof Load at -3 deg C.....	1.33 kN	1.62 kN
Average Creep-Equation Proof Load at -2 deg C.....	1.00 kN	1.35 kN *
Temperature Dependent Exponent, ω (Equ. 5.3).....	1.0	0.64

* Determined From the Step-Temperature Increase In Table 4.2, Tests #33 and #34

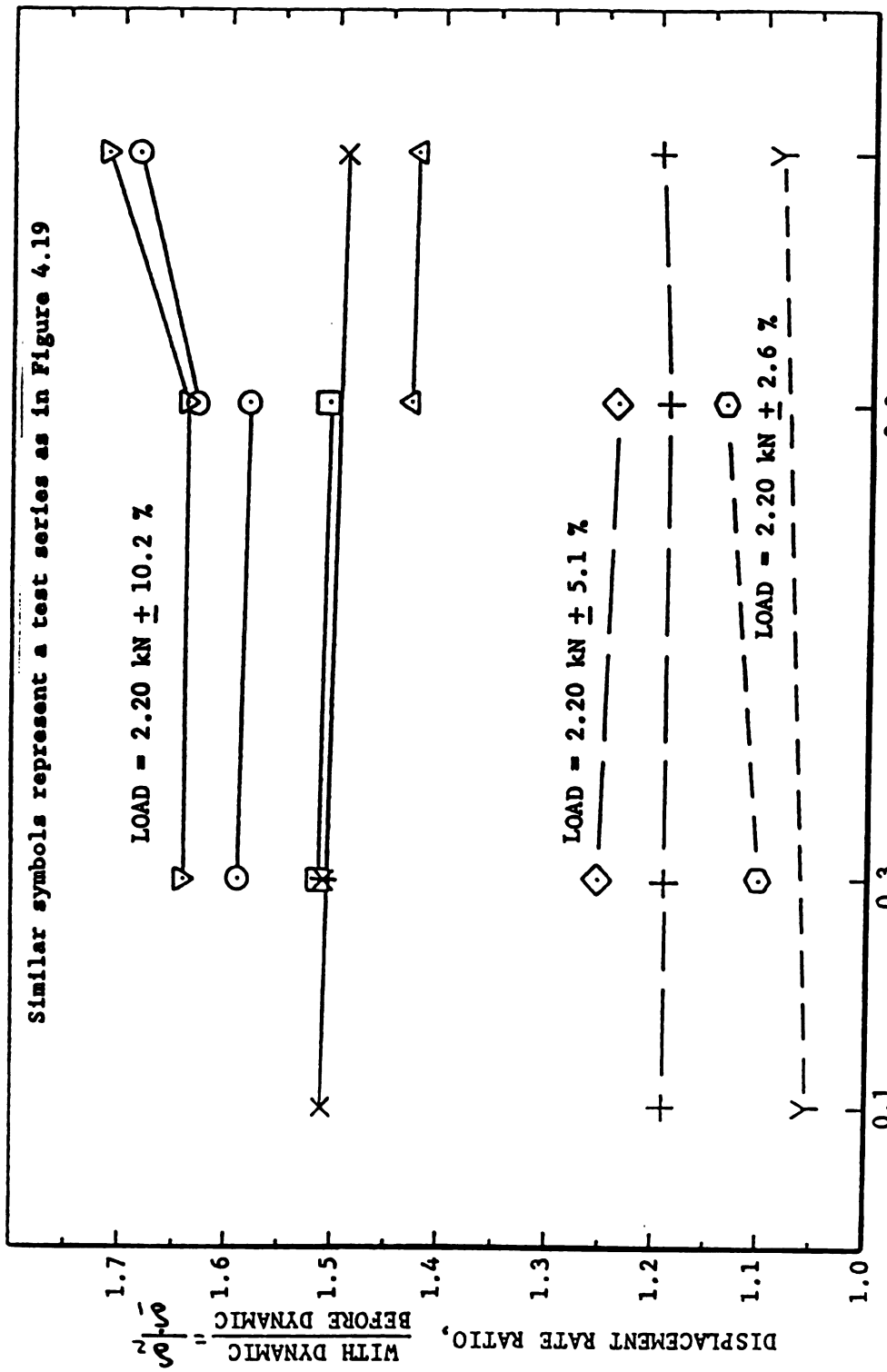

Figure 5.10. Dynamic loading effect on displacement rates (normalized) versus frequency.

set-up.

An increase in dynamic load amplitude significantly increased pile displacement rates over rates observed for sustained loads (Figure 5.10). Comparisons show rate increases roughly in proportion to the increase in load amplitudes, i.e., the rate was approximately doubled when load amplitude was doubled. Since several tests were run on one frozen sample, a creep rate measured just prior to application of the dynamic load might differ from rates for subsequent tests on the same sample. To compare tests performed at different initial creep rates, the ratio $\dot{\delta}_2/\ \dot{\delta}_1$ was plotted against $\dot{\delta}_1$ as shown in Figure 5.11. Data for each of the three best fit lines corresponds to a given dynamic load amplitude. The small negative slopes may show the effect of starting tests at various displacement rates before secondary creep was fully attained. Points on the left in Fig. 5.11 should be closer to the minimum or secondary creep rate. In addition, 3 shaded data points (indicated by a slash) represent displacement rate increases for a small static load increase. For a dynamic load amplitude equal to a static load increase, the dynamic rate increase always appeared as some fraction of the static rate increase.

The displacement rate ratios for static and dynamic short duration load increases are plotted against the percent of load increase in Figure 5.12. The cyclic load

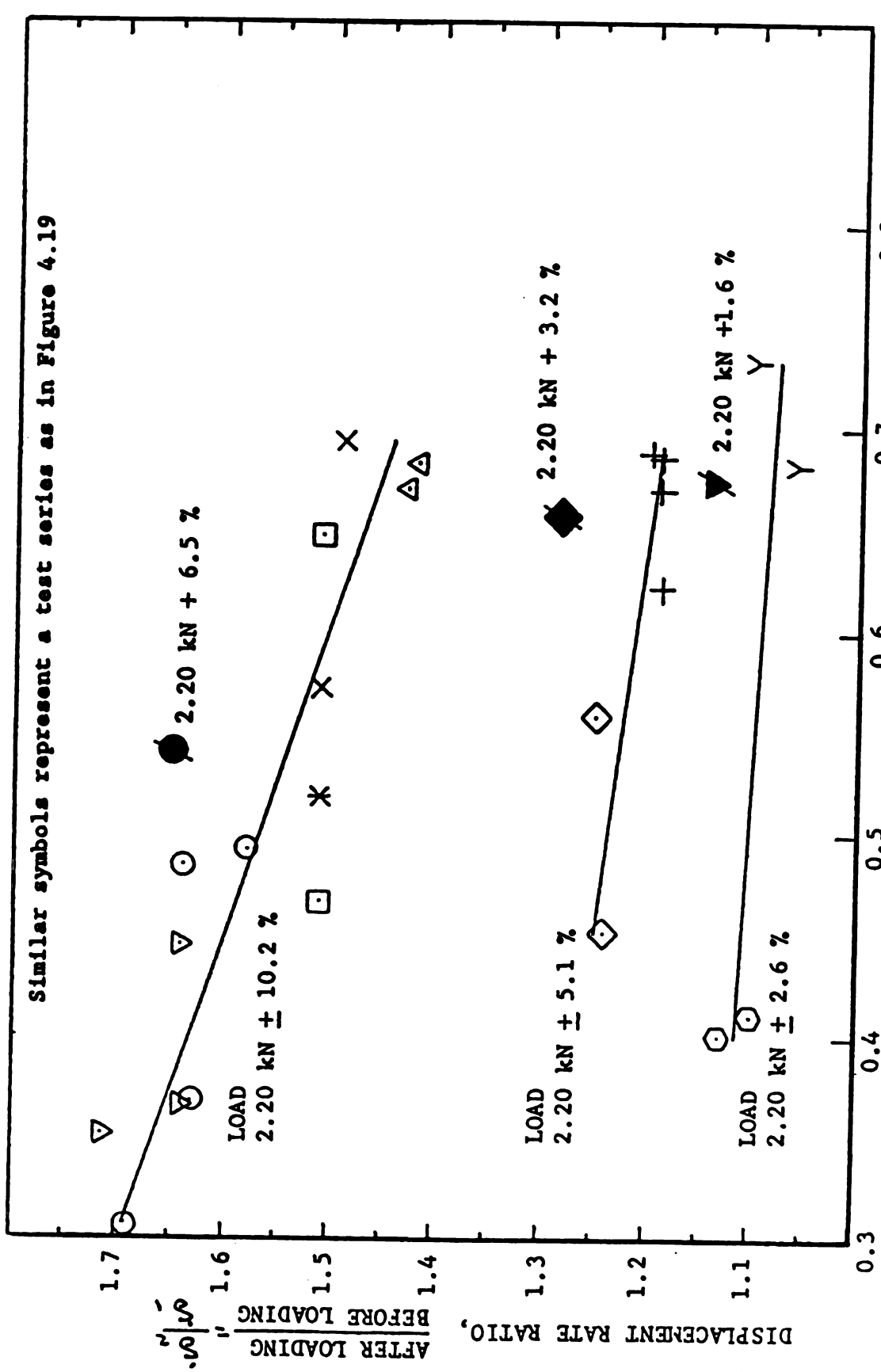

Figure 5.11. Displacement rate ratio versus displacement rate before dynamic (±) and static (+) loadings.

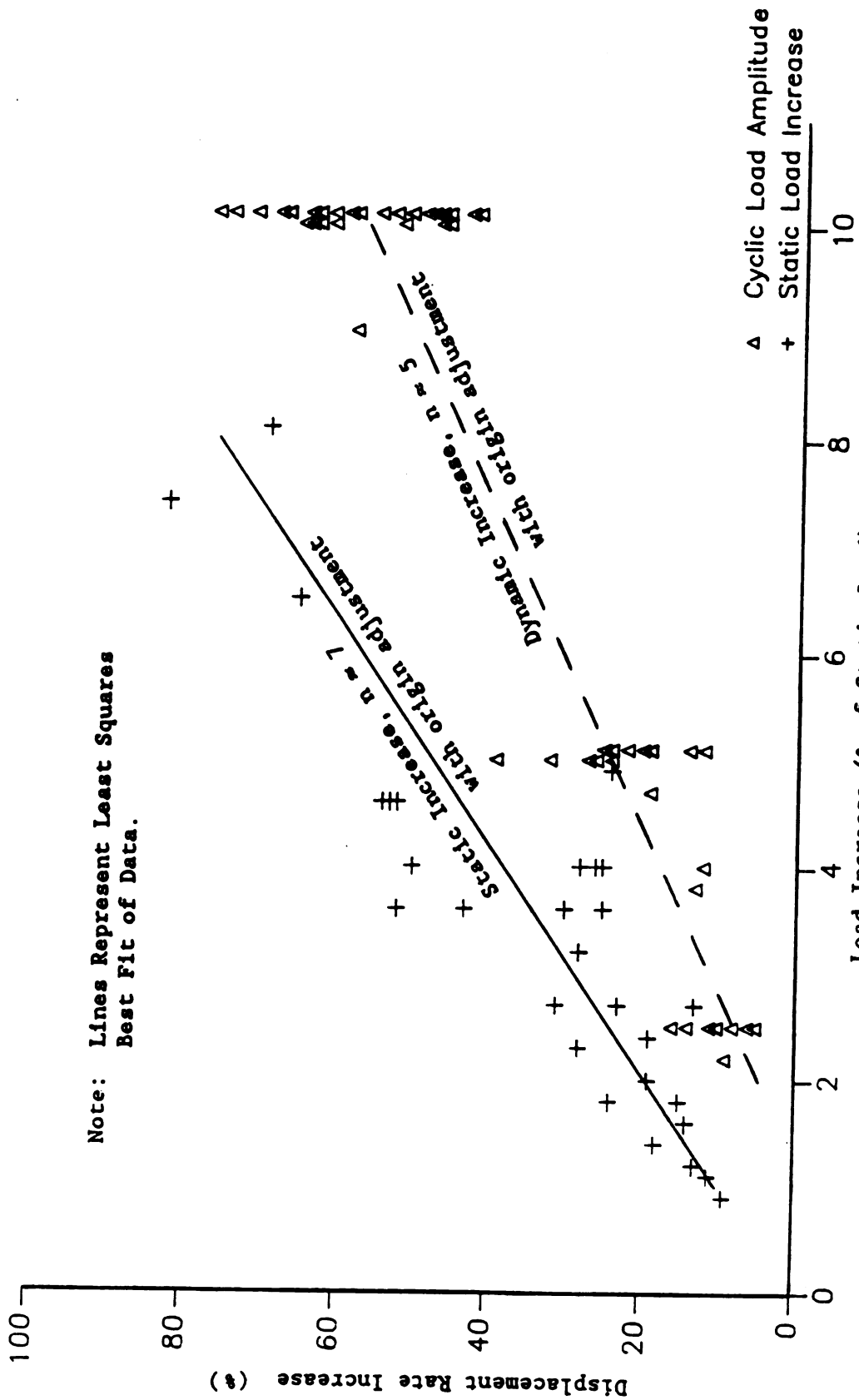

Figure 5.12. Displacement rate increases due to short duration load increases, static and dynamic.

amplitude is expressed as a percent of static load. Equations for the best fit lines to each group (Figure 5.12) illustrate that a superimposed cyclic load (amplitude X) would produce a short duration displacement increase roughly equal the increase produced by a static load increase (magnitude of 0.6 times X). The best fit line for static loading could be approximated by an n parameter of 7 while the best fit line for dynamic loading could be approximated (after adjusting the origin) by an n parameter of 5. The mechanism causing the shift of the best fit line for cyclic loading data is not known.

Available information on dynamic loading of lugged piles in frozen dense sand and ice are summarized in Figures 4.21(b) and 4.21(c), respectively. These early tests did not allow accurate measurement of displacement rate changes, but appear to show that cyclic loads have only a small effect on pile displacement rates in dense sand and ice.

A few cyclic load tests were applied to threaded piles in sand and ice. These tests show the same general relationship between cyclic loading and static loading for these piles. Results for Pile Test #86 (in sand), shown in Table 4.4, provides n parameter values between 2.5 and 3.5 with an average of about 2.9. Static loads added to similar piles as step loads or short duration loads during Pile Tests #67, #69, #80, and #79 indicate n parameter

values between 2.6 and 4.4 with an average of about 3.4. While the small number of tests performed do not provide a statistically good representation of this behavior, the implication of this comparison is that cyclic loading (at nonresonant frequencies) does not produce a large displacement rate increases in these piles. The effect, however, appears to be larger than that observed in lugged piles.

5.6. Limits of Model Pile Displacement

Differences in displacement limits, δ_M, had little effect on the initial displacement-time behavior of the model piles, but directly influenced the magnitude of the failure displacement, δ_F. Model piles with different displacement limits, curves 106 and 102 in Figure A.5, show a very similar settlement behavior up to tertiary creep, 8 mm for curve 102. Under similar conditions, a model pile with a larger displacment limit should begin tertiary creep after a greater displacement.

Piles with very short displacement limits, curves 103 and 101 of Fig. A.1, behaved differently from piles with longer displacement limits, curves 99 and 97. Inspection of split samples revealed that the shorter displacement limit samples appeared to have a smaller zone of compacted sand in front of the lug. Upon loading a pile with a very short displacement limit, shear quickly developed across

the observed failure surface, increasing the pile displacement rate, and producing failure before full development of the densified zone of sand. A graph of displacement limits versus failure displacements is shown in Figure 5.13. With more data, relationships similar to Figure 5.13 could be prepared to show the influence of pile diameter (to account for scale effects), pile lug size, lug spacing, load per lug, time to failure, different soils, and different temperatures on failure displacements.

For comparison purposes, experimental results have been summarized in Table 5.3. The load on each model pile was adjusted (to P') by subtracting the resistance (0.220 kPa) due to the pile section behind the lug. The area resisting load at failure (A_F) would then be the failure surface ahead of the lug and through the frozen sand plus the lug's outer surface (12.7 mm length). The adjusted load (P') was then divided by the shear surface (A_F) to provide the shear stress at failure (τ_F). All shear stresses at failure (850 to 1990 kPa) were shown to decrease with decreased time to failure t_F (t_F greater than 4 hours). If a model pile was loaded with a small load for a very long time, the shear stress at failure may continue to decrease asymptotically to approach the long term shear strength for the frozen sand at -3 deg C.

Displacement of threaded piles was limited by the pile's surface geometry. The relationship between thread

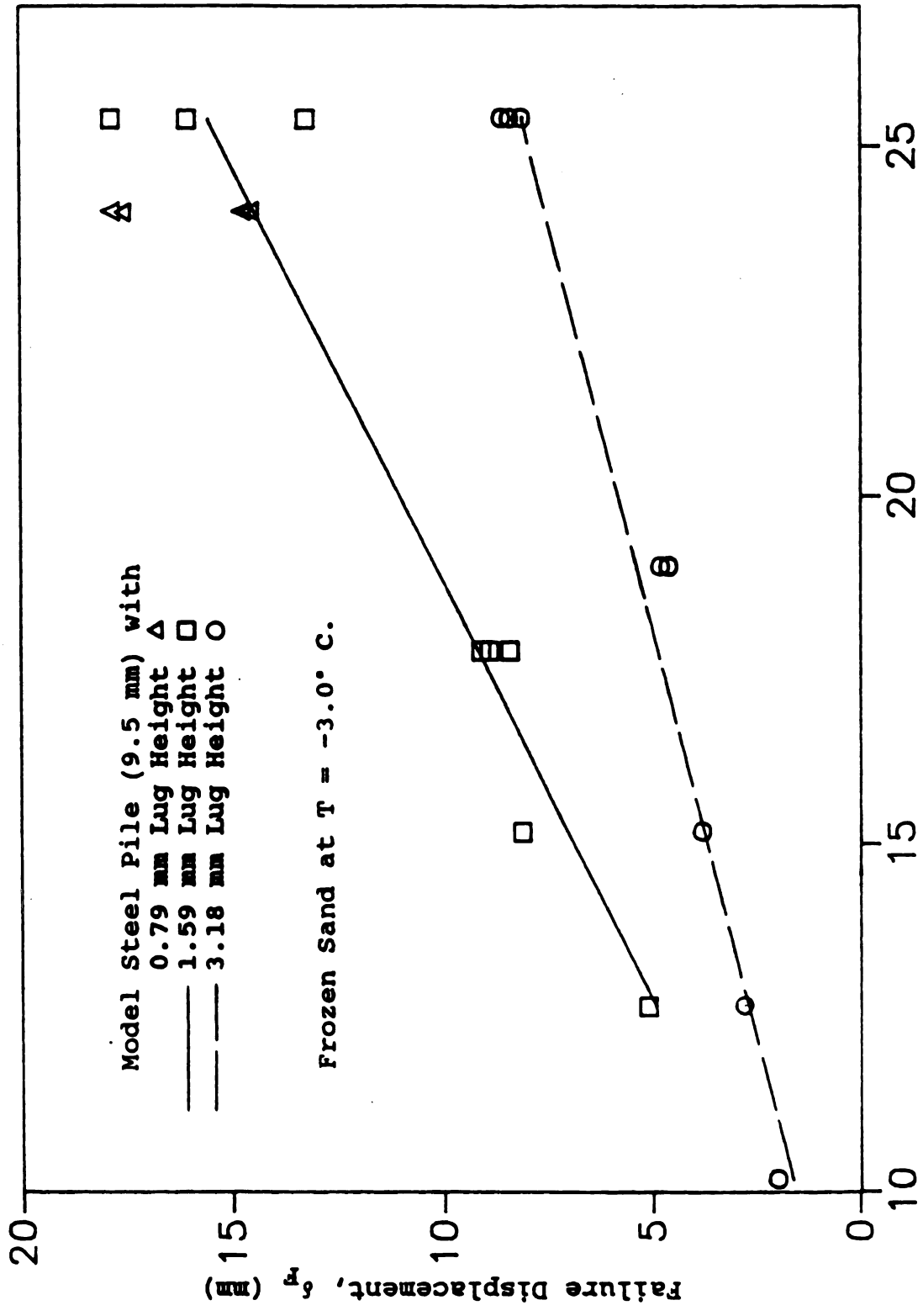

Figure 5.13. Relationship between displacement limit and displacement at failure.

Table 5.3. Lugged Pile Test Data at for Model Steel Piles Frozen in Sand at -3 deg C with Particle Sizes 0.42 to 0.59 mm.

Test No.	Pile Lug Height (mm)	Pile Load (kN)	Adjusted Pile Load (kN)	Displacement Limit δ_M (mm)	Displacement at Failure δ_F (mm)	Area of Shear at Failure A_F (cm^2)	Shear Stress at Failure τ_F (kPa)	Time at Failure t_F (hr)
111	3.18	3.10	2.68	25.4	8.1	14.9	1800	11.
107	3.18	2.21-3.10	1.80-2.69	25.4	8.6	14.7	1830	--
114	3.18	2.66	2.26	25.4	8.4	14.8	1520	24.
116	3.18	2.66	2.25	25.4	8.4	14.8	1510	26.
105	3.18	2.21-3.10	1.78-2.67	25.4	--	--	--	--
108	3.18	3.72	3.32	19.0	4.8	13.4	2500	1.5
110	3.18	3.10	2.69	19.0	4.6	13.5	1990	3.4
112	3.18	2.66	2.24	19.0	4.6	13.5	1650	9.8
99	3.18	2.21*g	2.21	15.2	3.8	12.0	1840	8.9
97	3.18	2.17*g	2.17	12.7	2.8	11.3	1930	4.2
103	3.18	2.21*g	2.21	10.2	2.0	10.4	2120	1.3
101	3.18	2.21*g	2.21	10.2	2.0	10.4	1990	1.1
113	1.59	2.66	2.24	25.4	17.8	8.1	2770	1.3*f
106	1.59	2.21	1.78	25.4	16.0	8.8	1940	8.5
117	1.59	1.77	1.35	25.4	13.2	9.9	1370	18.
115	1.59	1.77	1.38	17.8	8.4	8.8	1570	9.3
104	1.59	2.21	1.77	17.8	8.9	8.6	2060	3.9
102	1.59	2.21	1.79	17.8	8.4	8.8	2030	3.3
100	1.59	2.17*g	2.17	17.8	9.1	8.5	2560	2.0
98	1.59	2.21*g	2.21	15.2	8.1	7.9	2800	1.7
95	1.59	2.21	1.81	12.7	5.1	8.1	2230	3.3
118	0.79	1.77	1.36	24.1	14.5	7.8	1740	1.0
119	0.79	1.53	1.14	24.1	17.8	6.6	1730	2.6
121	0.79	1.34	0.97	24.1	14.7	6.6	1260	5.0
122	0.79	1.11	0.68	24.1	14.0	8.0	850	25.

*g pile shaft greased behind lug
*f possible faulty test, too fast.

spacing and pile displacement at the beginning of failure (tertiary creep) was illustrated by several figures in Section 4.7. While this data is limited, a review will allow several deductions to be made.

Thread spacing is plotted versus observed pile failure displacement for threaded piles frozen in uniform sized sand and polycrystalline ice in Figure 5.14. All threaded piles in polycrystalline ice began to fail after displacements approximately equal 0.15 to 0.20 mm. Examination of threaded piles after testing to failure in ice, showed a loss of some ice between the threads. This lost ice appeared to have been pushed past the shear surface, developed at the outermost edges of the threads, and into the surrounding ice matrix. This failure displacement approximately 0.15 to 0.20 mm) is not unlike the displacements (at peak pile capacity in Figure 5.6) associated with adhesion failure of smooth shaft piles. Tests of piles with very small threads (approaching the roughness of "smooth" shaft piles) may approach the behavior of smooth shaft piles.

Piles with the large size threads in frozen sand began to fail after a displacement nearly equal to the thread spacing. The explanation for these observations appear to be related to grain size (0.42 to 0.59 mm) of the frozen sand. These grains would fit between 1.06 mm and 1.58 mm thread spacings. Examination of these piles after failure

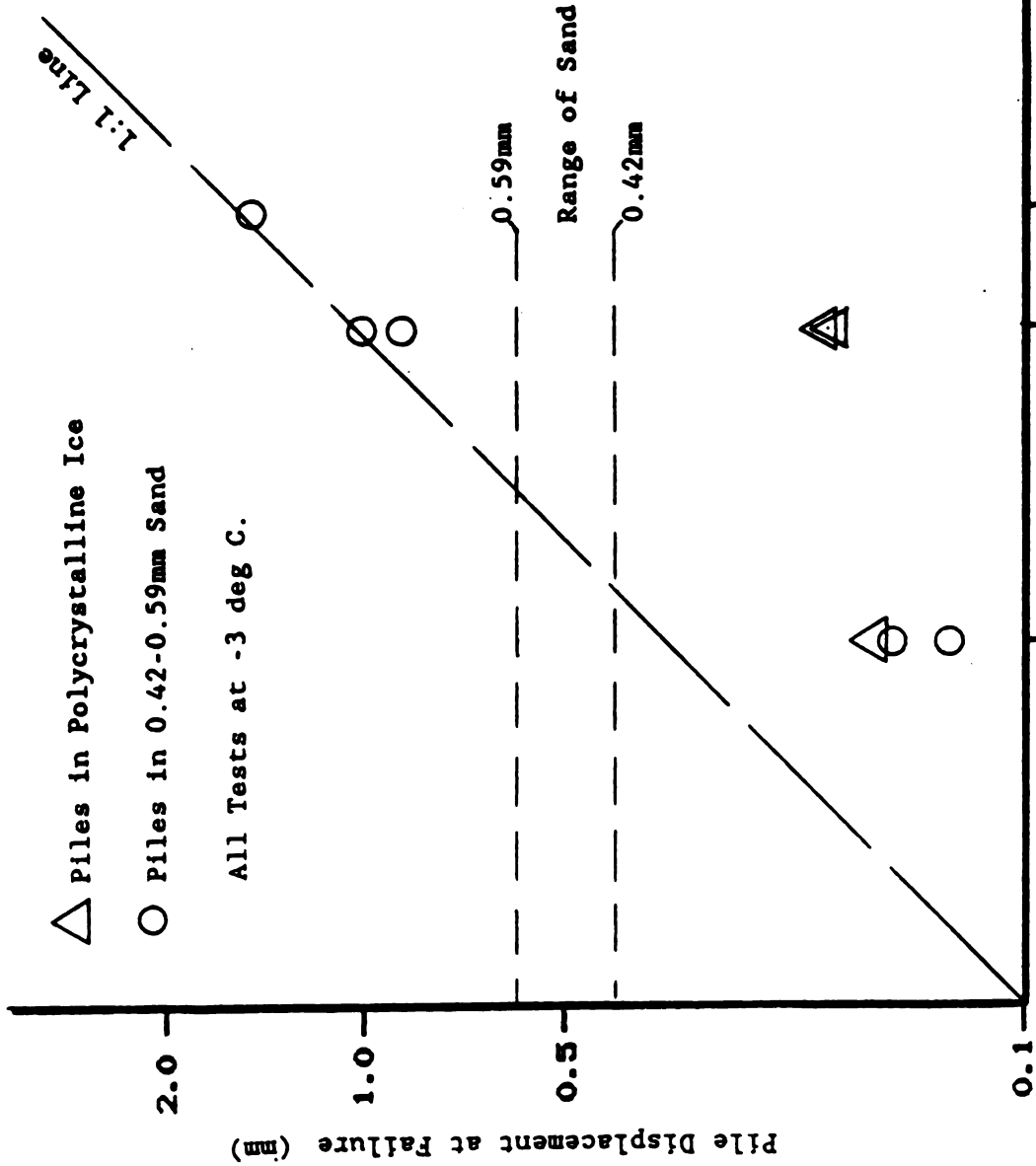

Figure 5.14. Comparison of thread spacing to pile displacement at failure.

in sand often showed only loose sand grains or empty spaces between threads. Before or during failure, ice and sand (now absent from these threads) must have been pushed out into the surrounding frozen sand. A displacement equal to the thread spacing may have been necessary to push all the interfering grains away from the cylindrical failure surface outside the outer thread edges before failure could begin. Some sand grains, although loosened, could have remained tightly interlocked with the threads and produced additional shear resistance.

The 0.42 to 0.59 mm sized sand grains could not fit between the smallest threads and did not develop a good interlock with this type of pile. Examination of these piles after testing to failure showed some striations along the shear surface where sand grains or pile roughness features had passed, but many areas showed only a smooth shear surface similar to the failure surface found after testing polycrystalline ice samples. Without a good interlock between the smallest threads and sand grains, the behavior of ice appears to have dominated.

Weaver and Morgenstern (1981a) report that an aluminum plate of given roughness developed sufficient load transfer to induce measureable shear deformation during shear tests of a frozen silt (sample with 30% of grain size less than the average plate roughness). This same plate showed an initial displacement at a frozen sand interface (average

grain size 200 times larger than the average plate roughness) but gradually developed sufficient load transfer to induce shear deformation within the sample. The frozen silt appeared to interlock well with the plate roughness compared to little interlock with the larger sand particles.

5.7. Comparison to Uniaxial Compression Tests

The adjusted n values in Table 5.1 can be compared to n values determined by Bragg and Andersland (1980) for unconfined compression tests of frozen sand with a solid volume faction of approximately 0.64. Bragg and Andersland (1980) estimated n values of 3.3 at -2 deg C and 8.7 at -6 deg C for strain rates less than 10^{-5}/sec. Interpolation between these temperatures yields n = 4.6 at -3 deg C. At strain rates greater than 10^{-5}/sec, very large n values would be obtained because of strength versus strain rate independence. The similarity between these n values and the n values observed for lugged piles is not surprising since the mechanical interaction developed during compression tests has similarities to the mechanical interaction with frozen soil ahead of a pile lug.

Bragg and Andersland's (1980) illustration of a ductile to brittle transition at strain rates greater than 10^{-4}/sec. may be related to the soil deformation process associated with a pile undergoing cyclic loading. It

appears that very small frozen soil zones, which are stressed rapidly during cyclic loading, would fail at the relatively small failure strain (less than 1%) associated with brittle fracture instead of the larger (greater than 4%) failure strain associated with ductile type creep deformation. Adjacent areas of frozen soil would then carry additional load and the overall pile displacement could increase.

Parameswaren (1979) performed a series of unconfined compression tests on frozen sand with a moisture content of approximately 20%. At strain rates below $3*10^{-6}$/sec, n values of 5.2 at -2 deg C and 8.2 at -6 deg C can be estimated from his data. An interpolation of these values yields an n value of 6.0 (at -3 deg C). At faster strain rates, these relatively high n values represent independence between strength and strain rate.

Parameswaren (1985) also superimposed cyclic loads of ±6.3% on larger static loads during creep compression tests of the same frozen sand (Figure 2.11). Table 5.4 includes this data and uses it with a variation of equation 3.4 in the form

$$\left(\frac{\sigma + \Delta\sigma}{\sigma}\right)^{n} = \dot{\epsilon}_2 / \dot{\epsilon}_1 \qquad (5.4)$$

where σ is initial stress, $\Delta\sigma$ is the amplitude of the cyclic load, $\dot{\epsilon}_2$ is the strain rate after load increase, and $\dot{\epsilon}_1$ is the strain rate before the load increase. The

Table 5.4. Temperature Adjustments for Parameswaren's (1985) Cyclic Uniaxial Compression Tests.

Initial Stress σ (MPa)	Stress Increase $\Delta\sigma$ (% / Hz)	Initial Strain Rate (Before Increase) $\dot{\epsilon}_1$ (10^{-8}/sec)	Strain Rate After Stress Increase $\dot{\epsilon}_2$ (10^{-8}/sec)	Temperature Adjusted Strain Rate $\dot{\epsilon}_2'$ (10^{-8}/sec)	$\frac{\dot{\epsilon}_2}{\dot{\epsilon}_1}$	$\frac{\dot{\epsilon}_2'}{\dot{\epsilon}_1}$
2.609	+6.3 /10	6.19	10.3	-	8.3	-
2.609	+6.3 /10	2.47	9.94	-	22.8	-
2.609	+6.3 /10	2.83	7.57	-	16.1	-
2.609	+6.3 /10	6.19	-	12.2 *	-	?
2.609	+6.3 /10	2.47	-	4.94	-	11.4
2.609	+6.3 /10	2.83	-	5.66	-	8.3

* Strain Rate Decrease is Not Realistic, Initial Rate May be In Primary Stage

large displacement rate increases observed in Figure 2.11 result in much larger n values as compared to values of 5.6 to 6.1 interpreted from Parameswaren's (1979) data involving only static loading and temperatures from -2.5 to -3.2 deg C.

During cyclic loading of Parameswaren's (1985) uniaxial compression samples, temperature increases did not quickly dissipate and the entire sample temperature increased as shown in Figure 2.11. The strain rate increase related to these temperature increases of -3.2 to -2.5 deg C can be estimated by first using equation 5.2 with ω = 0.64 to determine a relationship between creep loads which would produce equal strain rates at different temperatures. Thus

$$1.12 \quad P_{c(2.5)} = P_{c(3.2)} \qquad (5.5)$$

This relationship indicates that the load at -3.2 deg C must be 12% larger than the load at -2.5 deg C to produce equal strain rates. Taken one step further, a temperature increase from -3.2 to -2.5 deg C for a sample under a constant load would increase its strain rate to the rate resulting from a 12% load increase on a sample held at a constant temperature of -3.2 deg C. Equation 3.4 with n = 6.1 (interpolated for 3.2 deg C from Parameswaren's 1979 paper) can be rearranged such that

$$\left(\frac{1.12}{1}\right)^{6.1} = \dot{\epsilon}_2 / \dot{\epsilon}_1 = 2.0 \qquad (5.6)$$

This means that the strain rate should approximately double for a temperature increase of -3.2 to -2.5 deg C temperature increase. This adjustment is listed in Table 5.4 and the resulting n parameters are similar to those values found by static loading (Parameswaren, 1979) at constant temperatures. During static loading, measured temperature increases near a model pile on this project were found to be very small and quickly dissipated into the surrounding sample. Conditions for rapid heat dissipation are also likely to be observed around a full scale pile in frozen soil.

5.8 Comparison to Ladanyi's (1982) Cone Penetration Tests

From penetration tests conducted in varved silt at -0.3 deg C, Ladanyi (1982) estimated n values of 4 to 5 at penetration rates less than 18 mm/hr. Larger n values, 10 to 20, were estimated at penetration rates greater than 18 mm/hr. This behavior was associated with uniaxial compression tests (large n values) at strain rates above about 10^{-5}/sec.

Ladanyi (1976) has also compared a frozen soil element just ahead of a penetration rod with an element of soil within a compression test sample (at failure). He explained that the soil element, ahead of the advancing

penetration rod would change from the elastic to the plastic state in the same manner as the element in the compression test sample tested to failure. Ladanyi (1982) later proposed that it was more logical to compare the frozen soil behavior ahead of the penetration tip to an expanding hemispherical cavity with a diameter equal to the cone's diameter. This representation is shown in Figure 5.3a. Ladanyi stated that the creep equation parameters for ice poor or dense granular frozen soils should be obtained by static, stage-loaded cone penetration tests. These tests are not unlike the step loaded pile tests completed for this project.

After testing a series of model tapered piles, Ladanyi and Guichaoua (1985) proposed that an expanding cylindrical cavity theory, using a primary creep law (Ladanyi, 1972), was appropriate for tapered pile displacement in a frozen sand. Limited data did not fully support this theory. Movement of frozen sand around this study's model pile lug (which leaves a void behind the lug) is similar to cylindrical expansion.

5.9. Large n Values from Cyclic Loads on Model Piles

Parameswaren (1982) described how superimposed cyclic loads of $\pm$1.5% of the initial static load caused pile displacement rates to double. Figure 5.15 is from his paper shows the region of pile displacement (above 0.1 mm)

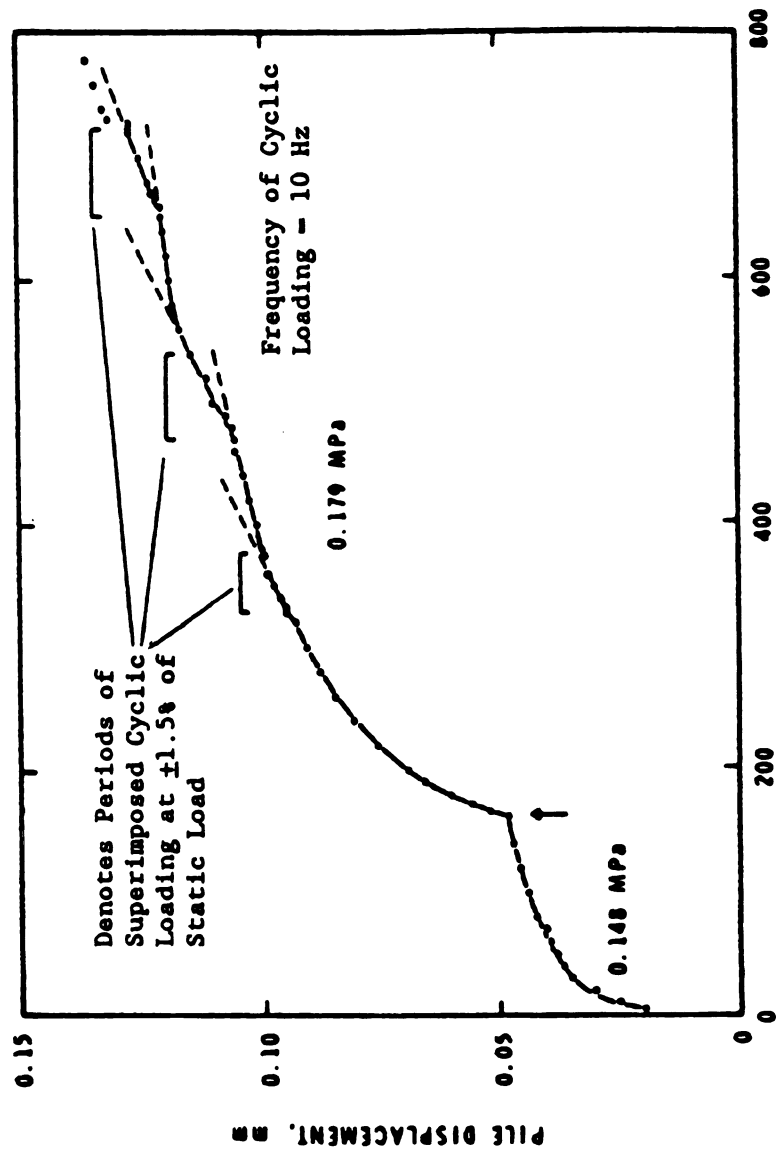

Figure 5.15. Displacement-time curve for concrete pile in frozen soil (Parameswaren 1982).

where a cyclic load of ±1.54% caused the displacement rate to approximately double, as indicated by the given displacement rates.

For a number of reasons, caution should be used when interpreting these results. Based on tests completed during this study, it is known that the displacement rate determined from a short duration test (section 2 in Figure 5.15) is relatively fast if compared to the displacement rate found at the end of a longer duration test (section 1 in Figure 5.15). It has also been shown that when a pile's load is reduced (sections 3, 5, and 7 in figure 5.15), a pile's displacement rate will be relatively slow for a period of time before regaining a displacement rate typical for this reduced pile load. From the information given, it is not clear if pile failure has started (although this seems unlikely at a displacement of less than 0.15 mm). The displacement rate increases in sections 2, 4, and 6 of Figure 5.15 would have been put into perspective if a small static load had been added (perhaps at section 4 in place of the cyclic loading) to produce a displacement rate similar to the rates produced by the cyclic loads.

To further examine this pile test, a variation of equation 3.4 can be used as:

$$\left(\frac{P + \Delta P}{P}\right)^{n} = \dot{\delta}_2 \,/\, \dot{\delta}_1 \qquad (5.7)$$

where P is the initial load and ΔP is the amplitude of the

cyclic load. A ±1.5% cyclic load that doubles the displacement rate can be shown as:

$$(1.015)^{n} = 2.0 \qquad (5.8)$$

which yields n = 46, a value considerably higher than the value of n = 8 given by Parameswaren (1982) for similar piles under static load increases.

Cyclic loads applied to various piles during this project gave n values equal to or less than the values found by static loading (see Table 4.3). Parameswaren's (1985) cyclic loading of uniaxial compression samples also appear to show, after being adjusted for temperature, n values approximately equal to static load n values. Assuming that heat generated at the pile/soil interface is quickly dissipated (as noted in this study), what could account for the large difference in n values between cyclic loading and dynamic loading?

This difference may be partly accounted for by considering basic harmonic loading theory. From Clough and Penzien (1975), a ratio of the maximum base force (force at the pile/frozen soil interface) to the applied force amplitude (force measured above the pile and frozen soil by a load cell) is called the transmissibility (TR) and is represented as

$$TR = M \left[1 + (2 \xi \beta)^2 \right]^{0.5} \qquad (5.9)$$

where M is the dynamic magnification factor

$$M = [\ (1 - \beta^2)^2 + (2\ \xi\ \beta)^2\ ]^{-0.5} \qquad (5.10)$$

with β defined as the ratio of applied frequency ($\bar{\omega}$) to the natural frequency (ω), thus

$$\beta = \frac{\bar{\omega}}{\omega} \qquad (5.11)$$

The damping ratio (ξ) is written as :

$$\xi = \frac{c\ \ \omega}{2\ k} \qquad (5.12)$$

where c (system damping coefficient), k (system spring constant), and ω (system's natural frequency of vibration) are the basic damped system parameters.

The TR values for the lugged and threaded piles used on this project are all close to 1 because the applied frequencies were all well below the natural frequencies of these pile/frozen soil systems. For this project, certain resonant frequencies developed due to parts of the test system which increased pile displacement rates. At 1 Hz, the static weights were induced to rotate clockwise and then counterclockwise which produced larger pile displacement rate increases. At 6.2 Hz, a long metal rod supporting the static weights would begin to vibrate and also produced displacement rate increases. These results were not included in the figures for this study because they represented a characteristic of the test system and not the behavior of model piles embedded in frozen soil

Although no information was given regarding damping of the pile/soil system, a conservative damping ratio of ξ = 0.16 (cyclic triaxial tests at 0.3 Hz on Ottawa sand at -2.5 deg C, Figure 2.10b) might be assumed. A second estimate of ξ = 0.03 (cyclic triaxial tests interpolated to 10 Hz for Ottawa sand at -4 deg C, Figure 2.10a) will also be considered. Parameswaren (1982) found that the amplitude of displacement between the pile and surrounding soil shown in Figure 5.15 was a maximum at a frequency of 8.72 Hz. Clough and Penzien (1975) explain that this peak response frequency would correspond to a value of β as

$$\beta_{peak} = [\ 1 - 2\ \xi^2\ ]^{0.5} \qquad (5.13)$$

Using this equation, natural frequencies at 8.95 and 8.73 may be determined for ξ values of 0.16 and 0.03 respectively.

If values for ξ = 0.16 and ω = 8.95 Hz are assumed, ω = 10 Hz can be used in Equation 5.10 to determine a TR = 2.4. A cyclic load of $\pm$1.5% of static load would become $\pm$1.5*(2.4) at the pile/soil interface. Using load increases of $\pm$3.6% in equation 5.7 yields an n value of 20. Assuming ξ = 0.03, ω = 8.73 Hz, and ω = 10 Hz would produce an n values of 15. These n values for cyclic loads are similar to the n values found from static loading only. Adjustments for temperature increases from cyclic loading

could decrease these n values to magnitudes associated with static loading.

5.10. Applications to Field Piles

Situations involving field piles will now be considered in light of the model pile test results contained in earlier parts of this dissertation.

5.10.1. Analysis of a Pile Failure

Lusher, et al. (1983) described a series of tests using 450 mm diameter field piles with 18 mm corrugations spaced at 300 mm intervals along the pile. For three soil types, these pipe piles were placed into 600 mm holes with a sand slurry. Once the sand slurry was frozen and the test temperatures had stabilized to -0.3 deg C (a coolant circulation system within the pile helped control temperatures), a series of incremental loads were added to each pile with each load maintained for a period of 3 days.

During test loading, pile displacements were measured at the top of the pile with reference to some fixed point away from the pile. As the pile settled, soil around the pile was moved or displaced. For those piles tested in clays and the ice rich silts at this relatively warm temperature, this deformation could occur at the pile/soil interface or entirely outside of the relatively stiff cylinder of frozen sand slurry. Analyzing their behavior

would require additional information.

Although creep parameters were not reported, the dense alluvial sands and gravels at Shaw Creek Flats in south-central Alaska would normally display a creep behavior similar to that of the frozen sand slurry. The frozen gravels should be stiffer than the sand slurry. Assuming that the surrounding natural soils are as stiff or stiffer than the frozen sand slurry, then pile movement and pile failure can be largely associated with deformation within the sand slurry.

Figure 5.16 summarizes displacement data for 3 pile tests conducted at Shaw Creek. The displacement-time curve for Pile #1 is shown at the top of this figure. All three curves are shown on the bottom part of this figure. To analyze the behavior of these piles, consider first the behavior of a combination of two model pile types: a small lugged pile and a threaded pile. A physical model of these combined characteristics might be analogous to a perforated lug threaded onto a rod which would then be frozen into a sand sample. The threaded portion of this composite model pile would quickly develop capacity but would start to fail after a small displacement (approximately 1 mm for a 1.06 mm peak to peak thread for the 9.52 mm diameter rods used in this study). As failure continued along the pile/sand interface, part of the pile capacity (held by these threads) is transferred to the lug.

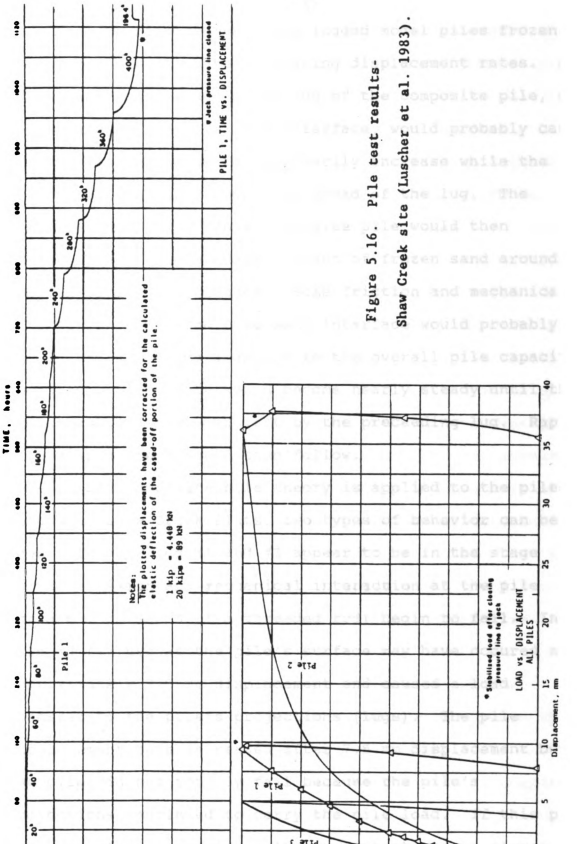

Figure 5.16. Pile test results-
Shaw Creek site (Luscher et al. 1983).

At 1 mm displacement, the lugged model piles frozen in sand were shown to have decreasing displacement rates. A transfer of pile load to the lug of the composite pile, due to failure at the pile/sand interface, would probably cause the displacement rate to temporarily increase while the frozen soil is fully compacted ahead of the lug. The displacement rate of this composite pile would then gradually decrease as displacement of frozen sand around the lug became established. Some friction and mechanical interaction along the pile/sand interface would probably remain and add a small amount to the overall pile capacity. The displacement rate would become nearly steady until the lug approached the void left by the preceeding lug. Rapid pile displacement would then follow.

If the composite pile theory is applied to the piles tested at Shaw Creek Flats, two types of behavior can be identified. Piles #1 and #3 appear to be in the stage before adhesion and mechanical interaction at the pile surface ("threads" of a threaded rod) begin to fail. In Pile #2 failure at the pile's surface may have occured at approximately 7.5 mm displacement and caused a load transfer to the pile's projections (lugs). The pile displacement rate increased after 7.5 mm displacement but the pile did not totally fail because the pile's projections continued to carry the pile load. If this pile had more closely spaced or larger projections, a slower

displacement rate would have been observed past the 7.5 mm displacement.

5.10.2. Comments on the Proposed ASTM Pile Standard

A proposed American Society for Testing and Materials (ASTM) "Standard Method of Testing Individual Piles in Permafrost Under Static Axial Compressive Load" (Neukirchner, 1988), was discussed earlier in Section 2.4. This method proposes that the test include two piles with two loads on each pile. The first load would be near 100% of the pile design load and should displace a relatively small amount until a steady creep rate is attained or until 3 days have passed. The second load, 200% of the design load, on each pile should cause failure with displacements reaching the point of accelerating rates at less than 25 mm. This process may take about 6-12 hours for the smaller pile load and about 3-5 days for the larger load. The two failure loads are used as a set of information, and the two creep loads are used together as a set in the proposed ASTM method.

Based on tests performed during this study, the approach proposed by this ASTM standard appears to be the right one. Loads causing failure are compared as a group while loads applied for shorter displacements are compared as another separate group. Directly comparing displacement rates determined at failure with displacement rates

determined after short displacements (as in short duration loads during this study) can give misleading information. Neukirchner (1988) explains (correctly) that this method should provide more useful pile loading information in a relatively economical and expedient manner, but cautions that tests from additional piles may be necessary.

Establishing a load-displacement relationship based on two data points can be risky if the two piles tested are not very similar. The "similar" piles in Figure 5.16 show significant variations. Displacement rate variations between model piles and even during a single model pile test was frequently encountered during this project. More data could be obtained from one pile if short duration type tests were applied at the end of a pile test (defined as when the pile displacement rate begins to increase).

It appears that a series of incremental-load type short-duration tests could be performed at the end of the standard pile test when the pile displacement rate is slowly increasing. This series of small loads (3 to 5%, 4 to 10%, and 9 to 15% of the initial load) could each be applied to the pile for short periods (10 to 30 minutes) before the initial pile load is restored. If the displacement rate before this series of loads were similar to the rate (including a short stabilization period) after the series, then a comparison between the three load increases could be considered. The relationship between

the three load increases and the n parameter determined between them would provide test data useful as an indication of agreement between the two piles tested. The expense of gaining this information would be minimal since the test piles and equipment are already in place.

5.10.3. Additional Pile Capacity from Driven Piles

Manikian (1983) discussed driving pipe piles into pilot holes filled with warm water (to decrease driving resistance). Driving piles with lugs would be difficult and could leave large voids behind each lug that reduce pile capacities. The pile corrugations discussed by Lusher, et al. (1983) could be added after driving but would require additional field time which is very expensive. Black and Thomas (1979) indicated that the 8 pile tests (distributed among three sites in Alaska) reported by Lusher, Black and McPhail (1983) cost over $5,000,000 in 1975. Pile modifications made during pile manufacture would be less expensive.

Before modifications to field piles can be considered, a method to install them is needed. Manikian (1983) decribed in detail how warm water (of a given temperature) had been added to pilot holes (of given diameter) and allowed to warm the surrounding frozen soil (for a given duration) to ease pile driving resistances. The relatively small volume of soil warmed by the water and by the action of pile driving was able to freeze again quickly. This

method could be taken one step further to ease the resistance of piles with "rougher" surfaces by including some combination of warmer water, larger pilot holes, or longer soil warming periods that would also keep freeze-back time to a minimum.

Roughness could be added to a pile surface so that the outside diameter was not increased but included grooves or indentations that, filled with the warmed soil during pile driving, would freeze solidly later. These roughness features should be equal to or larger than the grain size of the natural surrounding soil to produce a good interlock between soil and pile. Frozen soil within grooves could be considered similar to frozen soil (limited to 25 mm and less) ahead of model pile lugs. Pile capacity increases could be based on the length, depth, and shape of the pile indentations.

5.10.4. Needed Research on Pile Behavior

Several topics related to pile behavior under static and cyclic loads, described below, need further study.

a) Static and cyclic load effects on the behavior of frozen soil in shear at the pile/soil interface.
b) The long-term pile/soil interaction mechanism dependance on surface geometry needs to be described in greater detail.
c) The incremental-load type short-duration test sequence

would appear to have application to field pile load tests. Test procedures for field use need to be developed.

d) The pile displacement rate increase shown by Parameswaren (1982, 1984) should be considered during pile foundation design in permafrost. A field check of a pile's natural frequency could be developed.

SUMMARY AND CONCLUSIONS

6.1. Summary

Small cyclic loads superimposed on a static pile load will, in some frozen ground situations, increase pile settlement rates and significantly lower their design capacity. This situation may arise for piles in perennially frozen ground which are used to support vibrating machinery (turbines, power generators, or compressors) or traveling loads (cranes or fork lift trucks). Small cyclic loads, 3 to 5 percent of the long-term sustained load, were reported (Parameswaran, 1982, 1984) to accelerate settlement (displacement) rates of model piles embedded in frozen ground. The basic mechanisms by which small cyclic loads increase pile settlement rates and a suitable theory for estimation of this increase were objectives of this research.

This study used model steel piles in a laboratory setting to carefully change and control variables in order to increase our understanding of the processes responsible for friction pile settlement. Pile settlement rates due to static and incremental static loading were analyzed and compared to pile settlement rate increases due to superimposed dynamic loads. Variables controlled during these tests included cyclic load amplitude, frequency of load application, static load magnitude, and temperature.

Sand density and ice volume fractions were controlled during sample preparation. Model pile settlement in frozen ground is typically predicted on the basis of a creep equation relating pile load or pile-surface shear stress to pile displacement rates. Creep parameters were used to characterize soil type, soil/ice structure, temperature, and loading conditions. Experimental results showed that cyclic loads significantly increased model pile displacement rates over those observed for the sustained load, and that creep theory with the appropriate parameters will predict the effects of small dynamic loads on settlement rates.

Load capacity of friction piles in frozen ground is known to increase significantly when the pile surface is roughened by the addition of protrusions or lugs. A series of model steel piles with controlled surface geometries (lug size, shape, and spacing) were frozen in sand and loaded to provide additional information on the displacement mechanisms operating at the pile/frozen soil interface. The onset of increasing pile displacement rates (tertiary creep) was shown to be a function of lug height and spacing. A number of conclusions are presented in the next section.

6.2. Conclusions

The conclusions resulting fron this research project

will be presented under three headings: creep settlement parameters, dynamic load effects on settlement rates, and pile surface roughness and load capacity.

6.2.1. Creep Settlement Parameters

Displacement rates for most lugged piles decreased slowly with time throughout a given test and seldom reached a constant displacement rate. For these conditions, direct comparison of displacement rates or creep parameters between piles was difficult. To improve comparisons between tests, log(time)-log(displacement) plots were prepared using data obtained after a given displacement. This technique gave creep parameters which could be readily compared with like plots of similar pile test data.

Incremental loading for relatively short time periods eliminated some of the long-term pile displacement variability caused by small temperature changes, frozen soil heterogeneity, and decreasing displacement rates. Although these short-term tests may not accurately predict long term creep parameters, they did permit comparison of load variables such as dynamic-load amplitude and frequency with each other and with small static-load increases. Increasing a pile load by small steps, with each load held constant for a short duration, also decreased the effect of temperature, materials, and displacement variability, while it provided data that better predicted creep parameter (n)

values for long-term pile behavior.

6.2.2. Dynamic Load Effect on Settlement Rates

The technique developed to measure displacement rate changes for incremental static pile loads was used to measure displacement rate changes caused by dynamic loads superimposed on statically loaded model piles. Cyclic loads significantly increased pile displacement rates over those observed for a sustained load. Model pile displacement rates in frozen sand were observed to be essentially independent of frequency for small dynamic loads superimposed on a large static load in the range of 0.1 Hz to 10 Hz. The magnitude of rate increase was shown to be dependent on amplitude of the cyclic load. Frequencies that induced resonant responses in parts of the loading system were excluded from reported data.

Creep theory appears to be suitable for prediction of the change in pile displacement rates due to a small cyclic load. A superimposed cyclic load (amplitude X) would produce a short duration displacement increase roughly equal to the increase produced by a static load increase (magnitude of 0.6 times X). Compared to small static load increases, laboratory measurements indicated a reduction of the dynamic-load n to about 5/7's of the static-load n value when small dynamic loads were superimposed on larger static loads. This reduction in n appears to be

appropriate for evaluating the increase in settlement rates when nonresonant cyclic loading is superimposed on a static load. Pile capacity must then be adjusted for a given service life.

6.2.3. Pile Surface Roughness and Load Capacity

Load capacity of all model piles in frozen sand was dependent on a load transfer component acting at the pile/frozen soil interface. Mechanical interaction between frozen soil and model pile surface protrusions (lugs) provided the larger and more reliable long term load capacity.

A minimum lug spacing (greater than 10 mm for a 3.18 mm lug height) was needed to develop fully the mechanical interaction between frozen sand and the pile lug. Additional data are needed to completely define the relationship between lug spacing and lug size along with the influence of particle size, soil type, temperature, pile size, and loading conditions.

At lug spacings that fully developed mechanical interaction (greater than the minimum described above), the pile displacement-time behavior was relatively unaffected by lug space variations until it reached a critical displacement (start of pile failure). The relationship between critical failure displacement and lug spacing (displacement limit) was shown for 2 lug heights. It was

observed that shear stress on the remaining pile/soil contact area appeared to asymptotically approach the long term shear strength of the frozen soil. The mechanisms that initiated pile failure for these short term pile tests should be similar to those which operate during long term periods.

Limited information from tests with threaded-rod model piles indicated that thread heights and spacings larger than the sand particles fully developed pile/soil mechanical interaction. In comparison, tests with thread spacings less than the sand grain size did not fully develop mechanical interaction and showed a displacement behavior more like a threaded pile in polycrystalline ice. In polycrystalline ice, failure occurred at similar displacements for all threaded piles.

Based on the above observations, piles with surface irregularities much smaller than the adjacent sand grains will develop little pile/soil mechanical interaction during rupture of the adhesive bond component and during subsequent pile displacement. Frictional forces appeared to provide the major portion of any remaining pile capacity following a gradual loss of the adhesion bond along a relatively smooth pile.

APPENDIX A

FIGURES FOR DETERMINATION OF TABLE 4.1 CREEP PARAMETERS

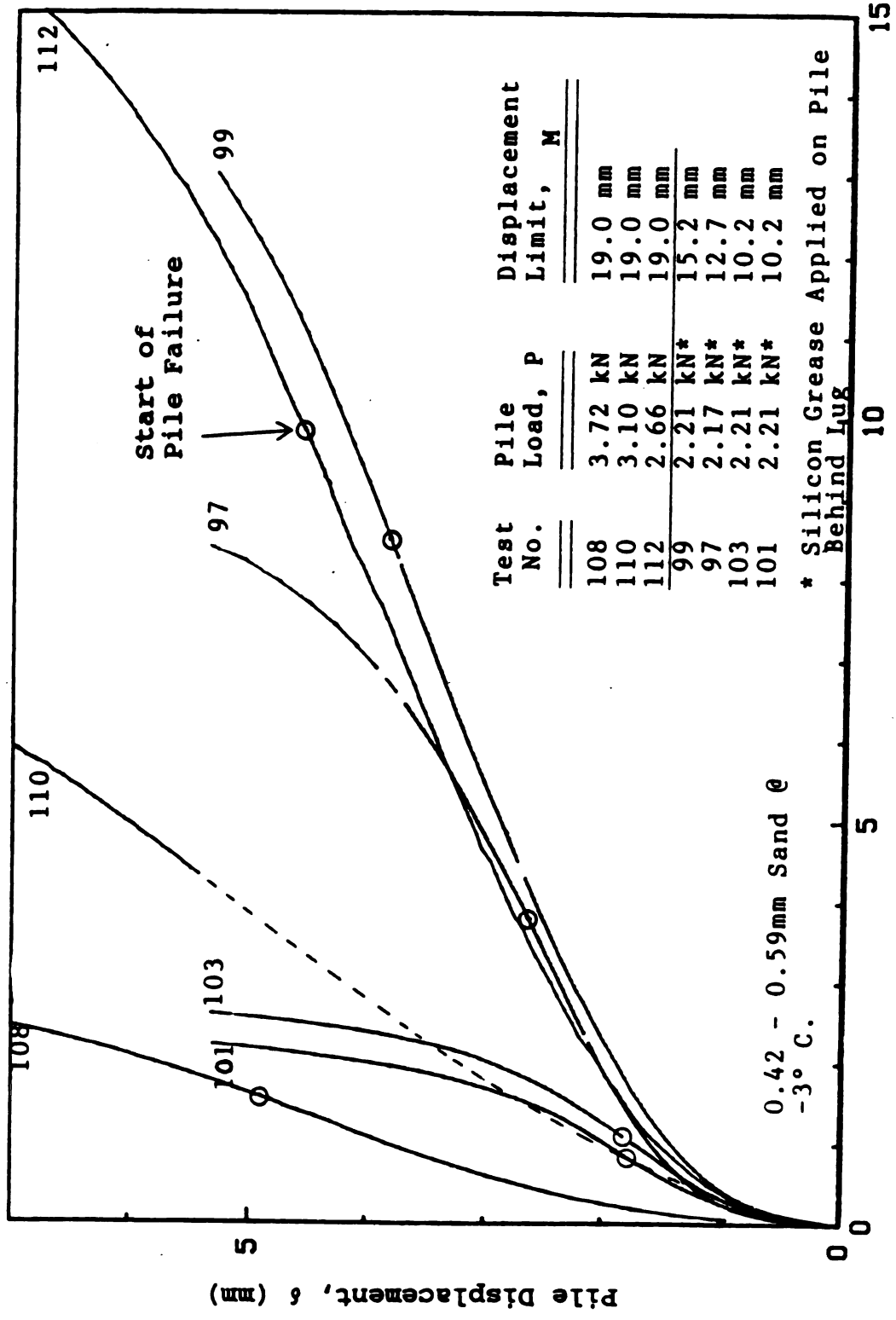

Figure A.1. Time-displacement curves for model steel piles in frozen sand at -3 deg C with 3.18 mm lug heights and 19.0 mm (average) displacement limits.

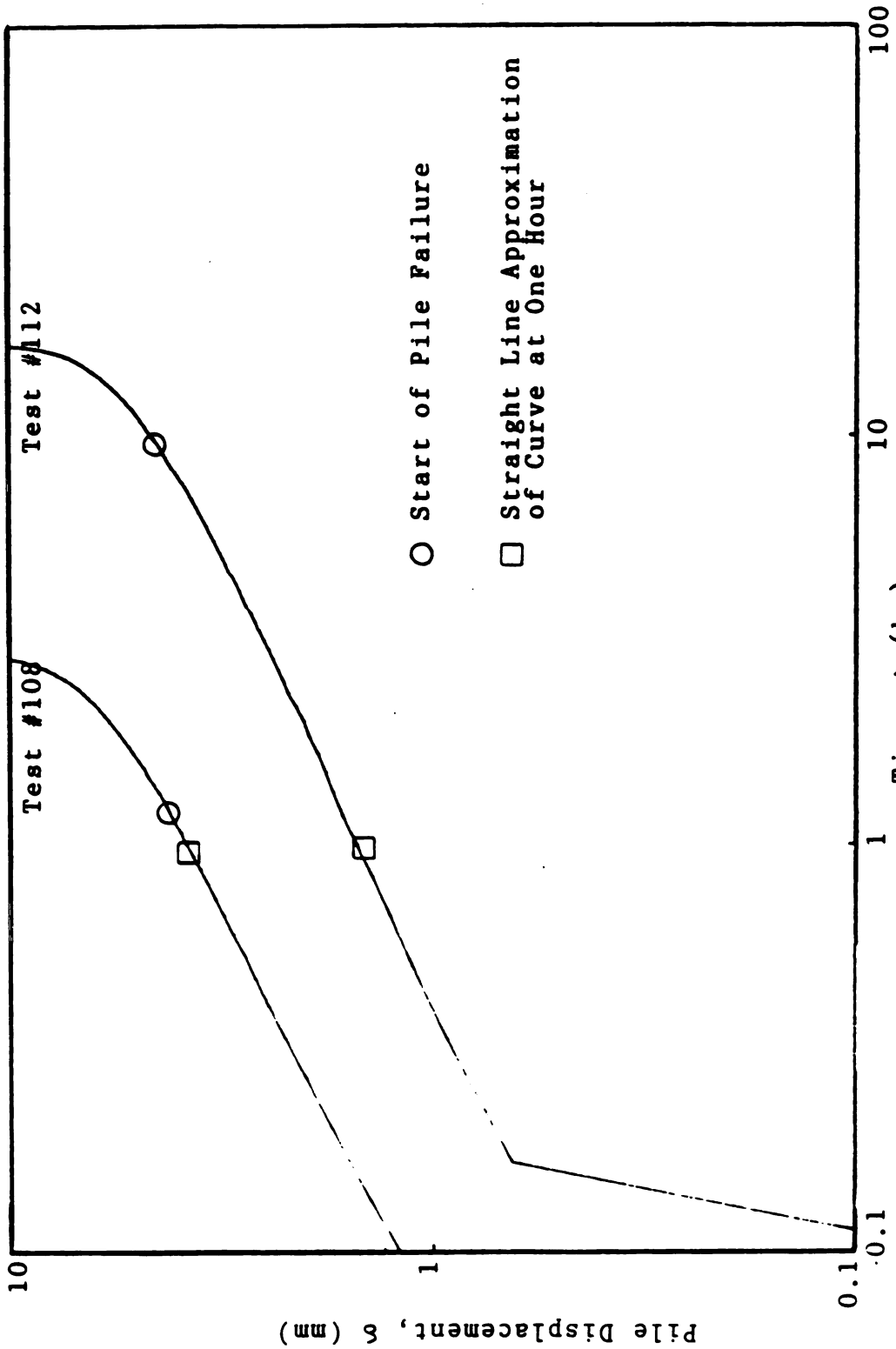

Figure A.2. Time-displacement curves for model piles in frozen sand at -3 deg C with 3.18 mm lug heights, 19.0 mm displacement limits. (a) 0 mm C-type plot starting points.

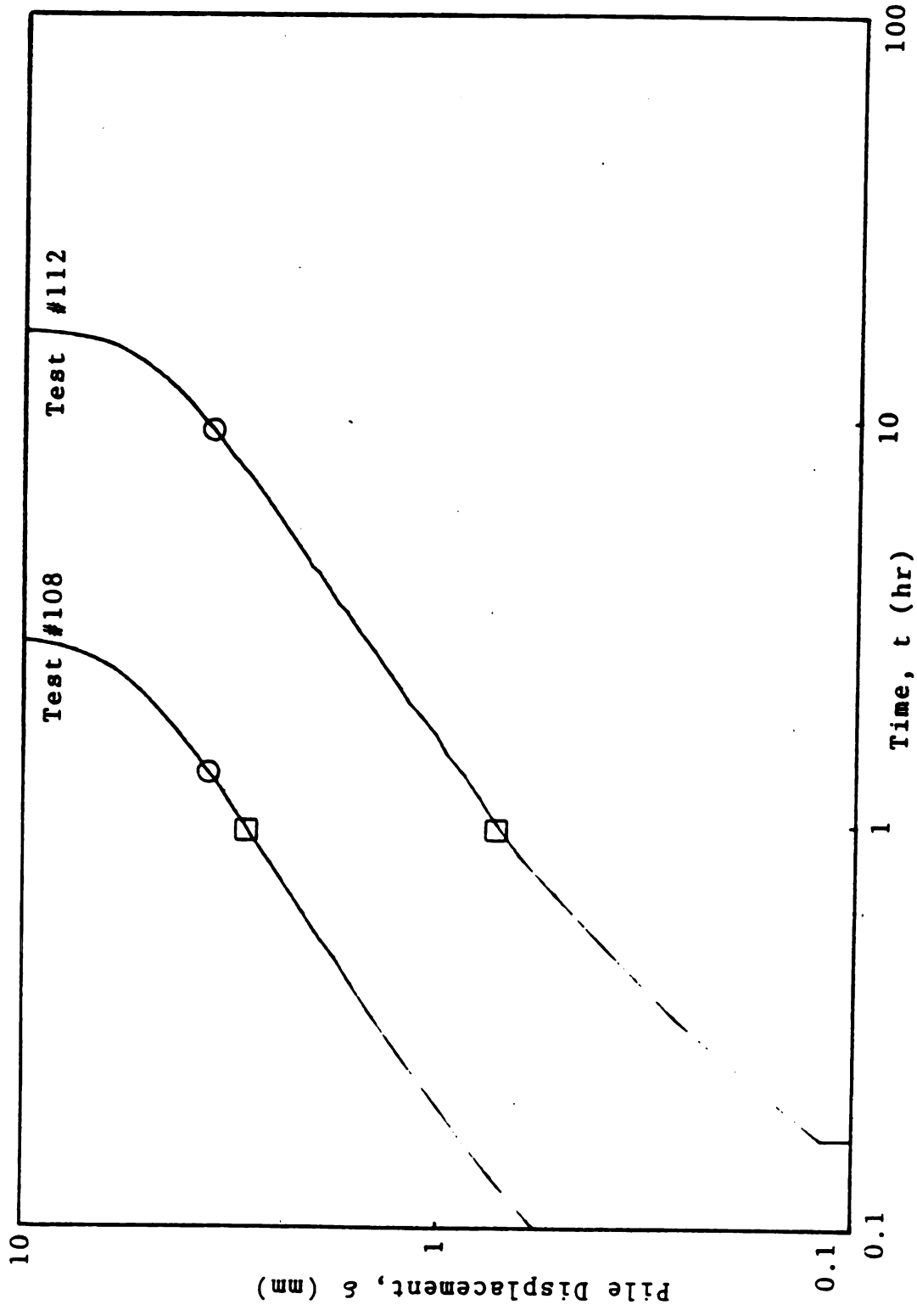

Figure A.2b. 1 mm C-type plot starting points.

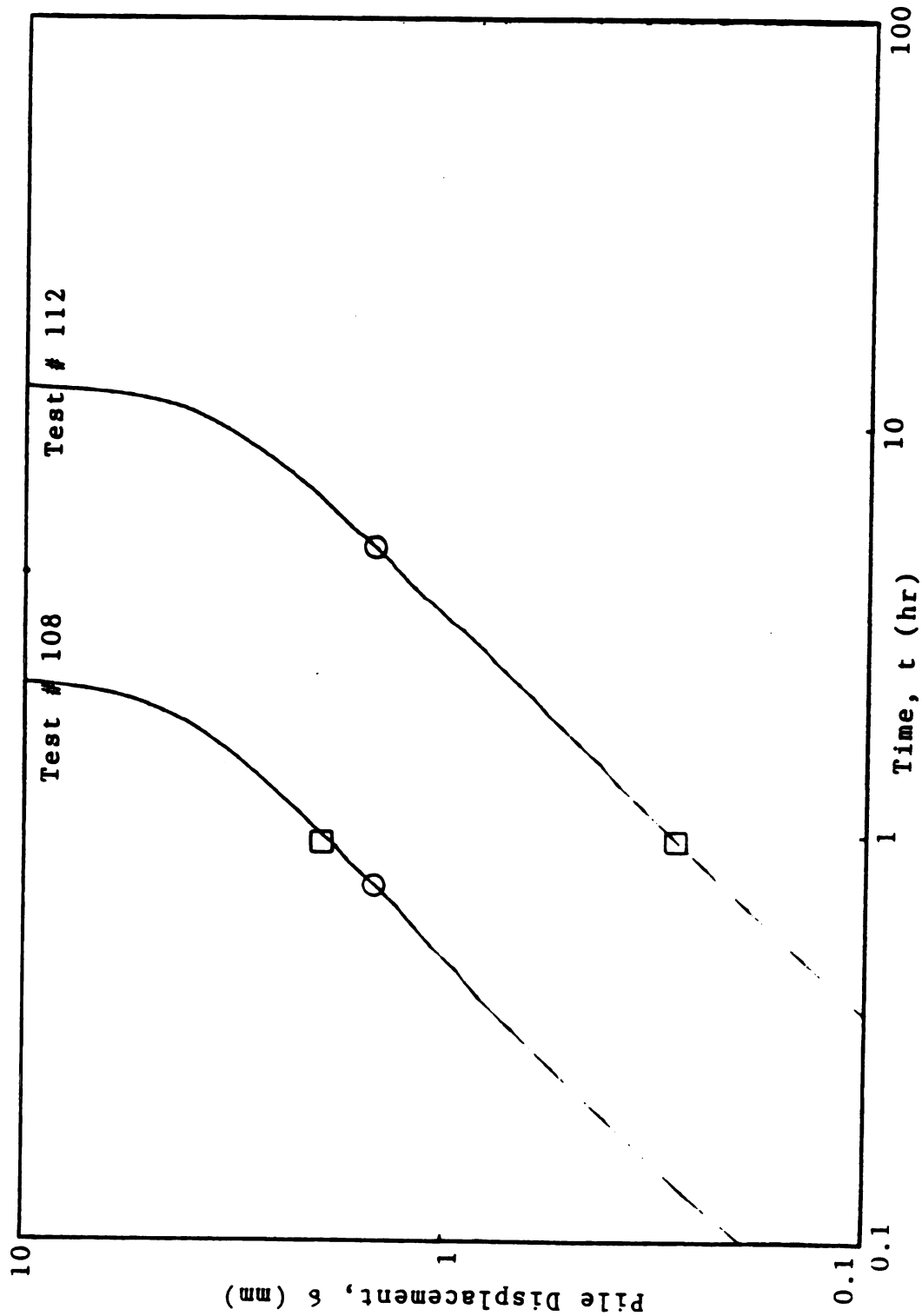

Figure A.2c. 3 mm C-Type plot starting points.

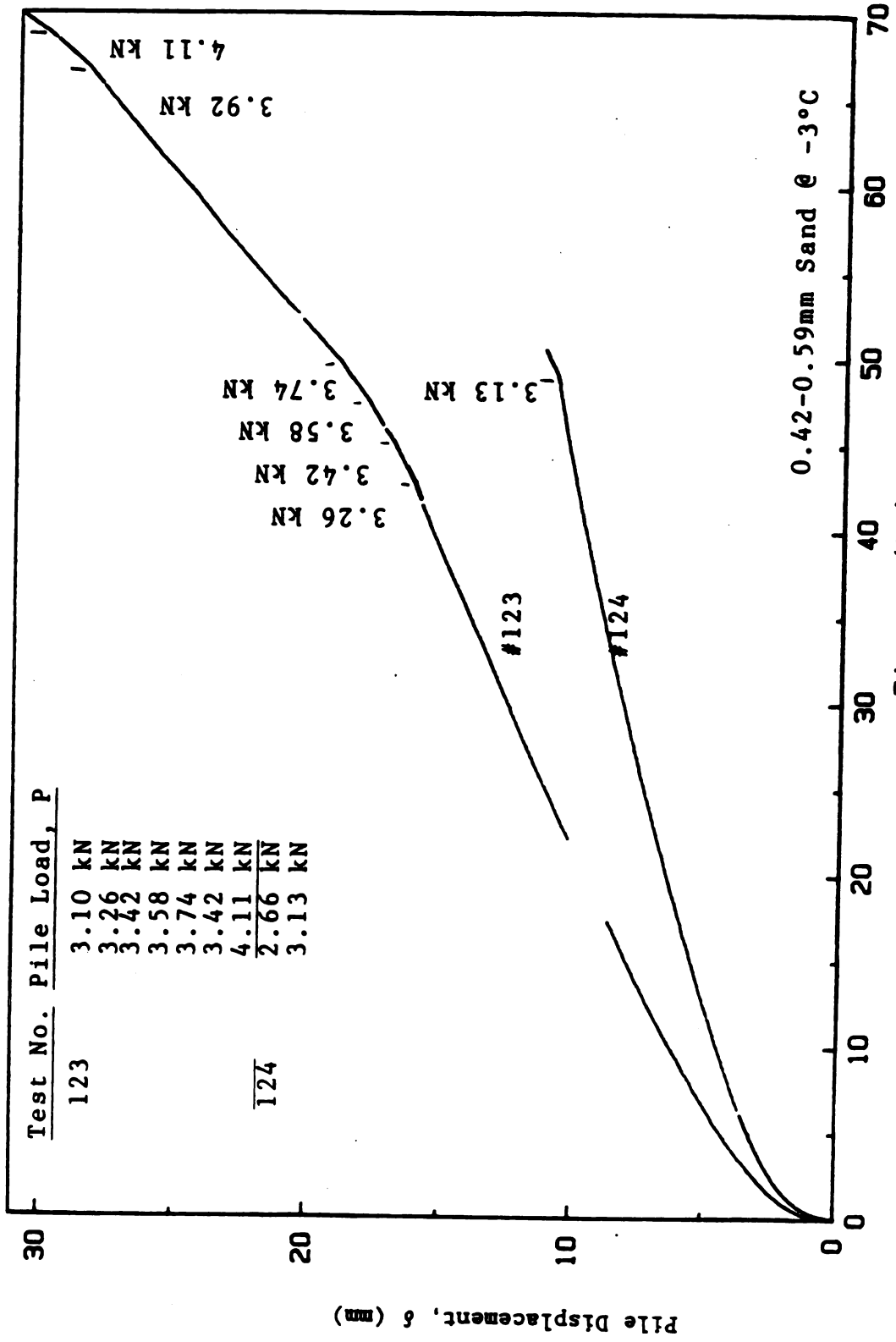

Figure A.3. Time-displacement curves for model steel piles in frozen sand at -3 deg C with 3.18 mm lug heights and 76 mm (average) displacement limits.

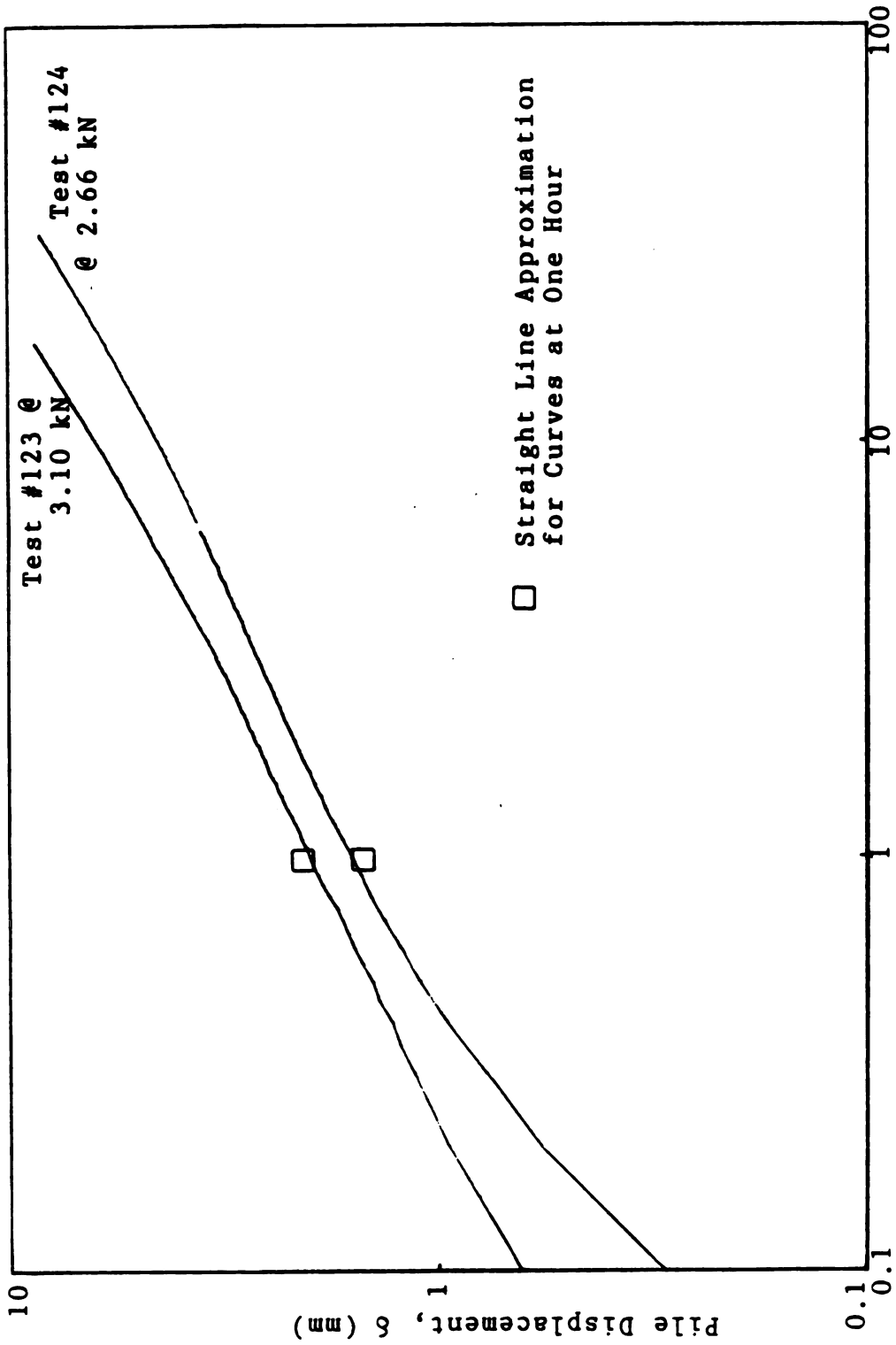

Figure A.4. Time-displacement curves for model piles in frozen sand at -3 deg C with 3.18 mm lug heights, 76 mm displacement limits. (a) 0 mm C-type plot starting points.

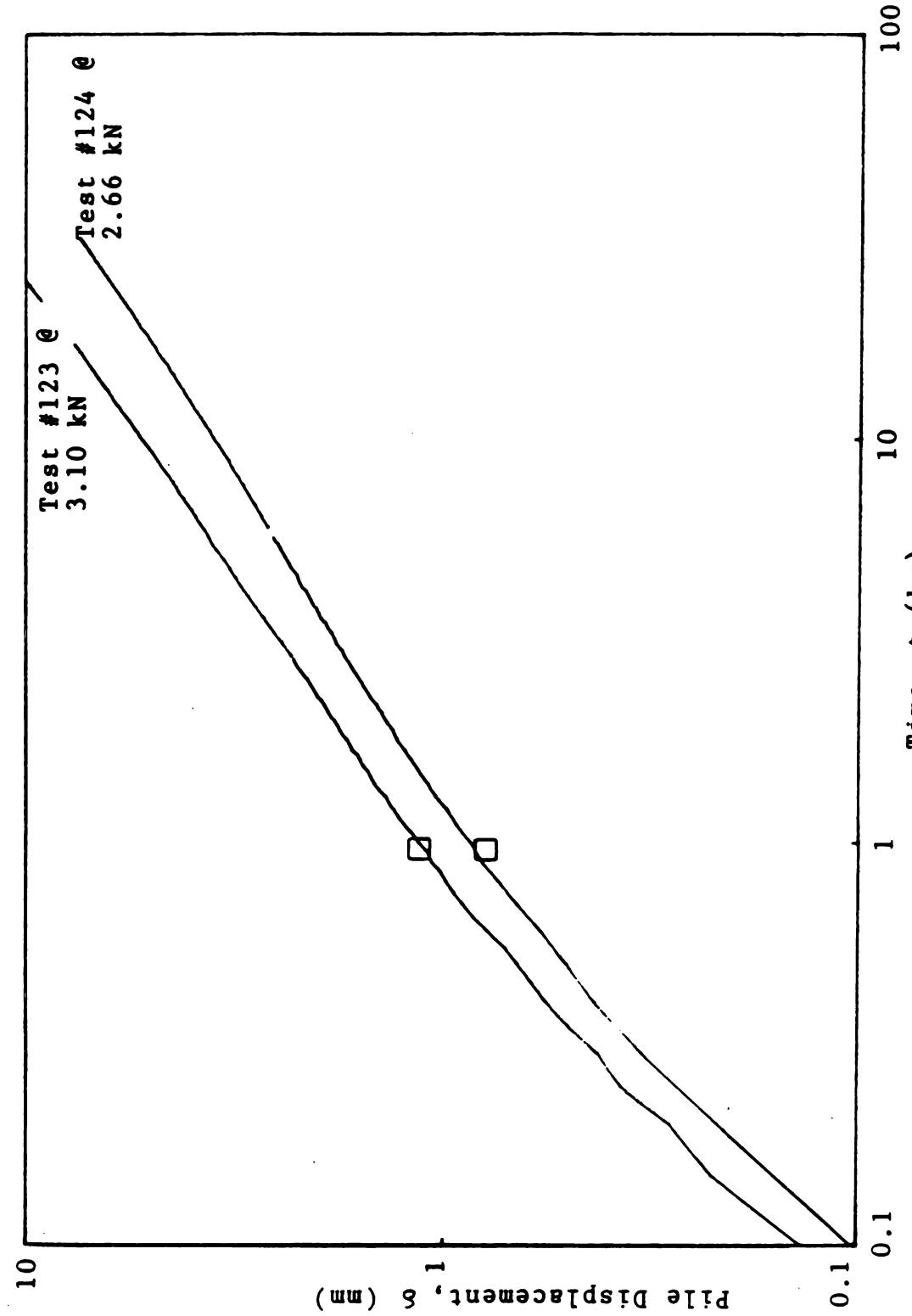

Figure A.4b. 1 mm C-type plot starting points.

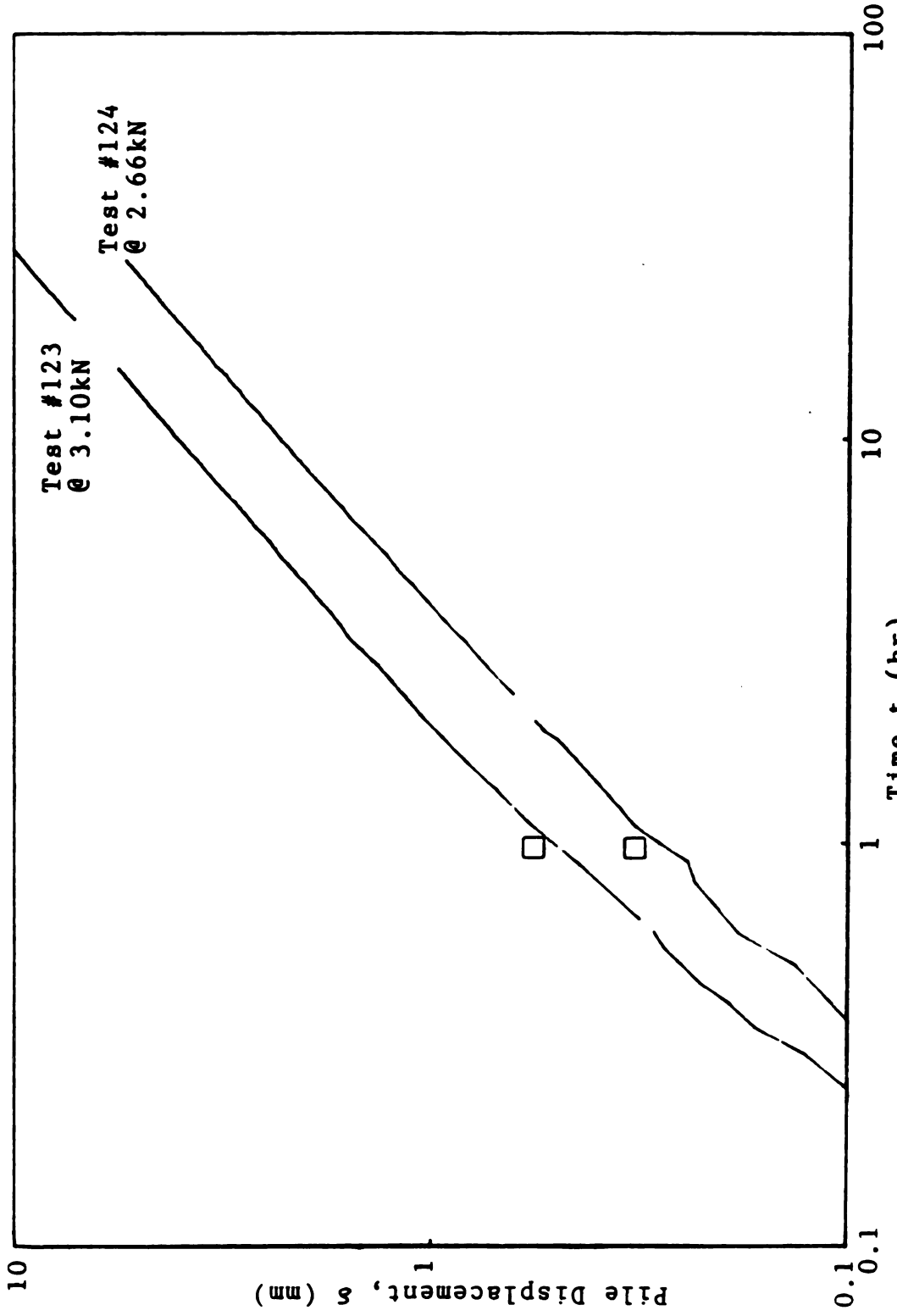

Figure A.4c. 3 mm C-Type plot starting points.

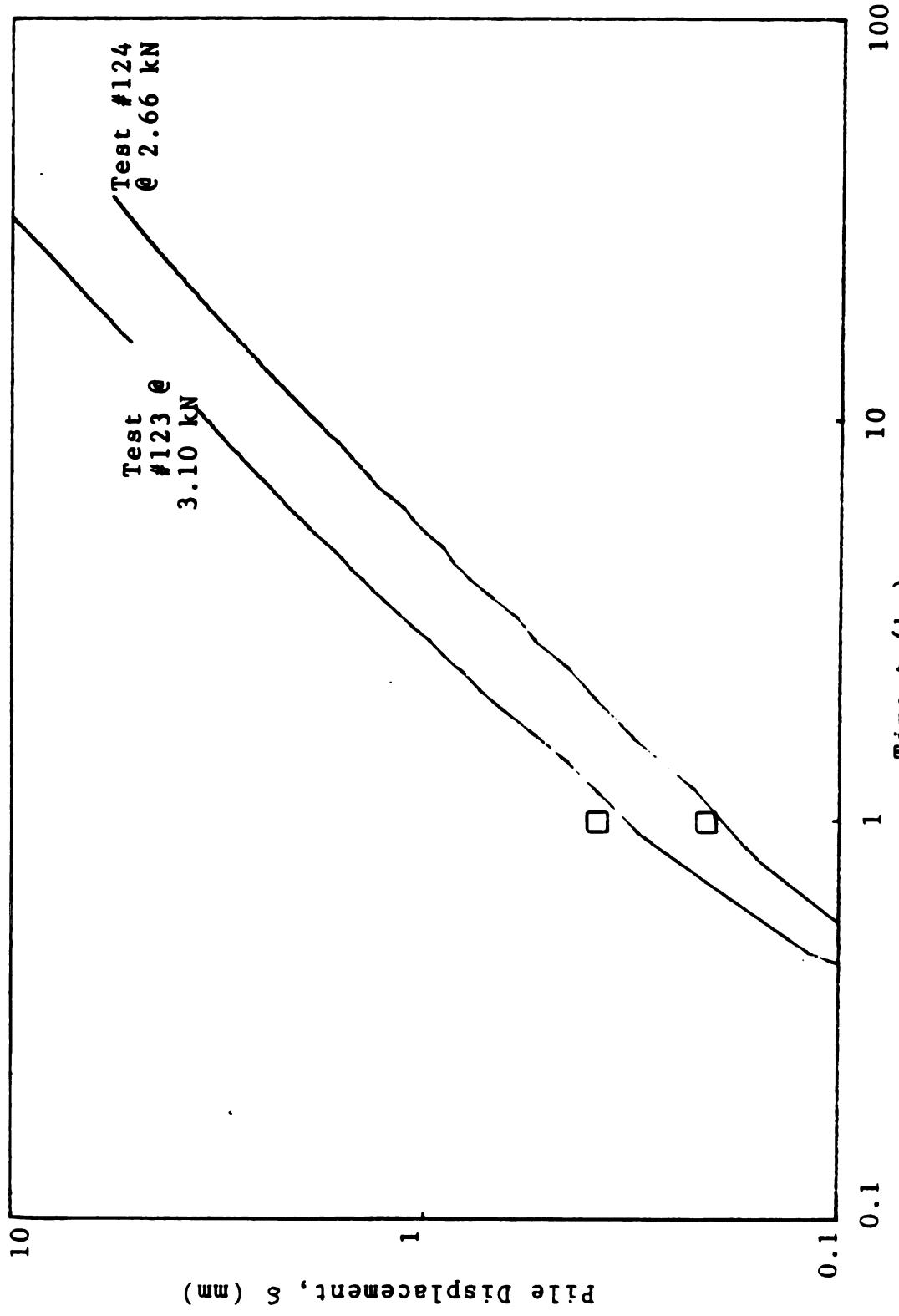

Figure A.4d. 5 mm C-Type plot starting points.

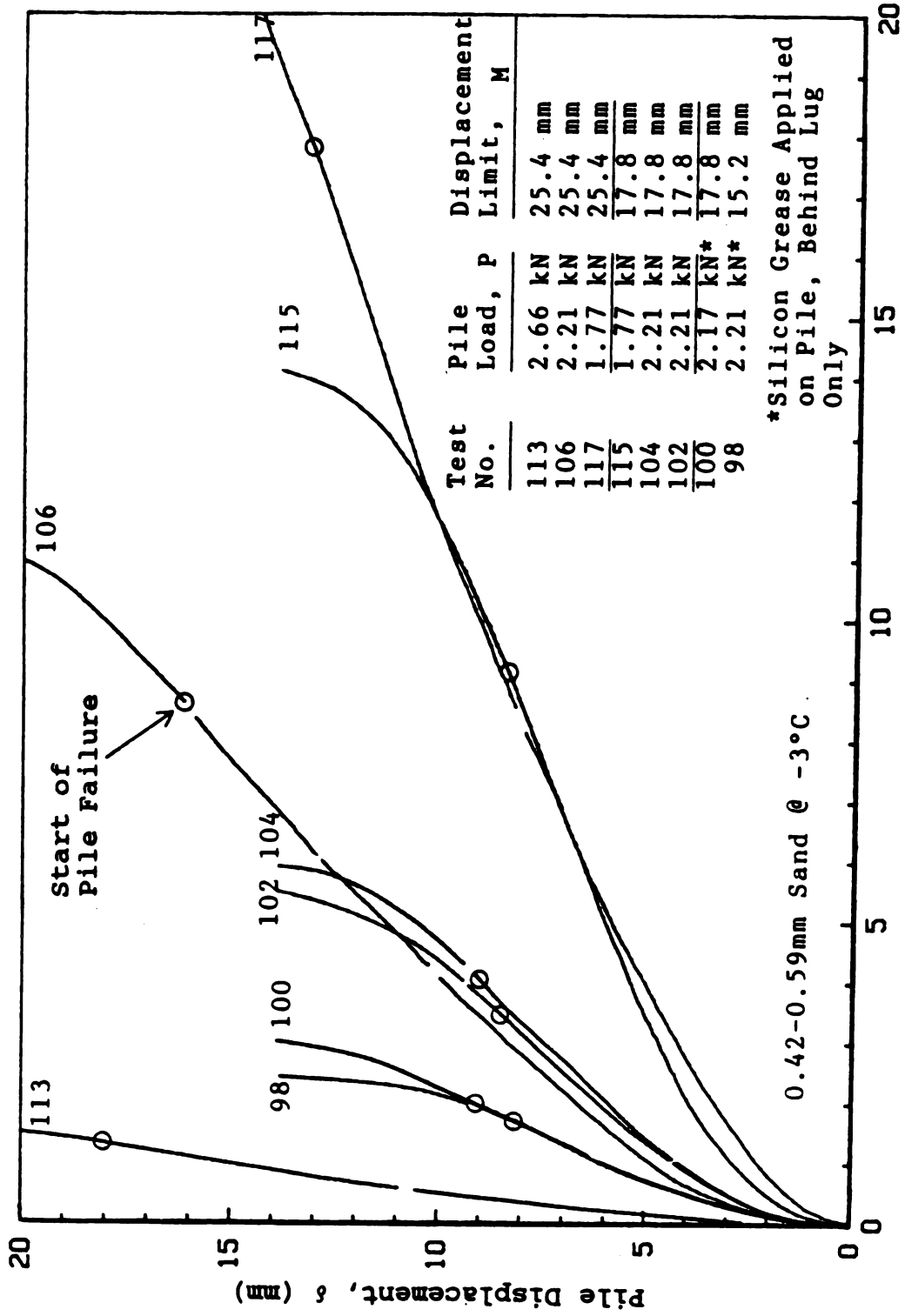

Figure A.5. Time-displacement curves for model steel piles in frozen sand at -3 deg C with 1.59 mm lug heights and 25.4 mm (average) displacement limits.

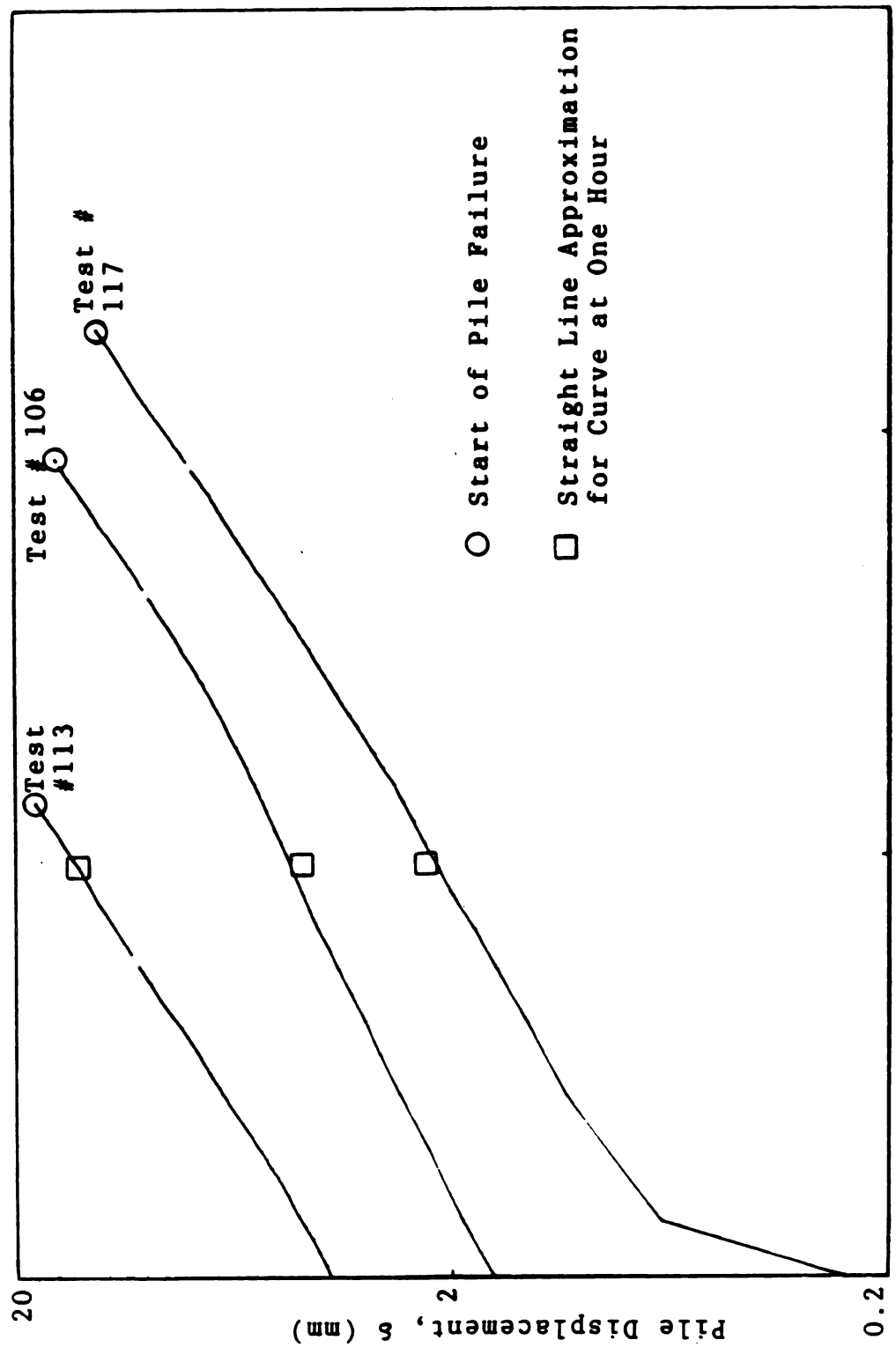

Figure A.6. Time-displacement curves for model piles in frozen sand at -3 deg C with 1.59 mm lug heights. (a) 0 mm C-type starting points and 25.4 mm displacement limits.

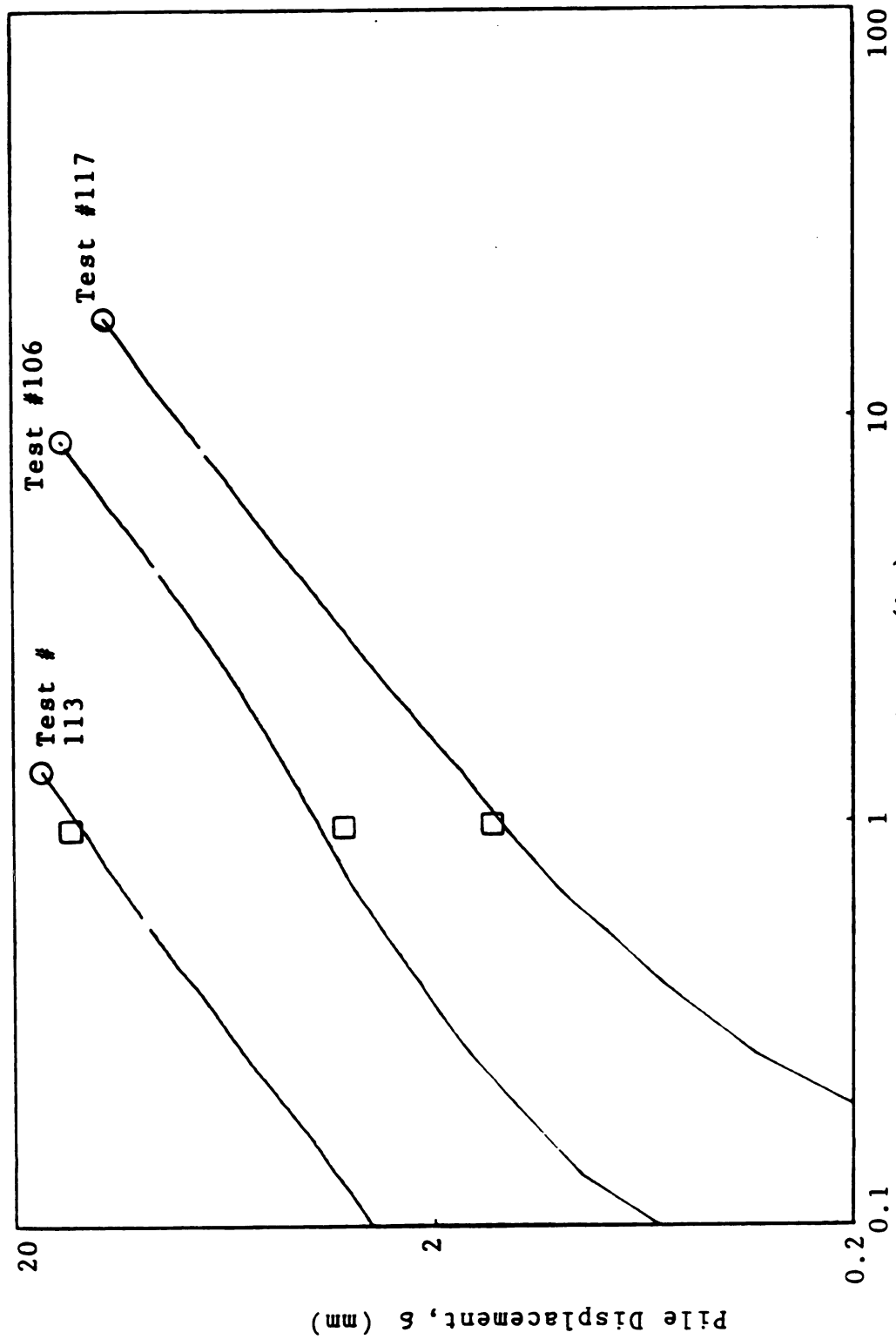

Figure A.6b. 1 mm C-type starting points and 25.4 mm displacement limits.

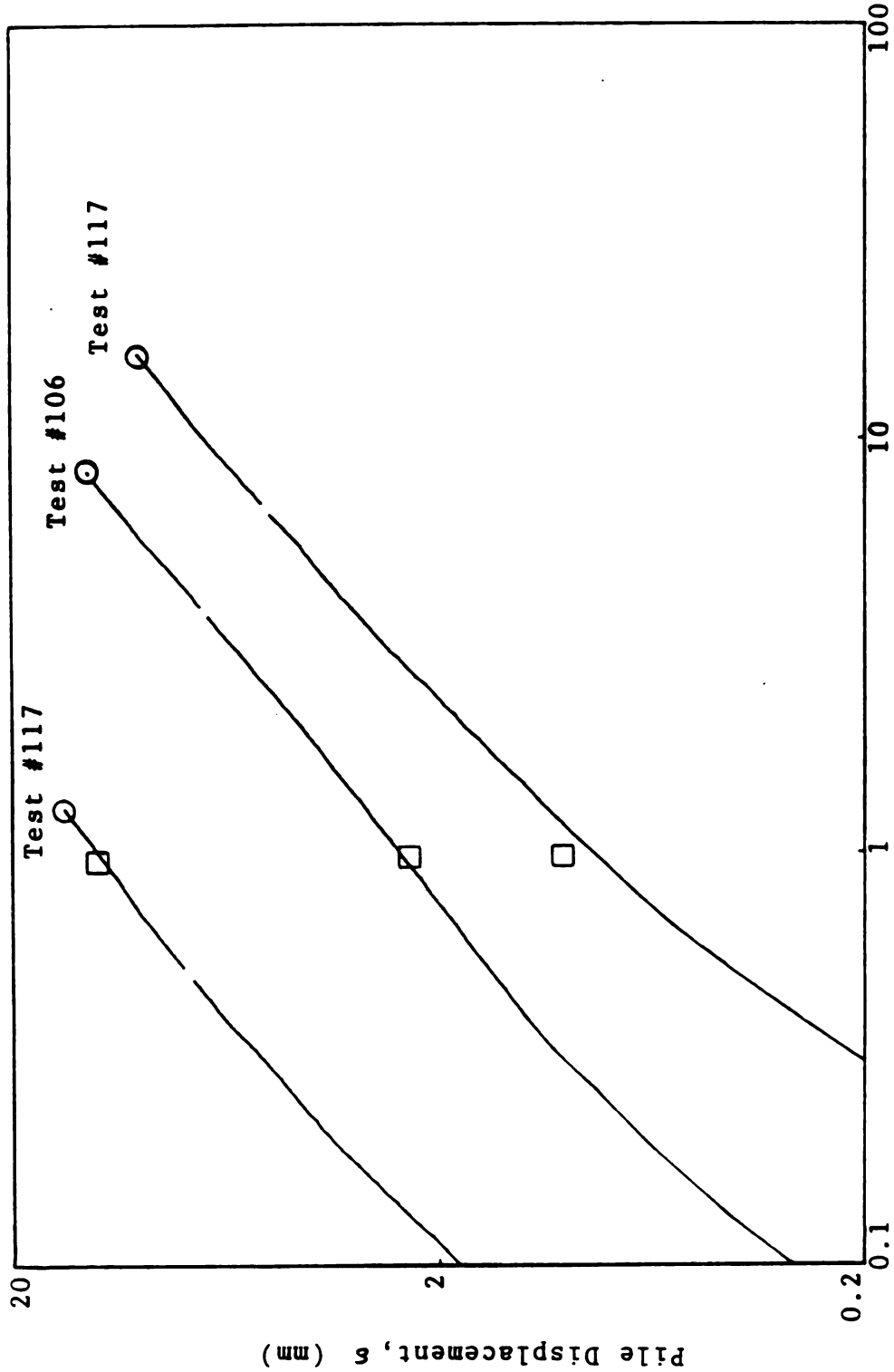

Figure A.6c. 3 mm C-type starting points and 25.4 mm displacement limits.

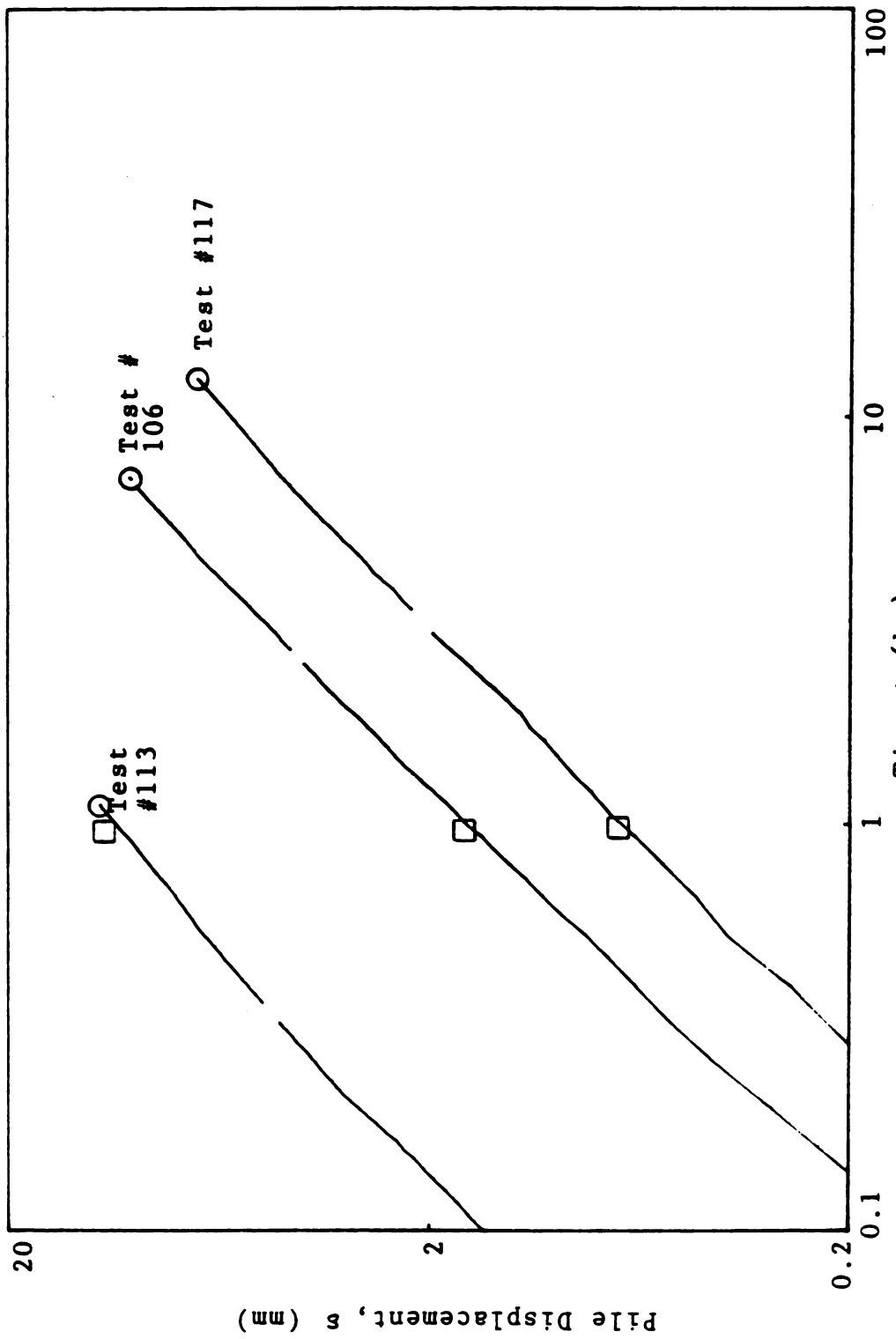

Figure A.6d. 6 mm C-type starting points and 25.4 mm displacement limits.

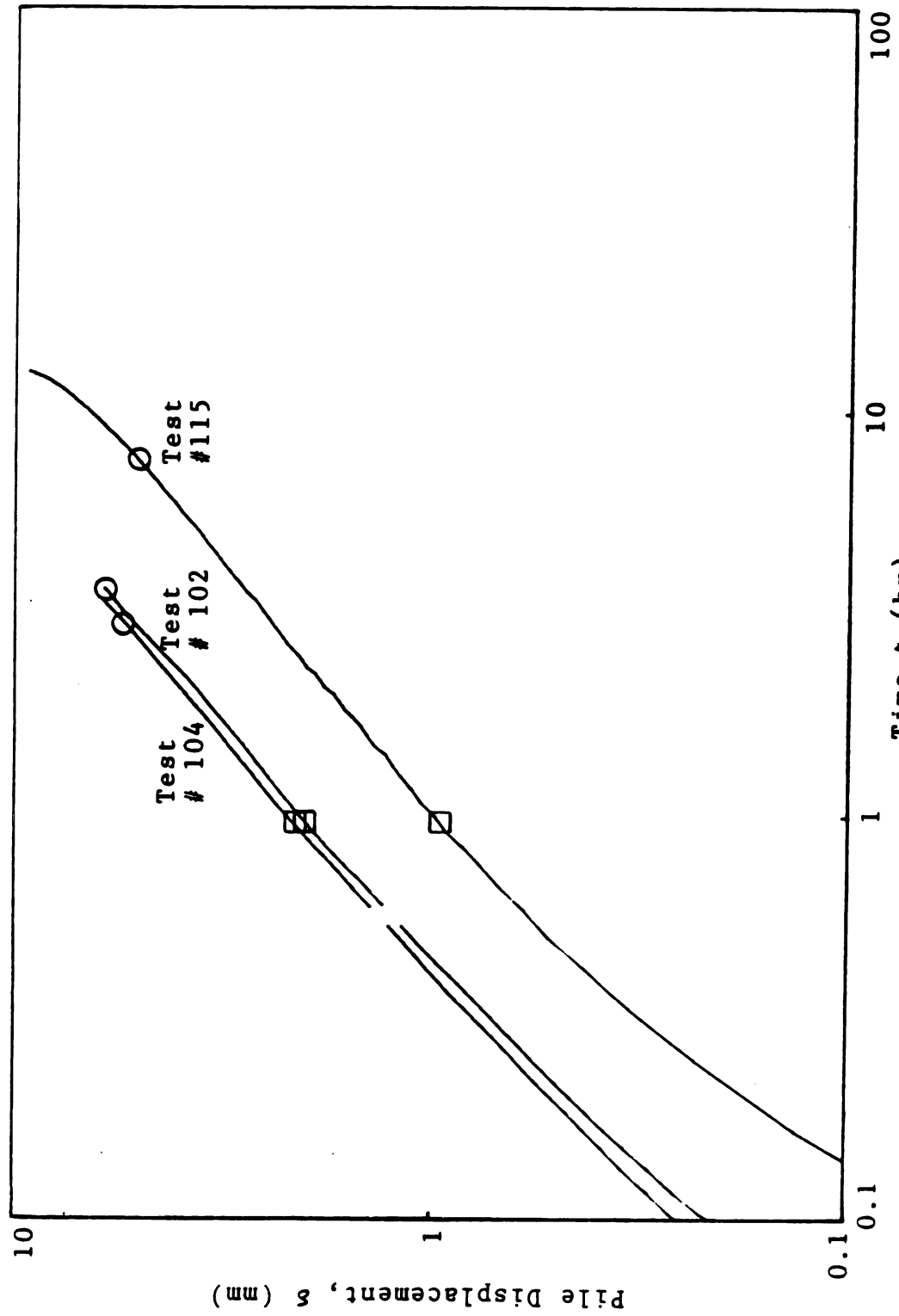

Figure A.6g. 3 mm C-type starting points and 17.8 mm displacement limits.

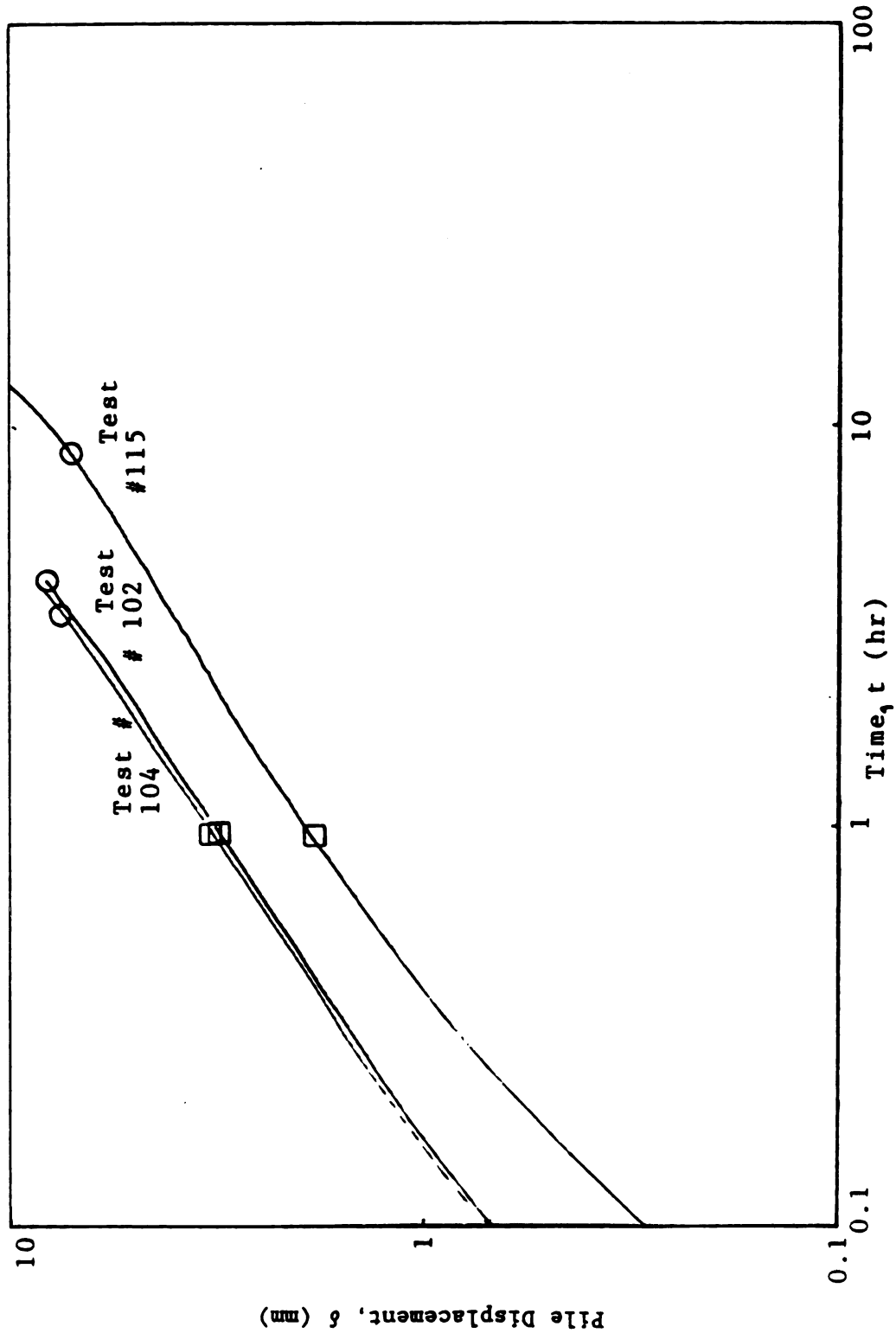

Figure A.6f. 1 mm C-type starting points and 17.8 mm displacement limits.

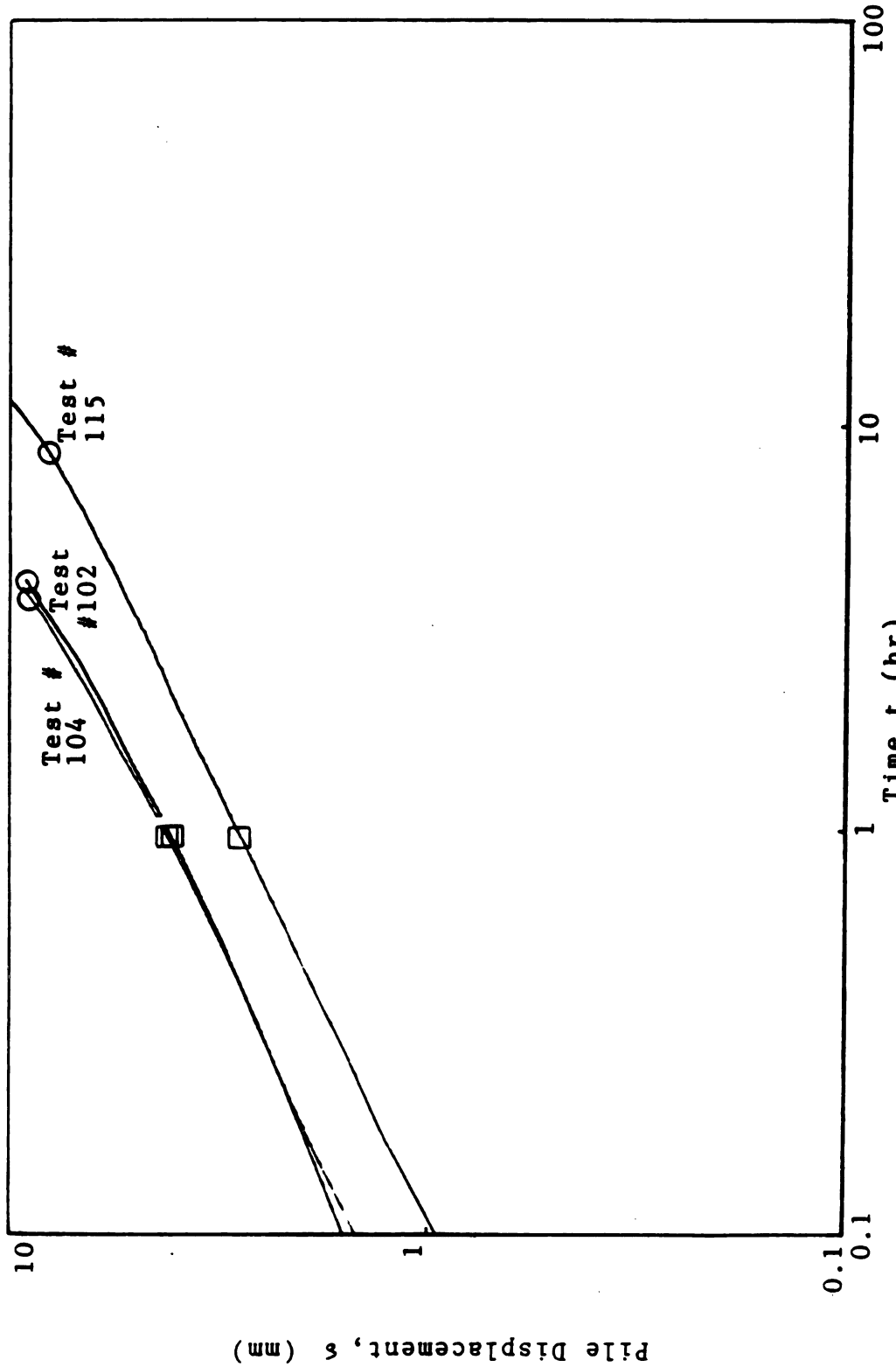

Figure A.6e. 0 mm C-type starting points and 17.8 mm displacement limits.

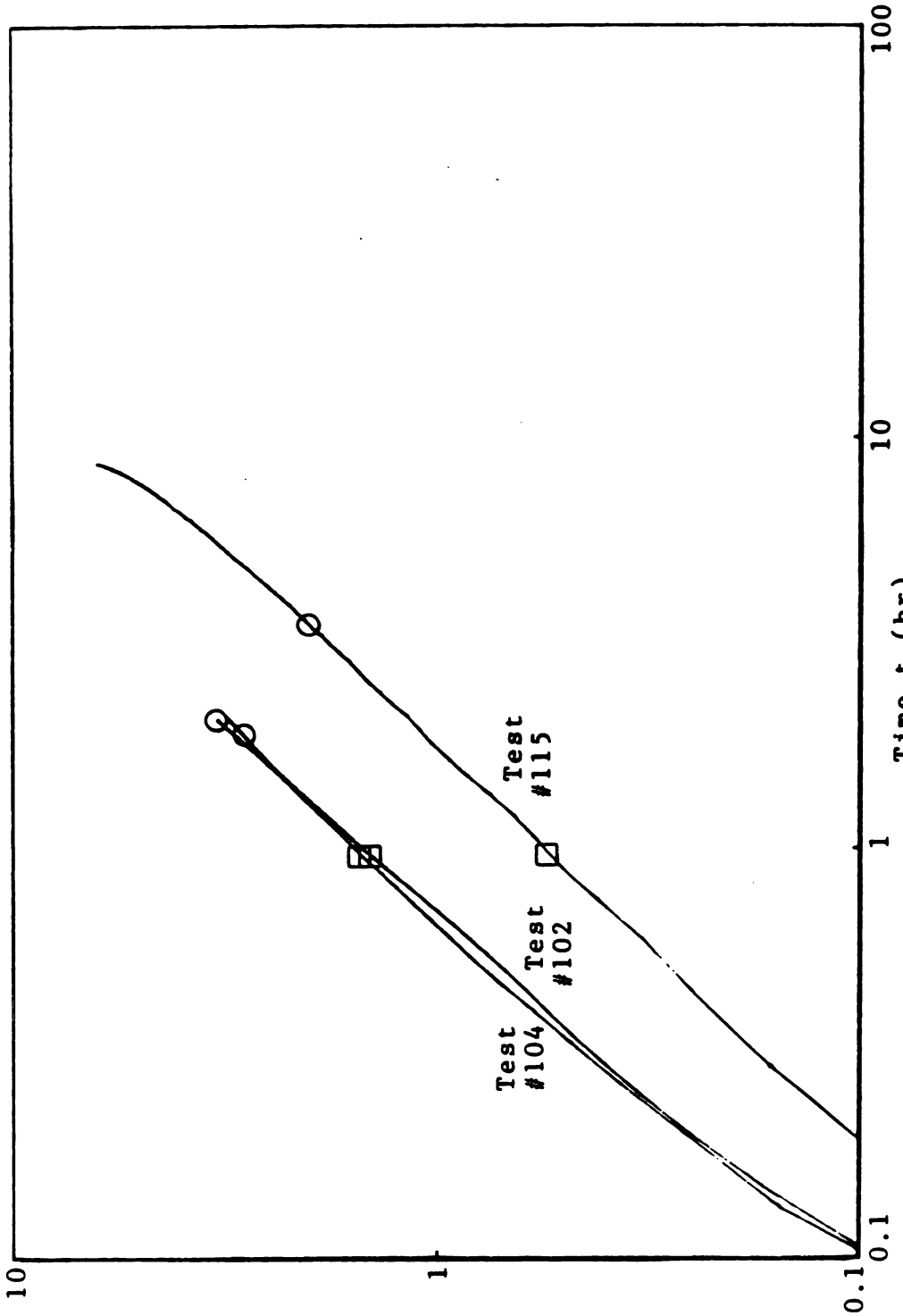

Figure A.6h. 6 mm C-type starting points and 17.8 mm displacement limits.

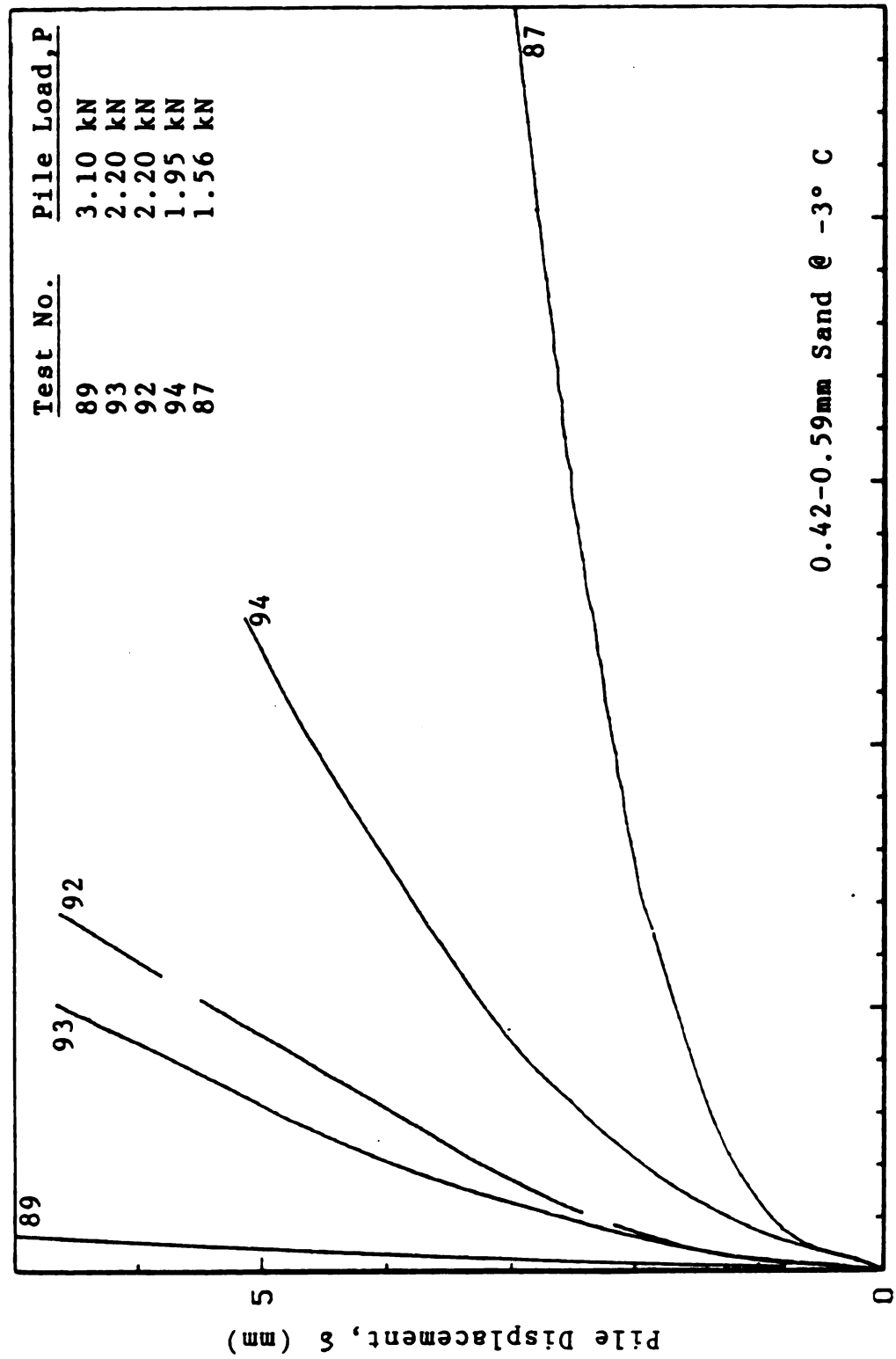

Figure A.7. Time-displacement curves for model steel piles in frozen sand at -3 deg C with 1.59 mm lug heights and 76 mm (average) displacement limits.

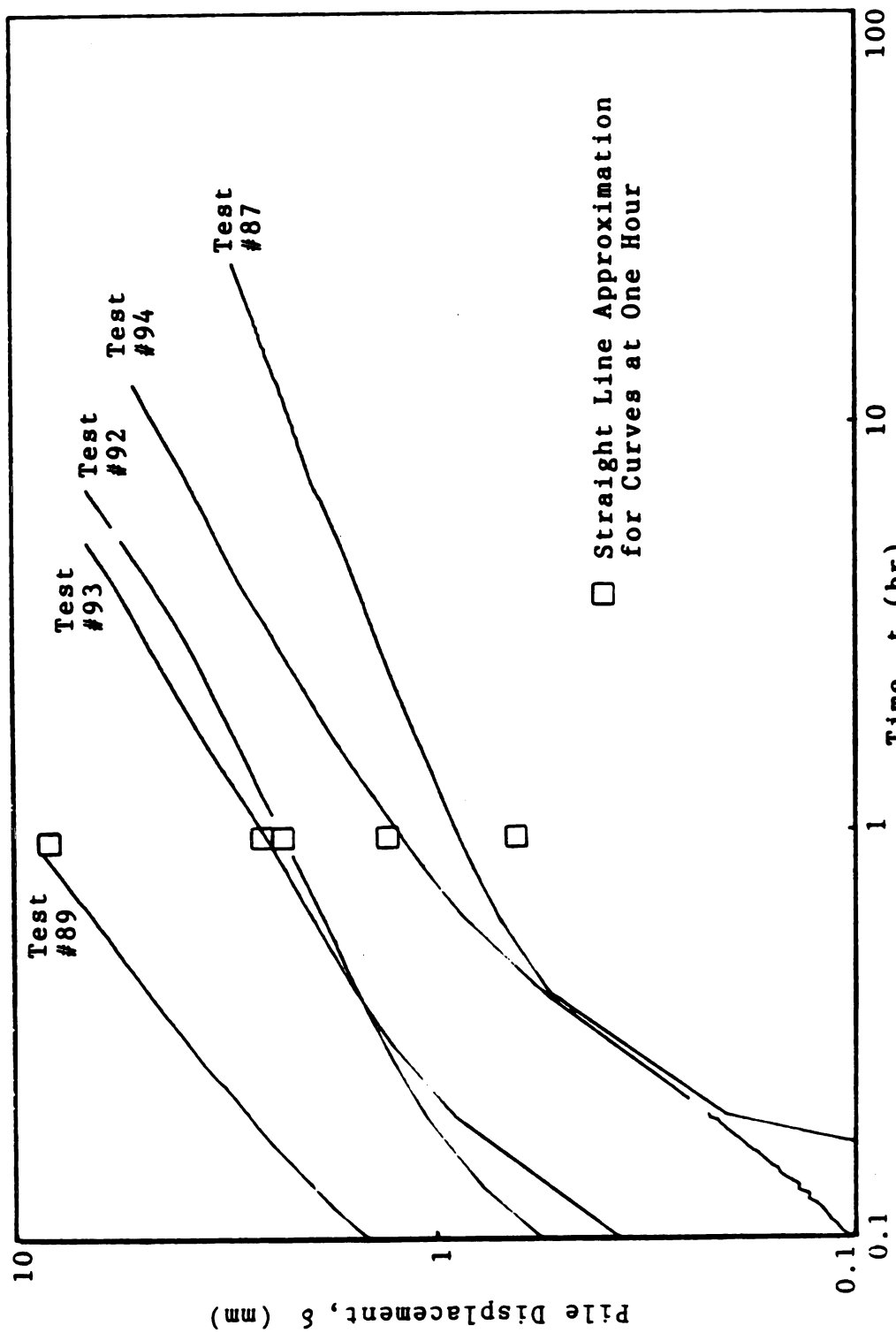

Figure A.8. Time-displacement curves for model piles in frozen sand at -3 deg C with 1.59 mm lug heights, 76 mm displacement limits. (a) 0 mm C-type plot starting points.

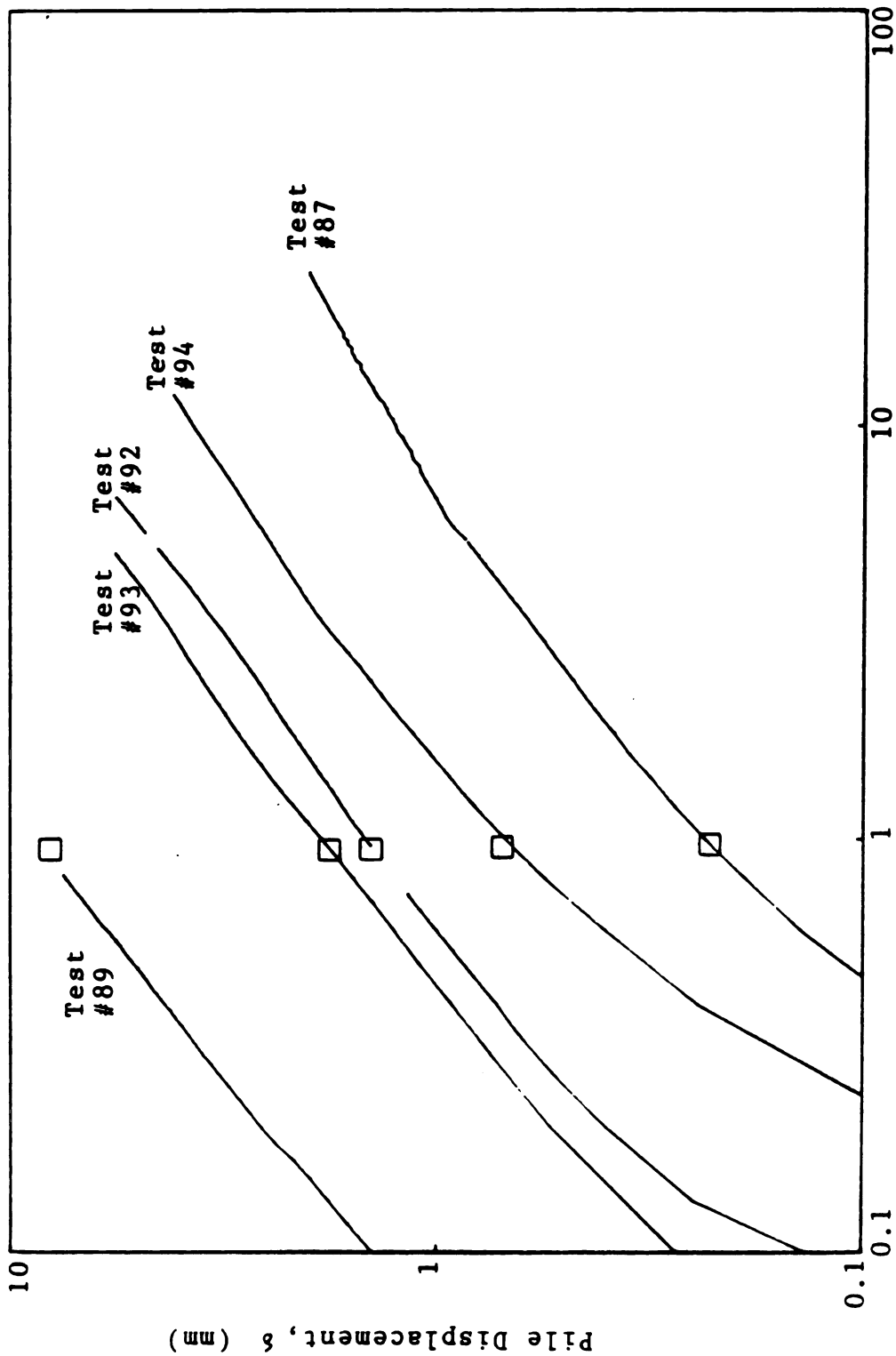

Figure A.8b. 1 mm C-type plot starting points.

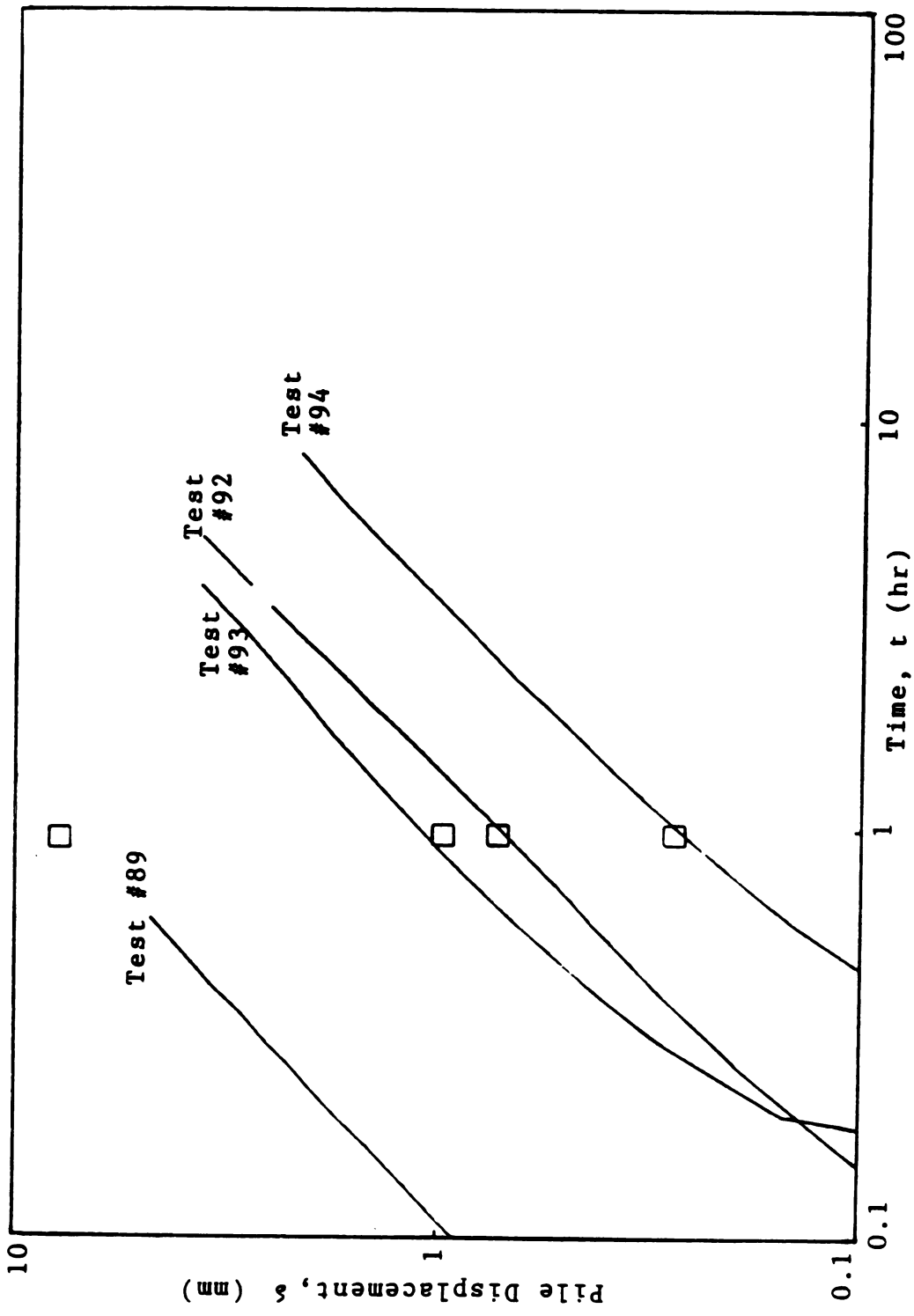

Figure A.8c. 3 mm C-Type plot starting points.

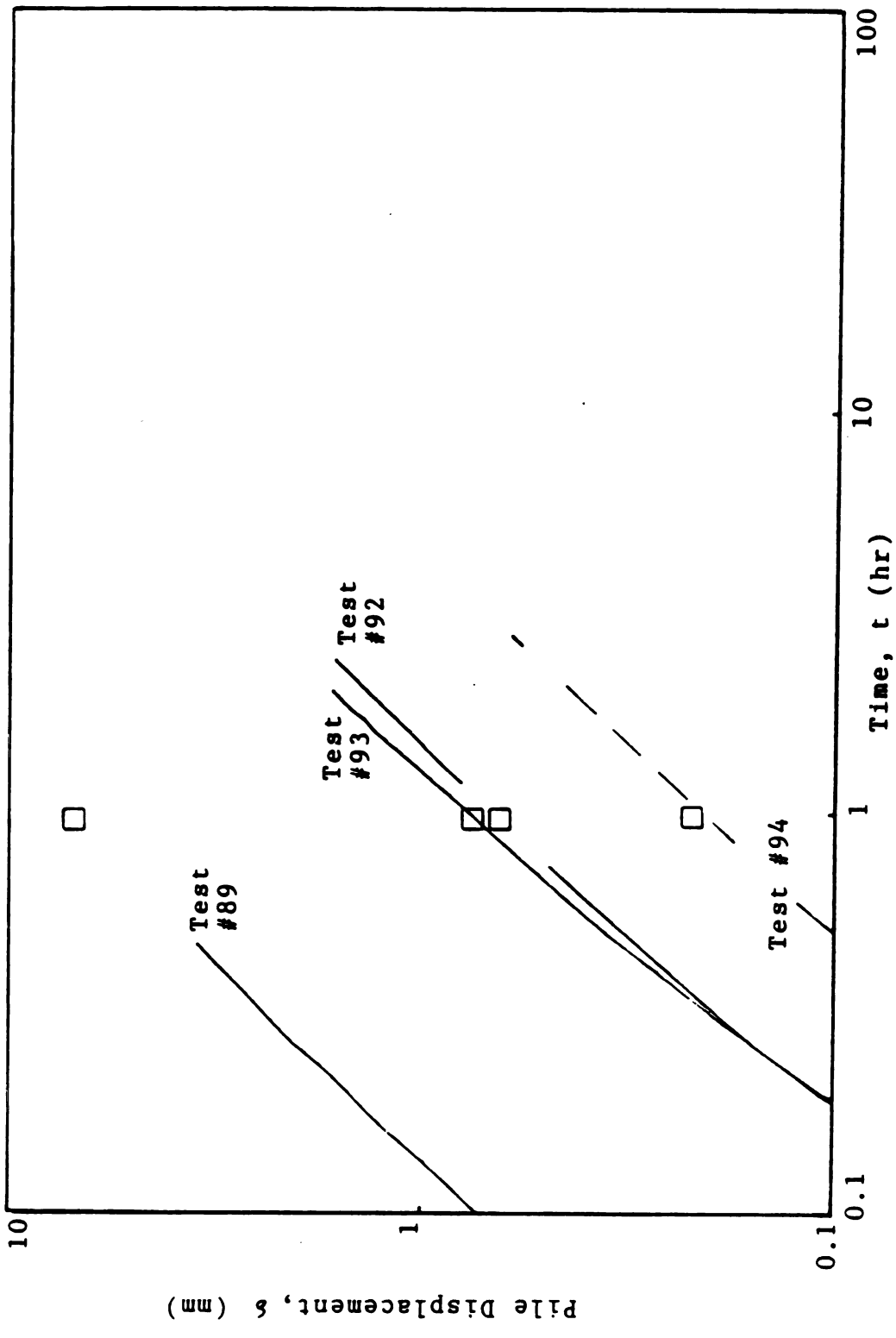

Figure A.8d. 5 mm C-Type plot starting points.

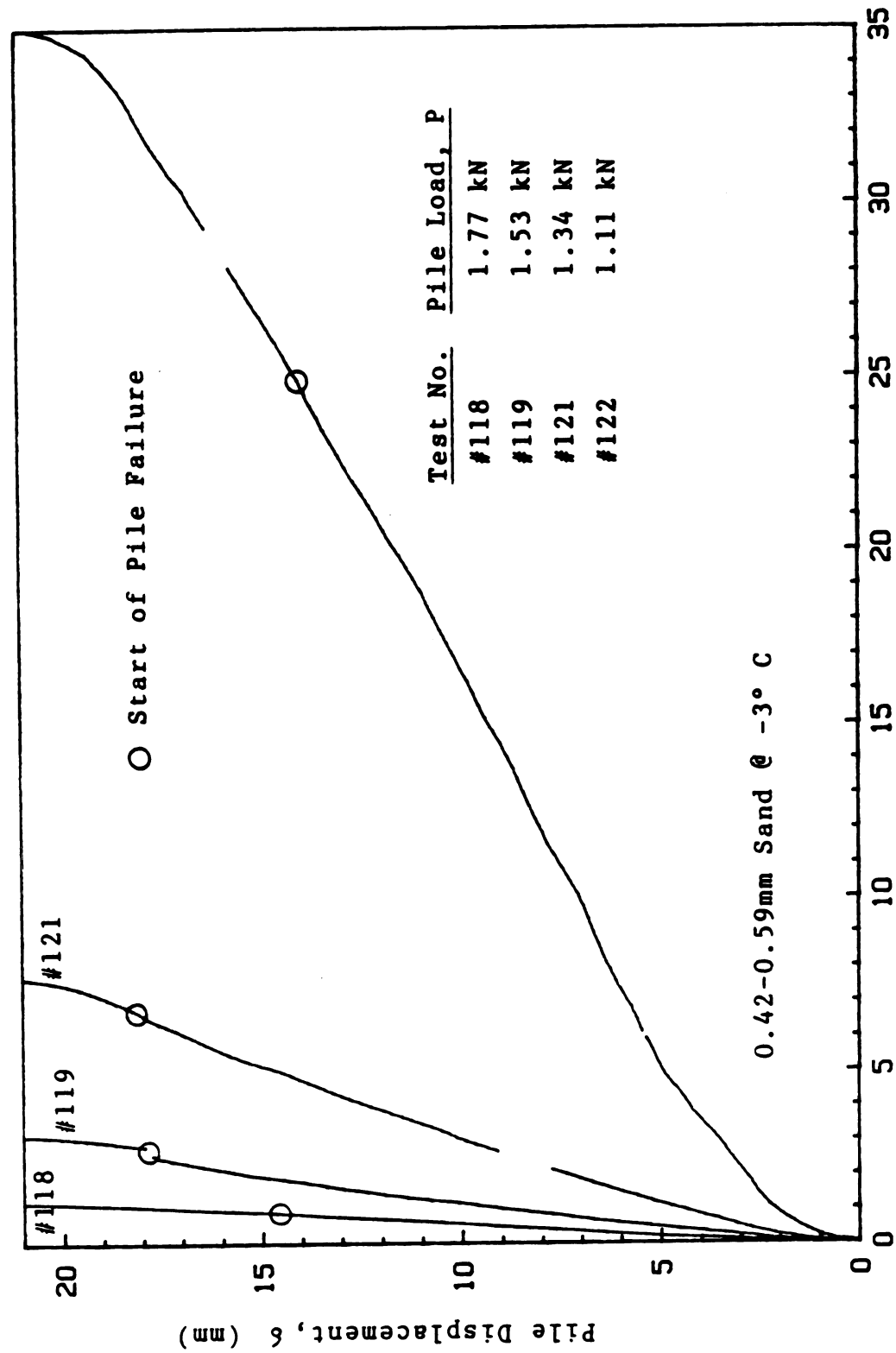

Figure A.9. Time-displacement curves for model steel piles in frozen sand at -3 deg C with 0.79 mm lug heights and 24.1 mm (average) displacement limits.

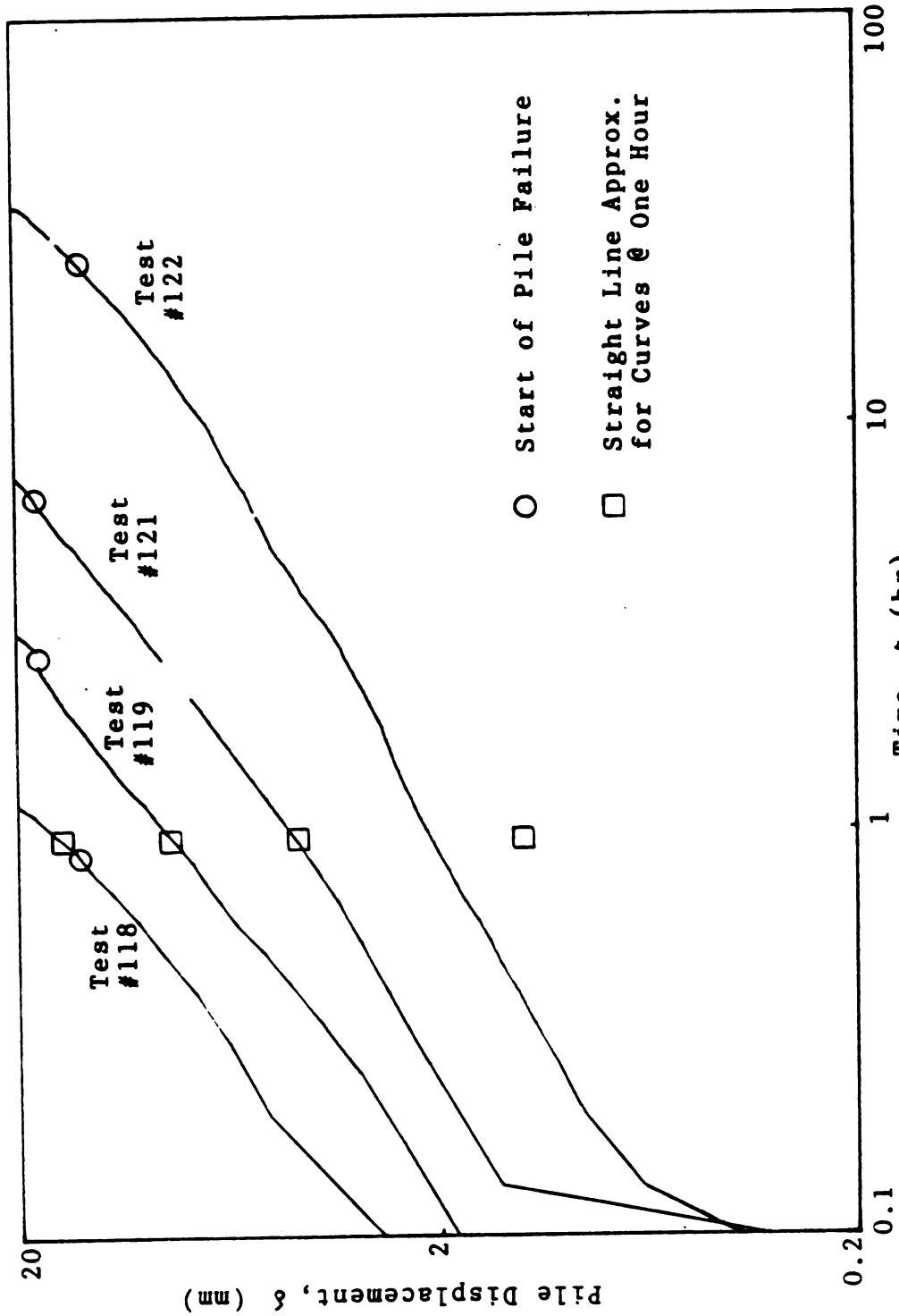

Figure A.10. Time-displacement curves for model piles in frozen sand at -3 deg C with 0.79 mm lug heights, 24.1 mm displacement limits. (a) 0 mm C-type plot starting points.

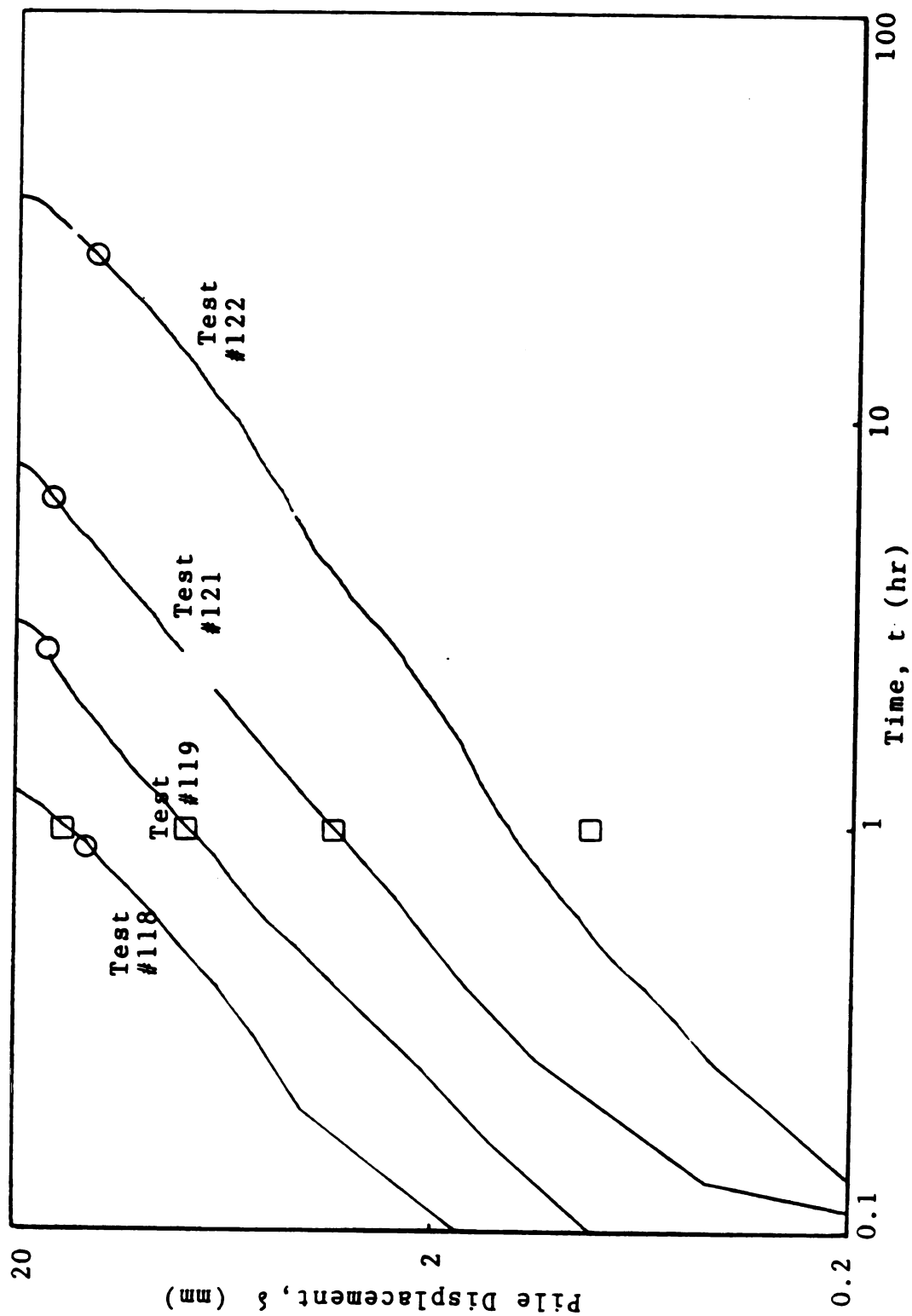

Figure A.10b. 1 mm C-type plot starting points.

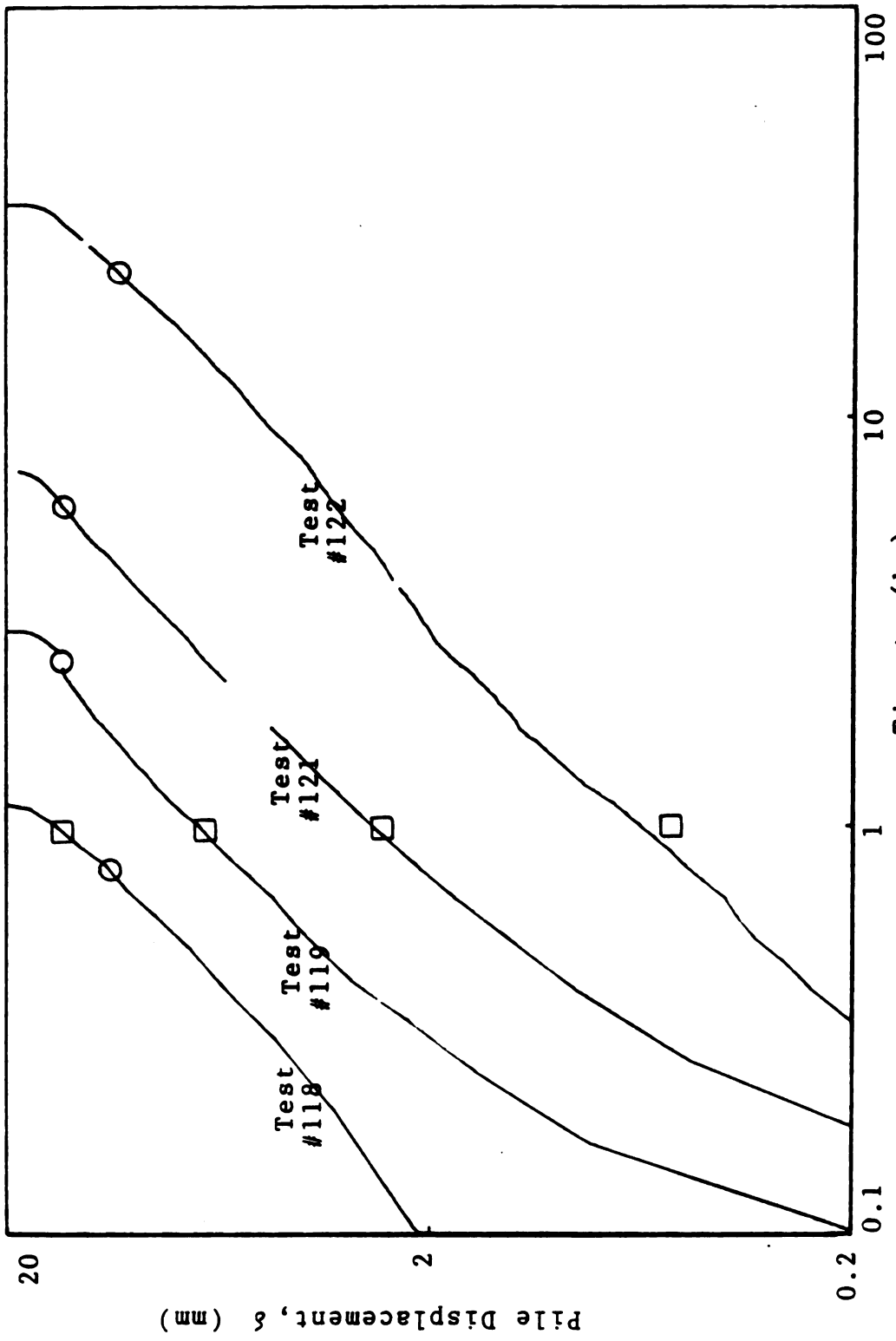

Figure A.10c. 3 mm C-Type plot starting points.

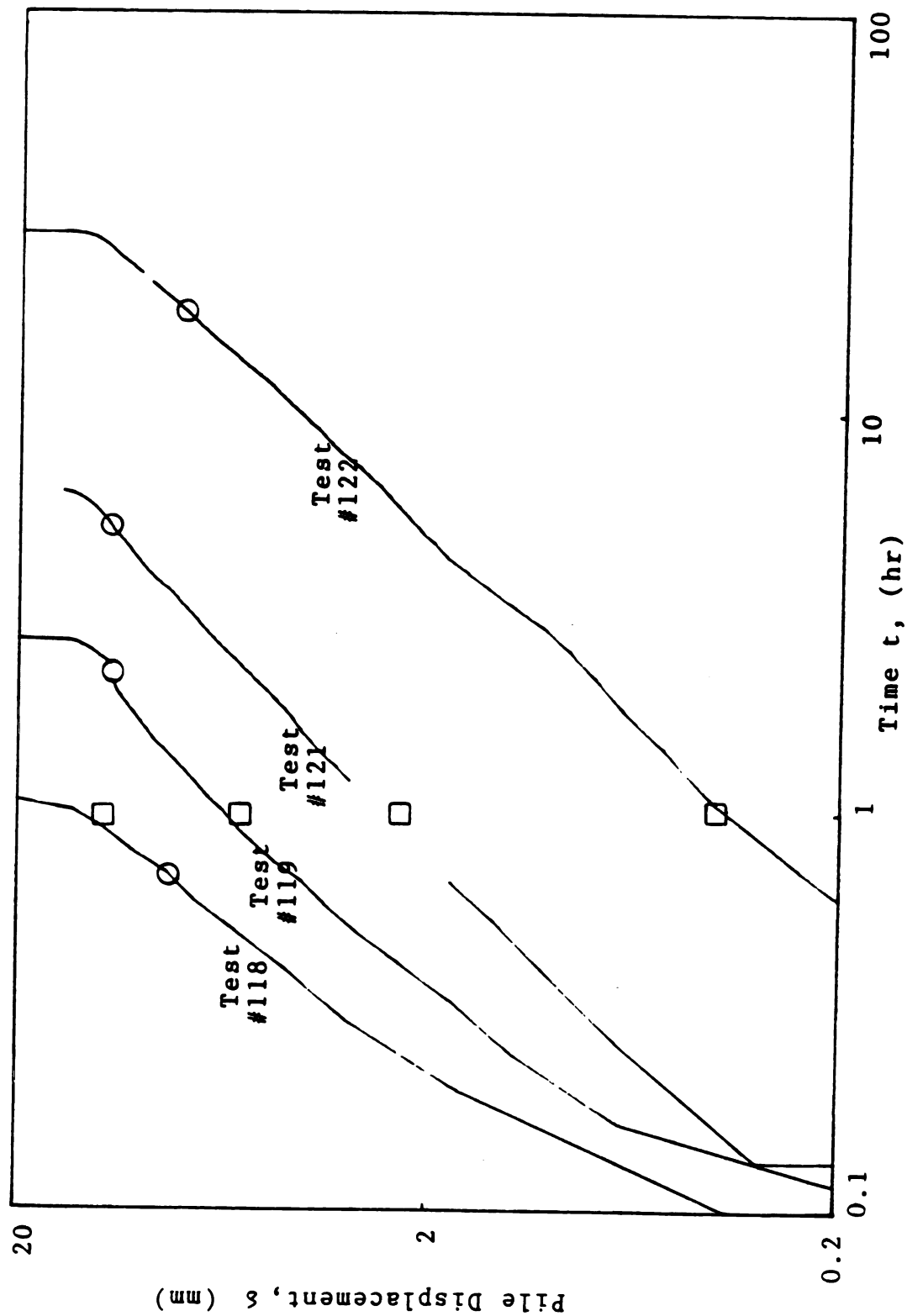

Figure A.10d. 6 mm C-Type plot starting points.

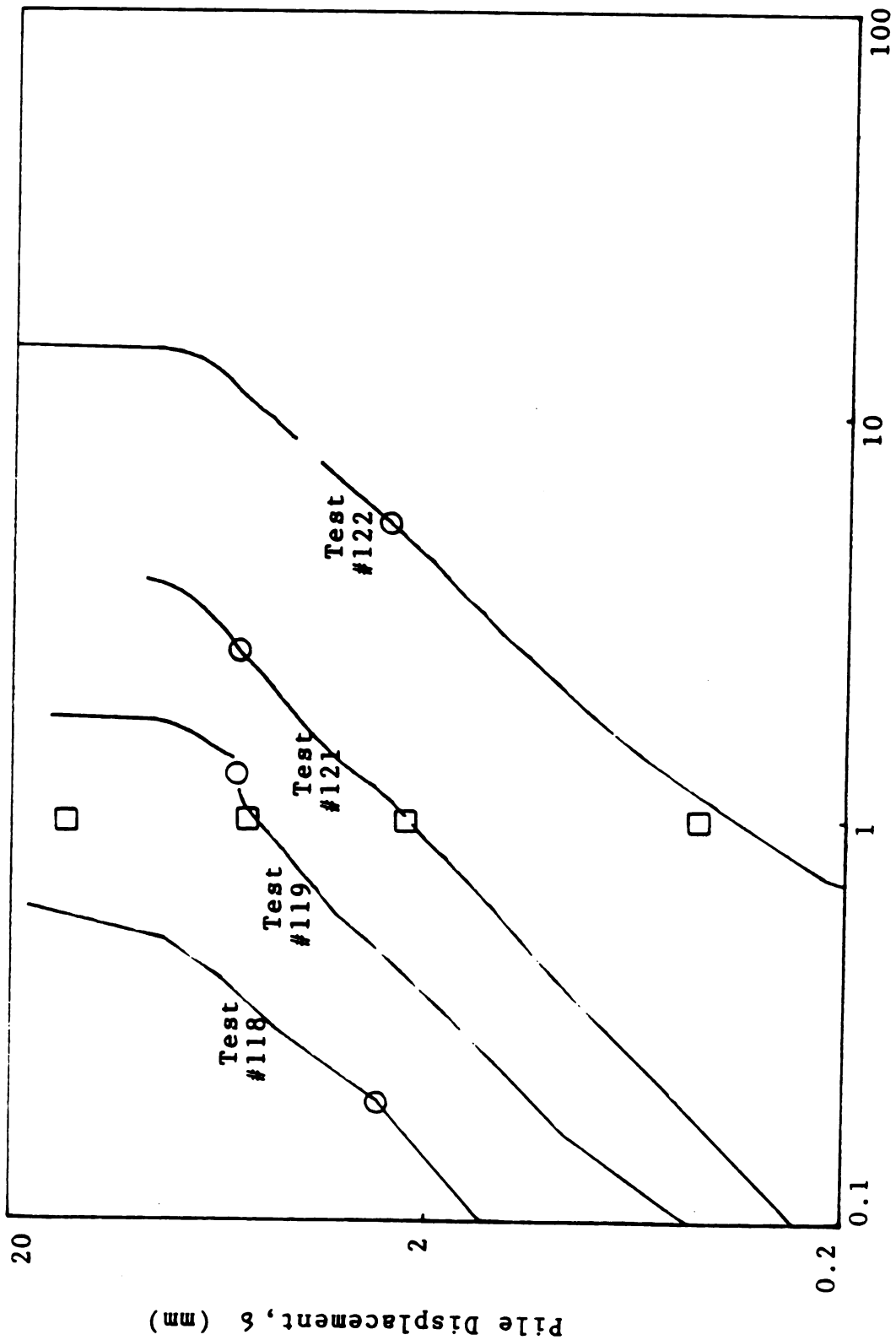

Figure A.10e. 12 mm C-Type plot starting points.

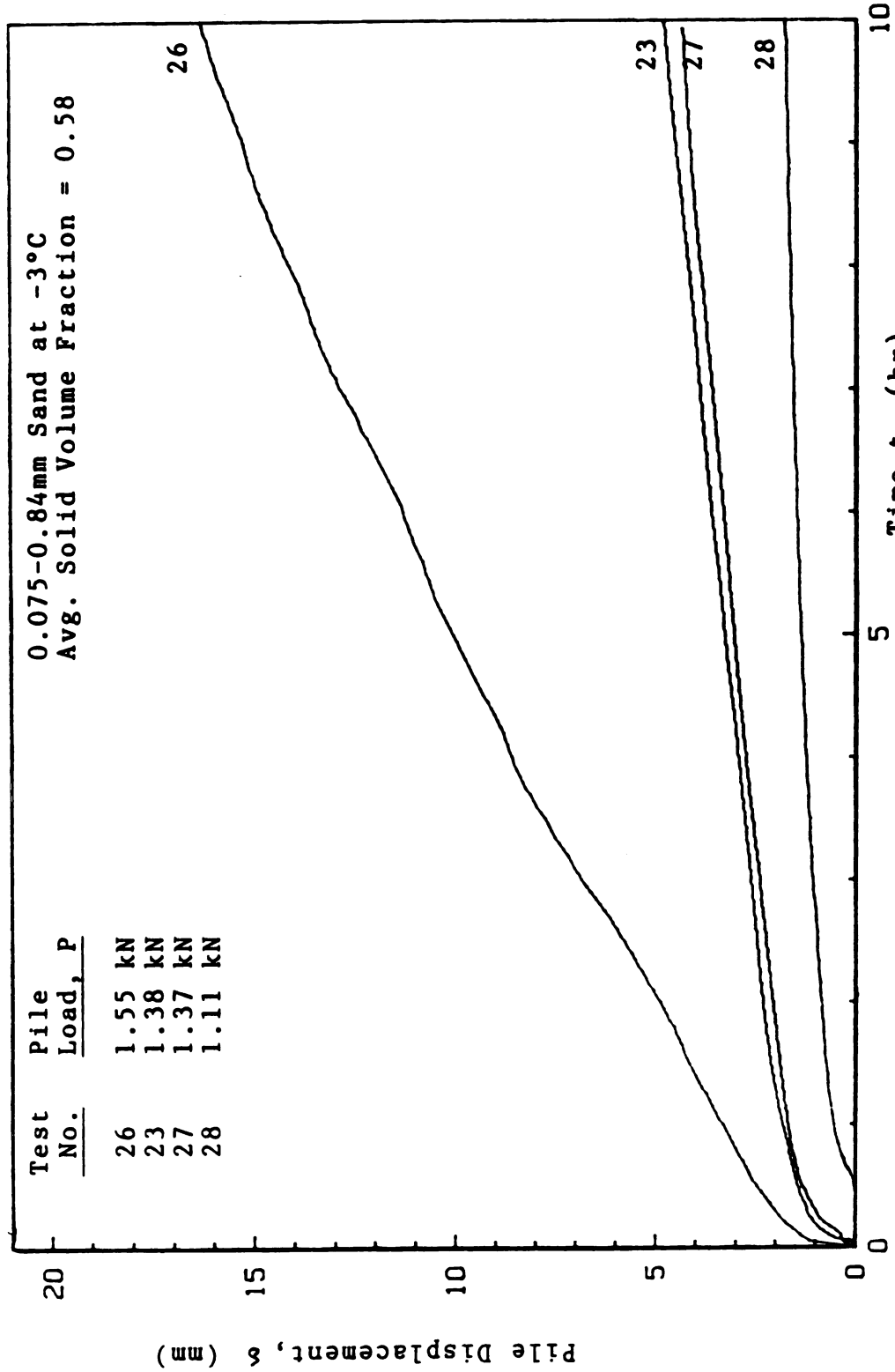

Figure A.11. Time-displacement curves for model piles in frozen sand (0.74 to 0.84 mm grain size) at -3 deg C with 0.79 mm lug heights and 76 mm (avg.) displacement limits.

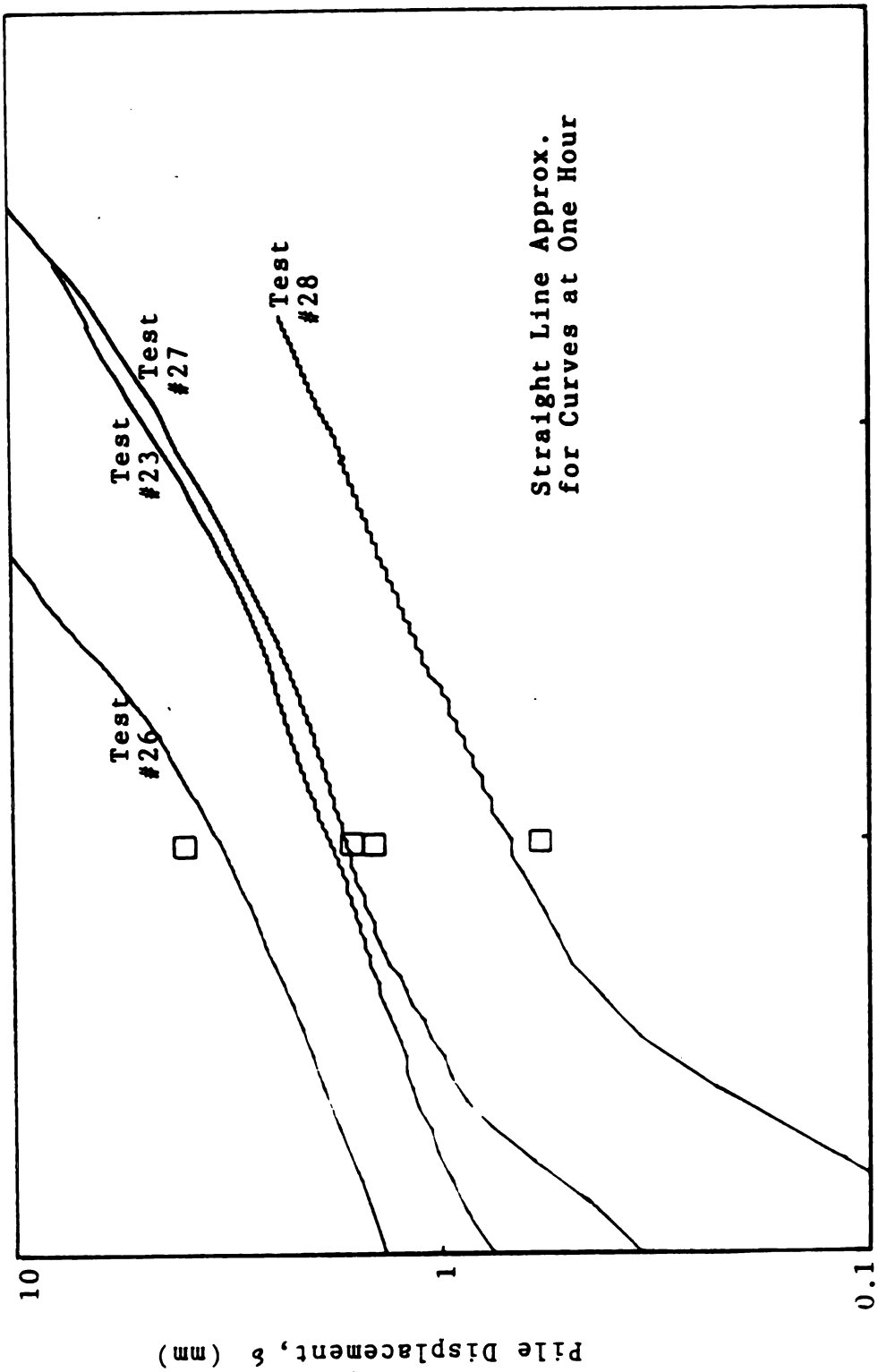

Figure A.12. Time-displacement curves for model piles in frozen sand at -3 deg C with 0.79 mm lug heights, 76 mm displacement limits. (a) 0 mm C-type plot starting points.

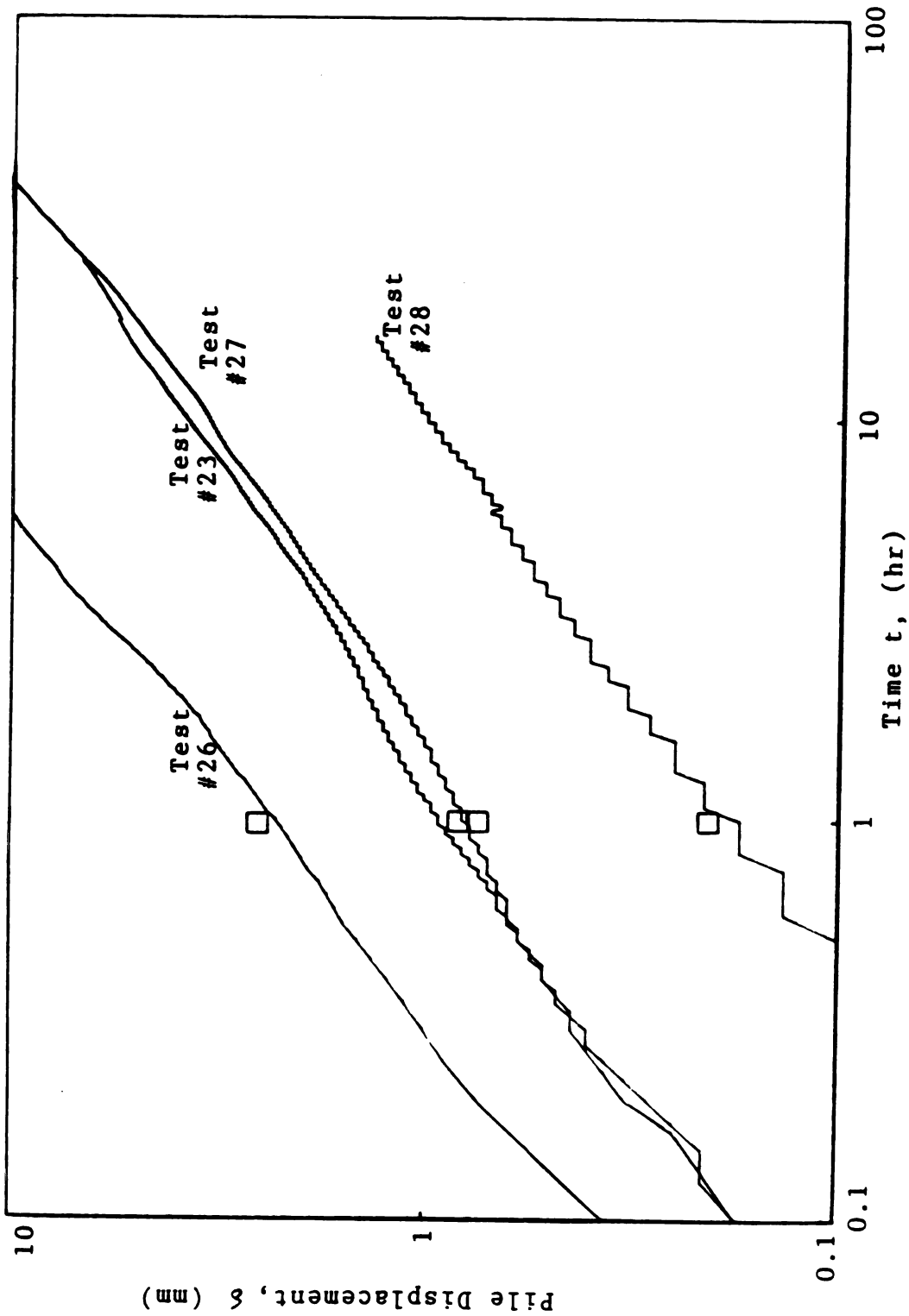

Figure A.12b. 1 mm C-type plot starting points.

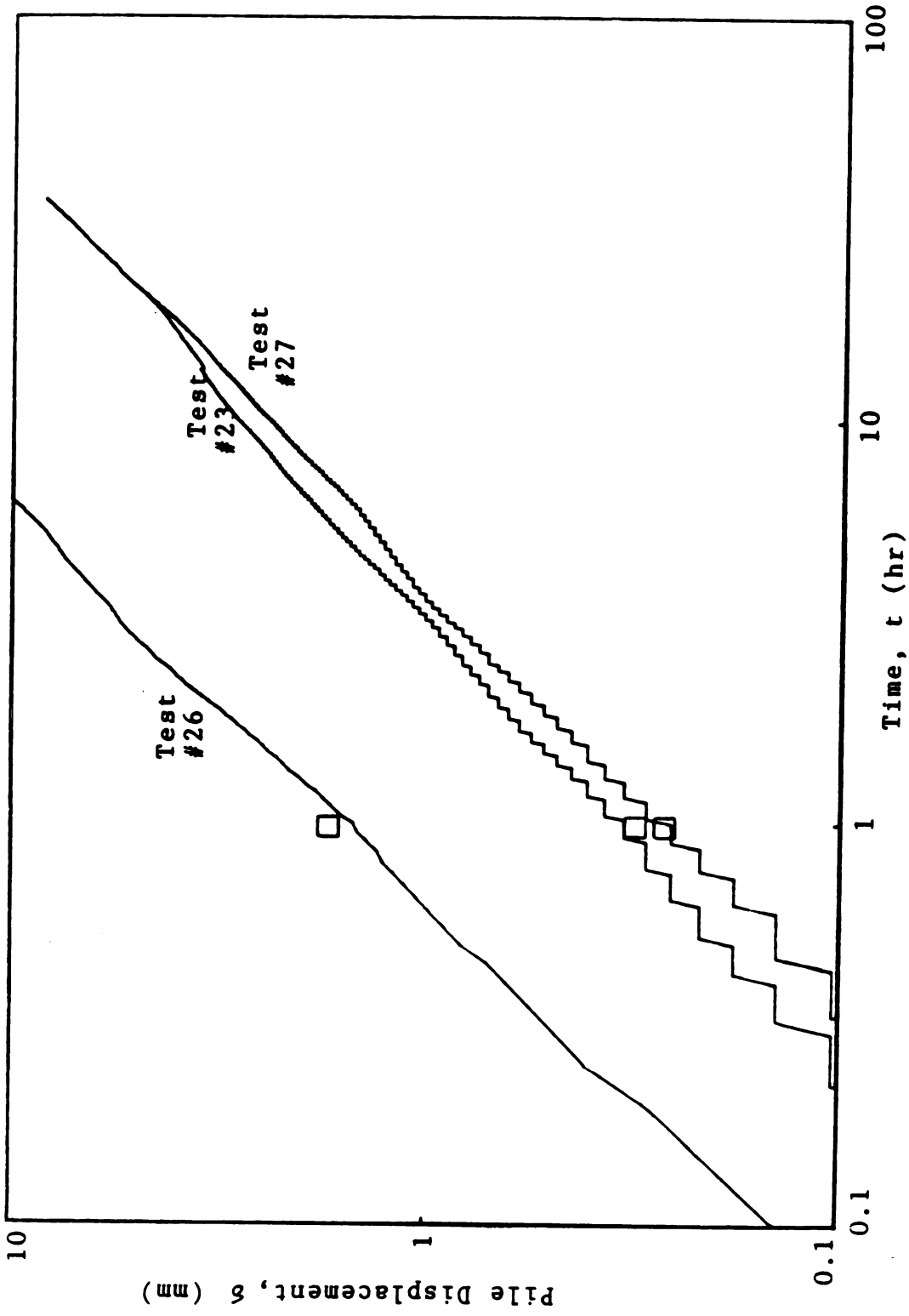

Figure A.12c. 3 mm C-Type plot starting points.

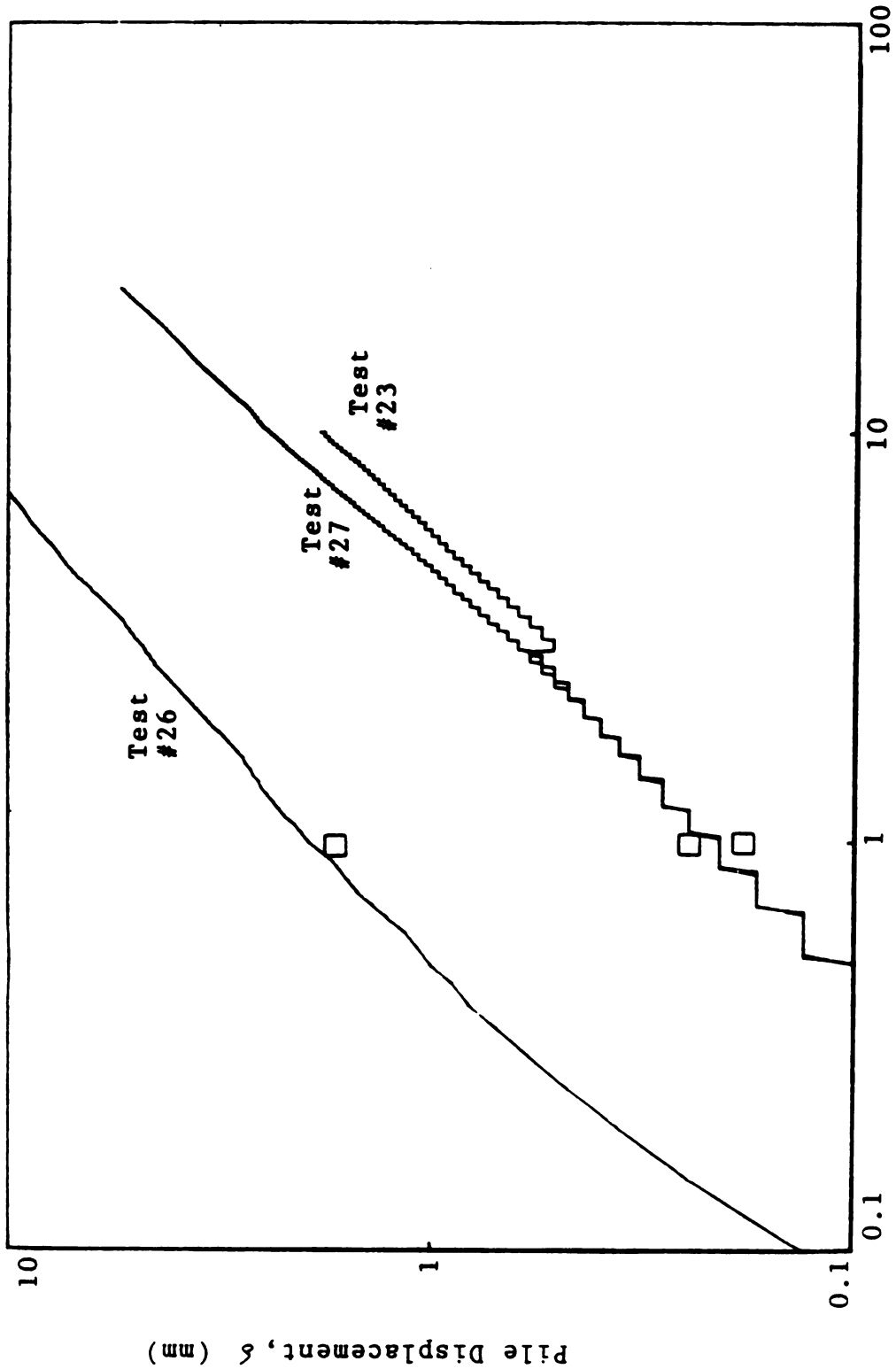

Figure A.12d. 6 mm C-Type plot starting points.

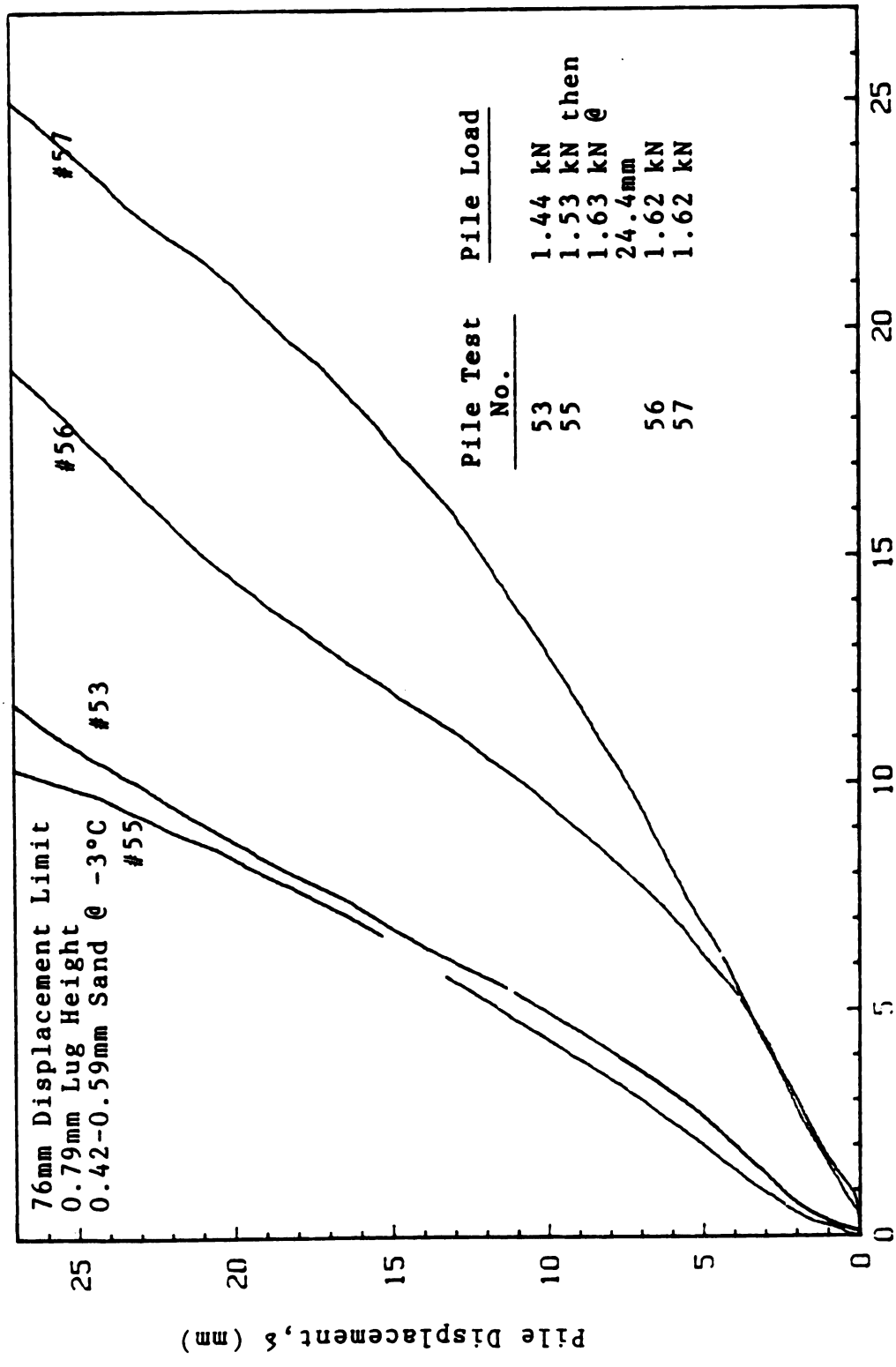

Figure A.13. Time-displacement curves for model steel piles in frozen sand at -3 deg C with 0.79 mm lug heights and 76 mm (average) displacement limits.

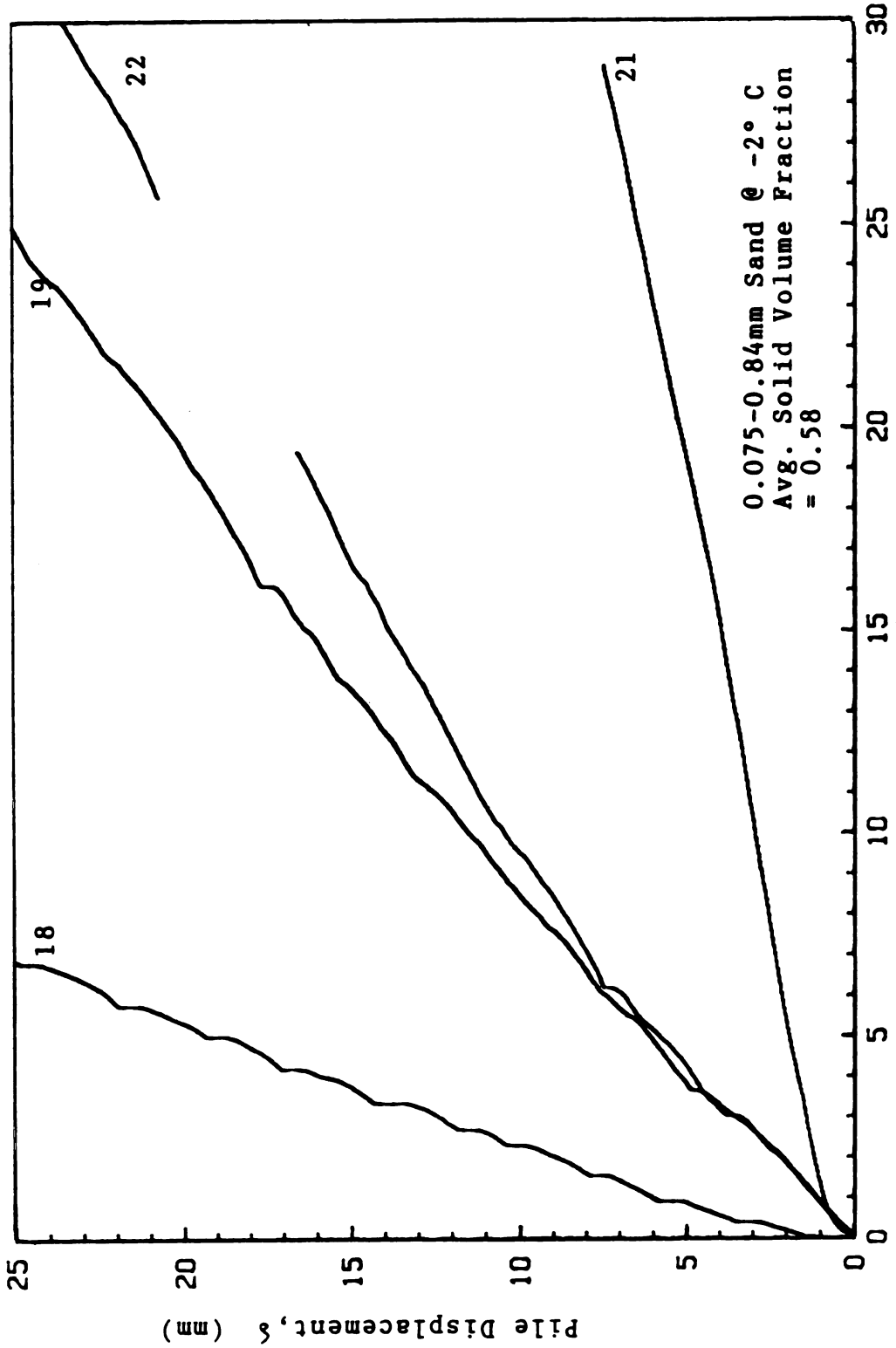

Figure A.14. Time-displacement curves for model steel piles in frozen sand (0.74 to 0.84 mm) at -2 deg C with 0.79 mm lug heights and 76 mm (average) displacement limits.

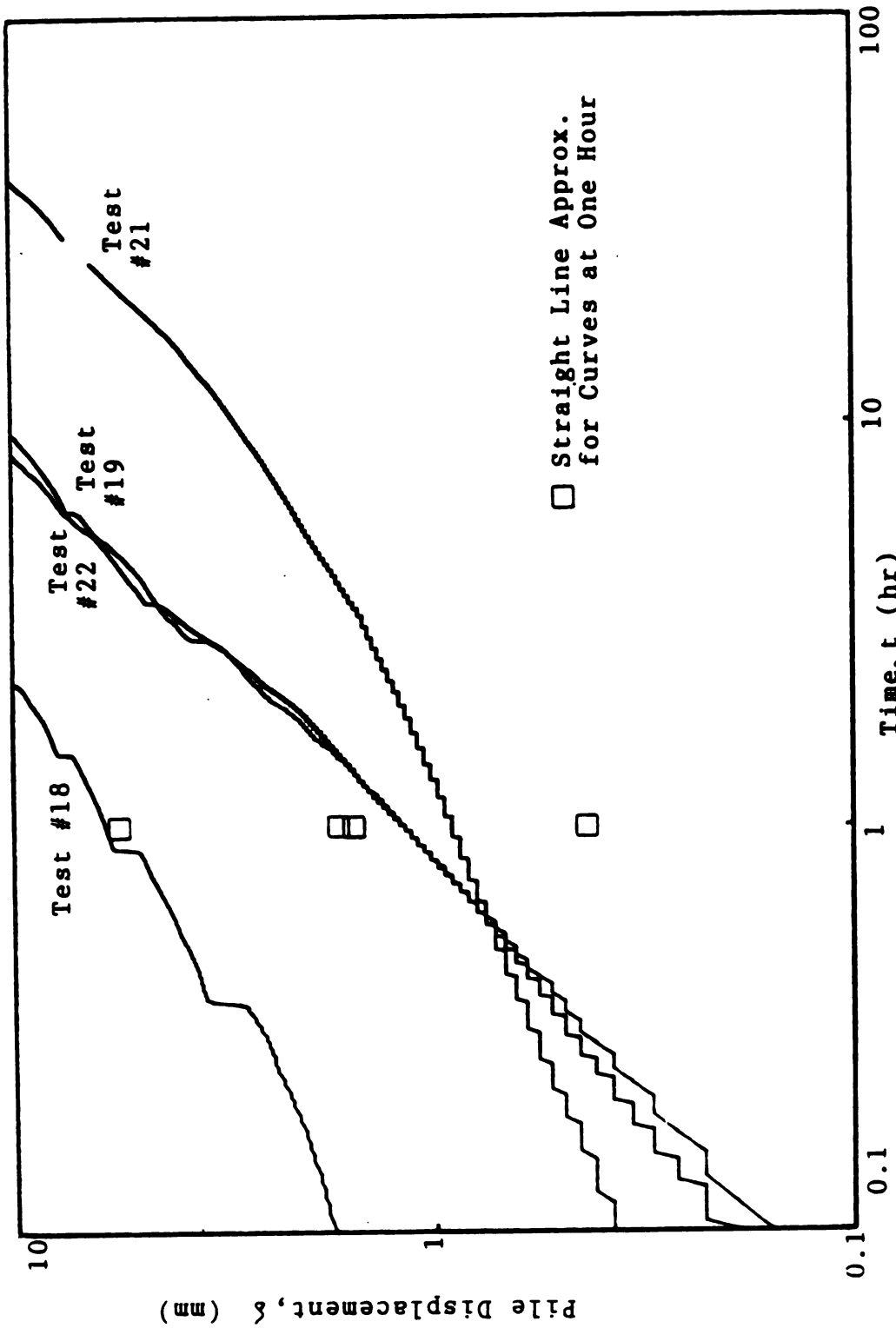

Figure A.15. Time-displacement curves for model piles in frozen sand at -2 deg C with 0.79 mm lug heights, 76 mm displacement limits. (a) 0 mm C-type plot starting points.

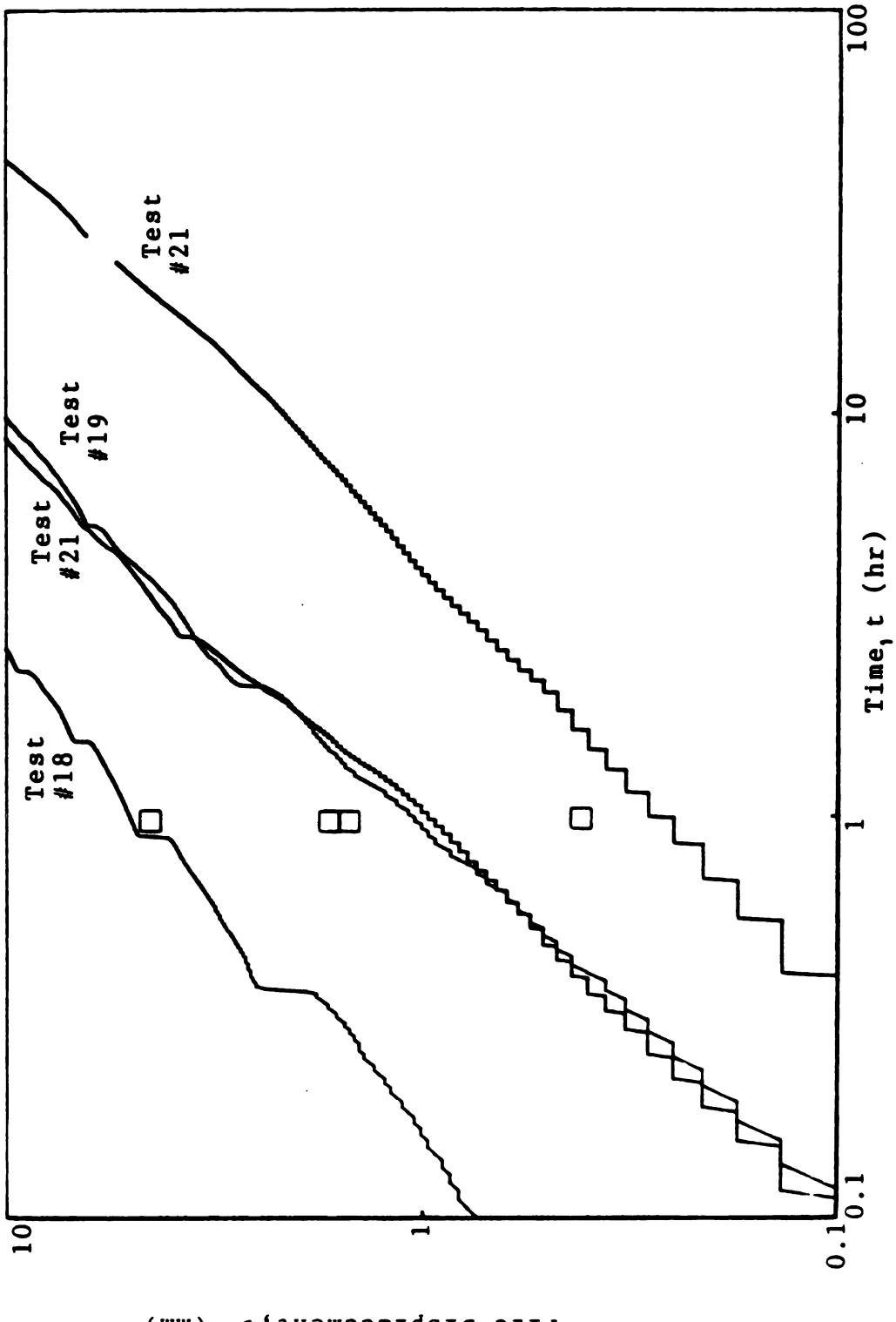

Figure A.15b. 1 mm C-type plot starting points.

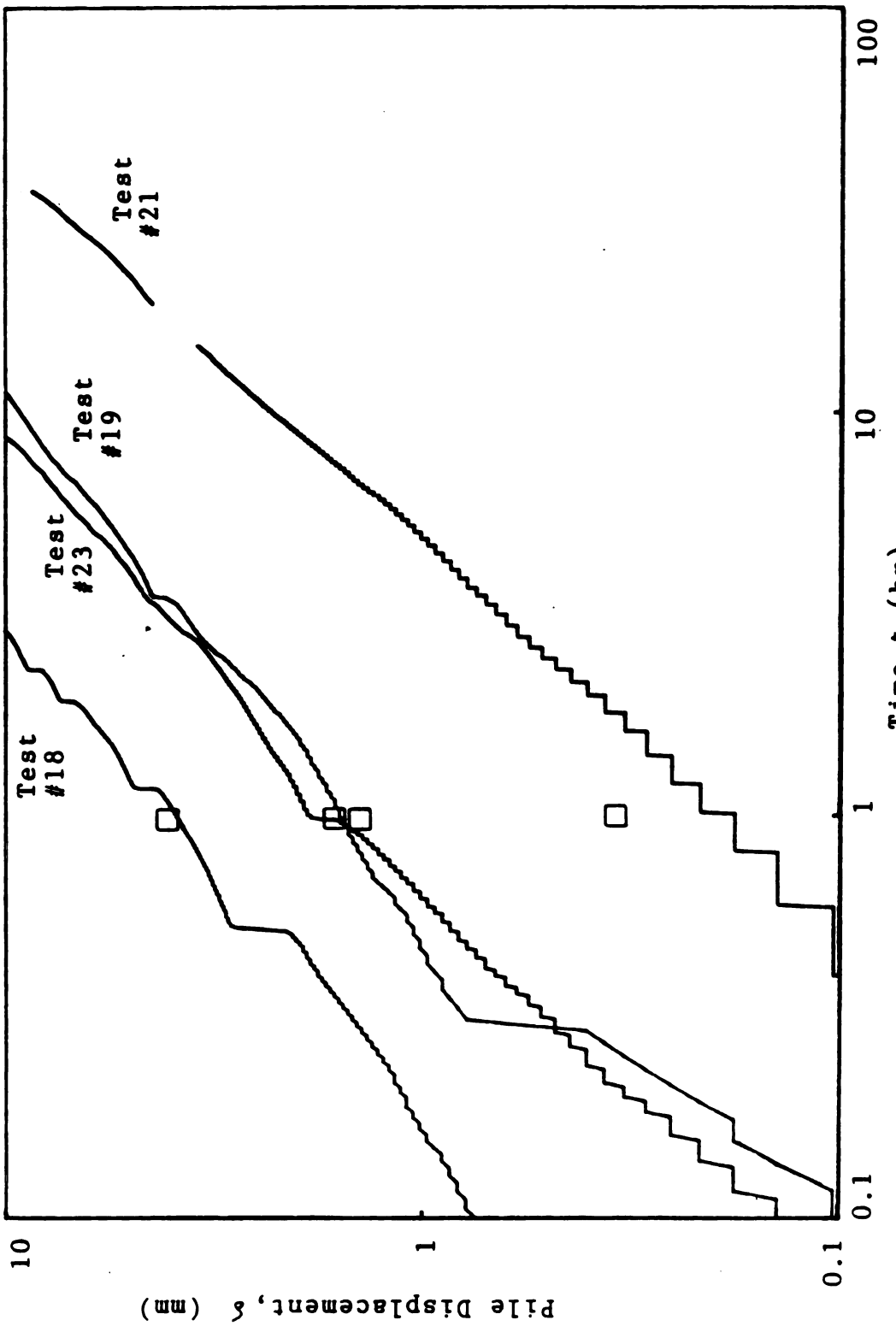

Figure A.15c. 3 mm C-Type plot starting points.

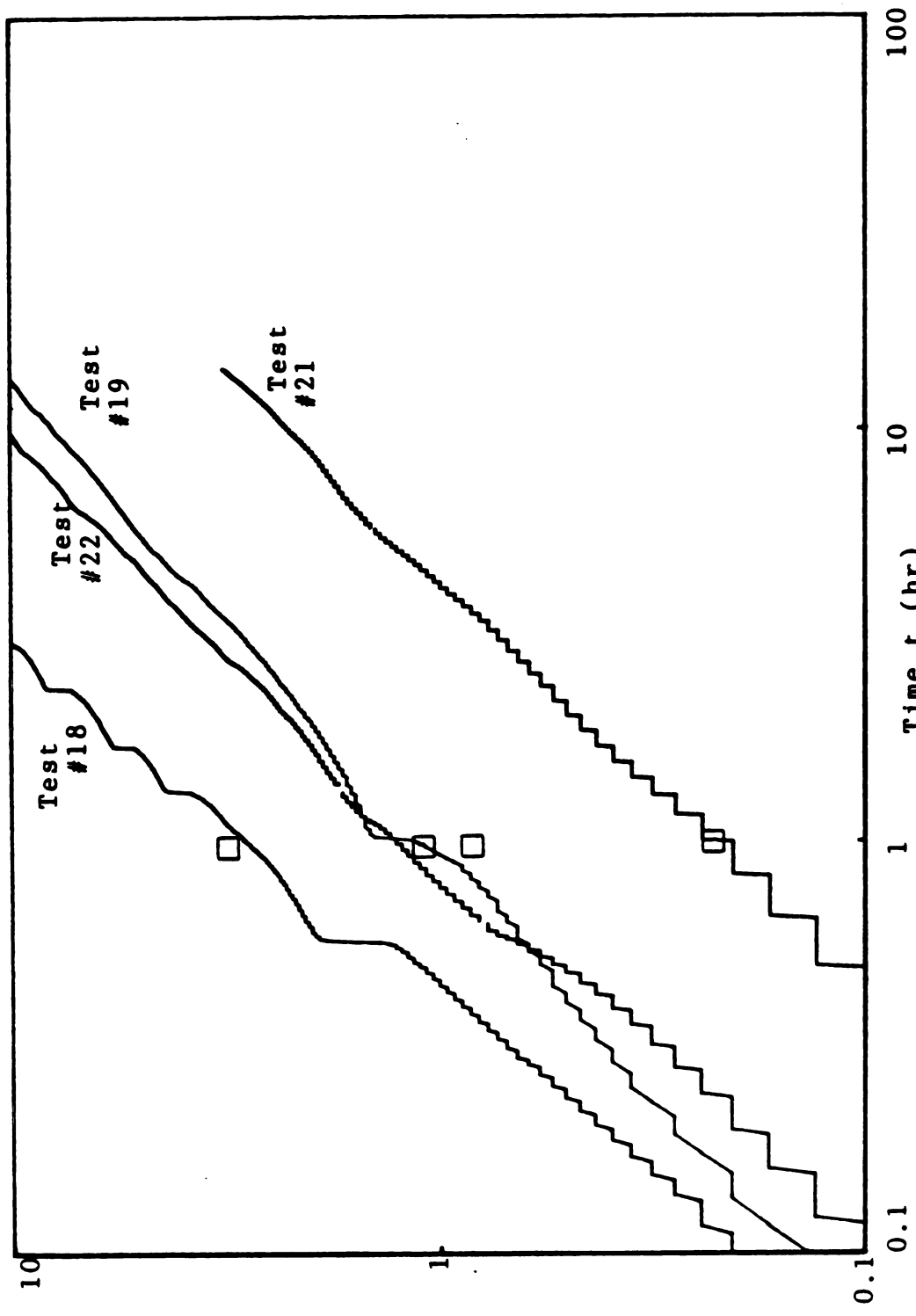

Figure A.15d. 6 mm C-Type plot starting points.

APPENDIX B

PILE TEST DATA

Table B.1. Tabulated Pile Test Data.

s-g: 0.074 to 0.84 mm grain size sand
s-u: 0.42 to 0.59 mm grain size sand
i : polycrystalline ice

Test No.	Figure No.	Test Temperature	Sand Type	Solid Volume Fraction	Ice Density	Embedment Ahead/Behind Lug	Lug Size	Thread Size /Pile Embedment
		deg C	*	%	g/cc	mm/mm	mm	mm/mm
1 through 17								
	Notes: Poor quality data due to coolant leaks and an inconsistent pile-loading system not shown.							
18	A.14	-2	sg	58.3	n/a	76/66.3	0.79	-
	Notes: Very small leak found after testing Mechanism for small displacement jumps unknown.							
19	A.14	-2	sg	58.1	n/a	76/62.9	0.79	-
20	B.1	-2	sg	57.8	n/a	76/62.1	0.79	-
	Notes: Large displacement rate increases, cause unknown.							
21	A.14	-2	sg	58.8	n/a	76/65.3	0.79	-
22	B.2	-2	sg	58.1	n/a	76/57.4	0.79	-
23	B.3	-3	sg	58.2	n/a	76/58.4	0.79	-
	Notes: Lever arm knife edges set on moveable rings for less static load variation.							
24	B.4	-3	sg	59.0	n/a	76/64.5	0.79	-
	Notes: Test appeared to be slow. Alignment problems or slightly higher vol./solids may be a factor.							
25	B.5	-3	sg	58.3	n/a	76/61.1	0.79	-
	Notes: Pile allignment estimated at 2 deg from vertical.							
26	B.6	-3	sg	58.0	n/a	76/62.1	0.79	-
27	B.7	-3	sg	57.6	0.90	76/59.7	0.79	-
	Notes: Coolant bath began to fail after approx. 12mm displ.							
28	B.8	-3	sg	58.1	0.92?	76/66.9	0.79	-
29	4.11	-3	sg	58.0	0.91	76/59.9	0.79	-

Table B.1. (cont.)

30	B.9	-3	sg	58.3	0.91	76/63.7	0.79	-
	Notes: Possible alignment problem during initial displ.							
31	B.10	-3	sg	62.4	0.93?	76/61.3	0.79	-
32	B.11	-3	sg	63.4	0.92	76/62.5	0.79	-
33	4.13	-3/-2	sg	64.5	0.93	76/62.1	0.79	-
34	B.12	-3/-2	sg	63.8	0.92	76/63.7	0.79	-
35	4.15	-3	i	0	0.90	76/76.4	0.79	-
36	n/a	-3	i	0	0.91	76/76.4	0.79	-
	Test Data: minutes 0, 8, 9, 10, 11, 11.32, 12 micrometers 0, 0, 38, 38, 114, 227, failure Pile load = 2.22 kN.							
37	n/a	-3	i	0	0.90	76/76.4	0.79	-
	Notes: Sudden pile failure at pile load = 2.67 kN.							
38	B.13	-3	i	0	0.89	76/76.4	0.79	-
	Notes: Silicon grease applied to pile before sample prep.							
39	B.14	-3	i	0	0.90	76/76.4	0.79	-
	Notes: Silicon grease applied to pile before sample prep.							
40	B.15	-3	i	0	0.89	76/76.4	0.79	-
	Notes: Sample behind lug broken away during initial displ.							
41	B.16	-3	i	0	0.90	76/76.4	0.79	-
	Notes: Teflon coating applied to pile before sample prep. Pile was turned to break adhesion before testing.							
42	B.17	-3	i	0	0.89	76/76.4	0.79	-
	Notes: Pile was turned to break adhesion before testing.							
43	B.18	-3	i	0	0.90	76/76.4	0.79	-
44	B.19	-3	i	0	0.90	76/76.4	0.79	-
45	B.20	-3	i+sg	32.6	n/a	76/76.4	0.79	-
	Notes: Ice chips mixed with 0.074-0.84 mm sand before adding chilled water. This sample was not uniform.							
46	B.21	-3	i	0	0.89	165.1/-	0.79	-

Table B.1 (cont.)

47	n/a	-3	i	0	0.89	76/76.4	0	-
	Notes: Pile without lug failed suddenly after 0.55kN added.							
48	B.22	-2	i	0	0.90	76/76.4	0.79	-
49	B.23	-3	i	0	0.89	76/76.4	0.79	-
50	n/a	-3	i	0	0.89	76/76.4	0.79	-
	Notes: Thermistor located 1.5 mm from pile shaft recorded approx. temp. increase of 0.06 deg C at time of rapid pile failure.							
51	4.16	-3	i	0	0.89	76/76.4	0.79	-
52	B.24	-2	i	0	0.90	76/76.4	0.79	-
53	A.13	-3	su	57.1	0.90	76/63.7	0.79	-
54	B.25	-3	i	0	0.89	76/76.4	0.79	-
55	A.13	-3	su	~57	~0.89	76/64.0	0.79	-
56	A.13	-3	su	57.4	0.90	76/63.7	0.79	-
57	A.13	-3	su	56.1	0.89	76/62.3	0.79	-
58	n/a	-3	su	57	0.91	76/62.1	0	-
	Notes: Pile load of 0.73 kN caused sudden failure.							
59	n/a	-3	su	57.1	0.89	76/60.7	0.79	-
	Notes: Coolant leak altered frozen sand around pile.							
60	4.8	-3	su	~57	~0.89	76/61.5	0.79	-
	Notes: Tapered lug used.							
61	B.26	-3	i	0	0.90	-	-	1.06/165.1
62	A.27	-3	i	0	0.91	-	-	1.06/84.9
63	4.29a	-3	i	0	0.90	-	-	1.06/23.8
64	4.29b	-3	i	0	0.90	-	-	1.06/80.3
65	B.28	-3	i	0	0.90	-	-	1.06/81.1
66	4.27	-3	i	0	0.90	-	-	0.35/87.4

Table B.1 (cont.)

67	B.29	-3	su	~57	~0.89	-	-	1.06/87.4
68	4.27	-3	su	~57	~0.89	-	-	0.35/87.1
69	B.30	-3	su	~57	~0.89	-	-	1.06/25.4
70	B.31	-3	su	~57	~0.89	-	-	1.06/33.3
	Notes: Coolant leak probably altered last portion of test.							
71	B.32	-3	su	n/a	n/a	-	-	1.06/79.4
	Notes: Pile coated with ice then surrounded with sand.							
72	4.28	-3	i	0	0.91	-	-	1.06/82.0
73	B.33	-3	su	n/a	n/a	-	-	1.06/81.8
	Notes: Pile coated with ice then surrounded with sand.							
74	B.34	-3	i	0	0.88	-	-	1.06/75.4
75	B.35	-3	i	0	0.91	-	-	1.06/87.6
76	B.36	-3	i	0	0.92	-	-	1.06/79.6
77	4.28	-3	i	0	0.91	-	-	1.06/79.4
78	B.37	-3	su	n/a	n/a	76/32.3	3.18	-
	Notes: Silicon grease applied to pile before sample prep. Short duration loads described in Table 4.3.							
79	B.38	-3	su	n/a	n/a	-	-	1.06/25.8
80	B.39	-2	su	57.1	0.90	-	-	1.06/54.0
81	B.40	-3	su	57.8	0.88	76/62.1	0.79	-
	Notes: Silicon grease applied to pile before sample prep. Short duration loads described in Table 4.3.							
82	B.41	-3	su	~57	~0.89	76/63.3	1.59	-
	Notes: Silicon grease applied to pile before sample prep. Short duration loads described in Table 4.3.							
83	n/a	-3	su	57.3	0.89	152.8/-	0	-
	Notes: Silicon grease applied to pile before sample prep. Pile load = 0.30 kN caused sudden failure.							
84	4.26	-3	su	60.2	0.91	-	-	0.35/51.6

Table B.1 (cont.)

85	B.42	-3	su	56.5	0.90	-	-	1.06/51.6
86	4.31	-3	su	57.8	0.95?	-	-	1.06/51.2
87	A.7	-3	su	56.4	0.89	76/63.3	1.59	-
	Notes: Short duration loads described in Table 4.3.							
88	B.43	-3	su	59.6	0.90	76.62.1	0.79	-
	Notes: Short duration loads described in Table 4.3.							
89	A.7	-3	su	56.7	0.85	76/63.7	1.59	-
	Notes: Short duration loads described in Table 4.3.							
90	4.25	-3	su	55.9	0.90	-	-	1.59/60.3
91	4.23	-3	su	58.3	0.89	-	-	1.06/52.4
92	A.7	-3	su	57.8	0.88	76/63.7	1.59	-
	Notes: Short duration loads described in Table 4.3.							
93	A.7	-3	su	57.9	0.90	76/63.7	1.59	-
	Notes: Short duration loads described in Table 4.3. Lever arm adjusted at 8.72 and 14.37 mm.							
94	A.7	-3	su	56.7	0.85	76/63.7	1.59	-
	Notes: Short duration loads described in Table 4.3. Lever arm adjusted at 11.58, 25.12, 34.44 mm.							
95	B.44	-3	su	56.8	0.90	12.7/60.5	1.59	-
96	n/a	-3	su	55.3	0.90	12.7/62.2	1.59	-
	Notes: Sample damaged during load system set-up.							
97	A.1	-3	su	57.4	0.87	12.7/61.7	3.18	-
	Notes: Silicon grease applied behind pile lug.							
98	A.5	-3	su	59.1	0.88	15.2/65.5	1.59	-
	Notes: Silicon grease applied behind pile lug.							
99	A.1	-3	su	57.1	0.88	15.2/65.5	3.18	-
	Notes: Silicon grease applied behind pile lug.							
100	A.5	-3	su	56.8	0.87	17.8/61.9	1.59	-
	Notes: Silicon grease applied behind pile lug.							
101	A.1	-3	su	57.3	0.87	10.2/60.7	3.18	-
	Notes: Silicon grease applied behind pile lug.							

Table B.1 (cont.)

102	A.5	-3	su	57.0	0.87	17.8/63.2	1.59	-
103	A.1	-3	su	~57	~0.89	10.2/ -	3.18	-
	Notes: Silicon grease applied behind pile lug.							
104	A.5	-3	su	58.5	0.89	17.8/65.7	1.59	-
105	4.1	-3	su	57.3	0.86	25.4/63.3	3.18	-
106	A.5	-3	su	57.5	0.87	25.4/63.7	1.59	-
107	4.1	-3	su	56.7	0.88	25.4/60.7	3.18	-
108	A.1	-3	su	56.9	0.87	19.0/61.2	3.18	-
109	B.45	-3	su	57.2	0.88	15.2/60.5	3.18	-
110	A.1	-3	su	57.1	0.86	19.0/61.7	3.18	-
111	4.1	-3	su	57.1	0.88	25.4/62.5	3.18	-
112	A.1	-3	su	57.1	0.87	19.0/62.5	3.18	-
113	A.5	-3	su	57.2	0.88	25.4/63.7	1.59	-
114	4.1	-3	su	57.1	0.88	25.4/59.3	1.59	-
115	A.5	-3	su	57.9	0.86	17.8/59.3	1.59	-
116	4.1	-3	su	57.2	0.88	25.4/62.1	3.18	-
117	A.5	-3	su	56.8	0.88	25.4/63.2	3.18	-
118	A.9	-3	su	57.2	0.82	24.1/61.5	0.79	-
119	A.9	-3	su	57.5	0.91	24.1/60.3	0.79	-
120	4.25	-3	su	56.5	0.83	-	-	1.59/51.
121	A.9	-3	su	57.2	0.89	24.1/56.2	0.79	-
122	A.9	-3	su	55.6	0.96?	24.1/61.5	0.79	-
123	A.3	-3	su	57.3	0.88	76/28.8	3.18	-
124	A.3	-3	su	57.6	0.89	76/30.0	3.18	-

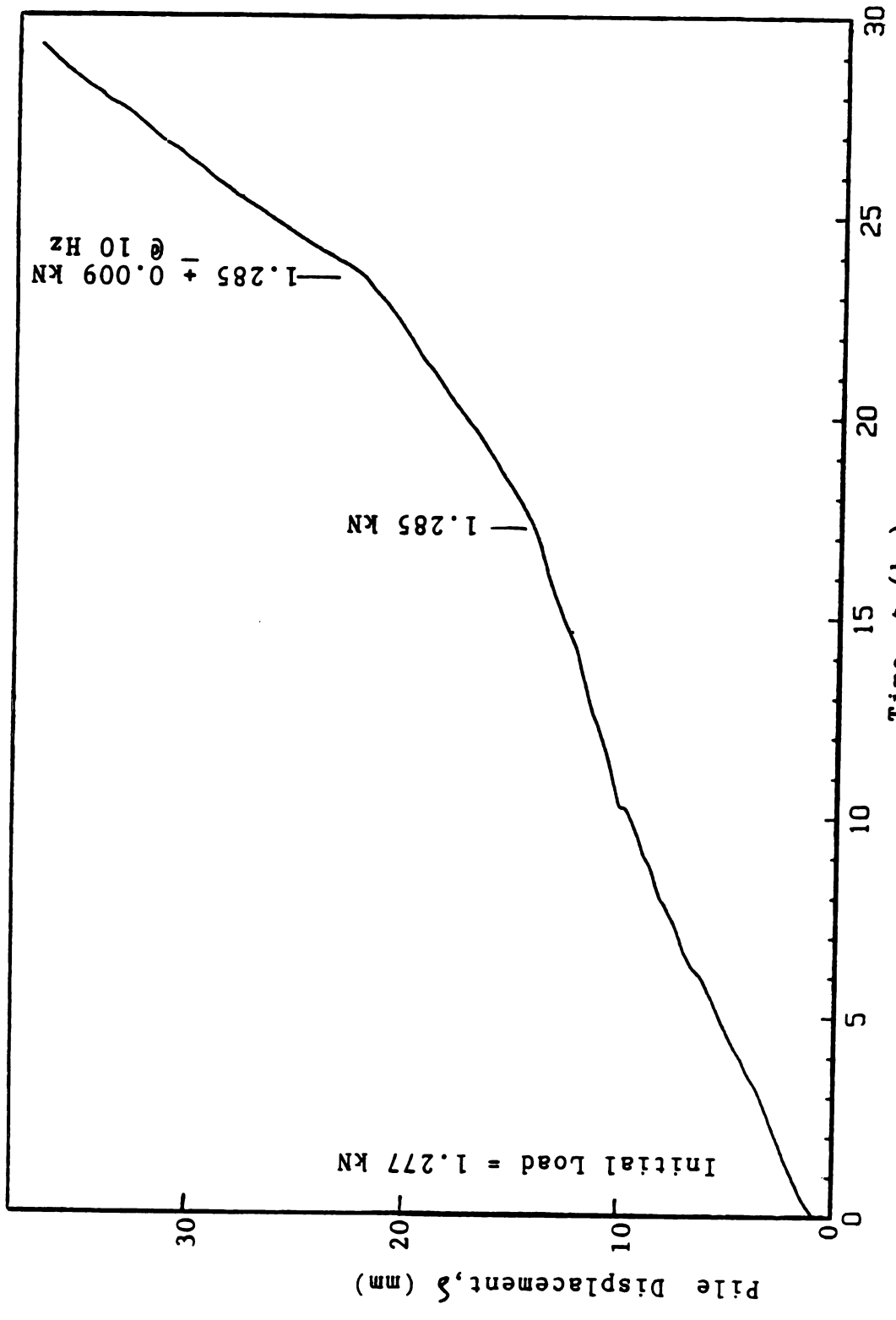

Figure B.1. Pile Test #20.

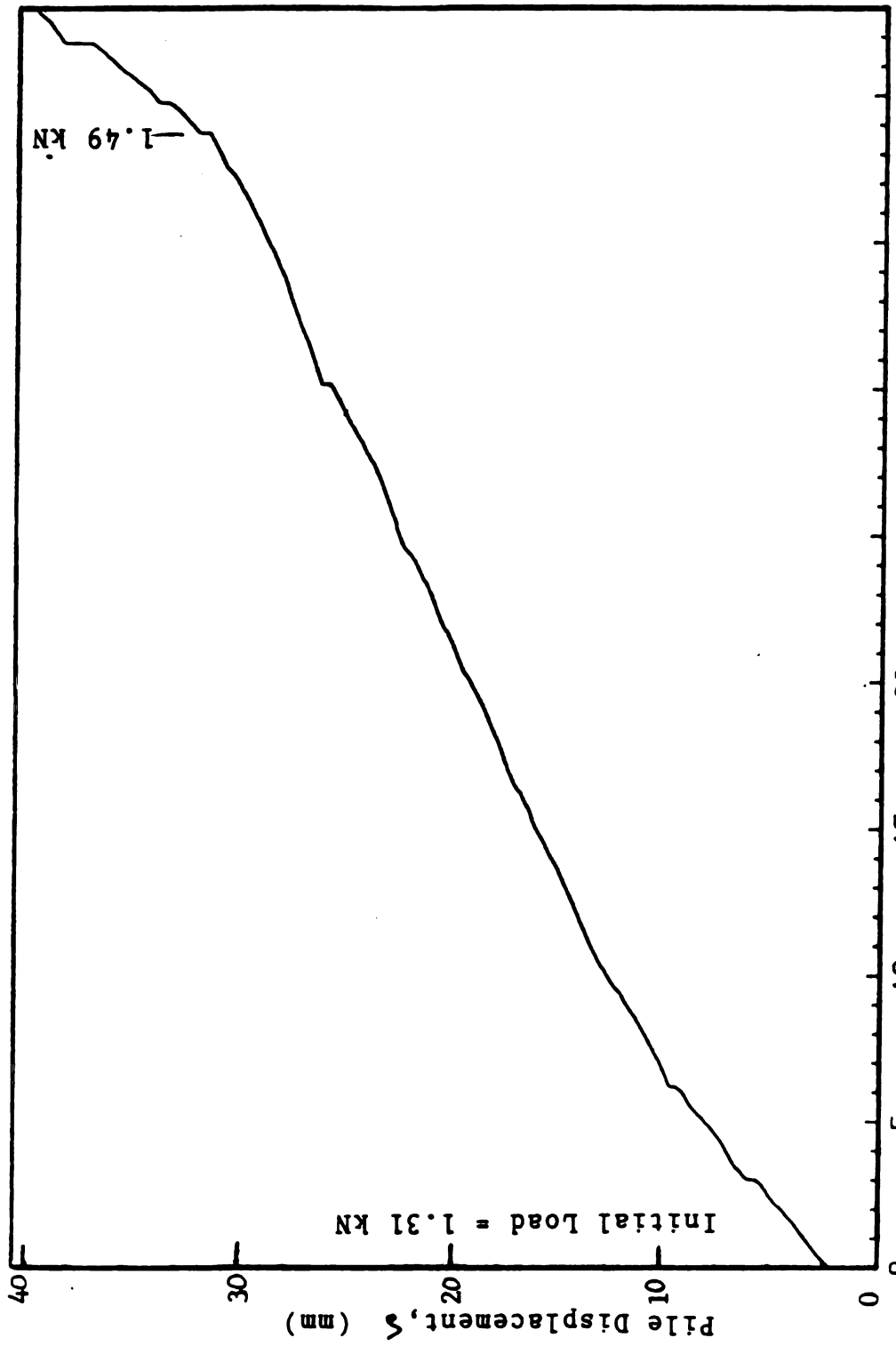

Figure B.2. Pile Test #22.

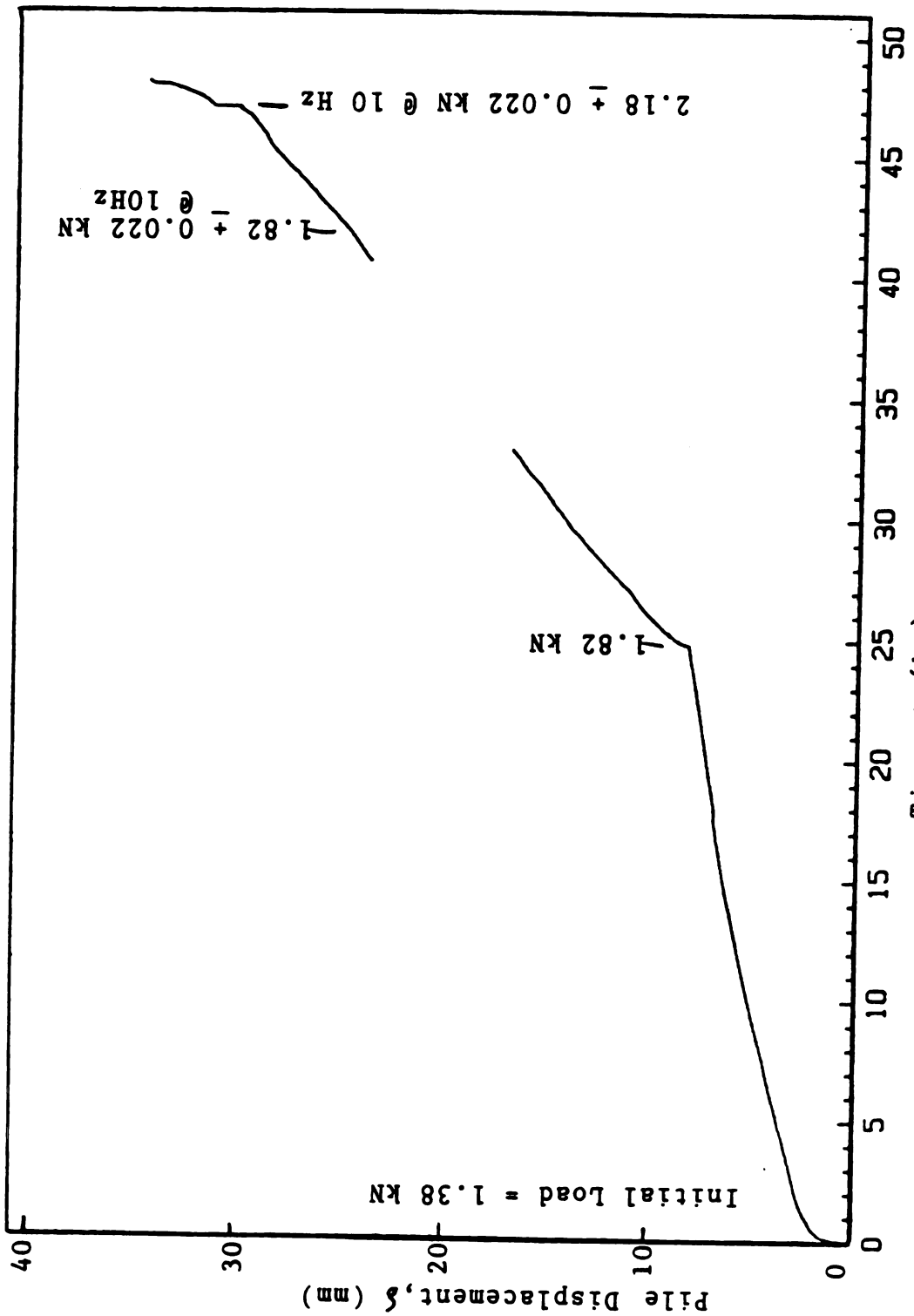

B.3. Pile Test #23.

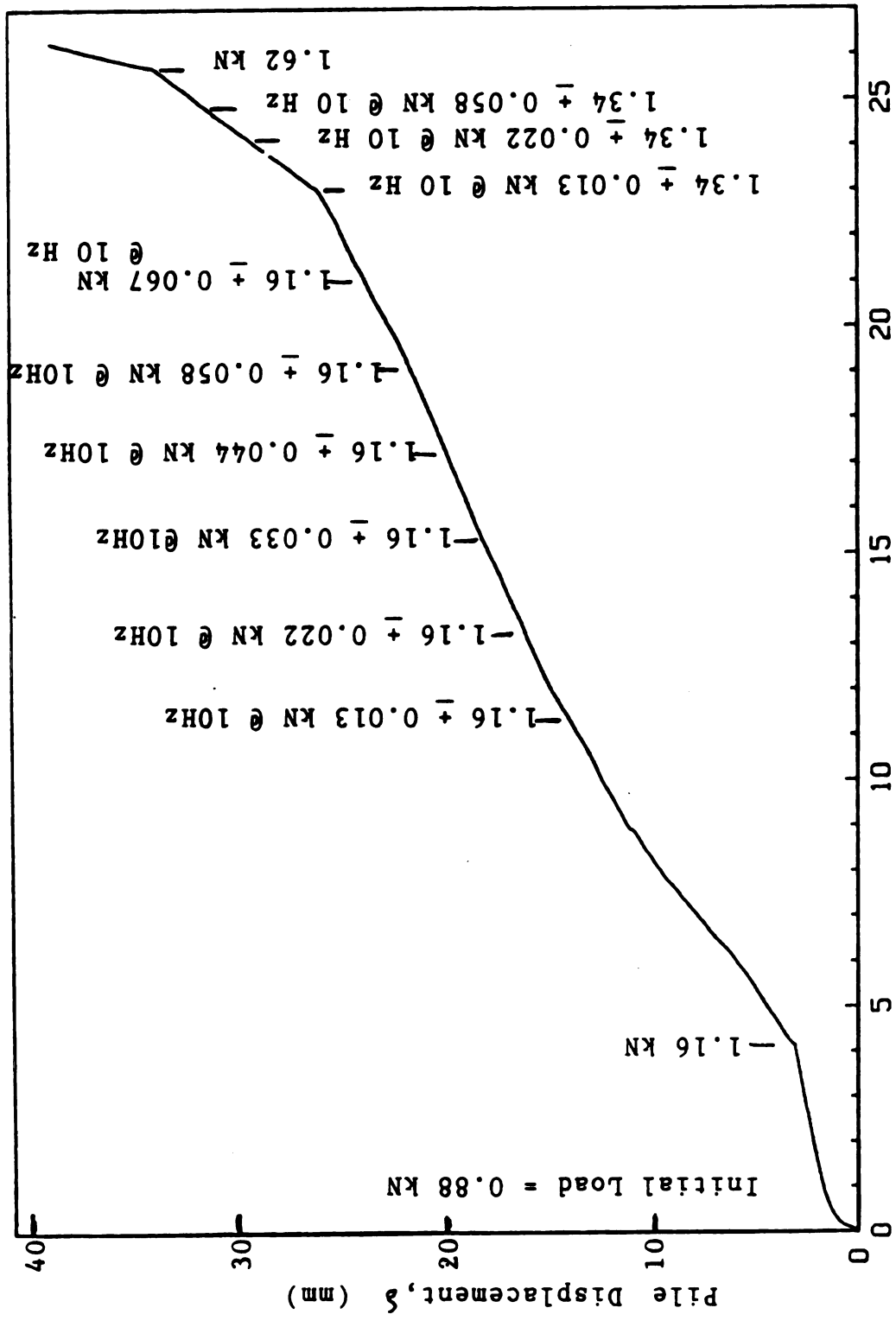

Figure B.4. Pile Test #24.

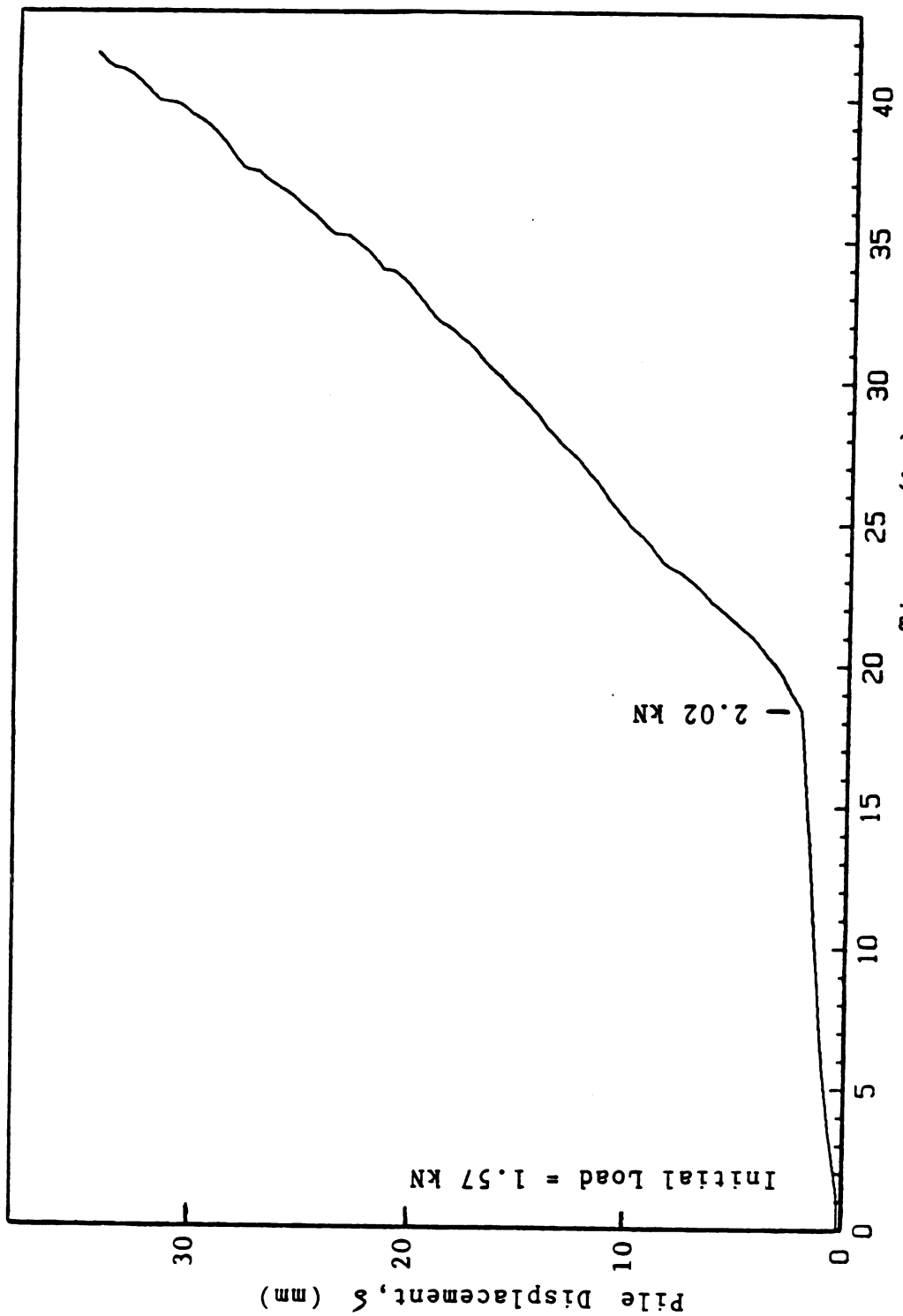

Figure B.5. Pile Test #25.

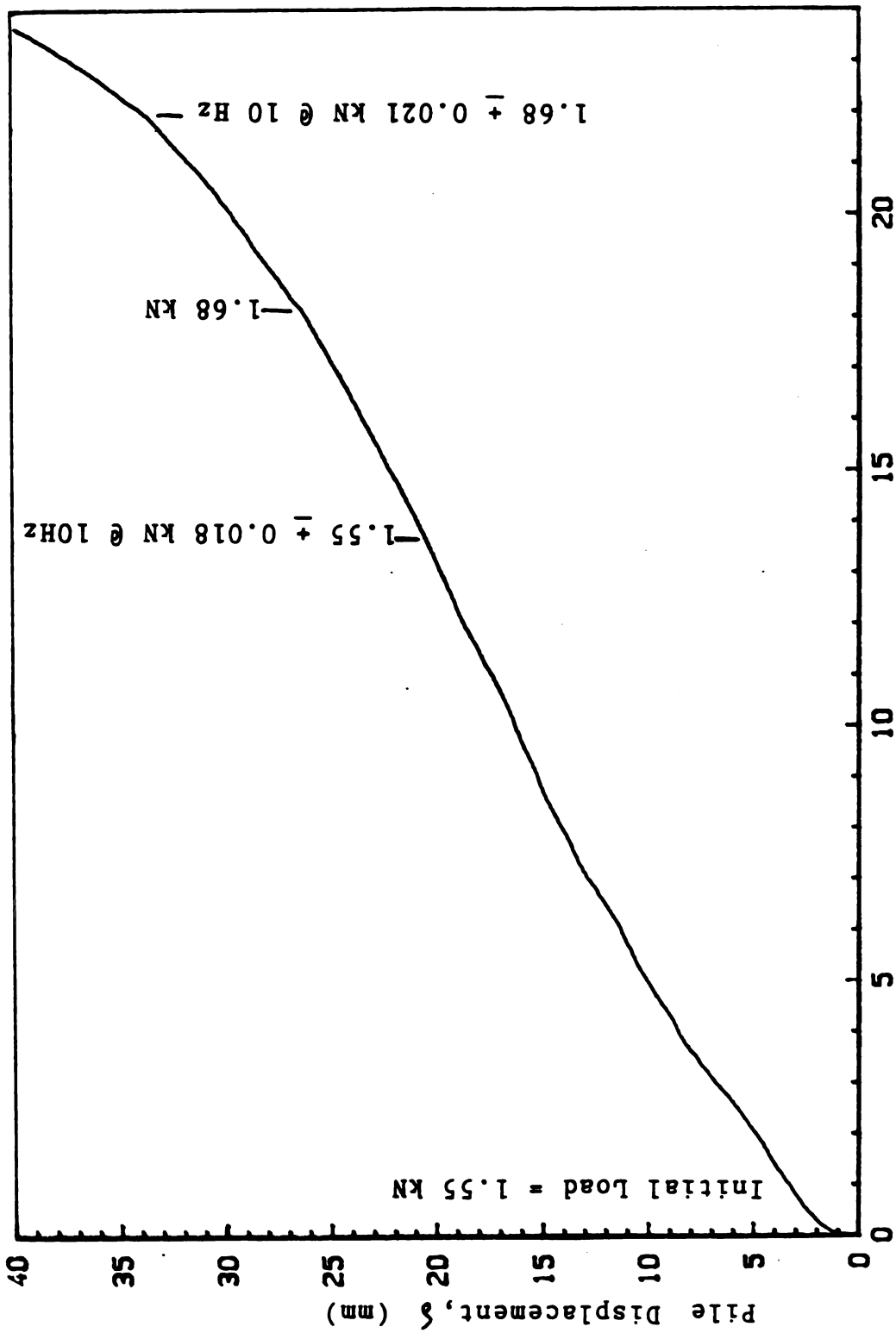

Figure B.6. Pile Test #26.

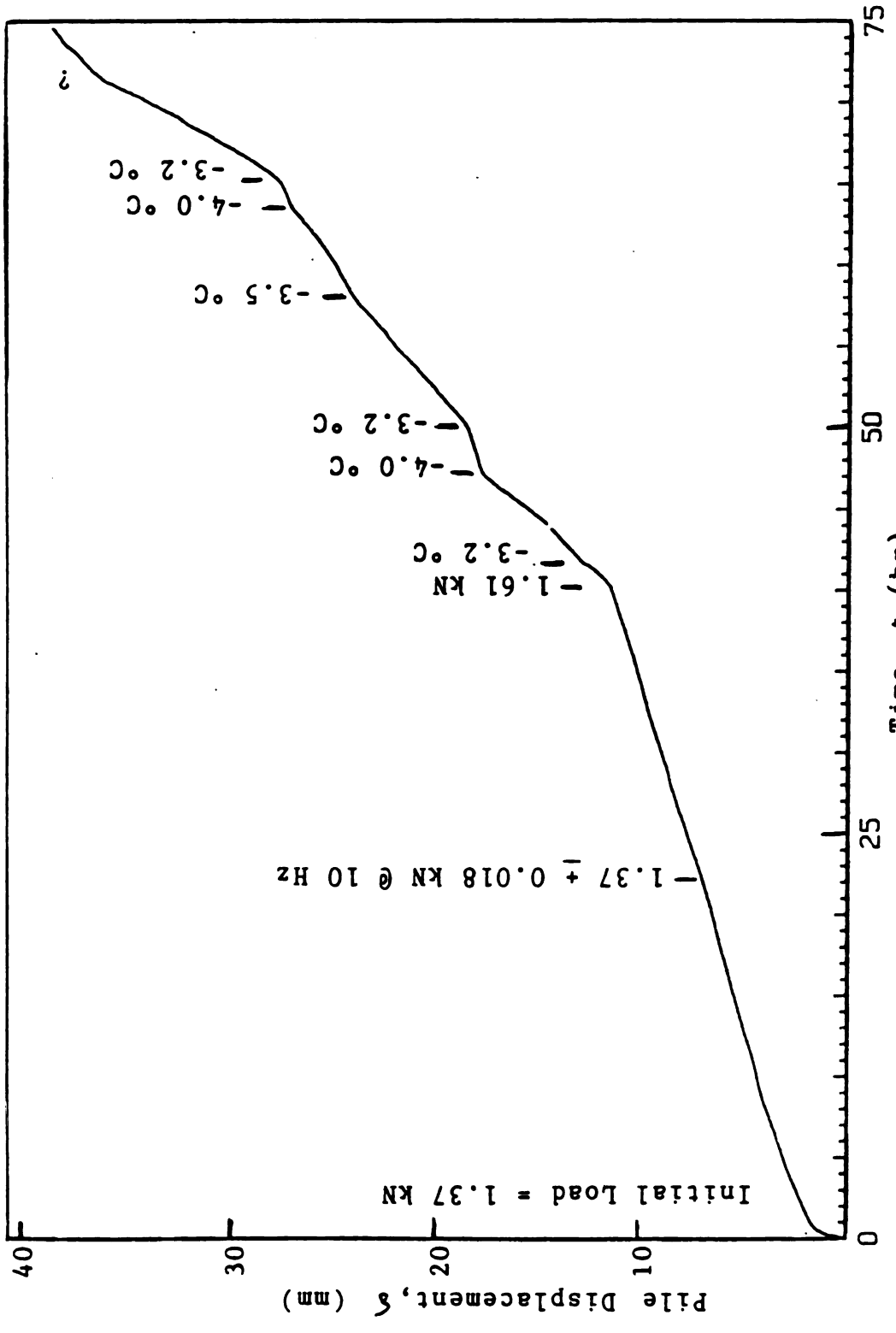

Figure B.7. Pile Test #27.

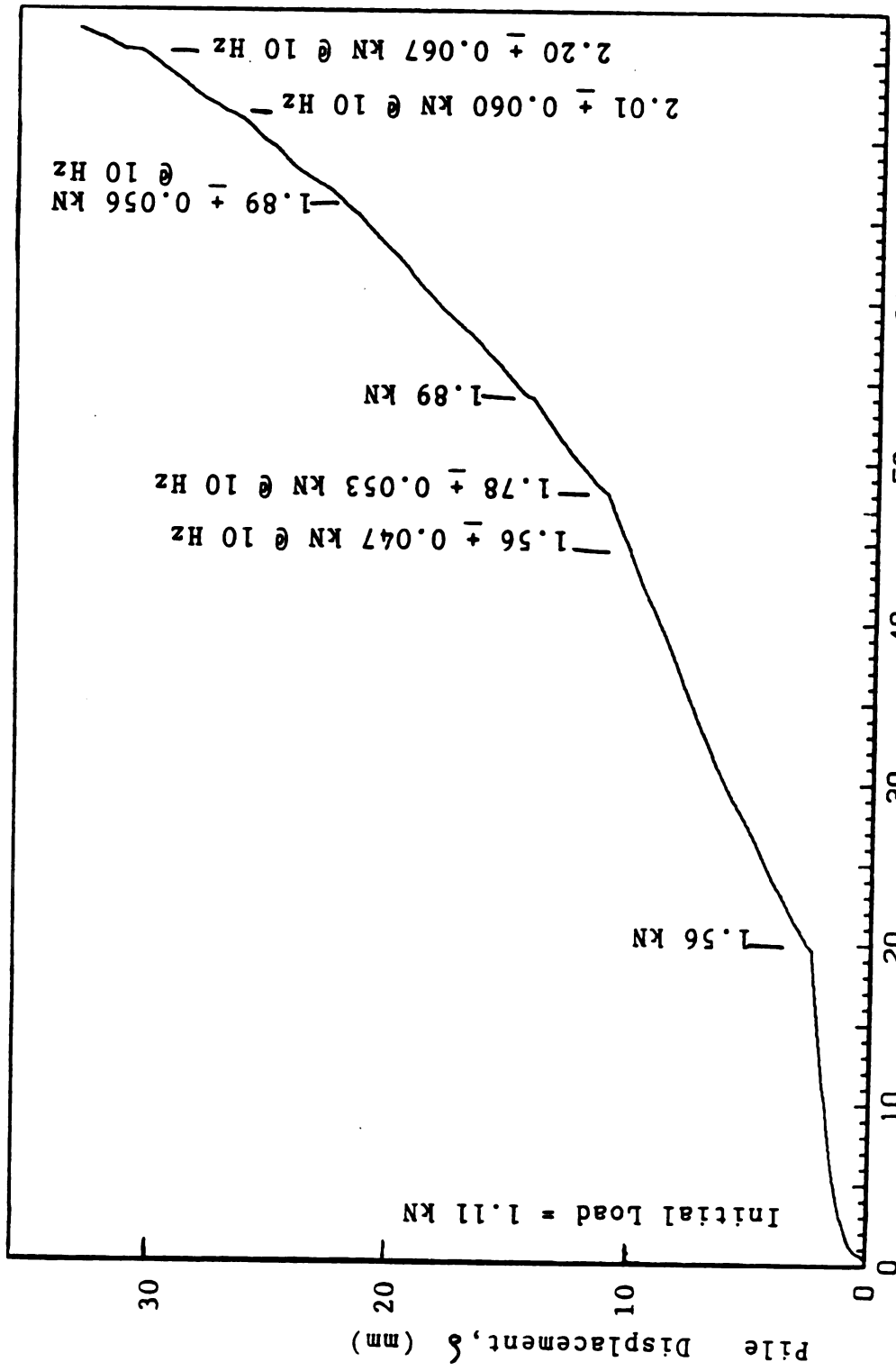

Figure B.8. Pile Test #28.

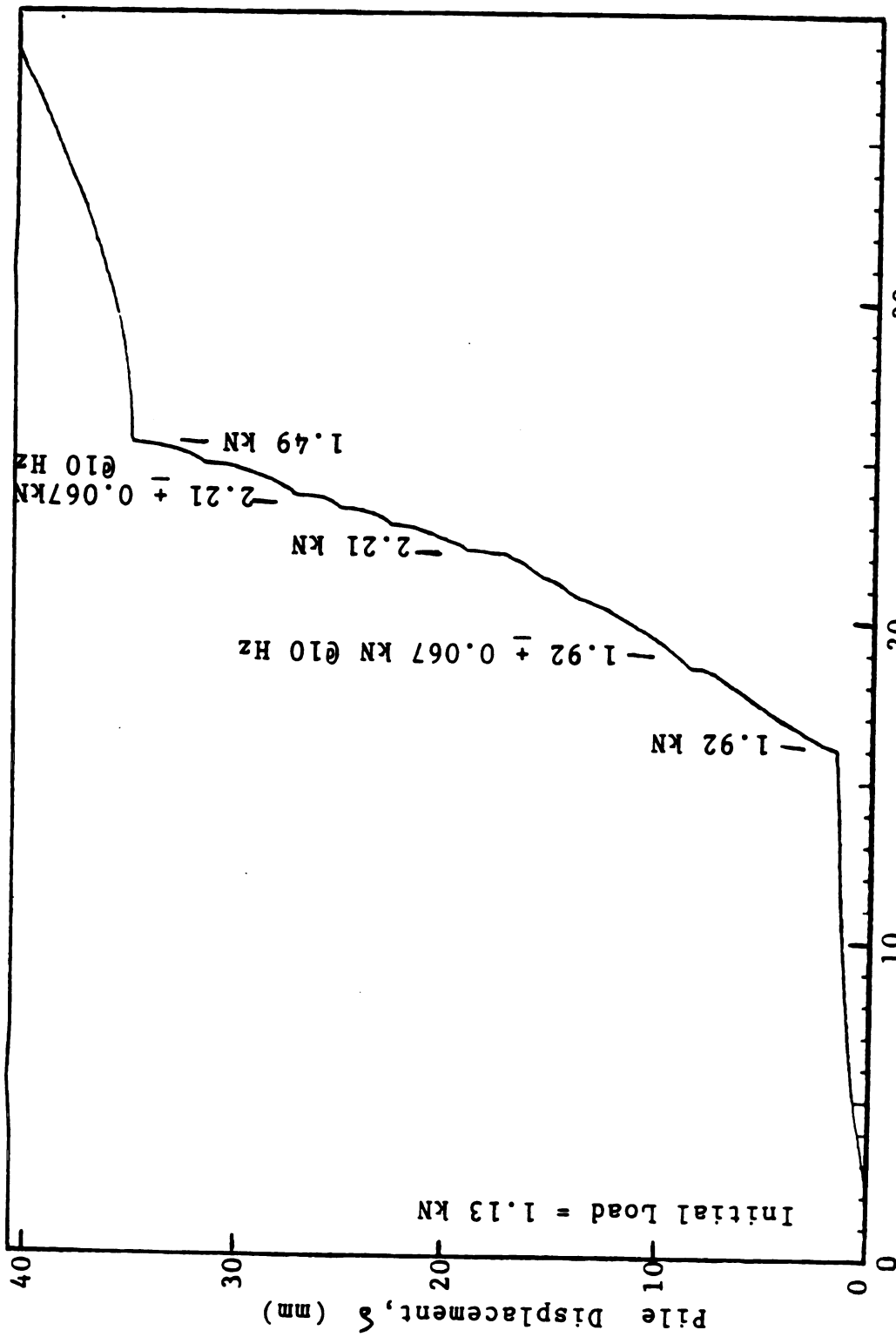

Figure B.9. Pile Test #30.

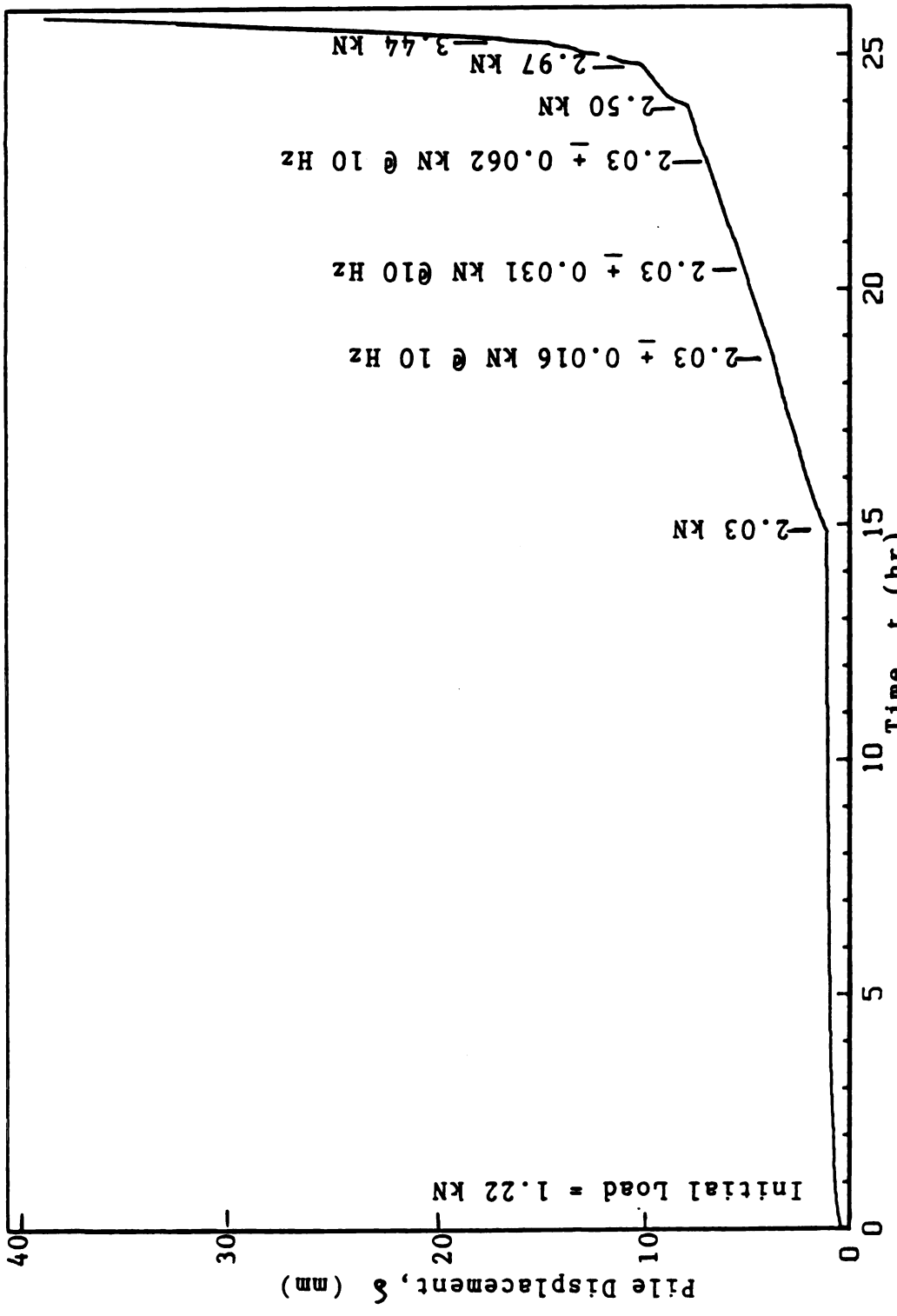

Figure B.10. Pile Test #31.

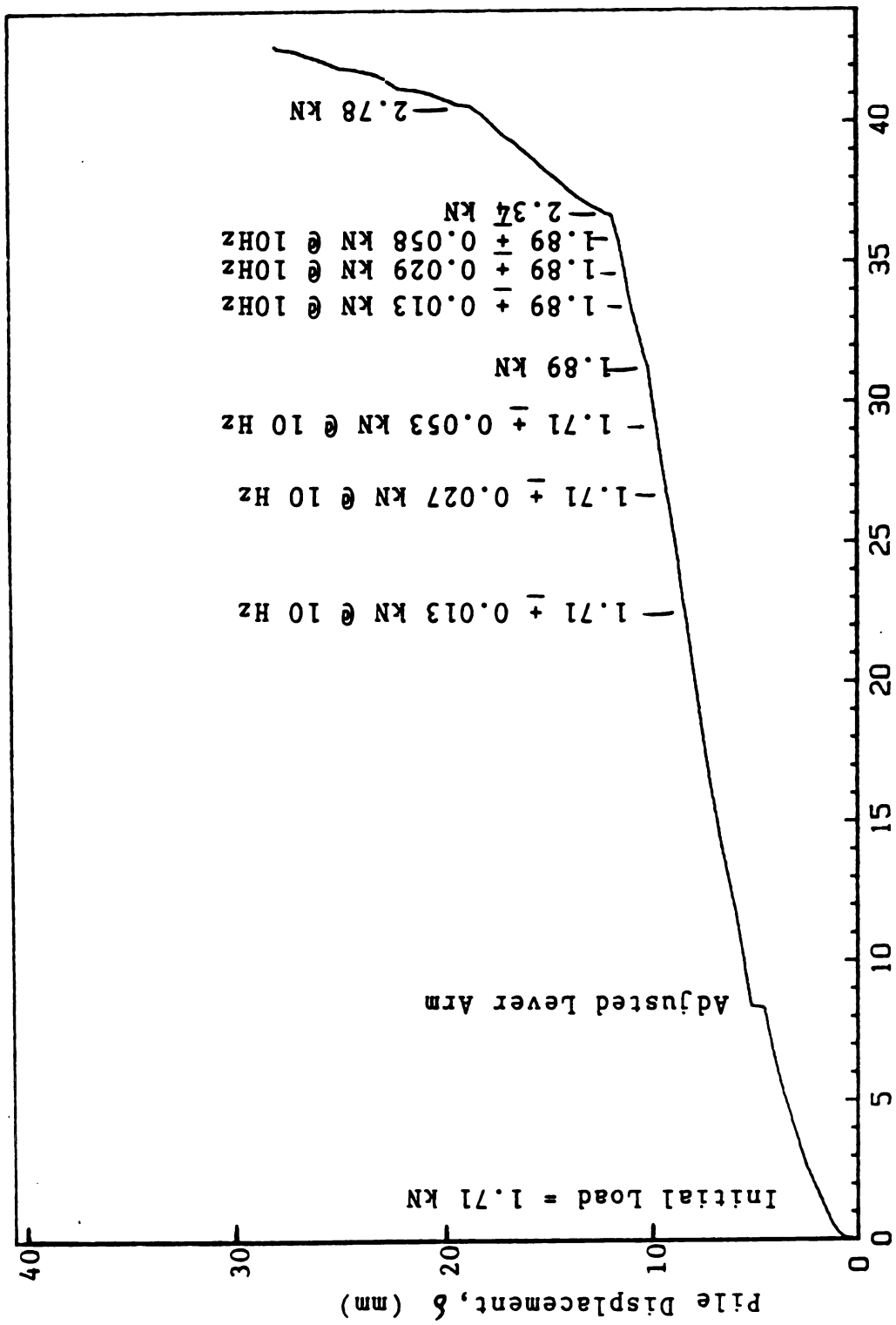

Figure B.11. Pile Test #32.

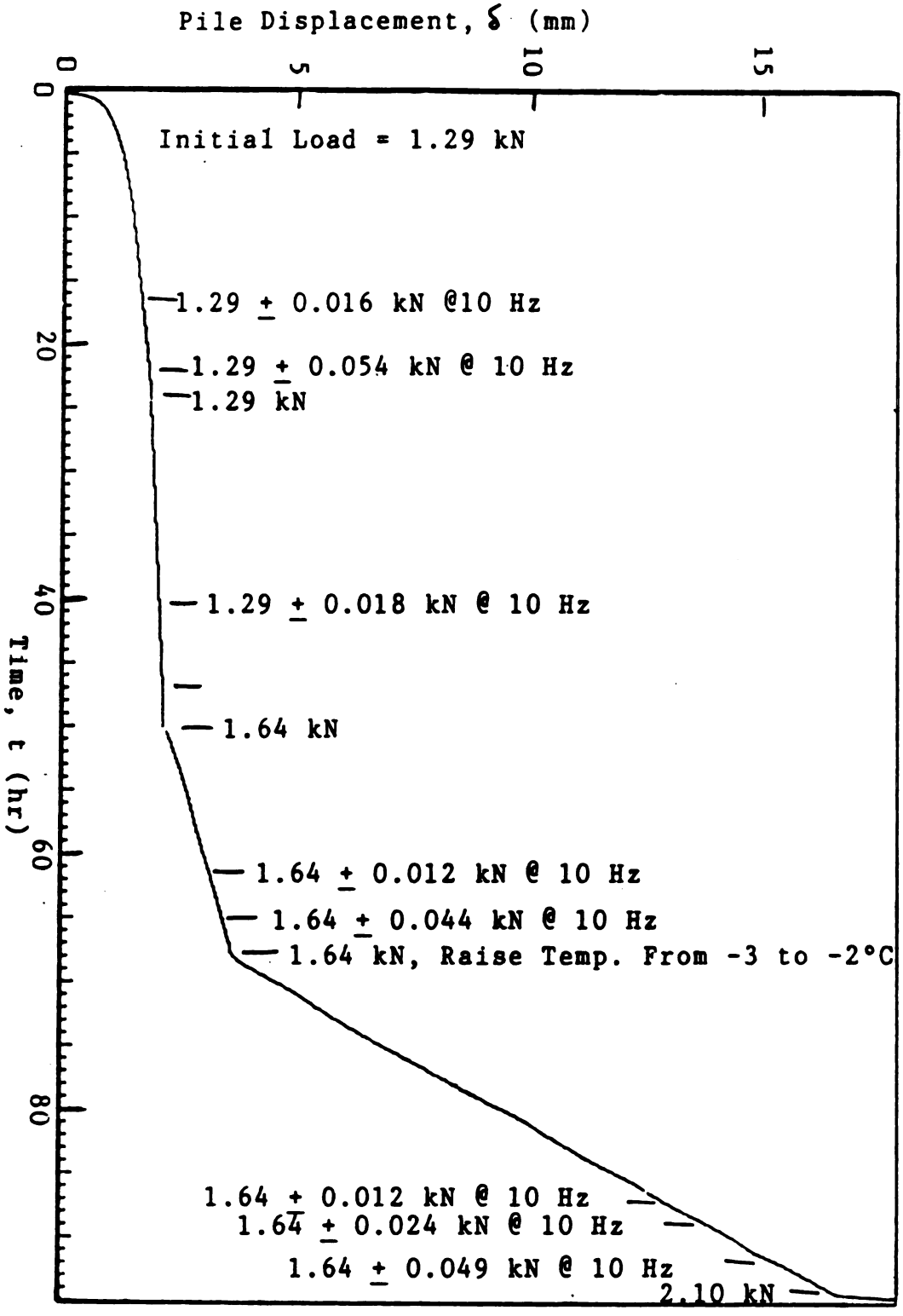

Figure B.12. Pile Test #34.

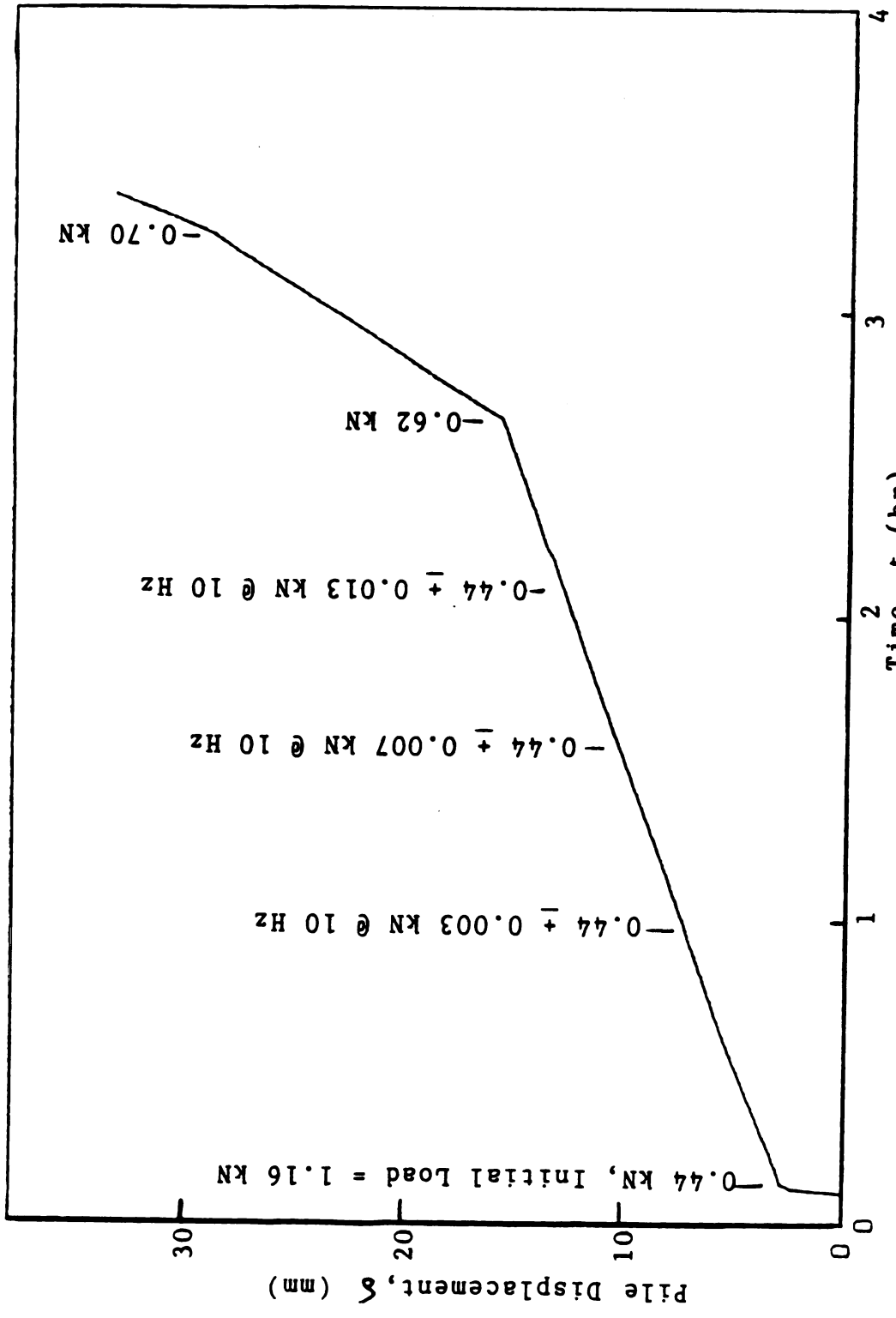

Figure B.13. Pile Test #38.

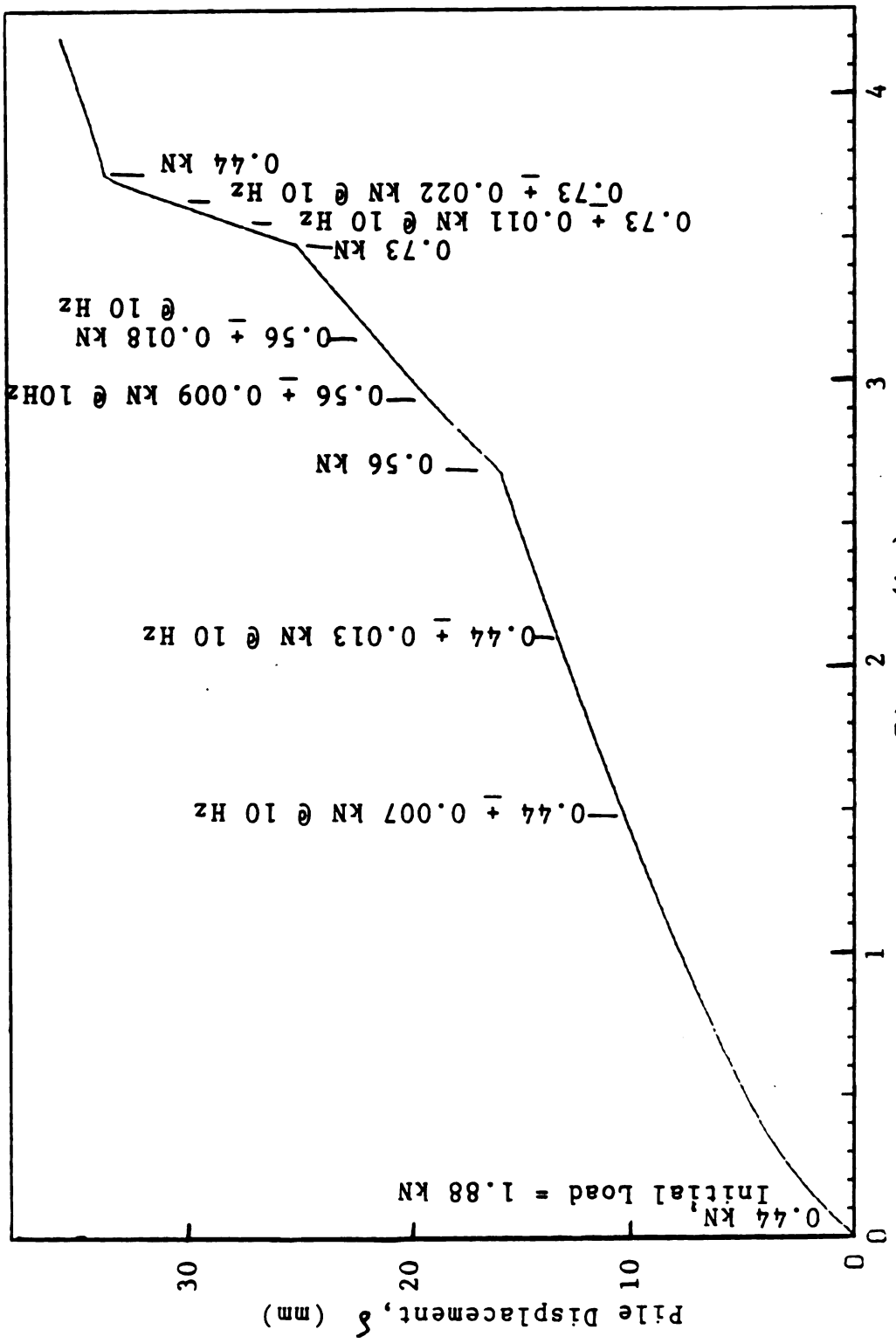

Figure B.15. Pile Test #40.

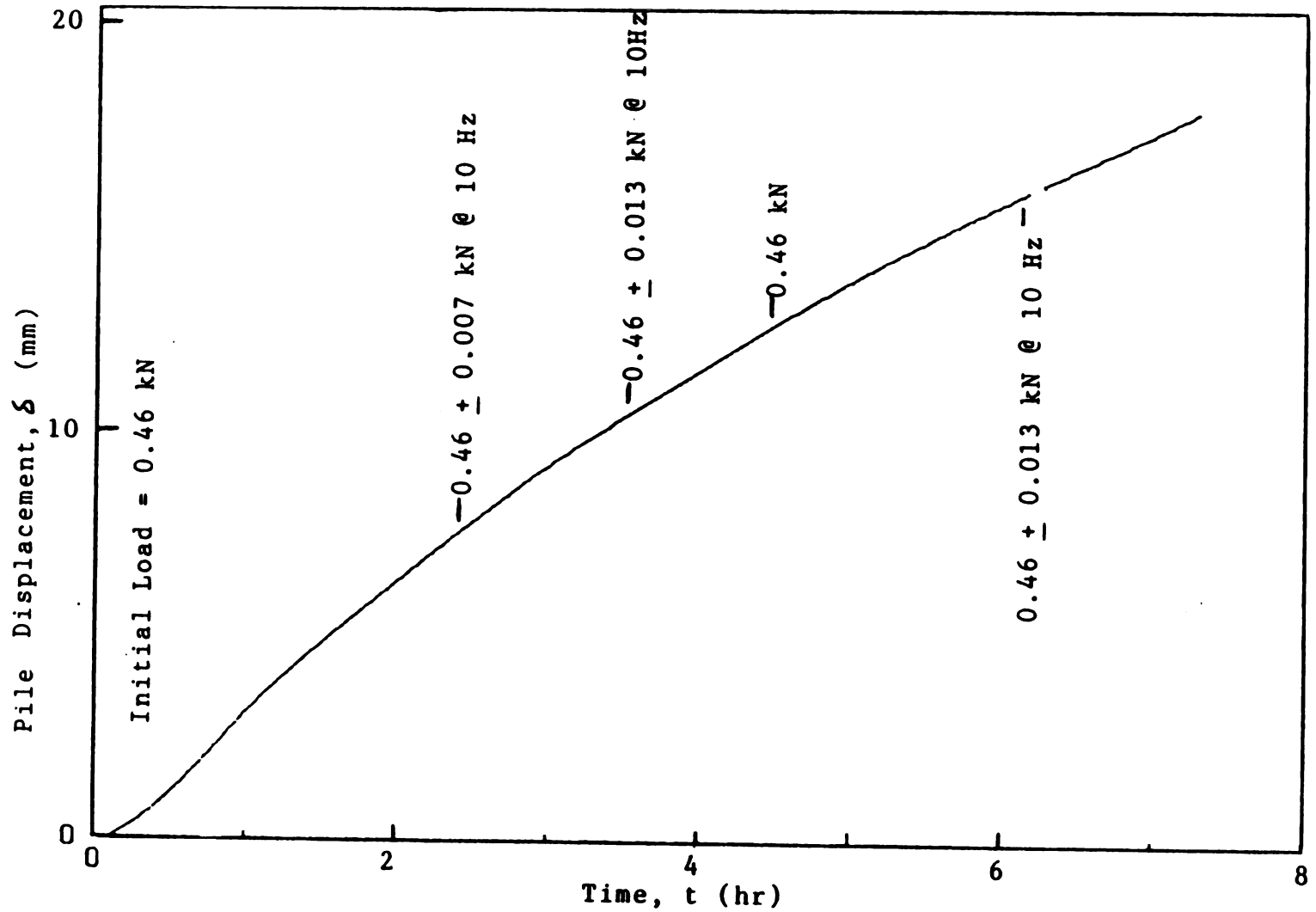

Figure B.16. Pile Test #41.

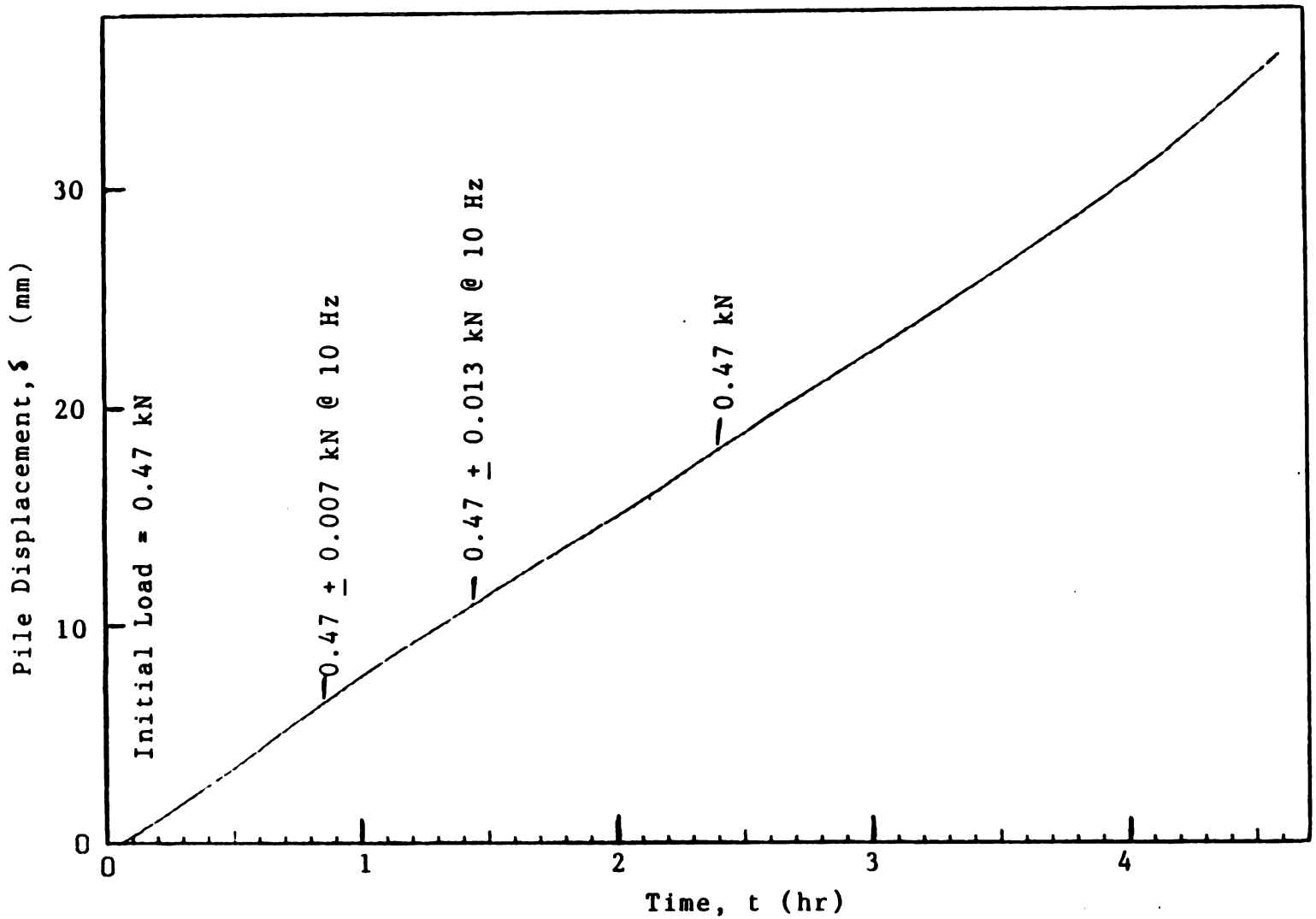

Figure B.17. Pile Test #42.

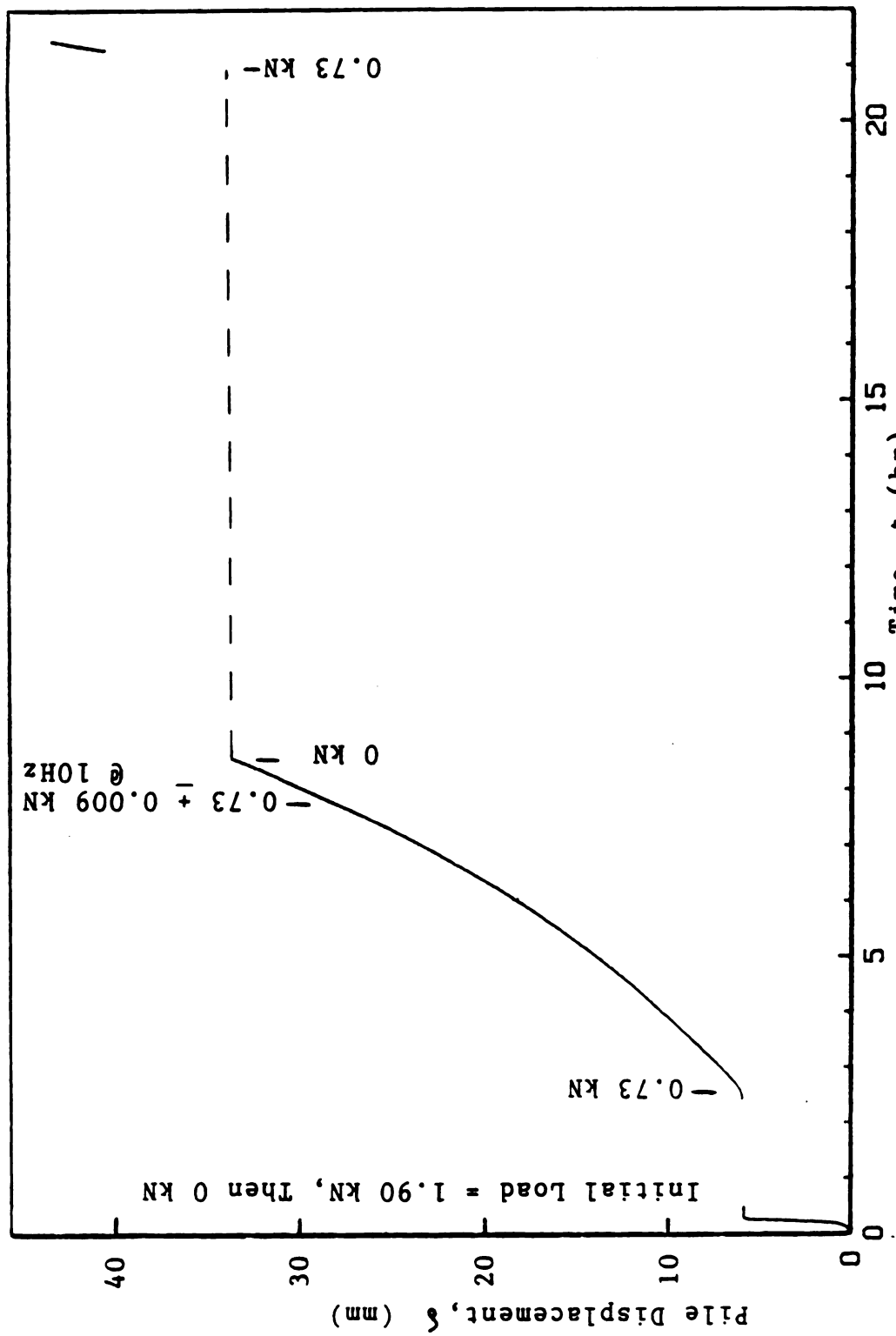

Figure B.18. Pile Test #43.

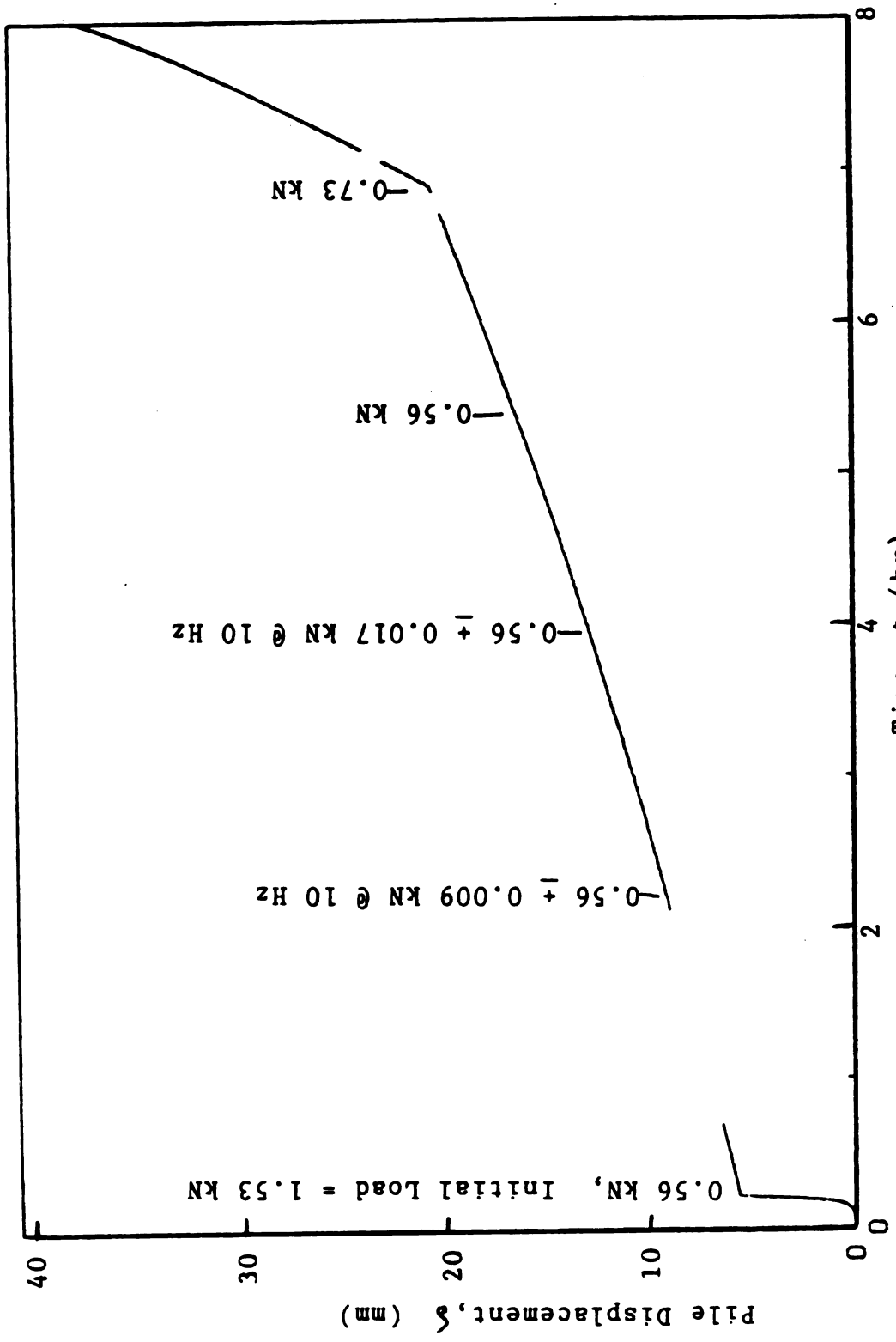

Figure B.19. Pile Test #44.

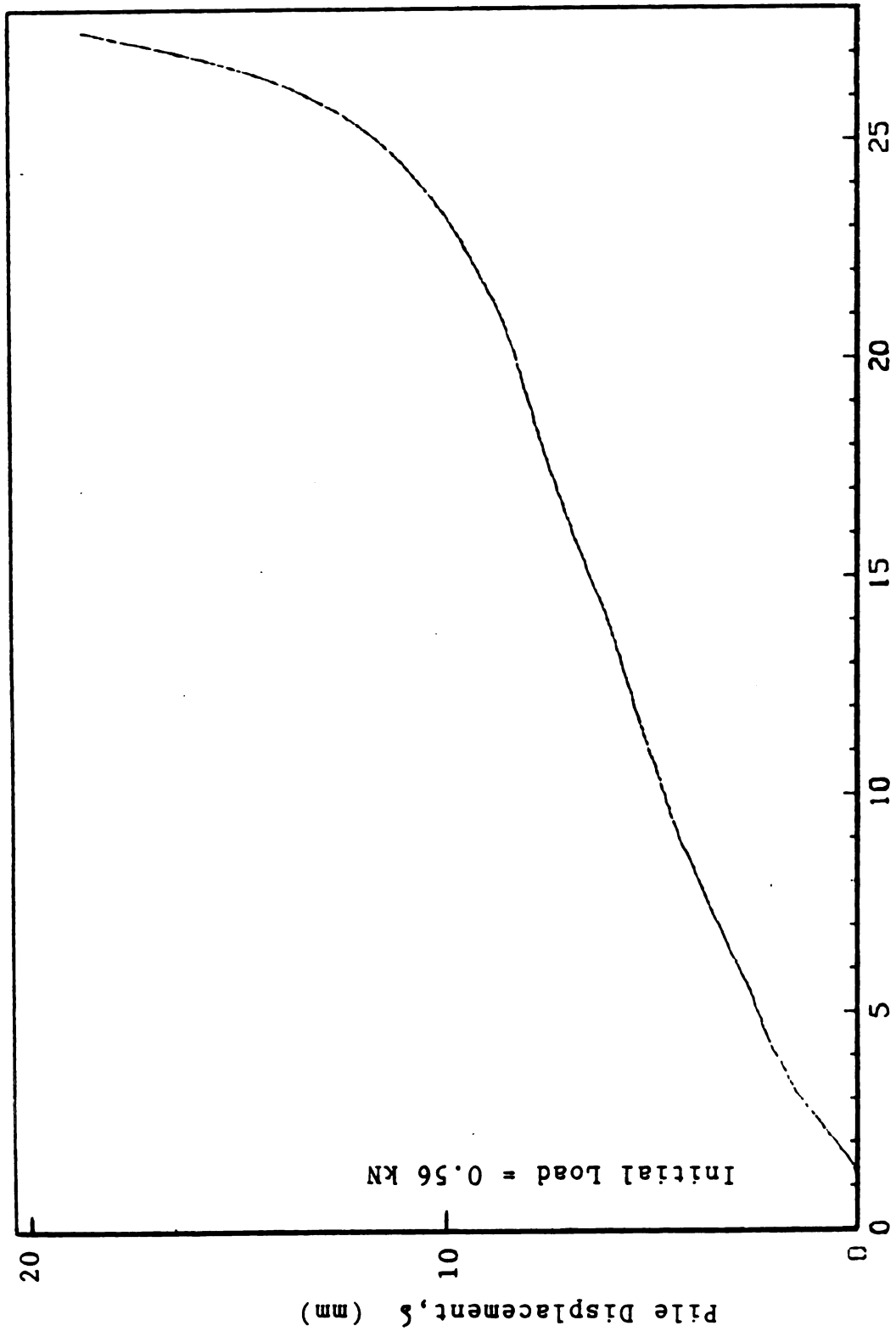

Figure B.20. Pile Test #45.

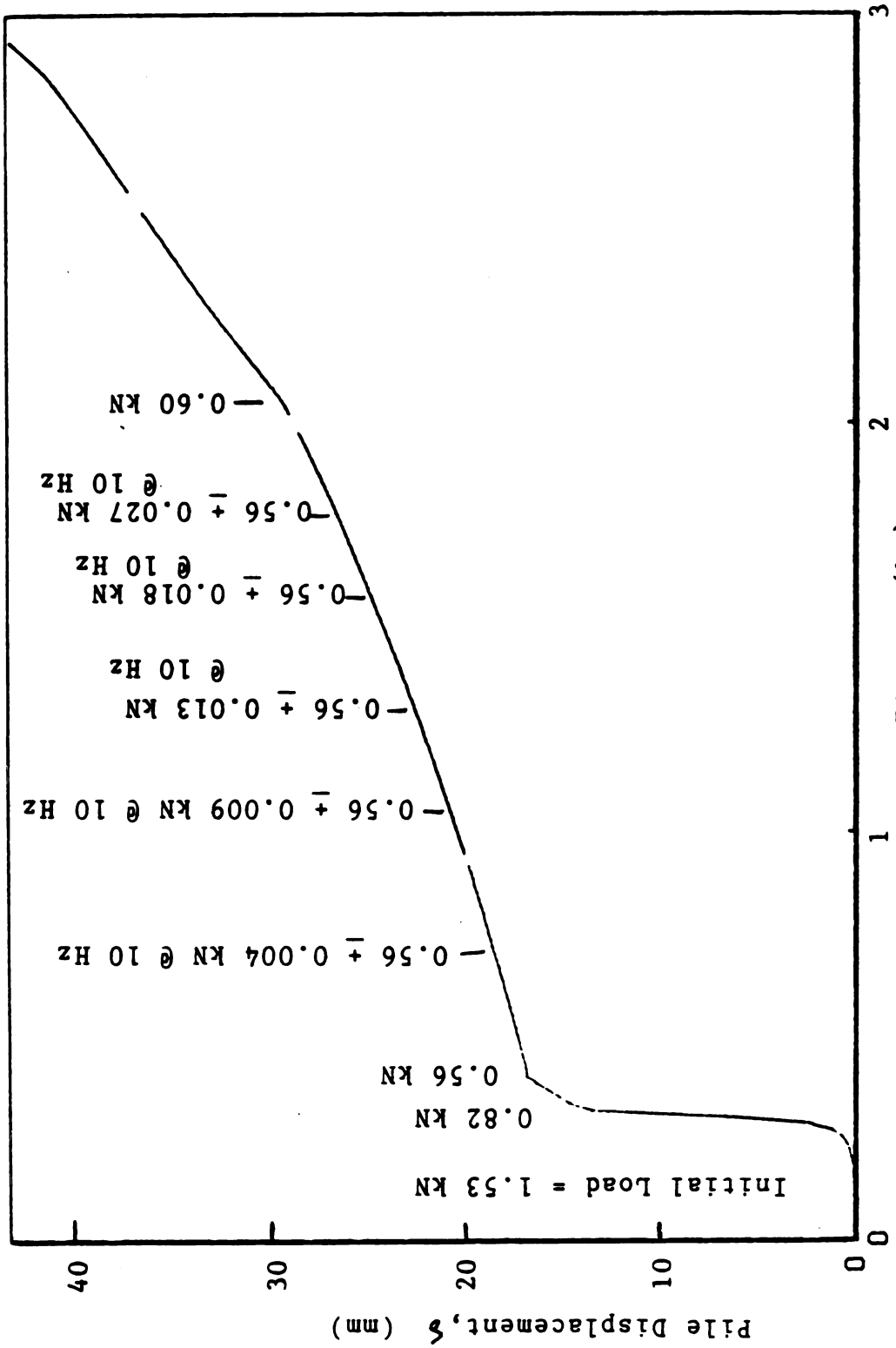

Figure B.21. Pile Test #46.

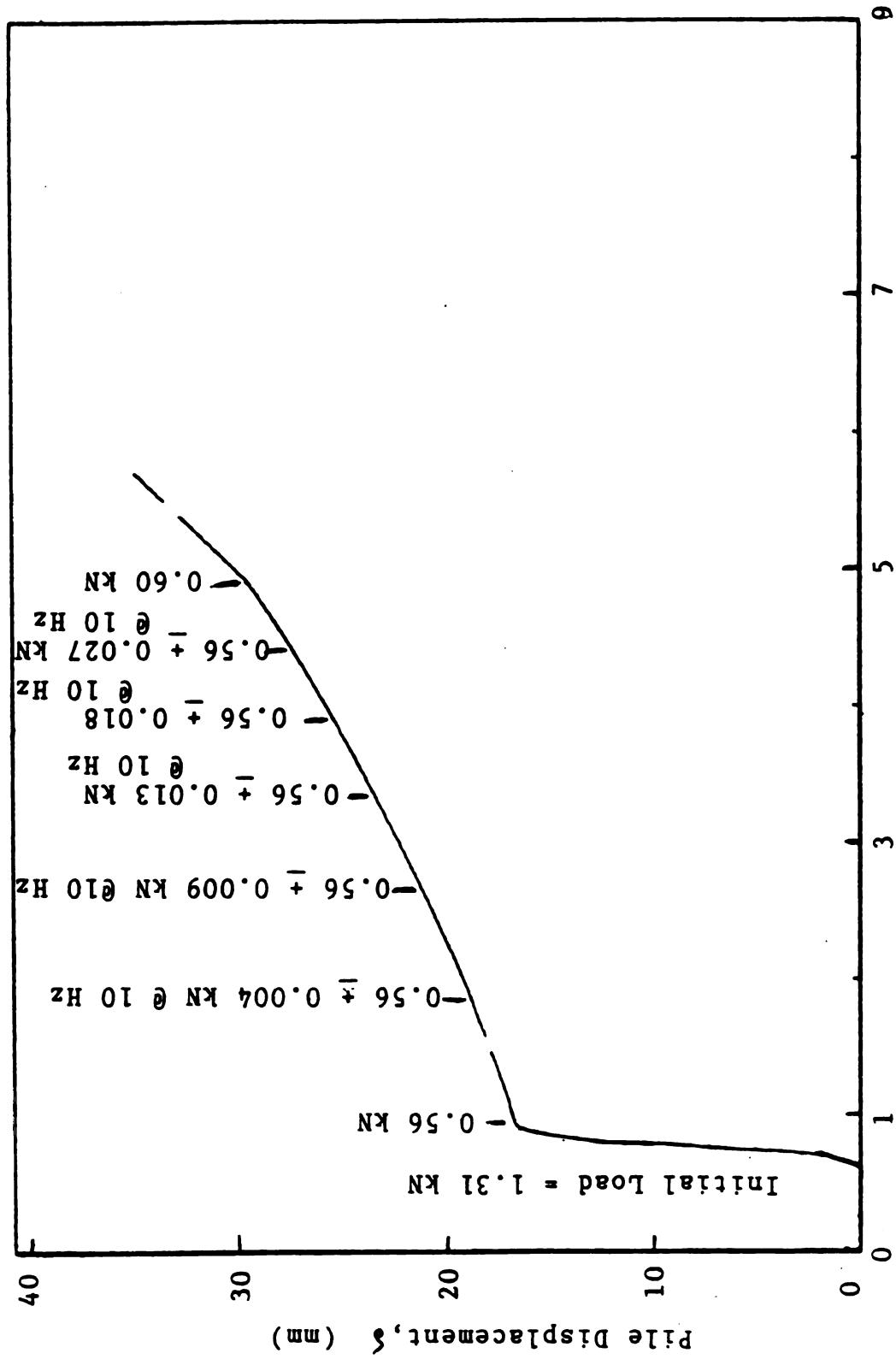

Figure B.22. Pile Test #48.

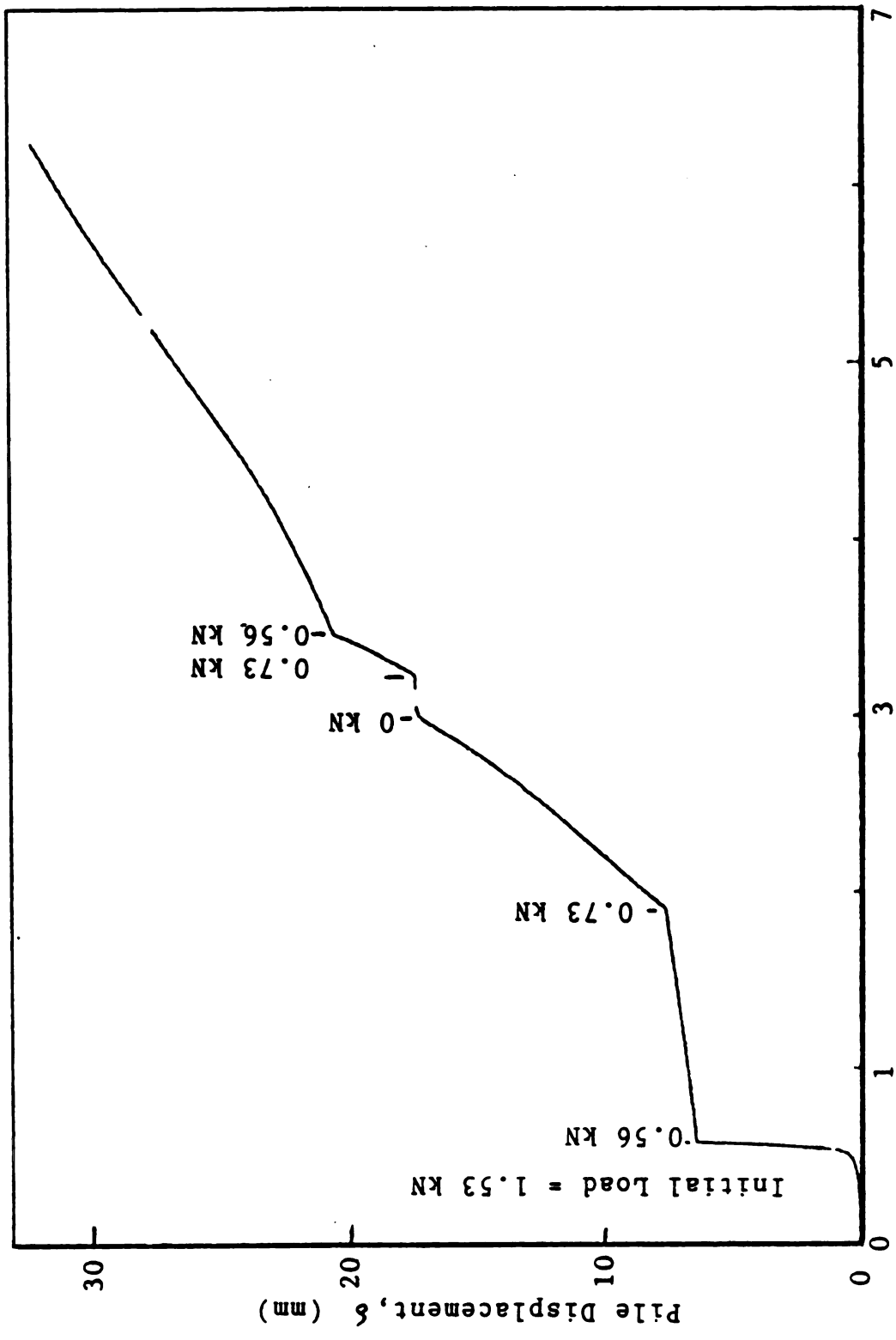

Figure B.23. Pile Test #49.

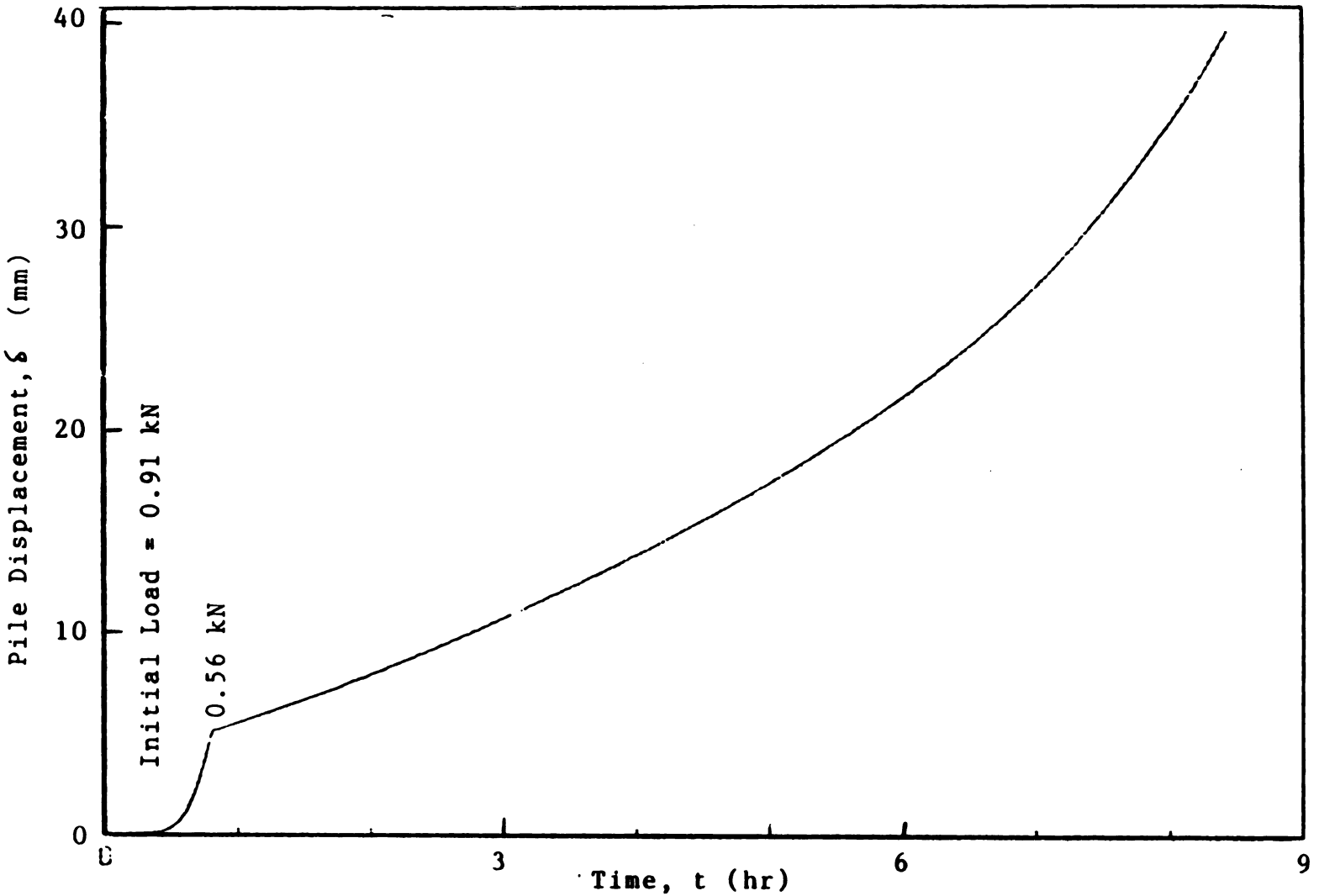

Figure B.24. Pile Test #52.

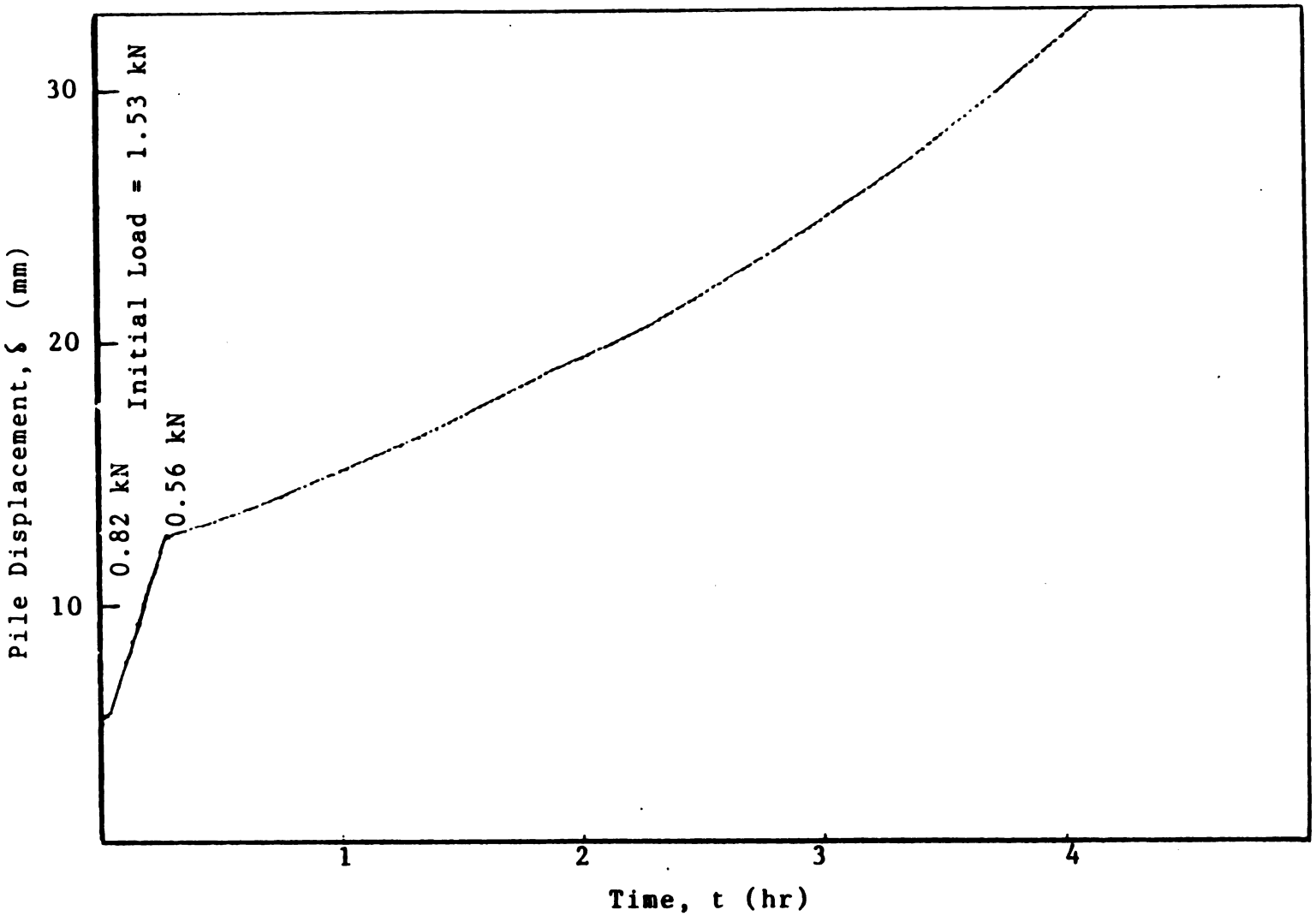

Figure B.25. Pile Test #54.

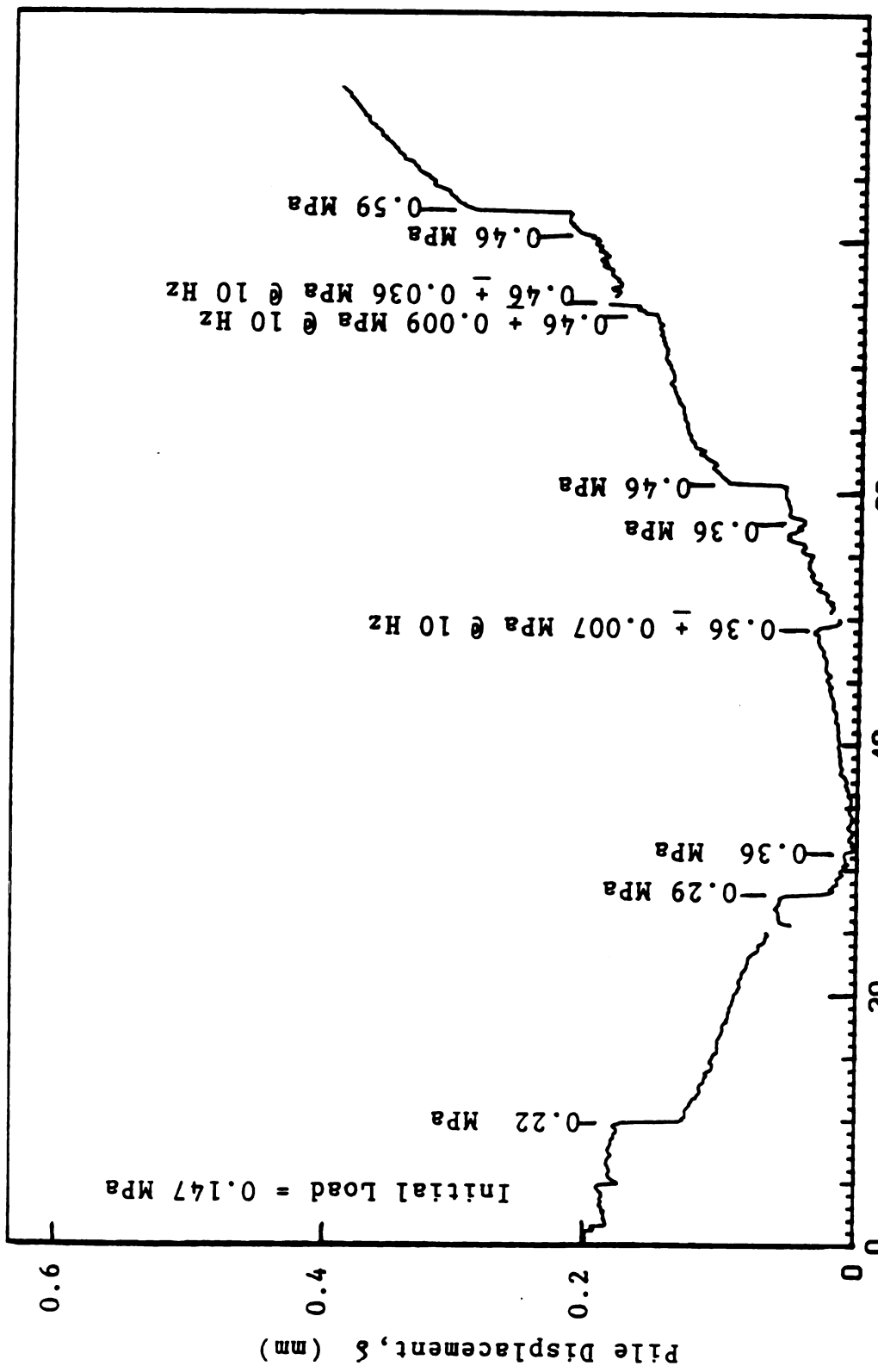

Figure B.26. Pile Test #61.

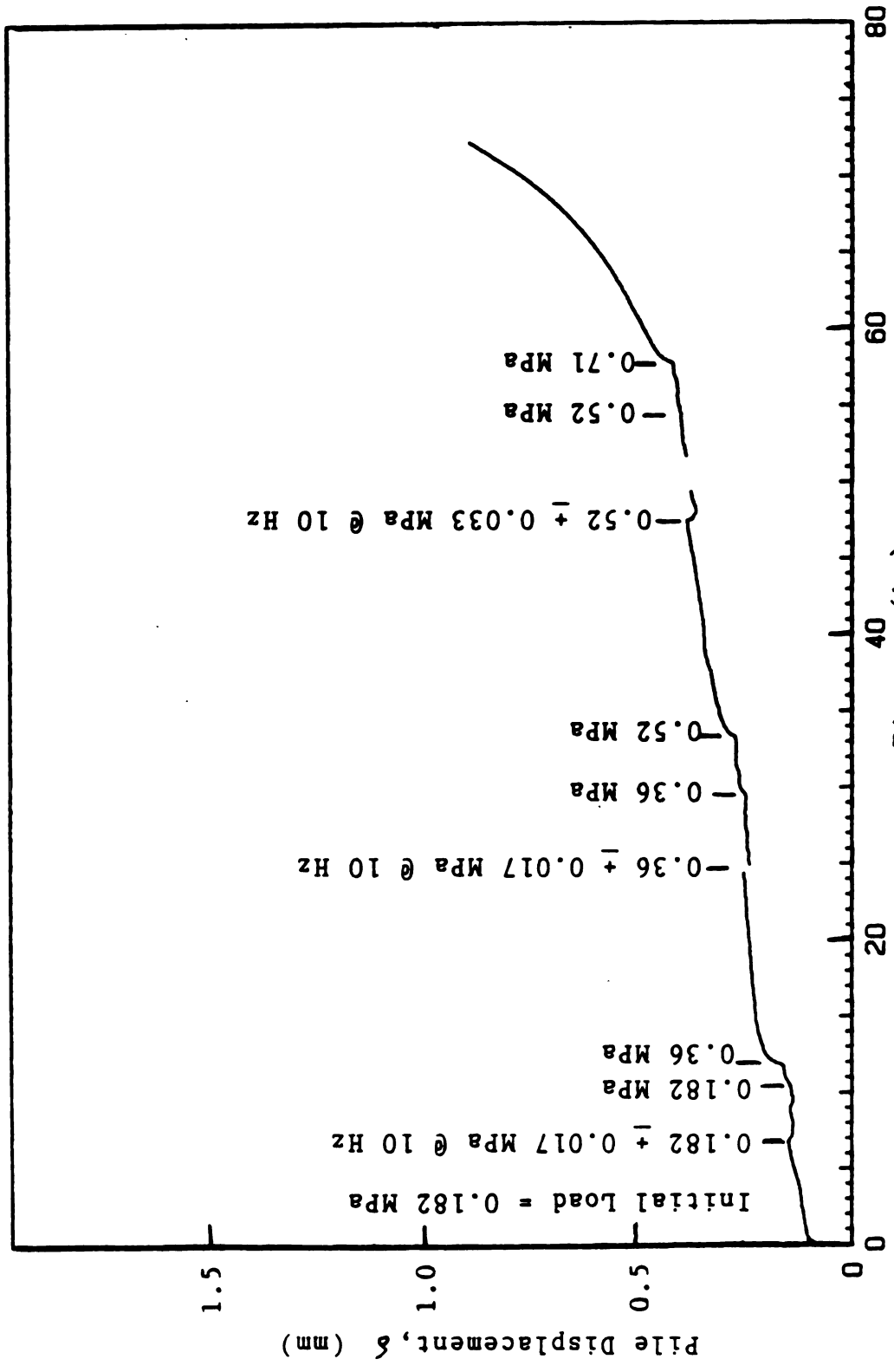

Figure B.27. Pile Test #62.

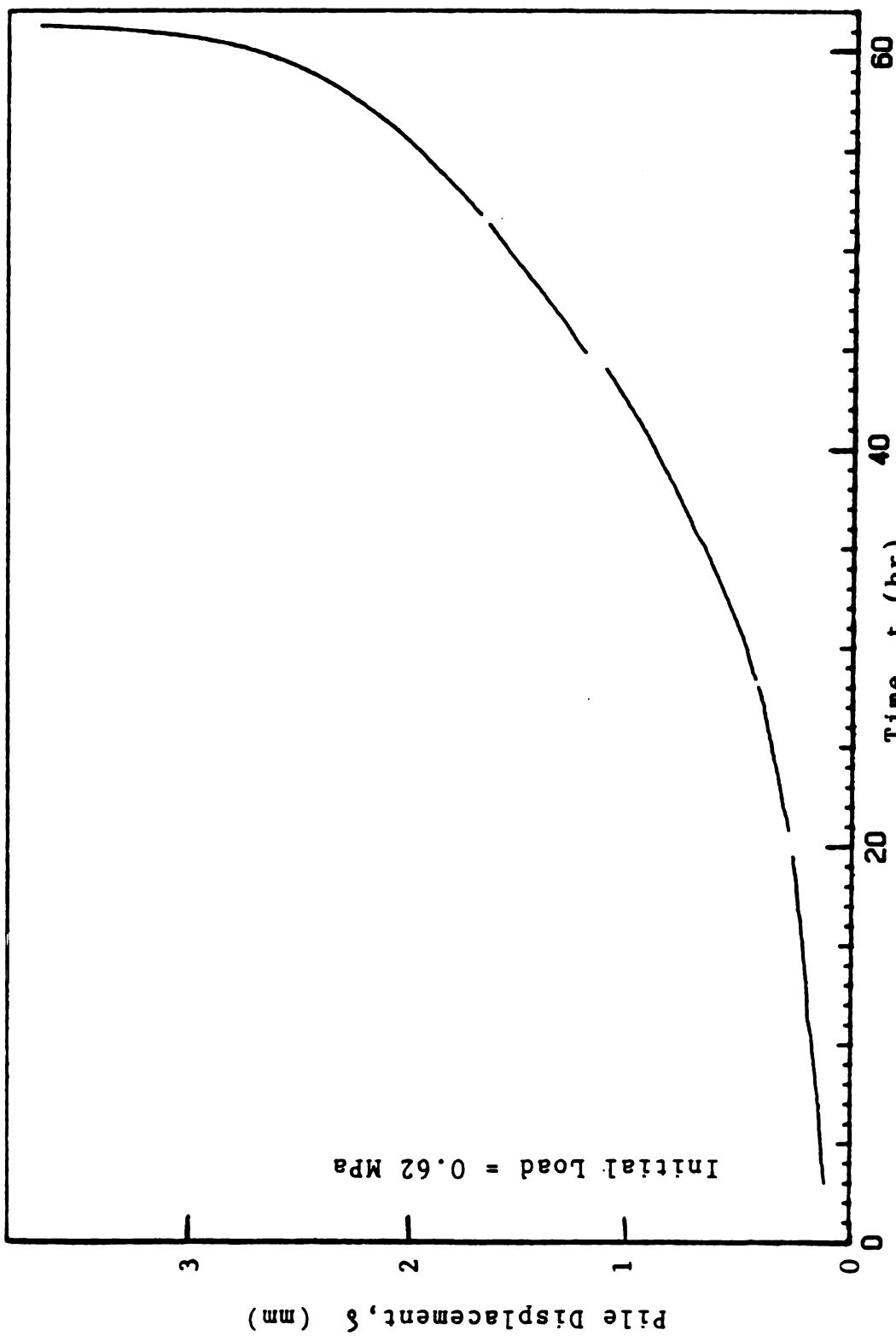

Figure B.28. Pile Test #65.

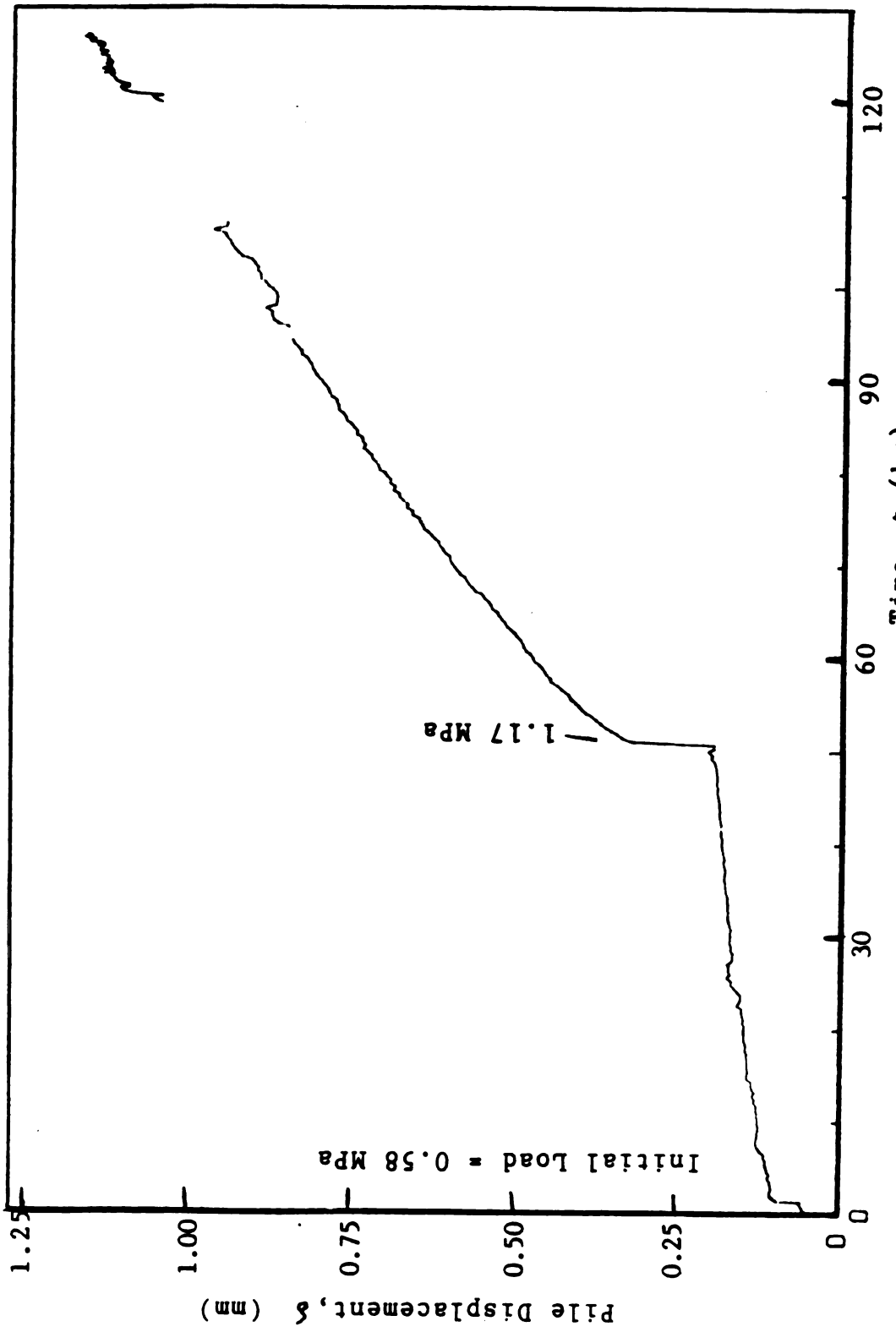

Figure B.29. Pile Test #67.

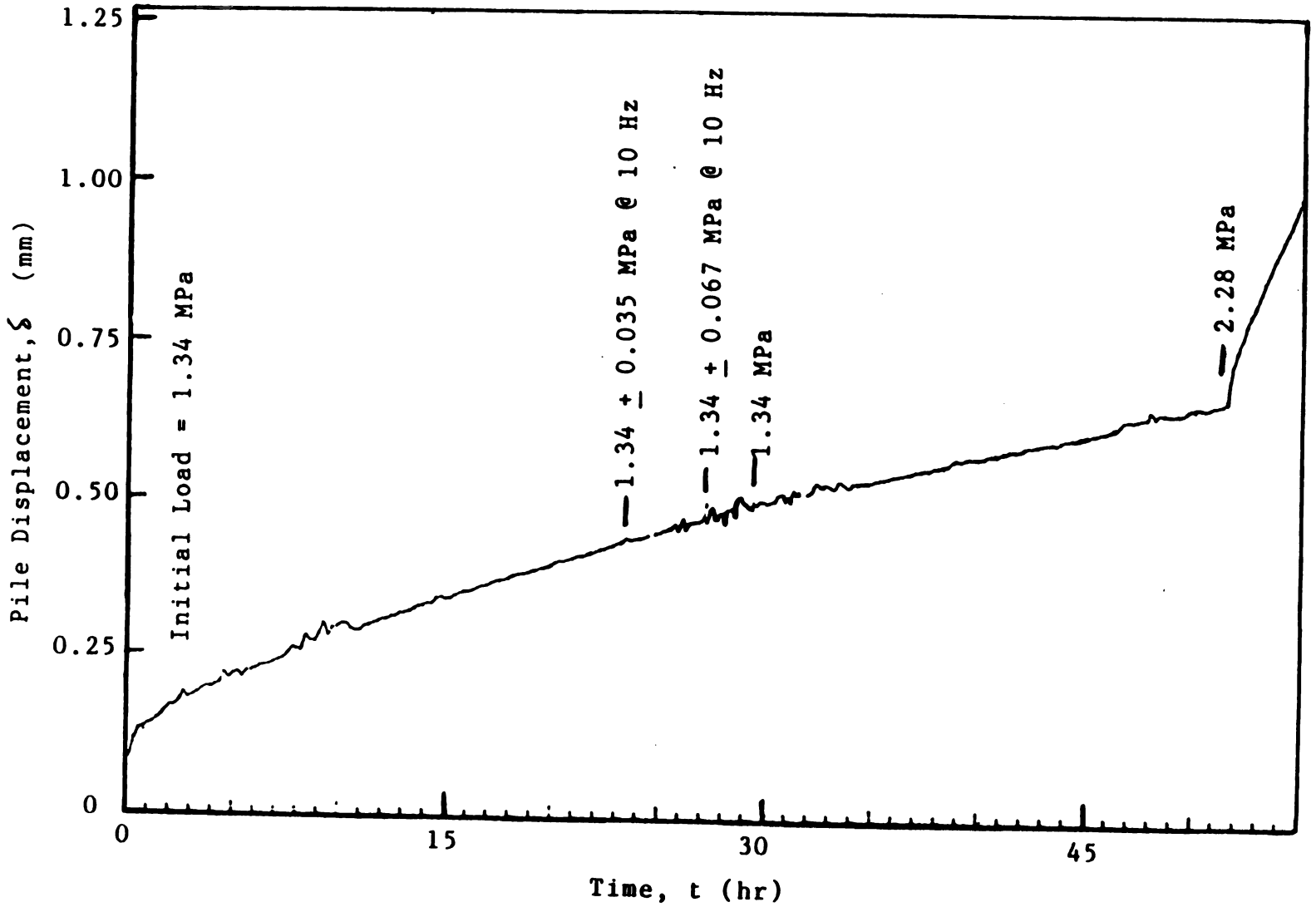

Figure B.30. Pile Test #69.

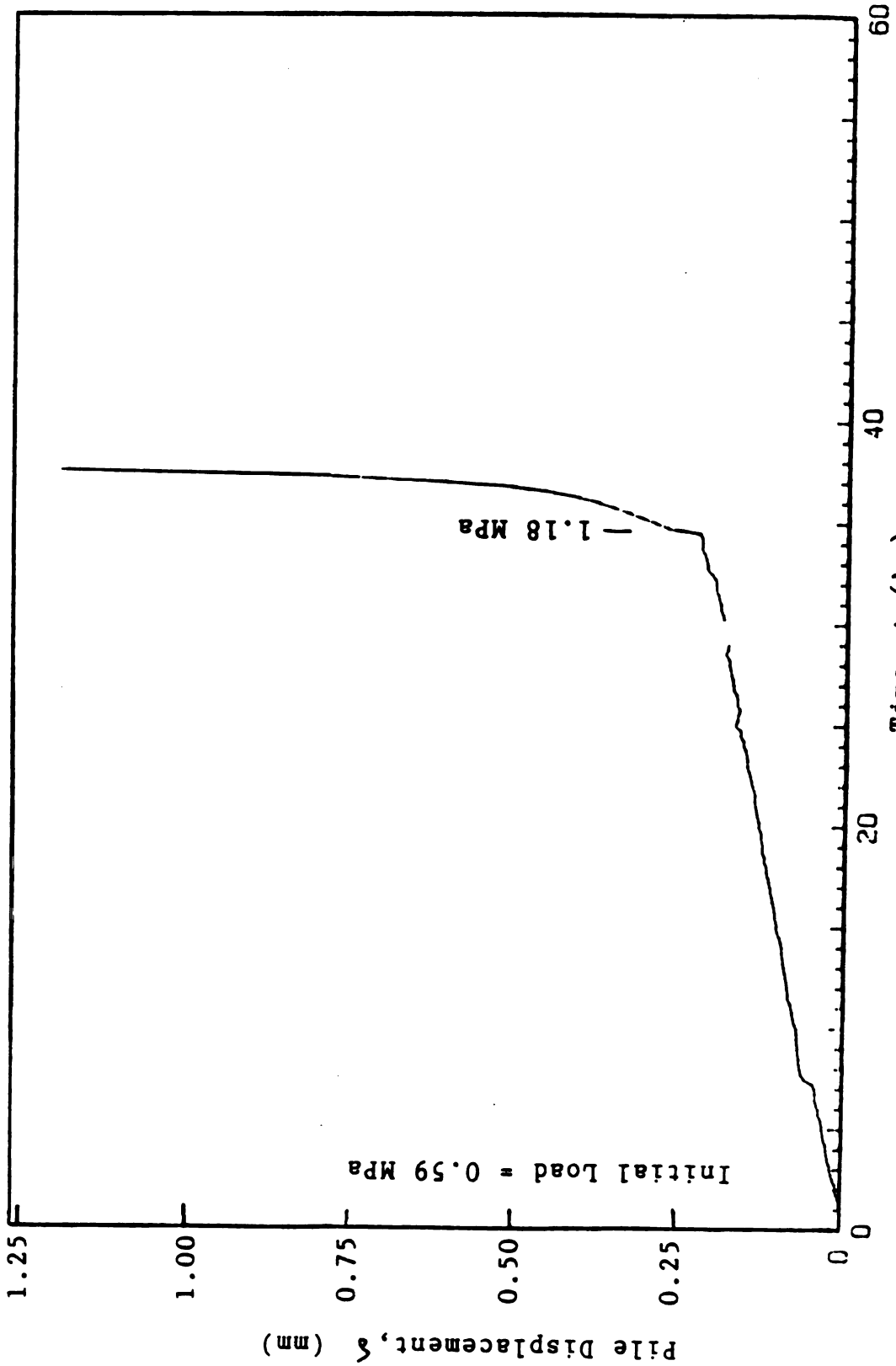

Figure B.31. Pile Test #70.

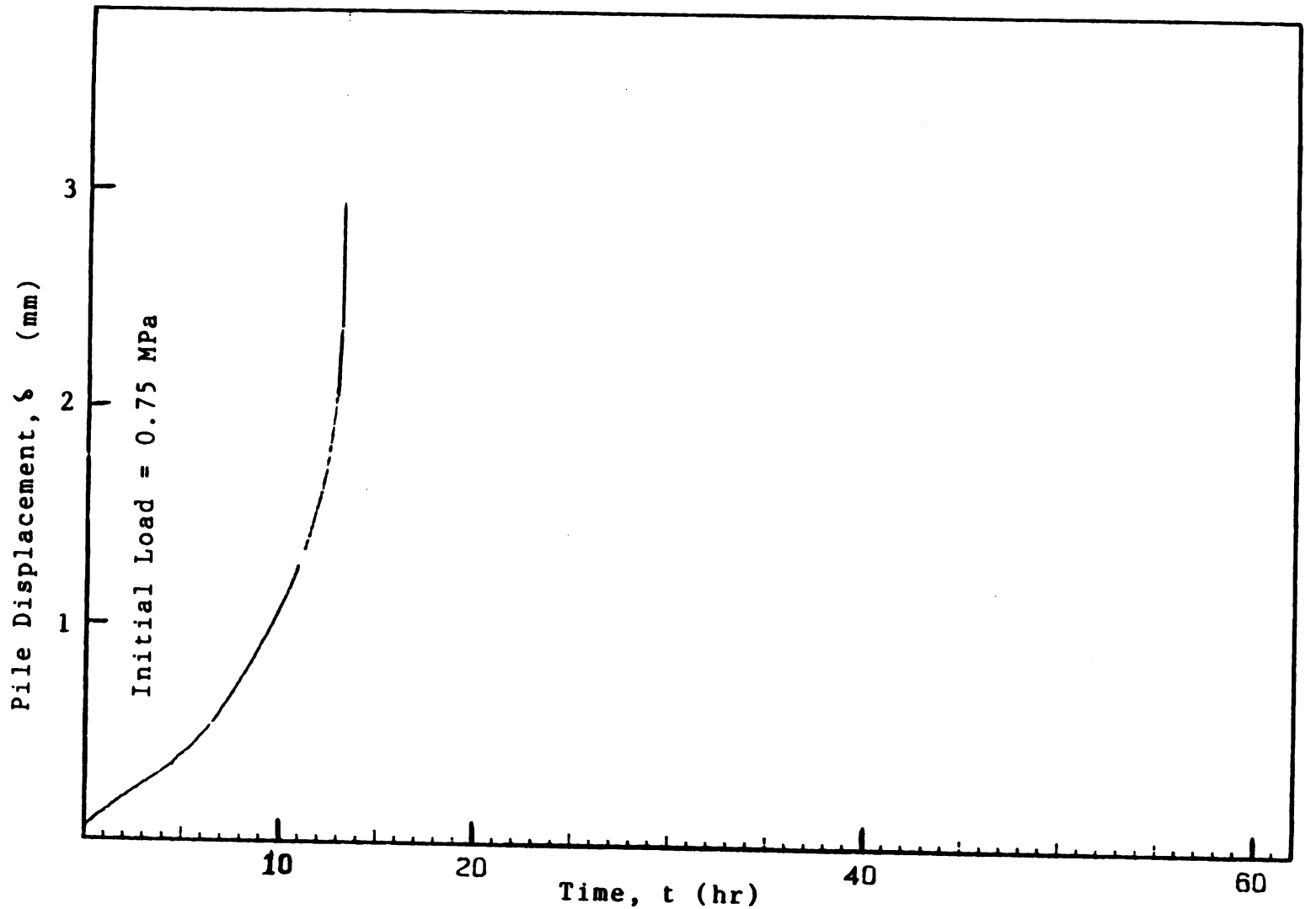

Figure B.32. Pile Test #71.

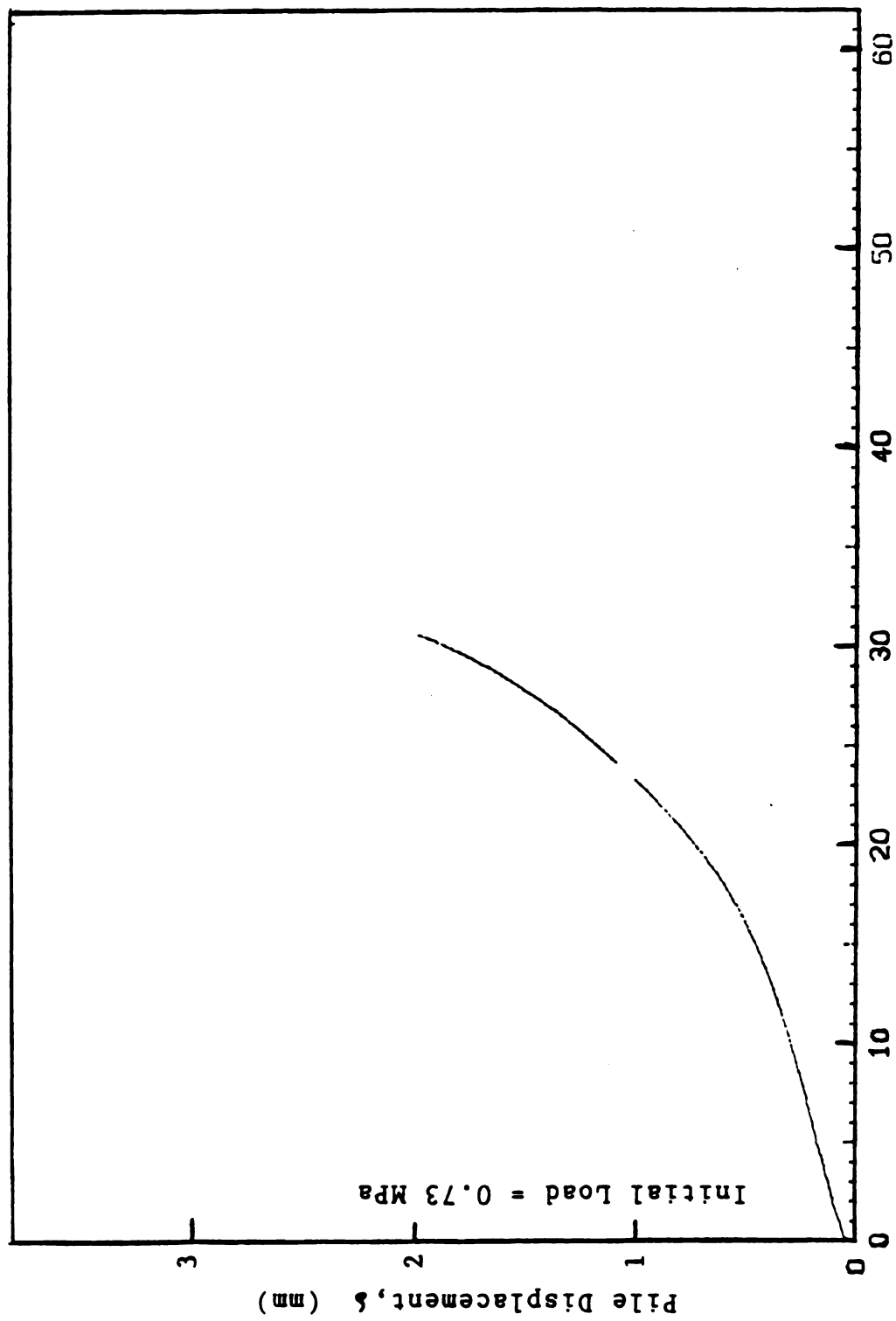

Figure B.33. Pile Test #73.

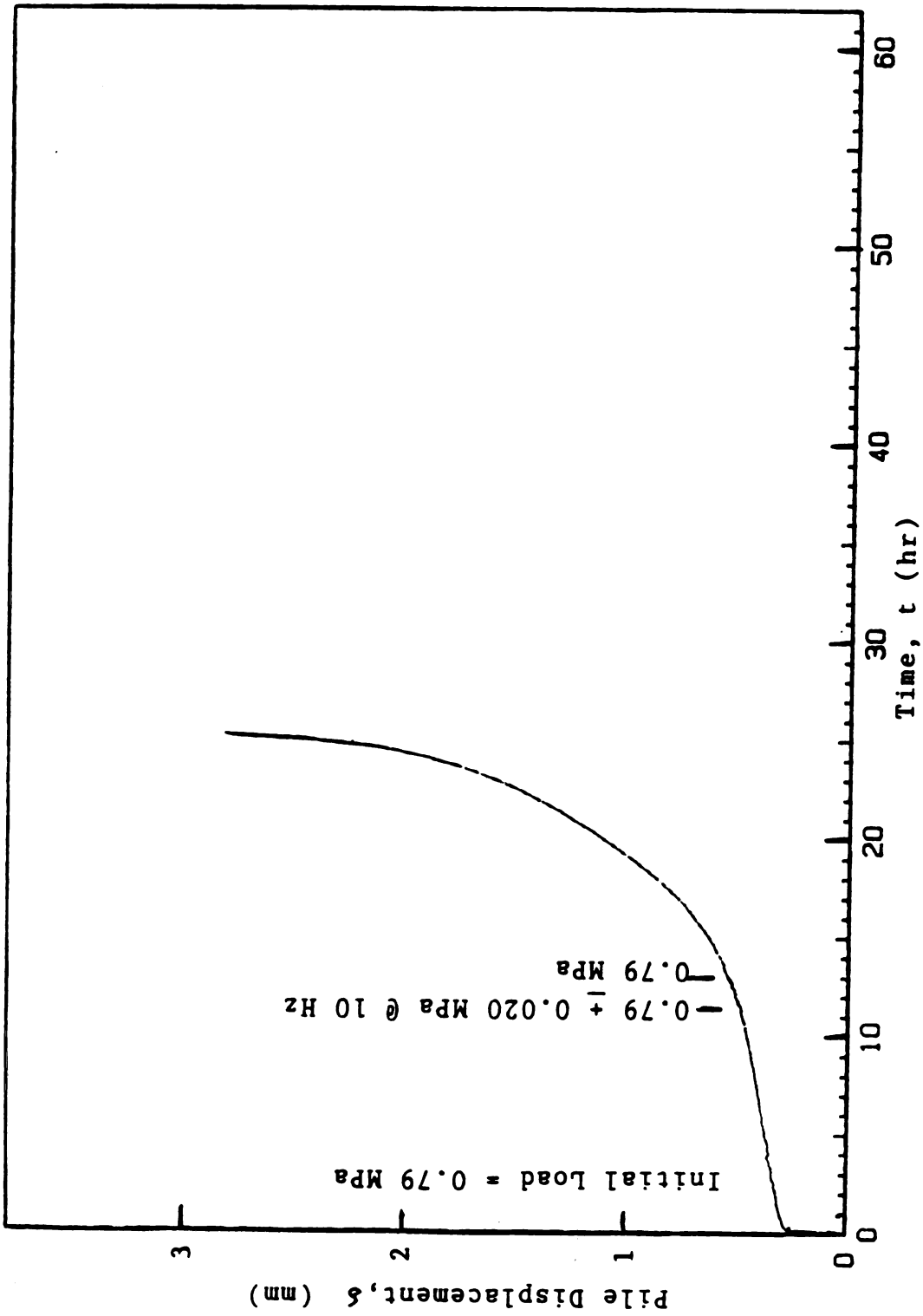

Figure B.34. Pile Test #74.

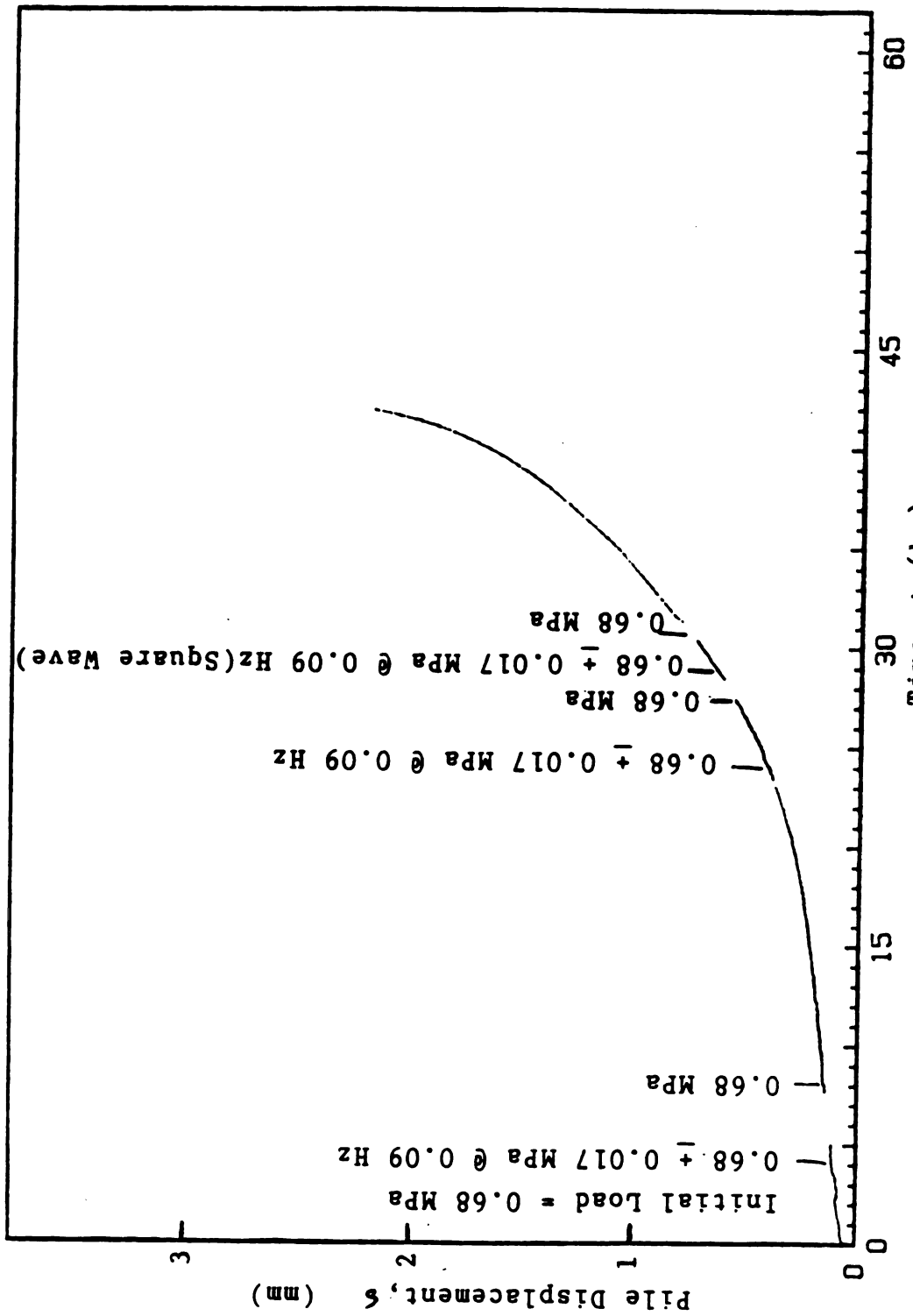

Figure B.35. Pile Test #75.

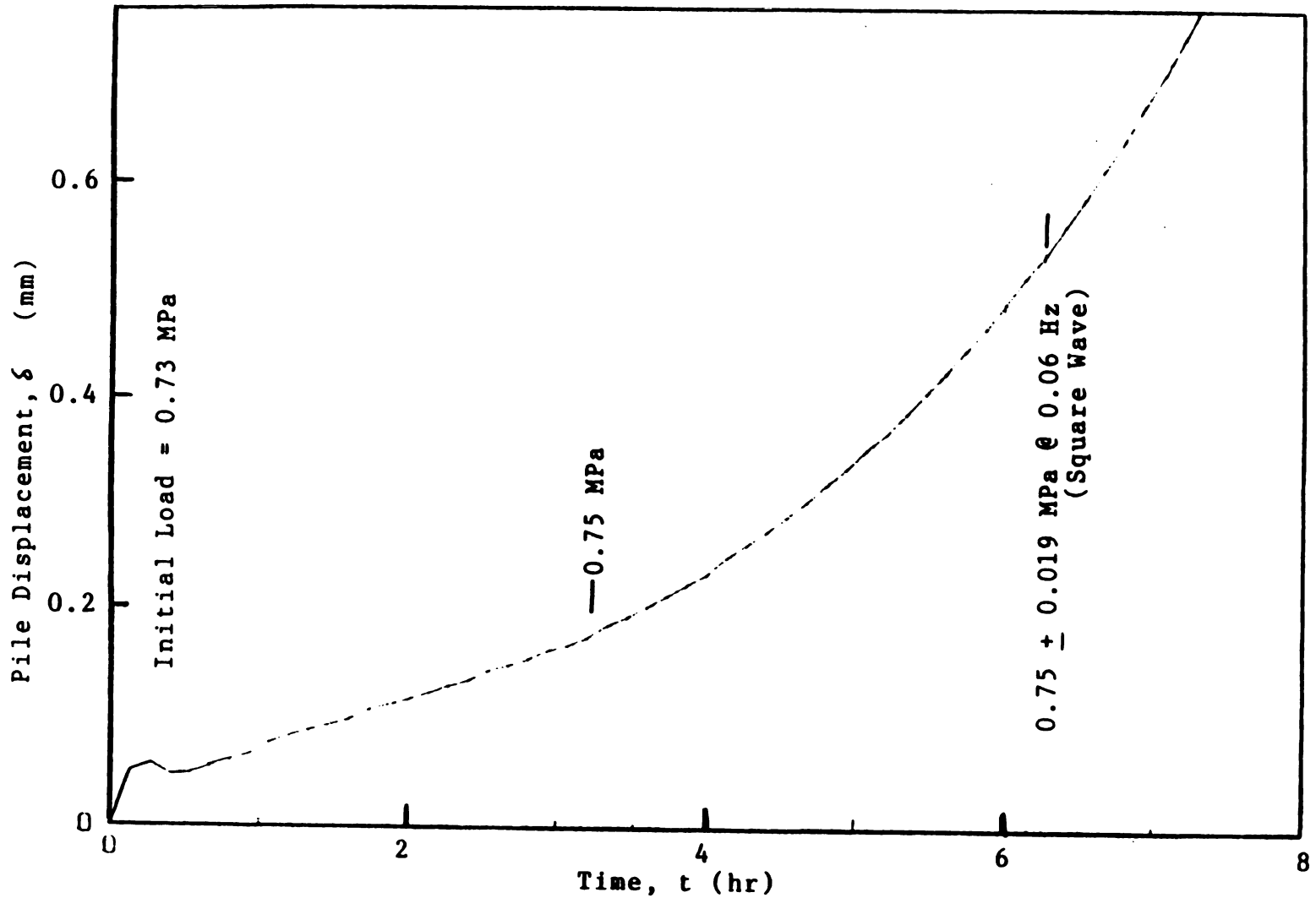

Figure B.36. Pile Test #76.

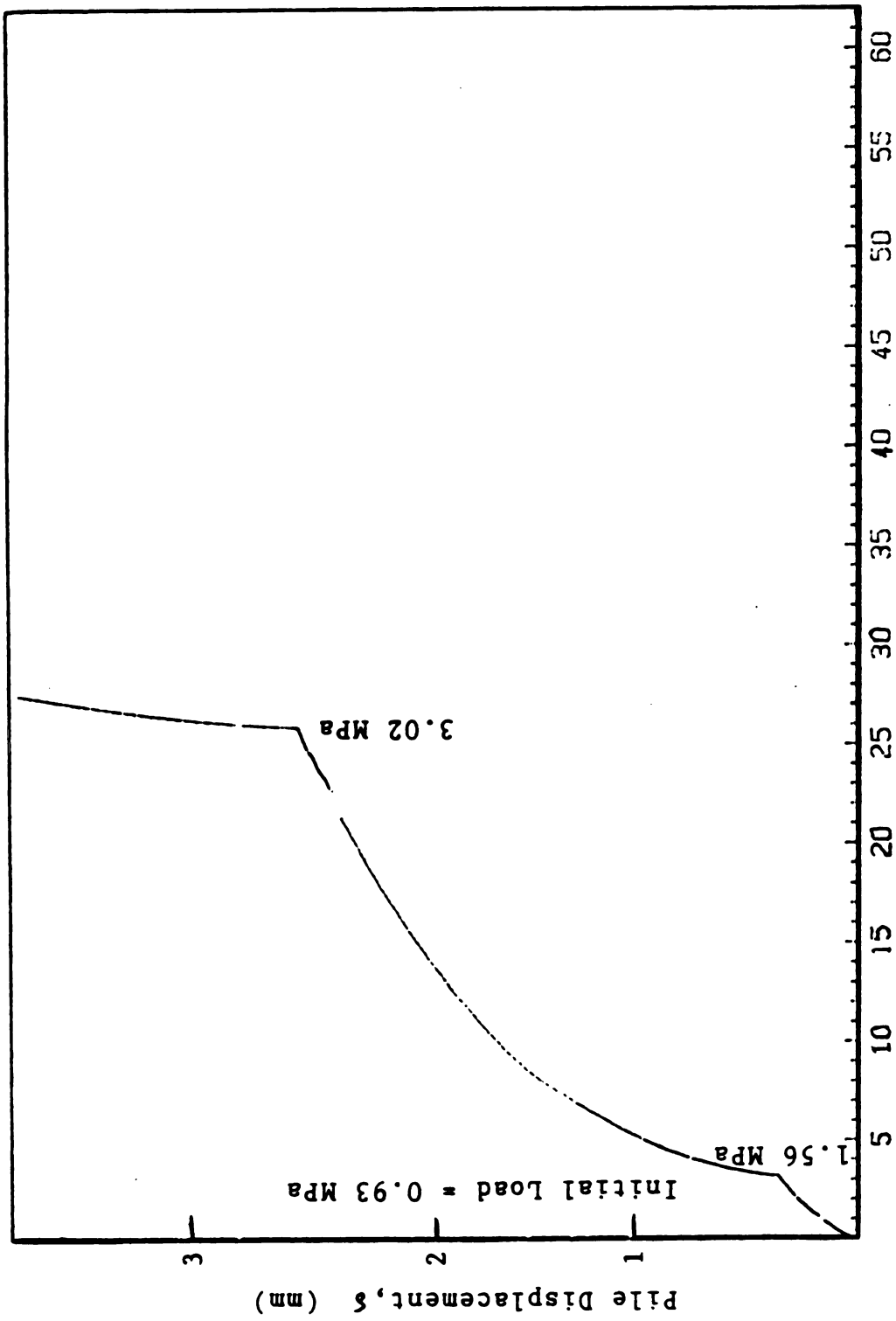

Figure B.37. Pile Test #78.

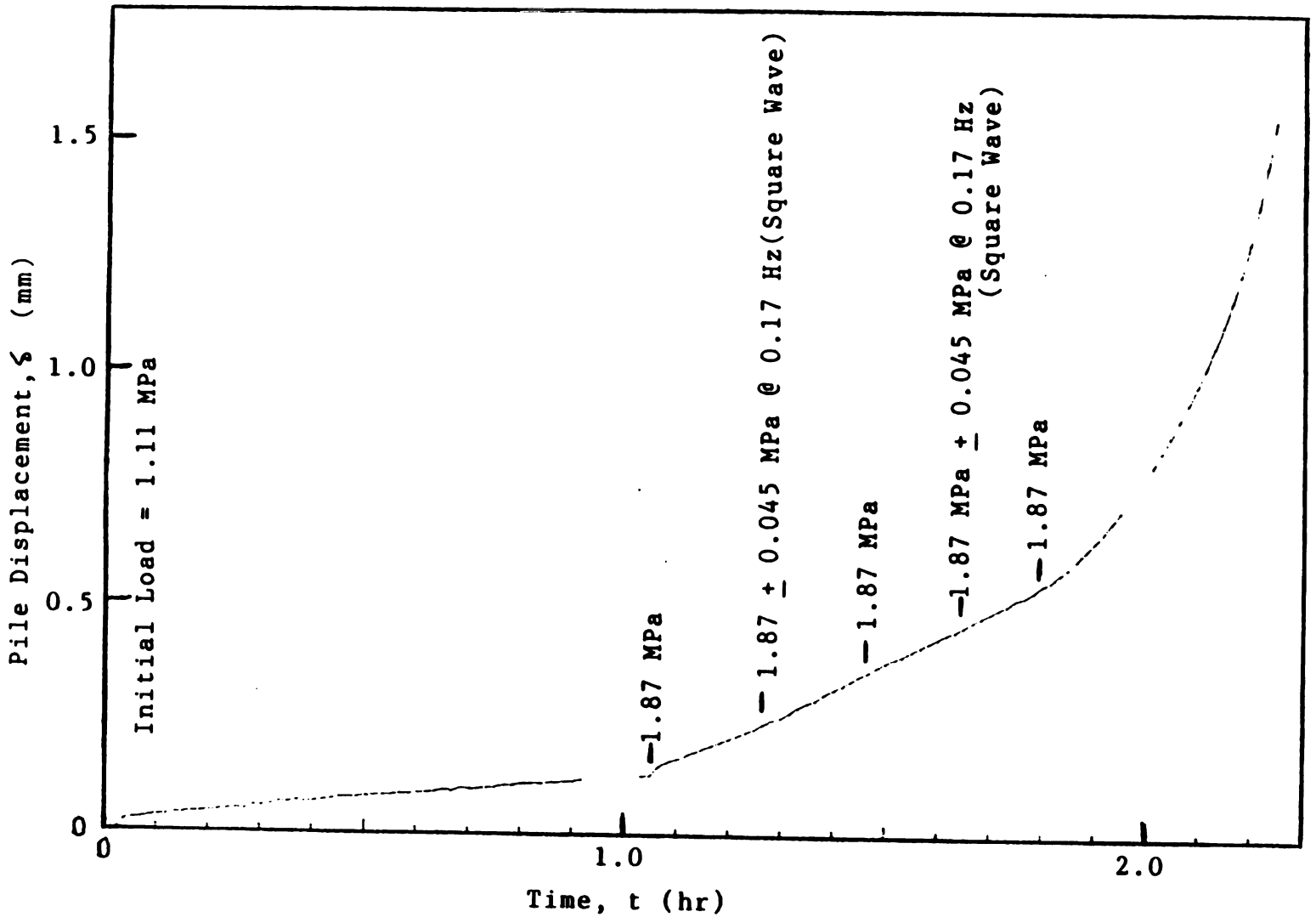

Figure B.38. Pile Test #79.

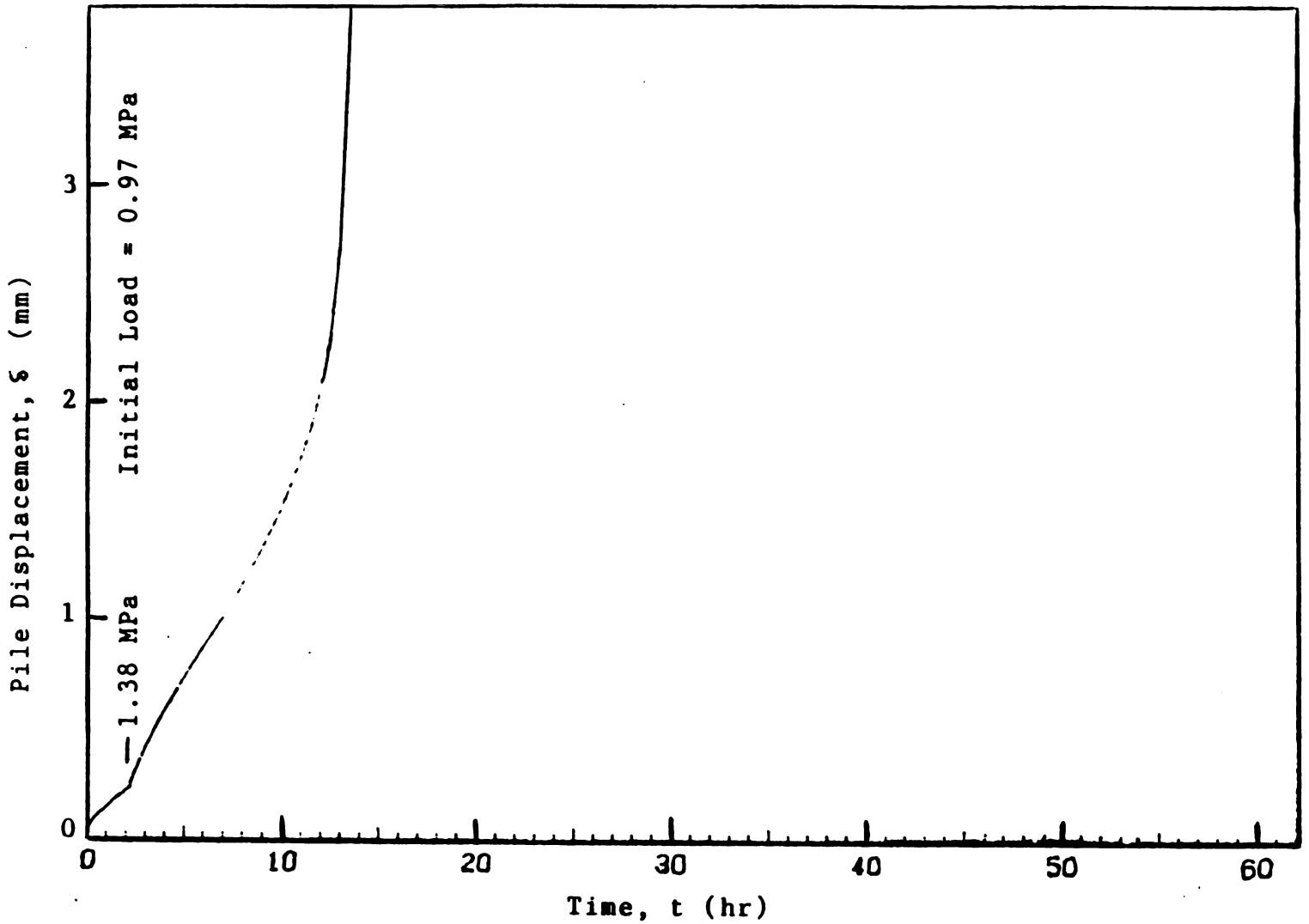

Figure B.39. Pile Test #80.

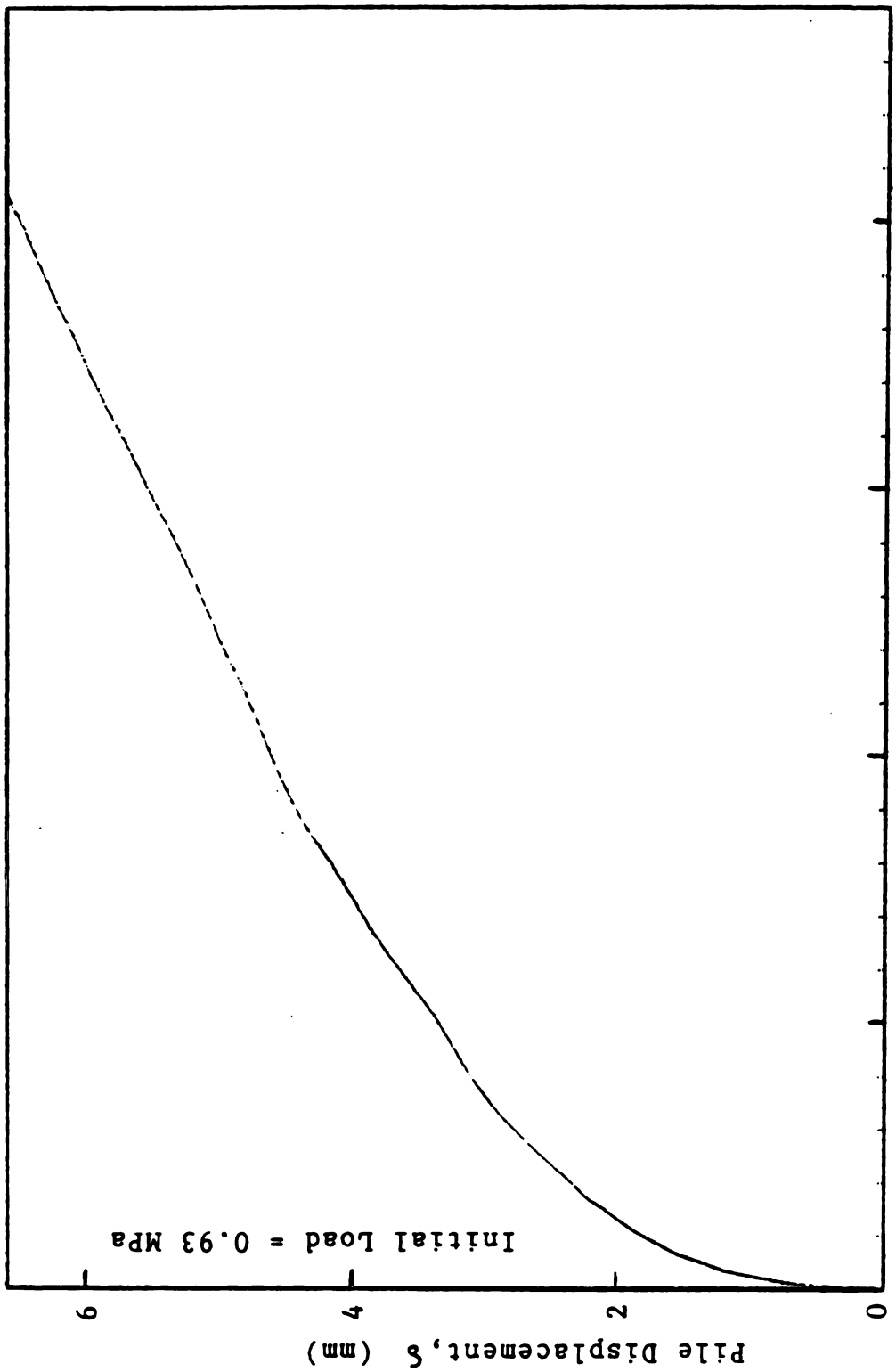

Figure B.40. Pile Test #81.

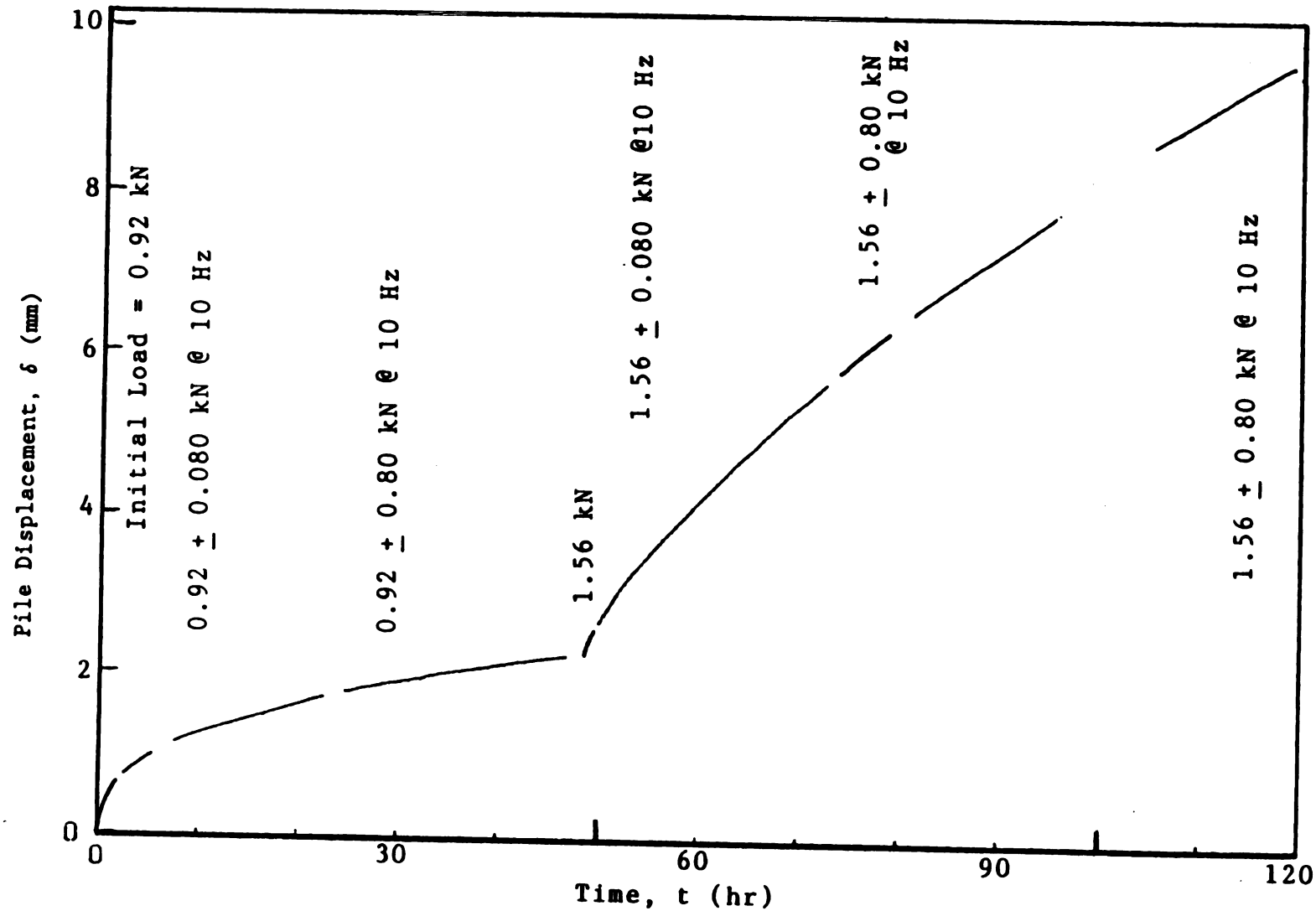

Figure B.41. Pile Test #82.

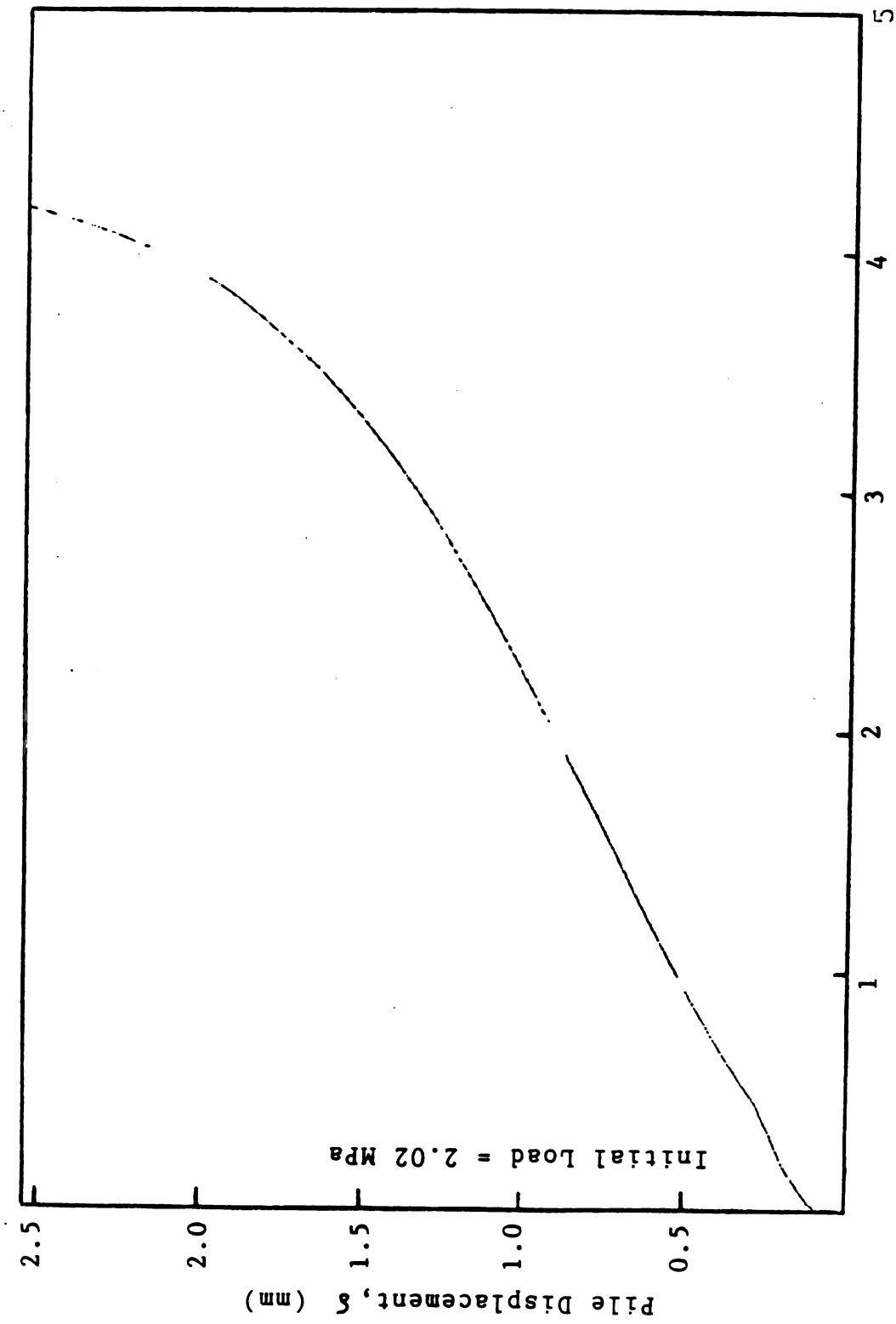

Figure B.42. Pile Test #85.

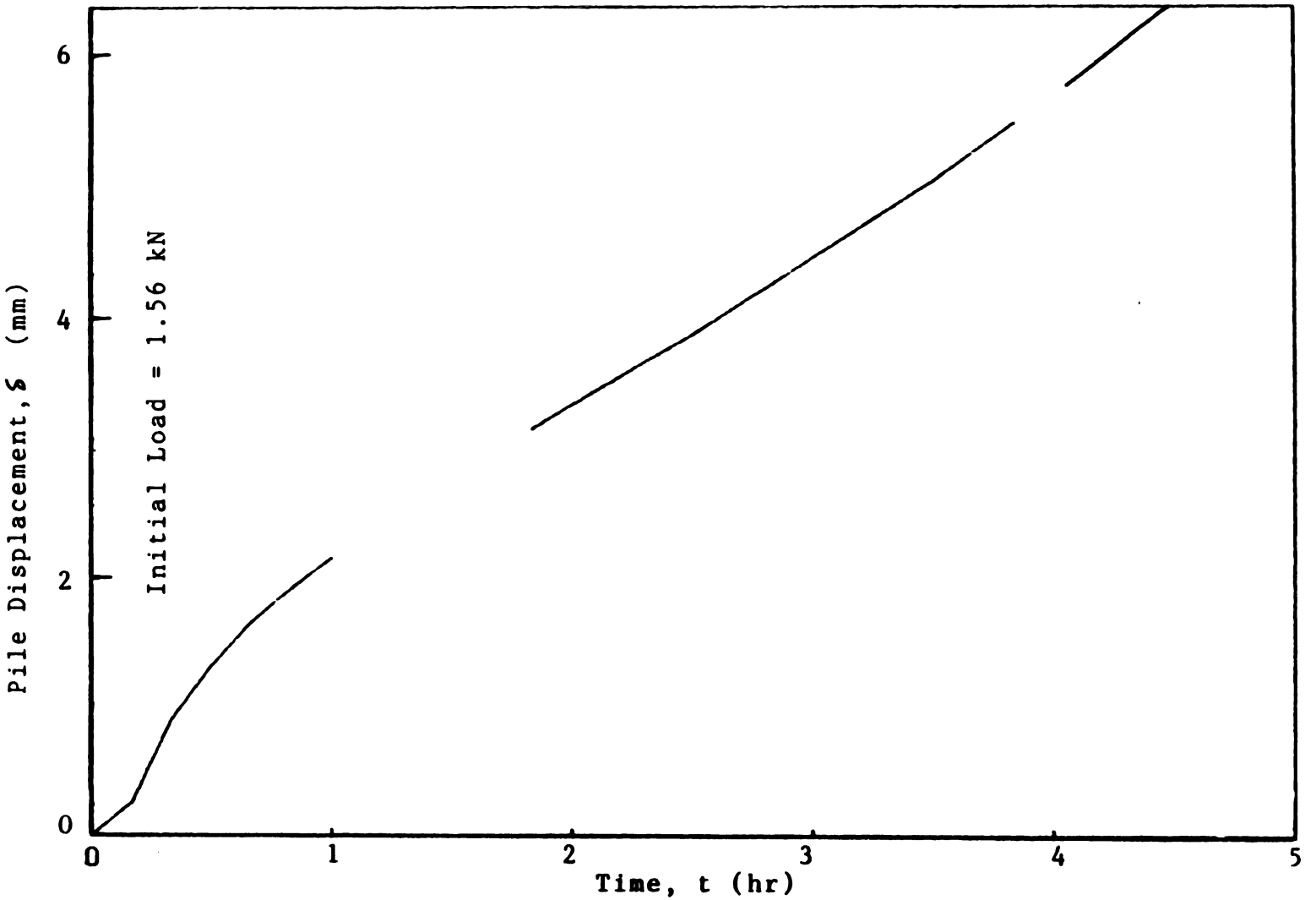

Figure B.43. Pile Test #88.

REFERENCE LIST

REFERENCES

Alkire, B.D. (1972). "Mechanical Properties of Sand-Ice Materials", unpublished Ph.D. Dissertation, Michigan State University, East Lansing, Michigan.

Alwahab, M. R. M. (1983). "Bond and Slip of Steel Bars in Frozen Sand," unpublished Ph.D. Dissertation, Michigan State University, East Lansing, Michigan.

Andersland, O.B. (1987). Chapter 8 in GROUND ENGINEER'S REFERENCE BOOK, edited by F.G. Bell, Butterworth and Co. (Publishers) Ltd., London.

Andersland, O.B.; and Akili, W. (1967). "Stress Effects on Creep Rates of Frozen Clay Soil," Geotechnique, London, Vol. 17, no. 1, pp. 27-39.

Andersland, O.B.; and AlNouri, I. (1970). "Time-Dependent Strength Behavior of Frozen Soil," J. Soil Mech. Found. Div. Am. Soc. Civil Eng., Vol. 96, No. SM4, pp. 1249-1265.

Andersland, O.B.; and Alwahhab, M.R.M. (1983). "Lug behavior for model steel piles in frozen sand," PERMAFROST, Proceedings 4th International Conference, National Academy Press, Washington, D.C., p. 16-21.

Andersland, O.B.; and Douglas, A.G. (1970). "Soil Deformation Rates and Activation Energies," Geotechnique, London, Vol. 20, No. 1, pp. 1-16.

Andersland, O.B.; Sayles, F.H.; and Ladanyi, B. (1978). "Mechanical Properties of Frozen Ground," Chapter 5 in GEOTECHNICAL ENGINEERING FOR COLD REGIONS, ed. by O.B. Andersland and D.M. Anderson., McGraw-Hill Book Co., New York.

Anderson, D.M.; Pusch, R.; and Penner, E. (1978). "Physical and Thermal Properties of Frozen Ground," Chapter 2 in GEOTECHNICAL ENGINEERING FOR COLD REGIONS (ed. by O.B. Andersland and D.M. Anderson), McGraw-Hill Book Co., New York.

Anderson, D.M.; and Tice, A.R. (1972). "Predicting Unfrozen Water Contents in Frozen Soils from Surface Area Measurements," Highway Research Record, No. 393, pp. 12-18.

Assur, A. (1963). "Discussion on Creep of Frozen Soils," PERMAFROST, Proc. 1st Int. Conference, Purdue University, Lafayette, Indiana, pp. 339.

ASTM (1988). "Piles Under Static Axial Compressive Load," ASTM-D1143.

Baker, T.H.W. (1978a). "Effect of End Conditions on the Uniaxial Compressive Strength of Frozen Sand", PERMAFROST, Proc. 3rd Int. Conference, Edmonton, Alberta, Vol. 1, pp. 608-614.

Baker, T.H.W. (1978b). "Strain Rate Effects on the Compressive Strength of Frozen Sand", Engineering Geology, 13, pp. 223-231.

Baker, T.H.W. (1979). "Strain Rate Effect on the Compressive Strength of Frozen Sand," GROUND FREEZING, First International Symposium, Bochum. (Edited by H. L. Jessberger), Elsevier Sci. Publ. Co., pp. 223-231.

Bishop, R.F.; Hill, R.; and Mott, N.G. (1945). "The Theory of Indentation and Hardness Tests," Proc. Phys. Soc., Lond. 57(3) pp. 147-159.

Bragg, R.A. (1981). "Properties for Sand-Ice Structural Systems," unpublished Ph.D. Dissertation, Michigan State University, East Lasning, Michigan.

Bragg, R.A.; and Andersland, O.B. (1980). "Strain Rate, Temperature, and Sample Size Effects on Compression and Tensile Properties of Frozen Sand," GROUND FREEZING, Second International Symposium, Trondheim, Norway, pp. 34-47.

Brown, J.; Rickard, W.; and Vietor, D. (1969). "The Effect of Disturbance on Permafrost Terrain," U.S. Army Cold Reg. Res. Eng. Lab., Spec. Rep. 138, Hanover, N.H.

Chaichanavong, T. (1976). "Dynamic Properties of Ice and Frozen Clay Under Cyclic Triaxial Loading Conditions," unpublished Ph.D. Dissertation, Michigan State University, East Lansing, Michigan.

Chamberlain, E.; Groves, C.; and Perham, R. (1972). "The Mechanical Behavaior of Frozen Earth Materials Under High Pressure Triaxial Test Condition," Geotechnique, London, Vol. 22, No. 3, pp. 469-483.

Clough R.; and Penzien J. (1975). DYNAMICS OF STRUCTURES, McGraw-Hill Book Co., New York.

Dillon, H.B.; and Andersland, O.B. (1966). "Predicting Unfrozen Water Contents in Frozen Soils," Canadian Geotechnical Journal, Vol. 3, No. 2, pp. 53-60.

Dufour, S.; Sego, D.C.; and Morgenstern, N.R. (1983). "Vibratory Model Pile Driving in Frozen Sand," PERMAFROST, Proceedings Fourth International Conference, National Academy Press, Washington. D.C., pp. 255- 260.

Eckardt, H. (1982). "Creep Tests With Frozen Soils Under Uniaxial Tension and Uniaxial Compression," Roger J.E. Brown Memorial Volume. Proceeding of the 4th Canadian Permafrost Conference Calgary, National Research Council of Canada, pp. 365-373.

Frost, H.; and Ashby, M.F. (1982). "Deformation Mechanism Maps" THE PLASTICITY AND CREEP OF METALS AND CERAMICS, Pergamon Press.

Glasstone, S.; Laidler, K.; and Eyring, H. (1941). THE THEORY OF RATE PROCESS, McGraw-Hill Book Co., New York.

Gold, L.W. (1970). "Process of Failure in Ice," Canadian Geotechnical Journal, Vol. 7, No. 4, pp. 405-413.

Gold, L.W. (1970). "Process of Failure in Ice," Canadian Geotechnical Journal, Vol. 7, No. 4, pp. 405-413.

Goughnour, R.R.; and Andersland, O.B. (1968). "Mechanical Properties of a Sand-Ice System," J. Soil Mech. Found. Div. Am. Soc. Civil Eng., Vol. 94, No. SM4, pp. 923-950.

Griffith, A.A. (1924). "The Theory of Rupture," 1st Int. Congress for Appl. Mech., Delft, pp. 55-63.

Haynes, F.D.; Karalius, J.A.; and Kalafut, J. (1975). "Strain Rate Effect on the Strength of Frozen Silt," U.S. Army Cold Reg. Res. Eng. Lab., Res. Rep. 350, p. 27.

Heydinger, A. G. (1987). "Piles in Permafrost," Journal of Cold Regions Engineering, American Society of Civil Engineers, Vol. 1, No. 2, pp. 59-75.

Hill, R. (1950). "THE MATHEMATICAL THEORY OF PLASTICITY," Clarendon Press, Oxford, England.

Hoekstra, P. (1969). "The Physics and Chemistry of Frozen Soils," Spec. Rep. 103, High. Res. B., pp. 78-90.

Hult, J.A.H. (1966). "CREEP IN ENGINEERING STRUCTURES," Blaisdell Publ. Co., Waltham, Mass.

Jellinek, H.H.G. (1957 a). "Tensile Strength Properties of Ice Adhering to Stainless Steel," USA SIPRE, Corps of Engineers, Wilmette, Ill., Res. Rep. 23.

Jellinek, H.H.G. (1957 b). "Adhesive Properties of Ice, Part 1," USA SIPRE, Corps of Engineers, Wilmette, Ill., Res. Rep. 38.

Jellinek, H.H.G. (1960 a). "Bonding of Flat Ice Surfaces-Some Preliminary Results," USA SIPRE, Corps of Engineers, Wilmette, Ill., Res. Rep. 61.

Jellinek, H.H.G. (1960 b). "Adhesive Properties of Ice, Part 2," USA SIPRE, Corps of Engineers, Wilmette, Ill., Res. Rep. 62.

Jellinek, H.H.G. (1960 c). "Some Frictional Properties of Thin Water Films," USA SIPRE, Corps of Engineers, Wilmette, Ill., Spec. Rep. 37.

Jellinek, H.H.G. (1967). "Liquid-Like (Transition) Layer on Ice," Journal Of Colloidal and Interface Science, Vol. 25, pp. 192-205.

Johnson, K.E. (1970). "The Correlation of Indentation Experiments" J.Mech. Phys. Solids. 18, pp. 118-126.

Johnston, G.H. (1963). "Pile Construction in Permafrost," PERMAFROST, Proceedings 1st International Conference, National Academy Press, Washington, D.C., pp. 477-481.

Johnston, G.H.; and Ladanyi, B. (1972). "Field Tests of Grouted Rod Anchors in Permafrost." Can. Geotechnical J., Vol. 9, pp. 176-194.

Kaplar, C.W. (1969). "Laboratory Determination of Dynamic Moduli of Frozen Soils and of Ice," U.S. Army, Cold Reg. Res. Eng. Lab., Hanover, N.H., Res. Rep. 163.

Kaplar, C.W. (1971). "Some Strength Properties of Frozen Soil and Effect of Loading Rate," U.S. Army, Cold Reg. Res. Eng. Lab., Spec. Rep. 159, Hanover, N.H.

Kovacs, A.; and Michitti, F. (1970). "Pile Driving by Means of Longitudinal and Torsional Vibrations," U.S. Army, Cold Reg. Res. Eng. Lab., Spec. Rep. 141, Hanover, N.H.

Lachenbruch, A.H. (1988). "Permafrost Temperature and the Changing Climate" PERMAFROST, Proceedings Fifth International Conference on Permafrost, Tapir Publishers, Trondheim, Norway, Vol. 2, pp. 1165-1170.

Ladanyi, B. (1966). "Failure Mechanism of Rock Under a Plate Load," Proc. First Cong. Int. Soc. Rock Mech., Lisbon, Port. 1, pp. 415-420.

Ladanyi, B. (1972). "An Engineering Theory of Creep of Frozen Soils," Canadian Geotechnical Journal, Vol. 9, No. 1, pp 63-80.

Ladanyi, B. (1976). "Use of the Static Penetration Test in Frozen Soils," Canadian Geotechnical Journal, Vol. 13, No. 2, pp. 95-110.

Ladanyi, B. (1981). "Mechanical Behavaior of Frozen Soils," MECHANICS OF STRUCTURED MEDIA (ed. By A.P.S. Selvadurai) Elsevier Scientific Publ. Co., New York, pp. 205-245.

Ladanyi, B. (1982). "Determination of Geotechnical Parameters of Frozen Soils by Means of the Cone Penetration Test", Proc. Symp. ESOPT II, Amsterdam, Vol. 2, pp. 671-678.

Ladanyi, B. (1985). "Use of the Cone Penetration Test for the Design of Piles in Permafrost", ASME Journal of Energy Resources Technology, 107, pp. 183-187.

Ladanyi, B.; and Guichaoua, A. (1985). "Bearing Capacity and Settlement of Shaped Piles in Permafrost", Proc. XI Intl. Conf. Soil Mech Found. Eng., San Francisco, pp. 1421-1427.

Ladanyi, B.; and Guichaoua, A. (1986). "Time Dependent Bond Regain in Driven Piles in Permafrost," Proceedings of the International Conference on Deep Foundation; Beijing, Vol. 1, pp. 2164-2169.

Ladanyi, B.; and Johnston, G.H. (1973). "Evaluation of In-Site Creep Properties of Frozen Soils with the Pressuremeter," PERMAFROST, Proc. 2nd Intl. Conf., N. American Contribution, Yakutsk, U.S.S.R., pp. 310-318.

Ladanyi, B.; and Johnston, G.H. (1974). "Behavior of Circular Footings and Plate Anchors Embedded in Permafrost," Canadian Geotech. Journal, 11, pp. 531-553.

Li, J.C. (1979). "Dynamic Properties of Frozen Granular Soils," unpublished Ph.D. Dissertation, Michigan State University, East Lansing, Michigan.

Linell, K.; and Lobacz, E.F. (1980). "Design and Construction of Foundations in Areas of Deep Seasonal Frost and Permafrost," U.S. Army Cold Reg. Res. Eng. Lab., Hanover, New Hampshire, Special Report 80-34.

Luscsher, U.; Black, W.T.; and McPhail, J.F. (1983). "Results of Load Test on Temperature Controlled Piles in Permafrost," PERMAFROST, Proceedings of the Fourth International Conference, National Academy of Science Press, pp. 756-761.

Manikian, V. (1983). "Pile Driving and Load Tests in Permafrost for the Kuparuk Pipelone System," PERMAFROST, Proceedings of the Fourth International Conference, National Academy of Science Press, pp. 804-810.

Marin, J.; Pao, Y.H.; and Cuff, G. (1950). "Creep Properties of Lucite and Plexiglas for Tension, Compression, Bending and Torsion," Trans. Am. Soc. Mech. Eng., 73, pp 705-718.

Mellor, M. (1979). "Mechanical Properties of Polycrystalline Ice," In: Per Tryde (Ed), Physics and Mechanics of Ice, IUTAM Symp. Copenhagen, Springer-Verlag, Berlin, pp. 217-245.

Mitchell, J.K.; Campanella, R.G.; and Singh, A. (1968). "Soil Crep as a Rate Process," J. Soil Mech. Found. Div. Am. Soc. Civil Eng., Vol. 94, No.SM1, pp. 231-253.

Nadai, A. (1963). THEORY OF FLOW AND FRACTURE OF SOLIDS, Vol. 2, McGraw-Hill Book Co., New York.

Neukirchner, R.J. (1988). "Standard Method for Pile Load Tests in Permafrost" PERMAFROST, Proceedings Fifth International Conference, Tapir Publishers, Trondheim, Norway, Vol. 2, pp. 1147-1151.

Nixon, J.F. (1987). "Pile Load Tests on Saline Permafrost at Clyde River, N.W.T." Canadian Geotechnical Journal, Vol. 25, No. 1.

Nixon, J.F.; and Lem, G. (1984). "Creep and Strength Testing of Frozen Saline Fine-Grained Soils," Canadian Geotechnical Journal, Vol. 21, pp. 518-529.

Nixon, J.F.; and McRoberts, E.C. (1976). "A Design Approach for Pile Foundations in Permafrost," Canadian Geotechnical Journal, Vol. 13, pp. 40-57.

Odquist, F.K.G. (1966). "Mathematical Theory of Creep and Creep Rupture," OXFORD MATHEMATICAL MONOGRAPH, Oxford University Press, London.

Odquist, F.K.G.; and Hult, J. (1962). CREEP IN METALLIC MATERIALS, Springer, Berlin.

Orth, W. (1985). "Deformation Behavior of Frozen Sand and Its Physical Interpretation," GROUND FREEZING, Proceedings Fourth International Symp., Sapporo, Japan.

Parameswaran, V.R. (1979). "Creep of Model Piles in Frozen Soil," Canadian Geotechnical Journal, Vol. 16, No. 1, pp. 69-77.

Parameswaran, V.R. (1982). "Displacement of Piles Under Dyunamic Loads in Frozen Soils," The Roger J.E. Brown Memorial Volume Proceedings, Fourth Canadian Permafrost Conference, Calgary, National Research Council of Canada, pp. 555-559.

Parameswaran, V.R. (1984). "Effect of Dynamic Loads on Piles in Frozen Soils," Third International Cold Regions Engineering Specialty Conference, Edmonton, Alberta, Canada. Vol. 1, pp. 41-52.

Parameswaran, V.R. (1985). "Cyclic Creep of Frozen Soils" GROUND FREEZING, Proceedings of the Fourth International Symposium, Sapporo, Japan, Vol. 2, pp. 201-206.

Richart, F.E., Jr.; Hall, J.R., Jr.; and Woods, R.D. (1970). VIBRATIONS OF SOILS AND FOUNDATIONS, Prentice-Hall, Inc., Englewood, N.J.

Ruedrich, R.A.; and Perkins, T.K. (1974). "A Study of Factors Influencing the Mechanical Properties of Deep Permafrost," Journal of Petroleum Technology, pp. 1167-1177.

Sayles, F.H. (1966). "Low Temperature Soil Mechanics," Technical Note 143, U.S. Army Cold Reg. Res. Eng. Lab., Hanover, New Hampshire.

Sayles, F.H, "Creep of Frozen Sand," U.S. Army Cold Reg. Res. Eng. Lab., Hanover, New Hampshire, Technical Report 190.

Sayles, F.H. (1973). "Triaxial and Creep Tests on Frozen Ottawa Sand," PERMAFROST, Proc. 2nd International Conference, North American Contribution, Yakutsk, U.S.S.R., pp. 384-391.

Sayles, F.H, (1974). "Triaxial Constant Strain Rate Tests and Triaxial Creep Tests on Frozen Ottawa Sand," U.S. Army Cold Reg. Res. Eng. Lab., Hanover, New Hampshire, Tech. Report 253.

Sayles, F.H.; and Epanchin, N.V. (1966). "Rate of Strain Compression Tests on Frozen Ottawa Sand and Ice" U.S. Army Cold Reg. Res. Eng. Lab., Hanover, New Hampshire, Technical Note 140.

Sayles, F.H.; et al (1987). "Classification and Laboratory Testing of Artificially Frozen Ground," Journal of Cold Regions Am Soc. Civil Eng., Vol. 1, No. 1, pp. 22-48.

Schmid, W.E. (1969). "Driving Resistance and Bearing Capacity of Vibro-Driven Model Piles," Performance of Deep Foundations, American Society for Testing and Materials, Special Technical Publication 444, p. 362-375.

Scott, F.S. (1969). "The Freezing Process and Mechanics of Frozen Ground," Cold Regions Science and Engineering Monograph 11-D1, U.S. Army Cold Reg. Res. Eng. Lab., Hanover, New Hampshire.

Soo, S. (1983). "Experimental and Numerical Analysis of Frozen Sand Structures," unpublished Ph.D. Dissertation, Michigan State University, East Lansing, Michigan.

Soo, S.; Wen, R. K.; and Andersland, O. B.(1986). "Flexural Behavior of Frozen Soil," Canadian Geotechnical Journal, Vol. 23, pp. 355-361.

Stelzer, D. L.; and Andersland, O.B. (1988). "Dynamic Load Effect on Settlement of Model Piles In Frozen Sand," PERMAFROST, Proceedings Fifth International Conference, Tapir Publishers, Trondheim, Norway, Vol. 2, pp. 1165-1170.

Stelzer, D.L.; and Andersland, O. B. (1988). "Creep Parameters for Pile Settlement Equations," OFFSHORE AND ARTIC OPERATIONS SYMPOSIUM - 1989, ed. by A. Ertas, D. Hui, and R.G. Urquhart, Am. Soc. Mech. Eng., New York, pp. 133-138.

Stelzer, D.L.; and Andersland, O. B. (1989). "Pile Roughness and Load Capacity in Frozen Soils", COLD REGIONS ENGINEERING, ed. by R.L. Michalowski, Proceedings of the Fifth International Conference, Am. Soc. Civil Eng., New York, pp. 226-235.

Stevens, H.W. (1975). "The Response of Frozen Soils to Vibratory Loads," U.S. Army Cold Reg. Res. Eng. Lab., Hanover, New Hampshire, Technical Report No. 265.

Thomas, H. P.; and Luscher, V.(1980). "Improvement of Bearing Capacity of Pipe Piles by Corrugations," Collection of Papers from a U.S. Soviet Joint Seminar, Leningrad, USSR, pp. 229-234.

Ting, J.M.; Martin, R.T.; and Ladd, C.C. (1983). "Mechanisms of Strength for Frozen Sand," Journal of Geotechnical Engineering, Am. Soc. Civil Eng., Vol. 109, No. 10.

Trimble, J.R.; and Mitchell, R.J. (1982). " A Comparison of Static and Repeated Loading Tests on Natural Frozen Soils," Proceedings of the 4th Canadian Permafrost Conference, pp. 433-439.

Tsytovich, N.A. (1960). "Bases and Foundations on Frozen Soil," NAS NRS, Publ. 804, Highway Research Board, Spec. Rep. 58.

Tsytovich, N.A. (1975). MECHANICS Of FROZEN GROUND, McGraw-Hill Book Co., New York.

Vinson, T.S. (1978). "Response of Frozen Ground to Dynamic Loading," Chapter 8 in GEOTECHNICAL ENGINEERING FOR COLD REGIONS, McGraw-Hill Book Co., New York.

Vinson, T.S.; Czajkowski, R.; and Li, J. (1977). "Dynamic Properties of Frozen Cohesionless Soils Under Cyclic Triaxial Loading Conditions," Michigan State University, Div. Eng. Res. Rep. MSU-CE-77-1.

Vyalov, S.S. (1959). "Rheological Properties and Bearing Capacity of Frozen Soils," U.S. Army Cold Reg. Res. Eng. Lab., Hanover, New Hampshire, Translation 74.

Vyalov, S.S. (1962). "The Strength and Creep of Frozen Soils and Calculations for Ice-Soil Retaining Structures," U.S. Army Cold Reg. Res. Eng. Lab., Hanover, New Hampshire, Translation 76.

Vyalov, S.S. (1963). "Rheology of Frozen Soils," PERMAFROST, Proc. 1st Int. Conf., NAS-National Research Council Publ. 1287, pp. 332-337.

Vyalov, S.S. (1965). "The Strength and Creep of Frozen Soils and Calculations for Ice-Soil Retaining Structures," U.S. Army Cold Reg. Res. Eng. Lab., Hanover, New Hampshire, Translation 76.

Vyalov, S.S.; Gorodetskii, V.F; Ermakov, V.F.; Zatsarnaya, A.G.; and Pekarskaya, N.K. (1969). "Methods of Determining Creep, Long Term Strength And Compressibility Characteristics of Frozen Soils," Technical Translation 1364, National Research Council of Canada, Ottawa.

Weaver, J.S. (1979). "Pile Foundations in Permafrost," unpublished Ph.D. Dissertation, University of Alberta, Edmonton.

Weaver, J.S., and Morgenstern, N.R. (1981 a). " Simple Shear Creep Tests on Frozen Soils," Canadian Geotechnical Journal, 18:217-229.

Weaver, J.S., and Morgenstern, N.R. (1981 b). " Pile Design in Permafrost," Canadian Geotechnical J., 18:357-370.